CRWR Online Report 10-01

Hydraulic Conductivity Measurement of Permeable Friction Course (PFC) Experiencing Two-Dimensional Nonlinear Flow Effects

by
Joshua Brandon Klenzendorf, Ph.D.
Randall J. Charbeneau, Ph.D.
Michael E. Barrett, Ph.D.

May 2010

CENTER FOR RESEARCH IN WATER RESOURCES
Bureau of Engineering Research
The University of Texas at Austin
J.J. Pickle Research Campus, Austin, TX 78712-4497

Acknowledgements

The authors would like to thank the Texas Department of Transportation for providing funding for this research study under project number 0-5220 and continuing to support the Civil Engineering program at The University of Texas at Austin through additional research opportunities. In particular, we would like to thank the TxDOT Project Director, Gary Lantrip, of the Austin District for his continued interest and support in the use of porous pavements. In addition, we would like to acknowledge Byron Kneipfel and coworkers at the TxDOT Asphalt Laboratory in Cedar Park, Texas for allowing me to use their facilities.

The authors appreciate the support and encouragement of the other members of our research group. Most importantly Brad Eck and all his work and contributions on this research study. Thank you also to Remi Candaele, Patrick Frasier, Cody Hudson, and Tina Stanard for their contributions to this research study and help in collecting data.

Hydraulic Conductivity Measurement of Permeable Friction Course (PFC) Experiencing Two-Dimensional Nonlinear Flow Effects

Publication No. ___________________

Joshua Brandon Klenzendorf, Ph.D.
Randall J. Charbeneau, Ph.D.
Michael E. Barrett, Ph.D.
The University of Texas at Austin, 2010

Permeable Friction Course (PFC) is a layer of porous asphalt pavement with a thickness of up to 50 millimeters overlain on a conventional impervious hot mix asphalt or Portland cement concrete roadway surface. PFC is used for its driver safety and improved stormwater quality benefits associated with its ability to drain rainfall runoff from the roadway surface. PFC has recently been approved as a stormwater best management practice in the State of Texas. The drainage properties of PFC are typically considered to be governed primarily by two hydraulic properties: porosity and hydraulic conductivity. Both of these hydraulic properties are expected to change over the life of the PFC layer due to clogging of the pore space by trapped sediment. Therefore, proper measurement of the hydraulic properties can be problematic. Laboratory and field tests are necessary for accurately determining the hydraulic conductivity of the PFC layer in order to ensure whether the driver safety and water quality benefits will persist in the future. During testing, PFC experiences a nonlinear flow relationship which can be modeled using the Forchheimer equation. Due to the two-dimensional flow patterns created during testing, the hydraulic conductivity cannot be directly measured. Therefore, numerical modeling of the two-dimensional nonlinear flow relationship is required to convert the measureable flow characteristics into the theoretical flow characteristics in order to properly determine the isotropic hydraulic conductivity. This numerical model utilizes a new scalar quantity, defined as the hydraulic conductivity ratio, to allow for proper modeling of nonlinear flow in two-dimensional cylindrical coordinates.

PFC core specimens have been extracted from three different roadway locations around Austin, Texas for the past four years (2007 to 2010). Porosity values of the core specimens range from 12% to 23%, and the porosity data suggest a statistical decrease over time due to trapped sediment in the pore space. A series of constant head tests used in the laboratory and a falling head test used in the field are recommended for measurement of PFC hydraulic characteristics using a modified Forchheimer equation. Through numerical modeling, regressions equations are presented to estimate the hydraulic conductivity and nonlinear Forchheimer coefficient from the measureable hydraulic characteristics determined during experimental testing. Hydraulic conductivity values determined for laboratory core specimens range from 0.02 centimeters per second (cm/s) to nearly 3 cm/s. Field measurements of in-situ hydraulic conductivity vary over a range from 0.6 cm/s to 3.6 cm/s. The results of this research provide well-defined laboratory and field methods for measurement of the isotropic hydraulic conductivity of PFC experiencing two-dimensional nonlinear flow and characterized by the Forchheimer equation. This methodology utilizes a numerical model which presents a proper solution for nonlinear flow in two-dimensions.

Table of Contents

List of Tables

List of Figures

Chapter One

Introduction

1.1 Background and Motivation

Urbanization and the development of land result in the natural land cover being replaced by impervious surfaces. Roadways, parking lots, sidewalks, and buildings are among the typical structures that result in impervious surfaces and prevent rainfall from naturally infiltrating into the ground and recharging groundwater supplies. The effects of urbanization on the hydrologic processes of an area include, but are not limited to, increased peak flows and increased flow velocities during rainfall events. This can result in stream erosion and increased likelihood of flooding. In addition, various pollutants are washed off of impervious surfaces and enter the surrounding waterways degrading the water quality of the area and adversely impacting the local ecosystem (ASCE, 1992). The source of pollutants come from a range of anthropogenic effects including but not limited to: oil and grease from vehicles, nutrients from fertilizers, waste from construction sites, and general trash or floatable debris. In order to alleviate the negative impacts of urbanization on the hydrologic cycle, a variety of stormwater best management practices (BMPs) can be used. These practices typically include detention/retention ponds, wet ponds, constructed wetlands, and sand filters (ASCE, 1992). BMPs are designed to retain stormwater runoff and release the water slowly after the storm event has passed. This helps to decrease the peak flow rates and decrease the likelihood of flooding. In addition, the stormwater quality improves while the water is retained through the settling of particles and infiltration into the ground. More recently, various low impact development (LID) practices have gained popularity and interest in order to improve the adverse impacts of urbanization. LID methods include the use of green roofs, bioretention cells, rain gardens, rain barrels, and porous pavement systems.

The focus of this dissertation and research study deals with one type of porous pavement which is described below.

Field et al. (1982) provide an overview of the advantages and disadvantages of using a completely porous pavement system. Completely porous pavement systems consist of a porous asphalt or porous concrete surface course as well as a porous reservoir base course and subgrade. The goal of porous pavement is to drain all the rainfall runoff into the reservoir base course and then allow the water to slowly infiltrate into the surrounding natural soil. This reduces the peak runoff flow rate and improves the water quality by removing pollutants from the road surface through filtering of sediment particles and the pollutants associated with sediment. In addition, porous pavement removes runoff from the surface which helps to improve driver safety. Less surface runoff reduces the potential for hydroplaning and reduces splash and spray from vehicles, which allows for better visibility. However, there have been concerns with respect to the structural integrity of a completely porous pavement system. In the use of traditional impervious roadways, the subgrade is designed for a specified compaction strength and to remain free of water in order to maintain adequate structural strength. With the use of completely porous pavements, water is allowed to infiltrate into the subgrade. This suggests that the structural strength of the roadway may be adversely impacted during rainfall events.

In an effort to avoid the structural concerns of completely porous pavement systems, a different approach is needed. Recently, many state departments of transportation have begun using only a porous surface course in order to take advantage of the driver safety benefits. A porous asphalt surface course serves as a sacrificial overlay in that it is expected to degrade and be replaced more frequently than conventional pavements with a typical design life of roughly 10 years (TRB, 2009). Void space in the porous asphalt is created by removing the fine aggregate from traditional asphalt mixes and increasing the volume of asphalt binder. This results in a porous matrix of large angular aggregate, on the order of one centimeter (cm) in diameter, held together by asphalt binder. The lack of fine aggregate allows for increased void space between the large aggregates. A porous surface course consists of a porous asphalt layer up to 50 millimeter (mm) thick with roughly 20% effective porosity on top of a conventional impervious hot mix asphalt concrete (HMAC) or Portland cement concrete roadway surface. Conventional roadway surfaces typically have a porosity of less than 5%. During a rainfall event, the water enters the pore space of the surface course and is removed from the surface. Water then flows laterally along the underlying impervious asphalt layer to the roadway shoulder. The water resurfaces at the shoulder where it flows into a ditch or drainage swale running parallel to the road. Figure 1.1 shows a schematic view of a typical porous surface course overlay.

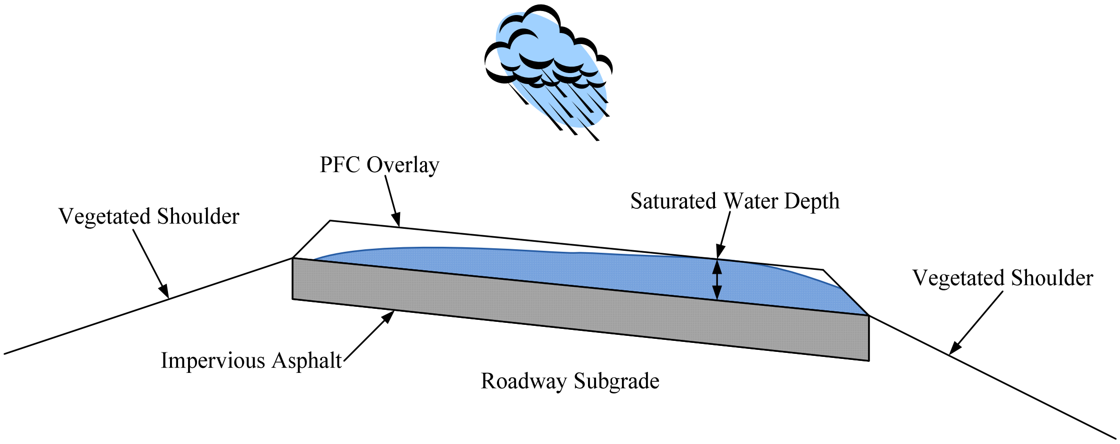

Figure 1.1 – Porous surface course overlay schematic

The decreased surface runoff provides numerous benefits which include better traction and decreased hydroplaning, a reduction of splash and spray from vehicles, increased visibility due to the decreased spray, and decreased light reflection from water on the road surface. These benefits are expected to reduce the number of accidents during rainfall events. Such a porous surface course has also been shown to reduce noise (Bendtsen and Andersen, 2005), increase skid resistance, and improve the quality of stormwater runoff by capturing pollutants in the pore space (Stotz and Krauth, 1994; Berbee et al., 1999; Pagotto et al, 2000; Barrett et al., 2006). In addition, porous surface courses are typically a few degrees cooler than conventional pavements and have been used to combat the urban heat island effect. However, the volume of runoff and peak flow rate are not drastically reduced as in a completely porous pavement system. Conversely, the structural strength of the roadway remains high because water is not allowed to enter the underlying roadway subgrade. The porous surface course system is the focus of this research study. This surface course is typically referred to as a permeable friction course (PFC) or previously referred to as open-graded friction course (OGFC). The PFC asphalt mix design that is being investigated for this research study is described in TxDOT (1993).

The advantages of the use of PFC also come with disadvantages, such as greater initial costs and shorter service life when compared to conventional pavements. The additional initial cost of PFC can be offset due to the improved water quality benefits. In general, a structural BMP is required to clean the stormwater runoff from a new development. The traditional BMPs, such as a sand filter, require the additional cost of land, concrete forms, and piping in order to treat the stormwater runoff, as well as scheduled maintenance. In certain cases, the additional initial cost of PFC is offset because a structural BMP is no longer required. Over time, clogging of the void space occurs due to the trapping of pollutants and suspended solids from the stormwater runoff (Fwa et al., 1999). This clogging is expected to reduce the impacts of the advantages associated with the drainage characteristics of the PFC. Therefore, understanding the hydraulic characteristics of PFC and the impact that clogging has on these characteristics is necessary in order to fully take advantage of the benefits associated with the use of PFC.

Currently, PFC is used primarily on roadways in order to take advantage of its driver safety benefits. PFC is not currently used solely for its benefits associated with improved water quality, although this is an area of on-going research. The Texas Commission on Environmental Quality (TCEQ) recently approved the use of PFC as a new stormwater BMP in the State of Texas on uncurbed roadways with a design speed of 80 kilometers per hour (km/hr) or greater. This allows for designers to utilize the water quality benefits of PFC when planning new projects. In order to take full advantage of the benefits of PFC, we must gain a better understanding of the hydraulic characteristics of the porous asphalt. A review of previous research conducted on PFC documented in the literature is provided in Chapter Two. The hydraulic characteristics of PFC are influenced by its porosity and hydraulic conductivity. It is expected that these two hydraulic characteristics are positively correlated. These parameters are, in general, not constant in space or time. The porosity and hydraulic conductivity of a PFC layer can change along the length and width of the roadway, but in general, we will assume homogeneous characteristics of these parameters. Furthermore, over time the pore space in the PFC can become clogged with sediment resulting in a decrease in porosity, and ultimately an expected decrease in hydraulic conductivity. Therefore, these parameters are not constant in time. Accurate measurement of these hydraulic characteristics is necessary to ensure adequate drainage of surface runoff and maintain the benefits of PFC. Related research is currently being conducted on the water quality improvements from a section of PFC compared to conventional HMAC. The smaller concentration in suspended solids observed in runoff from the PFC surface when compared to a conventional HMAC surface suggest that sediment is trapped in the pore space of the PFC over time. This is expected to result in a decrease in hydraulic conductivity and porosity over time. Being able to measure the in-situ hydraulic conductivity of a PFC layer at any given time is necessary to determine whether too much clogging has occurred and if the drainage benefits will persist for the next rainfall event.

This dissertation and related experimental and numerical research is a portion of the research study “Investigation of Stormwater Quality Improvements Utilizing Permeable Pavement and/or the Porous Friction Course (PFC)” funded by the Texas Department of Transportation (TxDOT) through research project number 0-5220. Researchers at the Center for Research in Water Resources (CRWR) at The University of Texas at Austin have been investigating both the hydraulic characteristics and stormwater quality improvements of PFC over the past several years (beginning in 2004). TxDOT currently uses PFC on several roadways around the City of Austin, as well as various other cities across the state. Creating a well defined methodology for the accurate measurement of the hydraulic characteristics of PFC both in the laboratory and in the field is one objective of the TxDOT research study which will be addressed in this dissertation. A second objective is the development of a numerical model to predict flow within PFC. The majority of this objective is addressed in the dissertation written by Eck (2010). However, the present dissertation will address numerical modeling of the nonlinear flow characteristics which have been observed to occur during hydraulic conductivity testing.

1.2 Research Objectives

This research study defines a methodology for measuring the hydraulic conductivity and porosity of a PFC overlay. PFC core specimens can be extracted from the roadway surface and analyzed in the laboratory to determine hydraulic conductivity and porosity. In addition, a field test can be used to determine the in-situ hydraulic conductivity of the PFC overlay. Hydraulic data collected over the past four years is analyzed to determine the changes in porosity and hydraulic conductivity at three different roadways around Austin, Texas (TX). Obtaining accurate measurements of the hydraulic characteristics and analyzing the change in these characteristics over time gives necessary information as to how the water quality and driver safety benefits of PFC will persist through time, and when maintenance or replacement of the PFC layer is needed. In addition, numerical modeling of the nonlinear flow regime observed in PFC during testing provides a better understanding of how these effects impact the flow of water through PFC. The objectives of this research can be divided into four major categories: evaluate hydraulic properties of PFC in the laboratory, evaluate hydraulic conductivity of PFC in the field, develop a numerical model of the nonlinear head distribution through a PFC core specimen, and analyze the change in hydraulic properties of PFC over time and at different locations.

1.2.1 Evaluate Hydraulic Properties in the Laboratory

The first objective, addressed in Chapter Three, is to evaluate both the hydraulic conductivity and porosity of PFC core specimens. This is accomplished through laboratory testing on the PFC core specimens using a series of constant head tests to determine the hydraulic conductivity, and a submerged unit weight method to determine the porosity. PFC core specimens were extracted from three roadways near Austin, TX (Loop 360, FM 1431, and RR 620) over the past four years (March 2007, February 2008, February 2009, and February 2010). Core specimens were not collected at FM 1431 in 2010 due to recent realignment of the roadway and abandonment of the previous coring location. A methodology for determination of the hydraulic conductivity for two-dimensional flow is described, and data collected from each core specimen is reported. Understanding of the hydraulic properties in a controlled laboratory setting is useful with respect to modeling of flow through the PFC layer for design purposes, such as the required thickness of PFC necessary to avoid surface runoff.

1.2.2 Evaluate Hydraulic Conductivity in the Field

Determination of hydraulic conductivity in the lab can be time consuming and may disturb the core specimen during the extraction process. Therefore, a quick, accurate field method for determination of hydraulic conductivity is necessary. This field test must be non-destructive so that the hydraulic properties of the PFC can be easily measured throughout the life cycle of the overlay. The field test will provide information on the extent of clogging that has occurred, as well as whether or not the benefits of PFC are likely to persist in the near future. Current field testing conducted by TxDOT is not sufficient to determine the hydraulic conductivity of the PFC overlay as mentioned in Section 2.3.2 and described in detail in Section 4.1. The second objective, addressed in Chapter Four, describes the test methodology and a new test apparatus developed at CRWR for determination of in-situ hydraulic conductivity using a falling head test. This allows for quick measurement of hydraulic conductivity using the principles established during lab testing for nonlinear flow. This information will help to determine the rate at which clogging occurs since the test can easily be conducted in the field at regular intervals.

1.2.3 Numerical Modeling of Hydraulic Characteristics

The third objective of this research, addressed in Chapter Five, is to develop a finite difference numerical model to analyze the nonlinear flow characteristics through PFC. During both lab and field testing, a nonlinear flow relationship exists between the flow rate and change in head for two-dimensional flow conditions. Therefore, the typical linear Darcy flow that occurs in most porous media is not sufficient to describe flow through PFC under testing conditions. This objective will determine the difference between the typical linear approximation to flow in porous media compared to the nonlinear flow observed in PFC cores. This is of particular interest due to the two-dimensional flow in PFC which has not been analyzed in detail in the past. The initial concern with nonlinear flow is to model the flow conditions that occur during the laboratory core tests used to determine hydraulic conductivity. The results of the numerical model will relate the measureable flow characteristics in the lab and field to the theoretical flow characteristics, which cannot be directly measured in two-dimensional flow, thereby determining a true hydraulic conductivity.

1.2.4 Analyze Hydraulic Properties based on Location and Time

Over time the hydraulic conductivity and porosity are expected to decrease due to the entrapment of sediment in the PFC pore space. The final objective, addressed in Chapter Six, will analyze the laboratory results and determine any statistical differences in the hydraulic properties of the PFC core specimens over time and from each roadway location. This information, together with water quality data collected at a PFC site, will help to determine when water quality benefits are no longer persistent based on changes in hydraulic conductivity. The experimentally obtained coefficients used to describe the nonlinear flow through PFC will be compared to empirical equations presented in the literature. This will help determine which previous work, if any, applies to flow through

PFC. Finally, analysis of the amount of trapped sediment in a PFC core specimen will help to determine if the improved water quality benefits are a result of filtering of the stormwater runoff or simply a decrease in source pollutants from the surface of vehicles due to decreased splash/spray.

1.3 Dissertation Organization

This dissertation describes the details of various testing protocols together with the data collected to date. The details of the numerical modeling techniques are presented as well. Chapter Two provides a review of related literature pertaining to previous research conducted on PFC, and a summary of flow equations through porous media describing both the linear and nonlinear flow relationships. Chapter Three provides the details of the laboratory testing conducted on PFC core specimens both for porosity and hydraulic conductivity measurements. Chapter Four provides the details of the field testing conducted on the PFC overlay for measurement of in-situ hydraulic conductivity. Chapter Five provides the details of the numerical modeling of nonlinear flow through porous media and describes the relationships between the measureable and theoretical coefficients needed to characterize the nonlinear flow properties. Chapter Six presents statistical analysis of the porosity and hydraulic conductivity data to determine any changes in hydraulic properties based on time and location. In addition, the hydraulic characteristics are compared to empirical equations in the literature. Finally, an estimate for the volume of sediment removed from the stormwater runoff and trapped within the PFC overlay is presented. Chapter Seven provides a summary of the research study and conclusions to each of the research objectives.

Chapter Two

Literature Review

A review of previous literature conducted on applicable porous media flow is summarized here. This will cover the typical linear Darcy flow through porous media at low velocity. Next, nonlinear flow at higher velocities is reviewed together with different models with which to characterize nonlinear flow. This includes theoretical development of nonlinear flow, estimation of nonlinear model coefficients, and experimental results for parallel and converging boundaries. Literature pertaining specifically to PFC is also reviewed. This includes the solution of steady state flow equations which model PFC flow as an unconfined aquifer, previous research results on methods for determination of hydraulic conductivity in porous asphalt, and additional literature pertaining to the water quality benefits of PFC. Finally, a short review of other issues addressed in this research is provided as well as how this research will expand the current literature.

2.1 Linear Flow Through Porous Media

Flow through porous media is typically characterized by the linear Darcy's law (Darcy, 1856). This is a well known law used in the field of groundwater, hydrogeology, engineering, and other fields of hydraulics. Virtually any textbook on these subjects will discuss Darcy's law (see for example Bear, 1972; Muskat, 1982; Fetter, 1994; and Charbeneau, 2000; among others). Darcy's law defines a linear relationship between flow rate and hydraulic gradient as given in Equation (2.1):

$$Q = -KIA \qquad (2.1)$$

In Equation (2.1), Q is the volumetric flow rate with units [L^3/T], K is the hydraulic conductivity [L/T], I is the hydraulic gradient [L/L], and A is the cross-sectional area of flow [L^2], where [L] represents units of length and [T] represents time. The negative sign is necessary because water flows from high hydraulic head to low hydraulic head, which is in the negative direction of the hydraulic gradient. The hydraulic conductivity is a measure of the ease with which a fluid flows through the porous medium.

Darcy's law is applicable to flow through most natural porous media systems. However, in general, it is only applicable for laminar flow and/or low velocity flow. The velocity can be found by first looking at the specific discharge, q:

$$q = \frac{Q}{A} = -KI \tag{2.2}$$

In Equation (2.2), q is the specific discharge or Darcy velocity [L/T], which is simply the volumetric flow rate per unit area. The actual fluid velocity through the porous media is greater than the specific discharge. This is due to the fact that the entire area is not available for flow due to the presence of solid material. Therefore, the average fluid velocity can be approximated using the effective porosity, n_e, of the porous media:

$$v = \frac{q}{n_e} \tag{2.3}$$

In Equation (2.3), v is the average fluid velocity [L/T] and n_e is the effective porosity of the porous media. The value of n_e is always less than unity, and for typical PFC overlays the effective porosity is approximately 0.2 or 20%.

The hydraulic gradient, I, is the change in hydraulic head with respect to each direction. Therefore, Darcy's law is actually a vector equation for multiple directions of flow. The hydraulic head is related to the elevation head, pressure head, and velocity head of the fluid. In most cases, the velocity head is relatively small and assumed to be equal to zero:

$$h = z + \frac{p}{\rho g} \tag{2.4}$$

Equation (2.4) defines the hydraulic head h [L] as the summation of the elevation head z [L] and pressure head, where p is the fluid pressure [M/L/T^2], ρ is the fluid density [M/L^3], g is the gravitational acceleration constant [L/T^2], where [M] represents units of mass. The hydraulic gradient is equal to the spatial change in hydraulic head. In Cartesian coordinates this is represented as:

$$I_x = \frac{\partial h}{\partial x},\ I_y = \frac{\partial h}{\partial y},\ \text{and}\ I_z = \frac{\partial h}{\partial z} \tag{2.5}$$

Equation (2.5) gives the hydraulic gradient in the *x*-, *y*-, and *z*-directions. Similarly, the hydraulic gradient can be given in two-dimensional cylindrical coordinates as:

$$I_r = \frac{\partial h}{\partial r}\ \text{and}\ I_z = \frac{\partial h}{\partial z} \tag{2.6}$$

Where *r* is the radial direction and *z* is the vertical direction. The third dimension in cylindrical coordinates is the θ-direction. However, for the purposes of this research study, there is no flow in the θ-direction.

The hydraulic conductivity *K* represents the ease with which water flows through the porous media and depends on both the fluid properties and porous media properties. The intrinsic permeability, given the symbol *k*, depends solely on the porous media properties and is related to the hydraulic conductivity as follows:

$$K = \frac{\rho g}{\mu} k \tag{2.7}$$

In Equation (2.7), μ is the fluid dynamic (absolute) viscosity [M/L/T] and *k* is the intrinsic permeability of the porous medium [L^2]. If *k* is known for a given porous medium, then the hydraulic conductivity can be calculated for any fluid properties. However, for this research study, we are only concerned with water as the fluid, so use of the intrinsic permeability is not necessary during testing. The intrinsic permeability can be estimated based on properties of the porous media such as porosity or grain size through various empirical equations. The following equation for *k* is calculated for the mean grain diameter d_{50} (Charbeneau, 2000):

$$k = \frac{{d_{50}}^2}{360} \tag{2.8}$$

In general, *k* can be represented by some appropriate length squared, divided by an empirically determined constant (Bear, 1972).

Since Darcy's law is actually a vector equation, the hydraulic conductivity is a tensor quantity for each direction. Therefore, in an anisotropic case, *K* will have a different value for each direction. However, for the purposes of this research, it is assumed that the hydraulic conductivity of PFC is isotropic, which results in K being a constant in space with only one value.

Finally, it should be noted that although the hydraulic conductivity is a constant when Darcy's law is applicable, the hydraulic conductivity represents the relationship between specific discharge and hydraulic gradient as the specific discharge approaches zero. This means that the hydraulic conductivity is the slope of the relationship between specific discharge and hydraulic gradient at zero. This is an important distinction necessary for nonlinear flow. We shall refer to the hydraulic conductivity as the specific discharge approaches zero as the "true hydraulic conductivity". In nonlinear flow, we can consider an "effective hydraulic conductivity," which is not a constant and changes as a function of the hydraulic gradient. This concept will be introduced in Chapter Five.

2.2 Nonlinear Flow Through Porous Media

The phenomenon of a nonlinear flow regime has been observed in numerous porous media experiments in the past. A clear understanding as to the cause of deviation from the linear Darcy's law has not been fully achieved. The causes of nonlinear flow have been debated in the literature and will be discussed here briefly. However, before the causes of nonlinear flow are discussed, two models used to characterize the nonlinear flow relationship are described, in addition to the transition between linear and nonlinear flow.

2.2.1 Forchheimer Equation

One of the most common equations used to characterize nonlinear flow is the Forchheimer equation (c.f. Reynolds, 1900; Forchheimer, 1901; Bear, 1972; and Charbeneau, 2000). Numerous attempts have been made to derive the Forchheimer equation and a discussion of these efforts is provided in Section 2.2.5. The Forchheimer equation relates the hydraulic gradient as a nonlinear function of specific discharge:

$$I = aq + bq^2 \tag{2.9}$$

In Equation (2.9), I is the hydraulic gradient and q is the specific discharge as defined above; the negative sign has been omitted for simplicity, but it is understood that the direction of flow is opposite the direction of increasing head. a [T/L] is the linear Forchheimer coefficient and b [T^2/L^2] is the nonlinear Forchheimer coefficient.

In the case of linear Darcy flow, $b = 0$ and $a = 1/K$. Therefore, at small specific discharge or low velocity, the q^2 term will be negligible and Darcy's law will be a good approximation to the Forchheimer equation. In this case, the hydraulic conductivity is equal to $1/a$, which is the slope of the nonlinear relationship as the specific discharge approaches zero. This agrees with our definition of "true hydraulic conductivity" given in Section 2.1. Interestingly, in the original writings of Darcy (1856), previous work cited by de Prony uses a very similar form of the Forchheimer equation to describe pipe flow. Although this equation was not applied to nonlinear flow in porous media, it is important to note its use prior to its application in porous media flow by Forchheimer.

The Forchheimer equation can also be represented in the following transformed form:

$$I = \frac{q}{K}\left(1 + \frac{q}{n}\right) \tag{2.10}$$

Equation (2.10) gives the Forchheimer equation as a function of the hydraulic conductivity K and transformed nonlinear Forchheimer coefficient n [L/T], where n is related to the previously described Forchheimer coefficients using the following relation:

$$n = \frac{a}{b} \tag{2.11}$$

This form of the Forchheimer equation is useful because if the value of n is known, then the ratio q/n can be compared to a value of one to determine if the nonlinear effects are significant for a given specific discharge.

In most cases in the literature, the Forchheimer equation is applied only to one-dimensional flow. However, in general it is applicable in multiple dimensions as a vector equation. The quadratic term creates some difficulty in representing the Forchheimer equation as a vector equation. Therefore, many researchers (Giorgi, 1997; Ewing et al., 1999; Moutsopoulos and Tsihrintzis, 2005; among others) have proposed the following representation of the vector Forchheimer equation in Cartesian coordinates:

$$\vec{I} = a\vec{q} + b\left|q\right|\vec{q} \tag{2.12}$$

In this case, the quadratic term is simply the magnitude of the specific discharge vector times the directional specific discharge vector. This allows both *a* and *b* to be tensor quantities for the anisotropic case. Wang et al. (1999) investigate numerical simulations of a model porous medium for the Forchheimer equation in three-dimensional Cartesian coordinates. They found that the tensor for both the linear and nonlinear coefficients can be represented as a diagonal matrix with two of the three values being the same magnitude. Therefore, they were only able to simulate two-dimensional anisotropic conditions. For the assumption of isotropic conditions, both *a* and *b* are constant scalars. In cylindrical coordinates, the vector Forchheimer equation is more complex and will be discussed in Chapter Five as used for the purposes of this research study.

The Forchheimer equation can also be expressed based on a pressure gradient instead of a hydraulic gradient. The pressure is related to the hydraulic head by $p = \rho g h$. Taking the gradient of the pressure term and relating it to the Forchheimer equation gives the following one-dimensional Forchheimer equation based on pressure:

$$-\frac{dp}{dx} = \frac{\mu q}{k} + b^{*}\rho q^{2} \tag{2.13}$$

In Equation (2.13), b^{*} has dimensions [1/L] and the Forchheimer coefficients can be related to the Forchheimer equation based on hydraulic gradient as follows:

$$a = \frac{\mu}{\rho g k} = \frac{1}{K} \text{ and } b = \frac{b^{*}}{g} \tag{2.14}$$

This form of the Forchheimer equation is useful when measuring the fluid pressure and also for determining the transition to nonlinear flow, as described in Section 2.2.3.

The linear Forchheimer coefficient, *a*, depends on both the properties of the porous media as well as the properties of the fluid. As expected, this is similar to the properties which are known to influence the hydraulic conductivity. The nonlinear

Forchheimer coefficient, b, depends only on the properties of the porous medium. It is related to the inertial forces which depend on the pore geometry of the porous medium.

2.2.2 Izbash Equation

The Izbash equation is another common equation used to describe the nonlinear flow relationship for high velocity (Izbash, 1931; Bordier and Zimmer, 2000). Also known as the power law, the Izbash equation is an empirical equation for which no formal derivation has been provided. The Izbash equation is as follows:

$$q = KI^{m} \tag{2.15}$$

In Equation (2.15), the specific discharge is represented as a power function of the hydraulic gradient with power m. For low velocity laminar flow, Darcy's law applies and $m = 1.0$. For fully turbulent flow $m = 0.5$. In most nonlinear flow cases, m has a value between 1.0 and 0.5. Clearly, if the Izbash equation is solved for the hydraulic gradient in the turbulent flow case, the hydraulic gradient is related to the specific discharge squared, as in the Forchheimer equation. Use of the Izbash equation is not directly considered in this research study. However, several previous research studies use this equation instead of the Forchheimer equation.

Although the Izbash equation can be shown to fit experimental data for nonlinear flow quite well, there is no theoretical derivation of the Izbash equation from first principles (i.e. conservation of mass and momentum). Therefore, the use of the Izbash equation is not an ideal situation. Furthermore, the Izbash equation assumes nonlinear flow for all values of specific discharge. As the specific discharge approaches zero, the Forchheimer equation approaches the linear Darcy's law relationship better than the Izbash equation. For these reasons, the Forchheimer equation is used in this research study.

2.2.3 Transition to Nonlinear Flow

The nonlinear flow relationship occurs for high velocity flows, but the transition to this nonlinear flow relationship is not well defined. Nonlinear flow occurs as a result of increased inertial forces, which are negligible for linear laminar flow conditions. Laminar flow may exist in many of the flow conduits of the porous media even if the overall flow is nonlinear. Therefore, nonlinear flow is not necessarily a result of fluid turbulence in the porous media but simply an increase in inertial effects which can no longer be neglected. Many researchers have attempted to provide a guideline as to when the onset of nonlinear flow occurs based on characteristics of the flow. The most common transition point is based on the value of the Reynolds number.

$$\mathrm{Re} = \frac{\rho q d}{\mu} \tag{2.16}$$

Equation (2.16) defines the Reynolds number Re as a function of the specific discharge, the fluid properties, and a characteristic length dimension, d. The Reynolds number is a nondimensional number that relates the ratio of microscopic inertial forces to viscous forces. In pipe flow, the Reynolds number can be used to determine the transition between laminar and turbulent flow based on the pipe diameter. However, in porous media flow, there is no uniform length dimension for which to characterize the flow due to the multiple flow paths, particle size distribution, etc. associated with the porous medium.

A common choice for the length dimension is to use some representative grain diameter size. The diameter of the grains in porous media is related to the size of the flow channels between the grains. Therefore, the mean grain diameter, d_{50}, is expected to represent the average flow channel diameter and will be used in this research study. In addition, a smaller grain size, d_{10}, is sometimes used and represents the smallest 10% of particle diameters. The reasoning behind this choice is that the smallest flow channels will govern the flow through the porous media. This suggests that the smallest flow channels will be the ones that restrict the overall flow through the media. Collins (1961) suggests the use of $d = (k/n_e)^{1/2}$, where k is the intrinsic permeability [L^2] and n_e is the porosity. Ward (1964) suggests the use of $d = k^{1/2}$. Therefore, there are many possibilities for the length dimension to be used in determining the Reynolds number.

The most common length dimension is to use d_{50} due to the ease with which it can be determined.

It is expected that in coarse grained media, linear flow conditions will exist for a Reynolds number less than some value between 1 and 10, when the Reynolds number is calculated based on the mean grain diameter, d_{50} (Bear, 1972). Laminar flow typically still exists until Re = 100 or larger, but a nonlinear flow relationship occurs prior to the onset of turbulence. This nonlinear relationship results either due to the flow properties or the material properties. The flow properties that produce nonlinear flow are a large specific discharge or hydraulic gradient. The material properties that create nonlinear flow are a large porosity or hydraulic conductivity (Sen, 1990). More specifically, the nonlinear relationship arises due to either large microscopic inertial forces or microscopic interfacial drag (viscous) forces (Hassanizadeh and Gray, 1987).

The use of the Reynolds number as an indicator for the presence of inertial effects, which result in nonlinear flow, has been debated in the literature. The reasoning behind this debate is that the Reynolds number represents microscopic flow conditions. It can be shown that even when microscopic inertial effects are significant, the macroscopic flow can remain linear, as in Darcy's law, for certain flow conditions. Therefore, Ruth and Ma (1992) suggest the use of a specific Reynolds number which they call the Forchheimer number. The length dimension in the Forchheimer number is equal to $b^* k_0$.

$$Fo = \frac{\rho q b^* k_0}{\mu} \tag{2.17}$$

In Equation (2.17), Fo is the Forchheimer number which is essentially a specific value of the Reynolds number. k_0 is the intrinsic permeability [L^2] as the specific discharge approaches zero. Ruth and Ma (1992) suggest that the intrinsic permeability is velocity dependant and the Forchheimer number can be used to determine if the nonlinear effects are negligible. When the Forchheimer number becomes experimentally significant with respect to a value of one, the nonlinear flow effects can no longer be ignored. The

Forchheimer equation based on pressure as represented by Equation (2.13) can be written in terms of the Forchheimer number as:

$$-\frac{dp}{dx}=\frac{\mu}{k}(1+Fo)q \tag{2.18}$$

From this representation of the Forchheimer equation, it can be seen that when the Forchheimer number becomes significant with respect to a value of one, nonlinear flow conditions will exist. Zeng and Grigg (2006) suggest a critical Forchheimer number for which the nonlinear effects become significant. They define the nonlinear effect, *E*, as the ratio of the pressure gradient consumed in overcoming liquid-solid interactions to the total pressure gradient as:

$$E=\frac{b^{*}\rho q^{2}}{-dp/dx}=\frac{Fo}{1+Fo} \tag{2.19}$$

Equation (2.19) relates the Forchheimer number to the nonlinear effects, *E*. *E* can be associated with the error of ignoring the nonlinear effects. Therefore, Zeng and Grigg (2006) show that if ten percent error is an acceptable limit of the nonlinear effects, the corresponding critical Forchheimer number would be Fo = 0.11. The use of the Forchheimer number, as opposed to the typical Reynolds number, provides a better estimate of when nonlinear effects become significant but requires knowledge of the material properties of the porous media.

2.2.4 Estimation of Forchheimer Coefficients

Many researchers have attempted to estimate the two Forchheimer coefficients from either a theoretical standpoint or a purely empirical development from experimental data. Sidiropoulou et al. (2007) provide a review of multiple empirical equations in the literature for estimating the Forchheimer coefficients, *a* and *b*. In addition, Li and Engler (2001) provide a literature review of empirical correlations for estimating the nonlinear Forchheimer coefficient only. A complete summary of all the equations will not be provided here. In Section 6.5 the numerical results obtained from this study will be compared with several empirical equations for estimating the Forchheimer coefficients. At this point, the empirical equations will be presented and briefly discussed. The typical factors used in many of these empirical equations are the fluid properties, porosity of the porous medium, and particle diameter of the porous medium. The majority of these empirical equations are based on laboratory experiments. Kelkar (2000) estimates the nonlinear coefficient for observations in the field and determined that the nonlinear coefficient is significantly greater when measured in the field compared to lab measurements. This claim is based on gas flow to a well and does not agree with the experimental data obtained in this research study and presented in Section 5.5.

There are several important empirical equations that will be discussed here due to their common reference in the literature. Ergun (1952) was among the first researchers to thoroughly investigate nonlinear flow effects through porous media. He claims the linear term of the Forchheimer equation represents viscous energy losses and the nonlinear term represents kinetic energy losses. Ergun expanded on the Kozeny-Carman equation and developed the following equations for the two Forchheimer coefficients:

$$a = \frac{150\mu(1-n_e)^2}{\rho g {n_e}^3 {D_p}^2} \tag{2.20}$$

$$b = \frac{1.75(1-n_e)}{g {n_e}^3 D_p} \tag{2.21}$$

where D_p is the diameter of the particles which make up the porous media. From these relationships, Ergun also derived two friction factors representing the relative viscous energy losses and kinetic energy losses, with respect to the total pressure drop for the flow, as a function of Reynolds number.

Ward (1964) conducted a dimensional analysis for nonlinear flow and determined the following empirical Forchheimer coefficients:

$$a = \frac{360\mu}{\rho g {D_p}^2} \tag{2.22}$$

$$b = \frac{10.44}{g D_p} \tag{2.23}$$

Ward uses the square root of intrinsic permeability as a length scale, where the intrinsic permeability is given in Equation (2.8). This length scale is used to define the Reynolds number:

$$\mathrm{Re}_k = \frac{\rho q \sqrt{k}}{\mu} \tag{2.24}$$

The symbol Re_k in Equation (2.24) means the Reynolds number is determined from the intrinsic permeability. Similar to Ergun, Ward determined a dimensionless friction factor as a function of Reynolds number for the porous media. The general friction factor is given as:

$$f_k = \frac{1}{\mathrm{Re}_k} + c_w \tag{2.25}$$

In Equation (2.25), f_k is the friction factor, and c_w is a constant that is a function of the porous media. For the porous media Ward conducted experiments on, he found c_w = 0.550. Ward also showed that at low values of Re_k where Darcy's law applies, $c_w = 0.0$ resulting in a linear relationship between f_k and Re_k on a log-log plot. As Re_k increases at the onset of nonlinear flow, a transition occurs and the full Equation (2.25) applies. Finally, at large Re_k, the friction factor is a constant equal to c_w. This type of graph is similar to the common Moody diagram for friction losses in pipe flow. Many subsequent research studies have referenced the work of Ergun and Ward and expanded on these models.

2.2.5 Causes of Nonlinear Flow

Darcy's law describes the specific discharge as a linear function of the hydraulic gradient given in Equation (2.2). This equation is only applicable for laminar flow at low velocities. Initially, it was thought that the onset of turbulent flow within the flow channels of a porous medium caused a deviation from Darcy's law. However, Hassanizadeh and Gray (1987) point out that deviations from Darcy's law are not caused by turbulence, as experimental data have shown nonlinear flow to occur for a Reynolds number near 10. Turbulence does not occur until the Reynolds number approaches a value of 300, suggesting that turbulence does not exist at the onset of nonlinear flow. Ergun (1952) states that pressure losses (or hydraulic head losses) are caused by kinetic energy losses and viscous energy losses. In linear flow, the kinetic energy losses are negligible and Darcy's law is applicable for low velocity where laminar flow typically occurs. Ward (1964) pointed out that there is no sharp division between laminar, transition, and turbulent flows in porous media due to the varying sizes of the flow channels. If turbulent flow occurs in some parts of the media, laminar flow may still exist in other parts of the porous media. In general, deviations from Darcy's law are typically attributed to increased microscopic inertial forces.

When investigating the causes of nonlinear flow, it is important to differentiate between the microscopic flow conditions and the macroscopic flow conditions. This distinction has been the focus of many developments in the literature which have attempted to derive the Forchheimer equation starting from the Navier-Stokes equations for conservation of momentum. Irmay (1958) was among the first to attempt a derivation of the Forchheimer equation from the Navier-Stokes equations for a model of spheres representing a homogeneous isotropic porous medium. Hassanizadeh and Gray (1987) suggest there are three possible mechanisms which cause nonlinear flow: turbulence, microscopic inertial forces, and increased microscopic drag or viscous forces. As previously mentioned, they rule out turbulence based on the value of the Reynolds number. By using an averaging technique on the Navier-Stokes equations, they conclude that the growth of microscopic viscous forces, or drag forces, on the pore walls at high velocity give rise to the nonlinear effects observed at the macroscopic scale. Ruth and Ma (1992) investigate the momentum equation at the microscopic scale and use an averaging theorem to obtain a macroscopic equation. They suggest that "as the Reynolds number is increased, inertial effects lead to secondary flow patterns" which cause circulation as the fluid flows past a particle. This secondary flow pattern is then dissipated due to viscosity. Ruth and Ma (1992) suggest that this viscous dissipation leads to a nonlinear increase in the pressure drop observed on the macroscopic scale and is a function of the Reynolds number. Ma and Ruth (1993) expand on the previous work and show that the microscopic inertial forces lead to a distorted velocity and pressure field which results in the onset of nonlinear flow effects. They go on to suggest that at high Reynolds number, both the inertial forces and viscous forces contribute equally to balancing the pressure gradient of the fluid.

Various other methods at deriving the Forchheimer equation have been attempted aside from averaging the Navier-Stokes equations. Giorgi (1997) attempts to derive the Forchheimer equation using the method of matched asymptotic expansions. The Forchheimer equation is constructed by using a permeability tensor which is a function of the fluid velocity and retaining the first two terms of the expansion, thereby deriving the quadratic term in the Forchheimer equation. Thauvin and Mohanty (1998) created a numerical model of a porous media network that allowed them to change various properties of the media such as porosity, tortuosity, pore size, pore throat radius, etc. and determine how those changes impact the Forchheimer coefficients. They then used regression to develop empirical equations useful for predicting the Forchheimer coefficients and compared those values with other equations in the literature. One finding of Thauvin and Mohanty (1998) relevant to PFC is the relationships they found for a decrease in pore size. As PFC becomes clogged with sediment it is expected that the pore size is decreasing. Thauvin and Mohanty (1998) showed that a decrease in pore size results in a decrease in porosity and permeability, and an increase in the nonlinear Forchheimer coefficient. Chen et al. (2001) use a homogenization method to derive the Forchheimer equation. In summary, the Forchheimer equation has been derived using various approaches, methods, and taking advantage of a range of approximations. There still appears to be a debate as to the actual causes of the deviation from Darcy’s law, but it is generally believed that increased inertial forces result in nonlinear flow. Finally, in general, there is very little literature available which derives the Izbash equation for modeling nonlinear flow from a theoretical standpoint. Therefore, the Forchheimer equation is preferred over the Izbash equation as a better representation of nonlinear flow.

2.2.6 Nonlinear Flow Solution in a Confined Aquifer

For this research study, many of the flow equations are presented in cylindrical coordinates to match the experimental laboratory setup. The majority of the literature describing nonlinear flow in a radial direction is related to groundwater wells in confined aquifers. Bear (1979) gives a steady state solution for Forchheimer flow in a confined aquifer around a discharge well. The solution gives the head profile at any radial distance r from the well. The radius of the well is R_w and the thickness of the aquifer is a constant t_a:

$$h(R_w) - h(r) = a\frac{Q}{2\pi t_a}\ln\left(\frac{r}{R_w}\right) + b\left(\frac{Q}{2\pi t_a}\right)^2\left(\frac{1}{R_w} - \frac{1}{r}\right) \qquad (2.26)$$

Therefore, the purely radial condition of Forchheimer flow in a confined aquifer has been solved, but no literature is available on a combination of radial and vertical Forchheimer flow or for an unconfined aquifer.

The previous derivation of the radial Forchheimer flow assumes steady state conditions. This assumption is not always applicable, resulting in the need for a transient solution. A transient solution has been developed for Darcy radial flow in a confined aquifer as described by the Theis equation (Theis, 1935). This equation relates the drawdown (change in head) to the Theis well function, which is a function of time. The Theis equation describes the development of the drawdown cone that results due to pumping as a function of time and radial distance for a linear flow relationship.

For nonlinear flow, an exact analytic solution for transient Forchheimer flow does not currently exist. However, some approximate transient solutions have been attempted by Sen (1988), Wu (2002), and Mathias et al. (2008) for radial Forchheimer flow to a well in a confined aquifer. Sen (1988) developed a transient solution similar to the Theis equation for linear flow applied to a well with a zero radius. A similarity solution was found through the use of the Boltzmann transformation, which results in a Bernoulli differential equation. However, it should be noted that Camacho-V. and Vasquez-C. (1992) suggest this transformation only applies to the linear flow case and is not valid for the nonlinear flow case. Sen (1992) replied to this comment and suggests that the transformation is valid but depends on the nonlinear Forchheimer coefficient. In either case, the solution by Sen (1988) consists of a modified well function that changes with time and with the nonlinear Forchheimer coefficient, *b*. For $b = 0$, the modified well function becomes the Theis well function for linear Darcy flow. It was shown that the drawdown for nonlinear flow increases more rapidly during a certain time interval when compared to the linear flow drawdown. When compared to the linear flow case, near the well location, the drawdown is always smaller for nonlinear flow, but farther away from the well, the drawdown is greater for nonlinear flow (Sen, 1987). Sen (1990) expanded on this original model and applied it to a well with a finite radius.

Wu (2002) uses the Warren-Root model, which treats fracture and matrix flow interactions using a double-porosity concept. Mathias et al. (2008) present a set of approximate solutions which include: a large time approximation derived from matched asymptotic expansions, a Laplace transform approximation for significant well-bore storage in turbulent flow, and a simple heuristic function for when the flow is very turbulent and the well radius is infinitesimally small. These approximations are then compared to equivalent finite difference solutions. The developments are useful in comparing the nonlinear transient flow conditions to the linear transient flow conditions. However, they only exist for the radial flow conditions observed in a confined aquifer.

2.2.7 Nonlinear Flow Investigation of Converging Boundaries

The experimental laboratory test setup used in this research study involves two-dimensional radial flow. Therefore, the flow paths will be diverging as flow exits the core specimen in the radial direction. Although there is no literature on two-dimensional diverging flows experiencing nonlinear flow conditions, there have been experimental tests in the past for flows with converging boundary conditions. Thiruvengadam and Pradip Kumar (1997) conducted experimental tests on a coarse grain porous media in a test setup with converging boundaries. They determined an exponential expression for the hydraulic gradient under radial flow conditions. The experimental tests, when corrected for porosity and wall effects, matched the theoretical equation for the hydraulic gradient suggesting that the flow can be modeled as radial flow. Venkataraman and Rama Mohan Rao (2000) expanded on the work by Thiruvengadam and Pradip Kumar (1997), and compared nonlinear flow in parallel boundaries to flow in converging boundaries. They mention that in the case of parallel flow, the hydraulic gradient is the same in the direction of flow. However, for converging boundaries, the cross-sectional area decreases in the direction of flow, resulting in a change in velocity, and a subsequent change in hydraulic gradient with the flow. It is typically assumed that the linear Forchheimer coefficient, a, is constant for both parallel boundaries and converging boundaries. However, it is possible that the nonlinear Forchheimer coefficient, b, changes for flows with converging boundaries. Therefore, Venkataraman and Rama Mohan Rao (2000) conducted experimental tests with porous media flow in converging boundaries using the empirical equations developed by Ward (1964) to determine the Forchheimer coefficients. They derived an altered Forchheimer equation for converging boundaries and determined two convergence factors which are useful for converting a and b for converging flow to the corresponding a and b for parallel flow. They determined that both the linear and nonlinear Forchheimer coefficients are, in fact, constants for converging flow when the convergence factor is used. Furthermore, they developed a graph of friction factor (determined empirically from Ward, 1964) versus Reynolds number for the Forchheimer equation which resembles the typical Moody diagram used for pipe flow (c.f. Hwang and Houghtalen, 1996). This graph uses Equations (2.24) and (2.25) determined by Ward (1964). Figure 2.1 shows the results of their experiments for various porous materials with converging boundaries once the Forchheimer coefficients were converted back to those for parallel boundaries. Both Ergun (1952) and Ward (1964) developed a similar graph as shown in Figure 2.1 for a single porous media experiencing parallel flow.

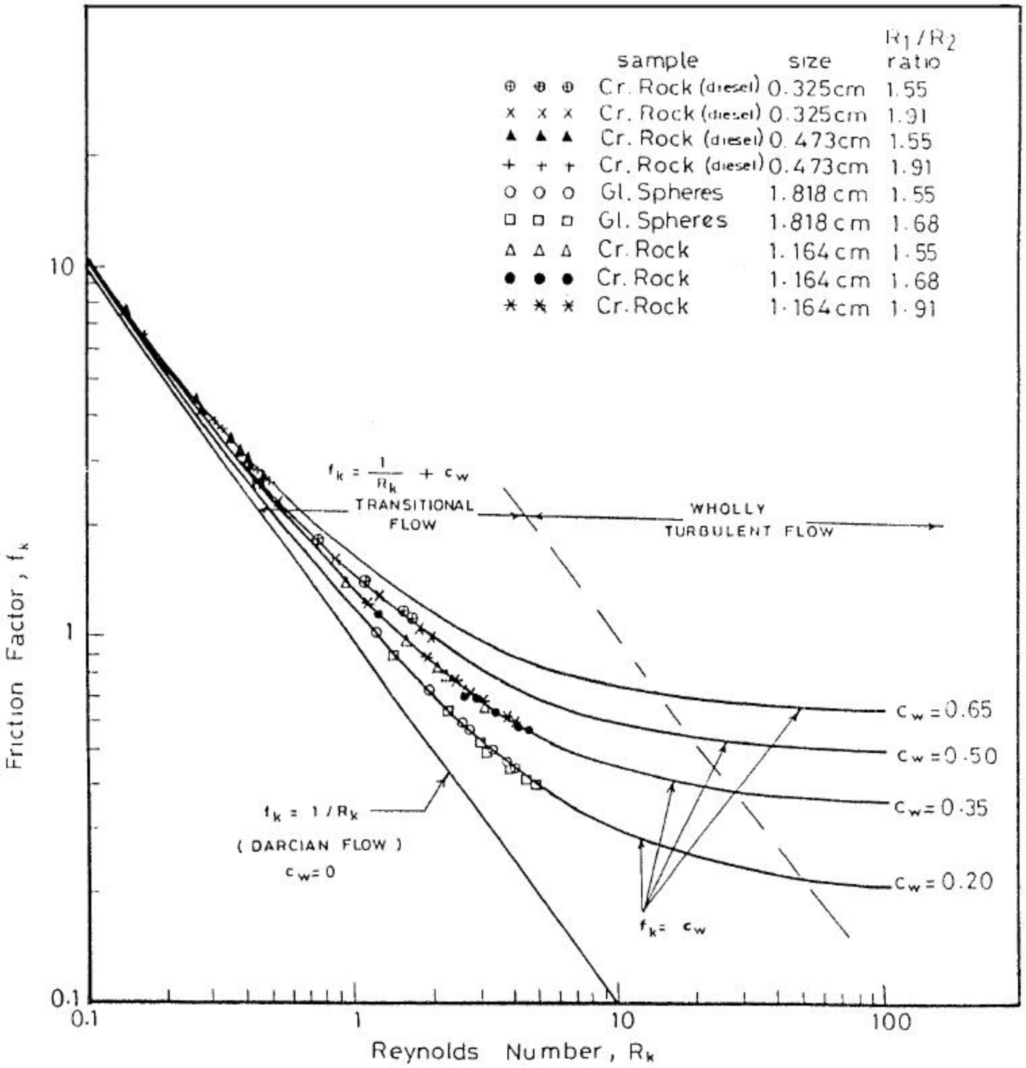

Figure 2.1 – Relationship between friction factor and Reynolds number for nonlinear parallel flow (source: Venkataraman and Rama Mohan Rao, 2000)

A similar relationship for the friction factor versus Reynolds number was previously presented by Venkataraman and Rama Mohan Rao (1998) for nonlinear flow conditions modeled with the Forchheimer equation. In this work, they analyzed experimental data presented in the literature for parallel flow and used the empirical relationships developed by Ward (1964). Reddy and Rama Mohan Rao (2006) continued the work on nonlinear flow with converging boundaries using a slightly different experimental setup. They suggest that the Forchheimer coefficients vary not only along the direction of flow, but also in the radial direction due to convergence. This contradicts the previous findings and Srivastava (2009) provides a discussion on this issue. Srivastava shows that the Forchheimer coefficients do not change because Reddy and Rama Mohan Rao (2006) are using an average hydraulic gradient. Furthermore, if the Forchheimer coefficients do change with the flow, then it would be expected that the hydraulic conductivity of a homogeneous isotropic porous medium changes if the flow is converging or diverging. Therefore, it can be shown that the Forchheimer coefficients are constant for both parallel and converging/diverging flows. This is an important aspect of the current research study since we will be investigating a diverging flow condition.

Goggin et al. (1988) developed a minipermeameter which uses air flow to determine the permeability of rock materials. The device essentially measures the pressure change as gas leaves a standpipe sealed on the rock surface. Flow is assumed to be a combination of vertical and diverging radial flow which is similar to the flow conditions used in this research, as described in Chapter Three. However, the no flow boundary conditions in this research study are not present in the analysis of the minipermeameter. Goggin et al. claim to have solved the Forchheimer equation for this two-dimensional flow problem, but they provide no details of the methods with which the equation is solved. As will be shown in Chapter Five, the solution of the Forchheimer equation in two-dimensions can be problematic and requires special consideration to solve. The problem setup proposed by Goggin et al. (1988) appears to be the most similar solution to what is considered in this research study. However, as mentioned, no information is provided on how this solution was obtained.

2.3 Permeable Friction Course Review

Previous research in the literature has been specifically conducted on PFC. These studies describe the analytic solutions of water depth profiles within a PFC layer, methodology for measuring hydraulic conductivity, and water quality improvements. An overview of additional benefits of porous pavements is provided briefly in Chapter One. These benefits include reduced splash/spray during rainfall events, improved traction, reduced chance of hydroplaning, improved stormwater runoff quality, and noise reduction. A recent report by the Transportation Research Board (TRB, 2009) provides an overview of construction and maintenance practices of PFC as well as the driver safety and environmental benefits of the use of PFC.

2.3.1 Water Depth Solutions

There have been several studies which have modeled flow through PFC under constant rainfall intensity in order to determine the water depth profile within the PFC. These studies have assumed linear flow utilizing Darcy's law and have only addressed one-dimensional flow at steady state. Essentially, the PFC layer can be modeled as an unconfined aquifer on a sloping impervious surface. It is assumed that there are small slopes in the water surface such that the Dupuit-Forchheimer assumptions apply. The Dupuit-Forchheimer assumptions state that the head in the unconfined aquifer is independent of the water depth such that only horizontal flow occurs. In addition, the assumption is made that the discharge is proportional to the slope of the water surface elevation (Charbeneau, 2000). The result of applying the Dupuit-Forchheimer assumptions is to convert the governing partial differential equation for flow to a first order nonlinear ordinary differential equation.

Jackson and Ragan (1974) were among the first to model flow through an entirely porous pavement. They developed numerical solutions to the Dupuit-Forchheimer assumptions which leads to the Boussinesq equation assuming Darcy flow conditions. The use of Darcy's law is only applicable when resistive forces dominate over inertial forces. Jackson and Ragan used an explicit central difference scheme (CDS) finite difference model to solve the Boussinesq equation for a pavement with zero slope in order to determine the effect of underdrain spacing on discharge rates. Yates et al. (1985a) develop an analytic solution for flow down a sloping unconfined aquifer under constant rainfall intensity. The Dupuit-Forchheimer assumptions are applied resulting in a second order nonlinear differential equation. The authors investigate a solution to this equation for two possible cases of boundary conditions. The first case is for a known downstream head and flux boundary, and the second is both a known downstream and upstream head boundary. They also determine the location of a groundwater drainage divide if it exists. Yates et al. (1985b) adds to the previous work by using a finite difference scheme to solve the governing nonlinear differential equation and then making additional assumptions to linearize the governing equation and comparing the results. Loaiciga (2005) solves essentially the same problem as Yates et al. for flow down an unconfined sloping aquifer. However, after applying the Dupuit-Forchheimer assumptions, Loaiciga uses a transformed variable to linearize the equations.

Ranieri (2002) was the first researcher to model water depths specifically within PFC. He developed a runoff model to determine the required PFC thickness necessary to contain the entire runoff within the pore space based on the roadway geometry, rainfall intensity, and PFC hydraulic conductivity. Ranieri starts with the Boussinesq equation and investigates two forms of the solution which essentially correspond to subcritical and supercritical flow conditions, as defined based on the magnitude of the rainfall intensity, hydraulic conductivity, and roadways slope. The theoretical model is validated with a laboratory experiment that simulated rainfall on PFC and measured the water depth within the pore space. Ranieri recognized that the flow regime within the PFC layer is nonlinear, and therefore introduced a factor which is multiplied by the hydraulic conductivity to account for nonlinear flow. The introduction of the factor follows the Lindquist-Kovacs theory which defines multiple flow regimes between laminar and turbulent flow conditions (Kovacs, 1981). The original Lindquist-Kovacs theory multiples the hydraulic conductivity by a factor which is a function of the Reynolds number. The Reynolds number for flow within a PFC layer changes along the flow path due to the continuous addition of water from the rainfall. Therefore, instead of altering the factor along the length of the flow path, Ranieri suggests the use of an empirical factor which depends on the rainfall rate, roadway inclination, and hydraulic conductivity. Ranieri (2007) expands on the earlier work and provides some minor corrections to the original model. A correction is made for the case when the upstream boundary condition is not impervious. In addition, it was recognized that in certain cases there exists a drainage divide within the PFC layer. Finally, the model is solved with a fourth order Runge-Kutta method in order to investigate how changes in roadway slope, rainfall intensity, PFC depth, and other design parameters effect the maximum water depth within the PFC.

Tan et al. (2004) use a commercially available three-dimensional finite element model to determine the effects of various roadway geometries on the drainage performance of PFC for both saturated and unsaturated flow conditions. They consider an anisotropic porous medium and developed design curves to determine the necessary PFC thickness based on longitudinal slope, cross slope, rainfall intensity, and pavement width. Charbeneau and Barrett (2008) provide analytic solutions to the governing equations of flow through PFC. These solutions expand on the previous work by Yates et al. (1985) and Loaiciga (2005) by investigating three ranges of rainfall intensity and a variety of boundary conditions which influence the analytic solutions. In addition, Charbeneau and Barrett address the issue of saturated PFC flow with the addition of overland sheet flow, which is not addressed in the previous works, and suggest a method for determining the spacing of underdrains. Figure 2.2 depicts a typical water depth profile within the PFC layer.

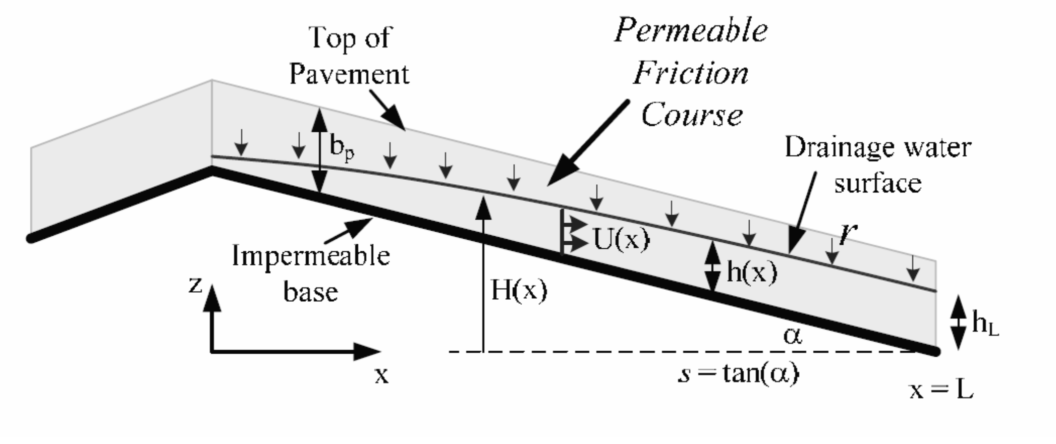

Figure 2.2 – Water depth profile in PFC (source: Charbeneau and Barrett, 2008)

Eck et al. (in press) provide a correction to Charbeneau and Barrett (2008) by addressing the criteria for the onset of surface overland sheet flow. In summary, the majority of the work conducted on water depth solutions within PFC are typically for steady state, constant rainfall conditions, with a known hydraulic conductivity assuming Darcy's law applies. Therefore, since the hydraulic conductivity is one of the major influencing factors for these models, accurate measurement of the hydraulic conductivity is needed.

2.3.2 Hydraulic Conductivity Measurements

Previous studies have been conducted on methods to measure the hydraulic conductivity of porous asphalt mixes. Tan et al. (1997) describe a falling head test to measure the one-dimensional hydraulic conductivity under a nonlinear flow relationship. They use a pressure transducer to measure the water depth as it falls through a porous asphalt sample which is formed to fit the test apparatus. The nonlinear flow conditions are modeled from the Izbash equation and a one-dimensional hydraulic conductivity is measured. Fwa et al. (1998) investigate additional materials as well as measure both horizontal and vertical hydraulic conductivity. The resulting hydraulic conductivity in both directions are very similar, suggesting the media they tested is isotropic. Tan et al. (1999) develop an automatic field permeameter utilizing a falling head test to determine the three-dimensional hydraulic conductivity. The three-dimensional hydraulic conductivity is then converted to an effective isotropic hydraulic conductivity using a correction factor based on the wetted zone of the PFC during testing as determined from a commercially available finite element model. However, this finite element model does not account for surface runoff which is observed during field testing as a result of improper modeling of the underlying impervious boundary. One-dimensional laboratory tests were then conducted in order to determine the anisotropy of the porous asphalt by comparing to the effective isotropic hydraulic conductivity. The anisotropy ratio of horizontal to vertical hydraulic conductivity is reported to range from 1.1 to 2.5 for various porous asphalt mix designs. Fwa et al. (2001a) provide results for in-situ hydraulic conductivity using their automatic field permeameter and found a range in hydraulic conductivity from 0.5 centimeters per second (cm/s) to 4.5 cm/s. These studies all utilize the Izbash equation for nonlinear flow and do not directly measure the hydraulic gradient for three-dimensional flow conditions. In order to solve this problem, they use a finite element model which does not accurately simulate the flow conditions observed due to the lack of surface runoff.

Clogging of the porous asphalt with sediment from stormwater runoff is expected to decrease the hydraulic conductivity over time. Therefore, Fwa et al. (1999) define a test methodology to compare the relative clogging potential of multiple porous media mix designs. Tan et al. (2000) improve on this test procedure and compare the clogging results to the theoretical Giroud model developed for sediment retention and clogging of geotextile fibers. The theoretical model defines the hydraulic conductivity as a function of the mass of sediment trapped for a given thickness of porous media. Tan et al. (2003) compare the experimentally determined decrease in hydraulic conductivity to the theoretical Kozeny-Carmen equation and introduce an empirical constant which can be used to characterize the clogging potential of the porous medium. In order to combine all the work on measurement of hydraulic conductivity and clogging potential of porous asphalt, Fwa et al. (2001b) present a rational method for designing a porous pavement drainage layer. Chai et al. (2004) incorporate this methodology and simulate flow conditions on a porous pavement for both short-term and long-term urban drainage control using a finite element model for both saturated and unsaturated porous media flow.

There are several documented testing devices used in the field to estimate the relative drainage capacity of a porous asphalt surface course. The method described by Tan et al. (2002) provides the best estimate of hydraulic conductivity. However, as previously mentioned, this method uses the Izbash equation and assumes a three-dimensional permeability based on a finite element method, which does not account for surface runoff. This device has a standpipe radius of 7.5 cm centered on a base plate with a radius of 25 cm. In addition, there are several other devices currently being used which estimate drainage capacity but do not give any indication of the actual hydraulic conductivity that is necessary for modeling flow through PFC. Isenring et al. (1990) describe a field test developed by the Institute for Transportation, Traffic, Highway and Railway Engineering (IVT) of the Switzerland Institute of Technology called the IVT permeameter. The IVT permeameter is essentially a vertical pipe which is placed on the porous asphalt surface and sealed with putty at the base. A falling head test is conducted and the drainage capacity is expressed as the time needed to drain 2.27 liters (L) of water through the PFC. A similar test procedure described in TxDOT (2004a) is used in the State of Texas. The drainage capacity is reported as the time to drain 5.1 L of water. Van Heystraeten and Moraux (1990) investigate porous asphalt in Belgium and show an outflow meter used to measure in-situ drainage capacity. Although they give little information on this device, it appears to work as a double-ring infiltrometer. Finally, in the State of California, drainage capacity is determined by creating a circular trough in the surface of the porous asphalt and expressing drainage capacity as the time needed for water to flow out of the trough (see Caltrans, 2004). Although there are a variety of testing procedures currently being used, none of these give an actual estimate of the hydraulic conductivity of the porous asphalt. These methods are best suited during construction when the porous asphalt is being compacted. After each pass of the compaction vehicle, the falling head test can be easily conducted. Once the drainage capacity reaches a specified level, compaction of the layer is complete and construction of the PFC layer is finished. Although useful during the construction process, these methods provide no useful information for modeling of flow through PFC for design or maintenance purposes.

2.3.3 Water Quality Benefits

The use of porous pavements has been shown to decrease the concentration of multiple contaminants typically found in stormwater runoff. Although the pollutant removal process has not been determined, it is generally thought that the porous pavement either acts as a filter to remove pollutants, or rather pollutants are simply not washed off vehicles due to the reduction in splash/spray on the roadway. Stotz and

Krauth (1994) were among the first to document the water quality benefits of porous asphalt. They monitored a porous asphalt overlay in Germany for one year and compared pollutant loadings to those from a nearby impervious roadway. It was shown that there was a reduction in filterable solids by approximately 50% when comparing porous asphalt to the impervious roadway. Ranchet (1995) studied porous asphalt overlays in France with impervious stone-matrix roads and found the greatest pollutant reductions were for zinc, copper, and hydrocarbons. Berbee et al. (1999) monitored both impervious and porous asphalt surfaces in the Netherlands and found significant pollutant reductions for lead, copper, zinc, and suspended solids. A similar study by Pagotto et al. (2000) in France showed a reduction in suspended solids and heavy metals when comparing impervious roadways to porous asphalt roadways. Barrett et al. (2006) investigate the pollutant concentrations from an impervious roadway to those from the same roadway after it is overlain with a layer of PFC in the State of Texas. Pollutant removal is then compared to removal from a vegetated buffer strip. Barrett and Shaw (2007) report an additional years worth of data to these findings. Stanard et al. (2008) provide a more in-depth description of the monitoring site as well as updated results. Stanard (2008) and Frasier (2009) also present details on the construction of multiple monitoring sites and provide the water quality data to support the use of PFC as a stormwater BMP in the State of Texas.

2.4 Hydraulic Characteristics of Conventional Pavements

A quick review of literature on conventional impervious pavements is useful to get an idea of the relative magnitude of values for hydraulic characteristics of various pavements types. Masad et al. (1999) investigate methods for determining the porosity of conventional impervious asphalt mix designs. Multiple porosity measurement methods were used, including the specific gravity (submerged unit weight) method, optical image analysis method, and x-ray tomography analysis method. All three methods compared favorably. Porosity measurements on PFC core specimens reported in this dissertation will use both the submerged unit weight method and image analysis method. Masad et al. (1999) report a range of porosity in conventional asphalt from 1.5% to 11% depending on the amount of compaction, with most samples having a porosity of less than 3%. Similarly, Krishnan and Rao (2001) report porosity values of 2-3% for conventional asphalts. Therefore, porosity values in PFC are significantly larger than for conventional asphalt.

Comparing values of hydraulic conductivity between conventional asphalt and PFC is also useful. The assumption is made that the underlying conventional pavement surface is impervious when modeling flow through PFC. Masad et al. (2004) report an average hydraulic conductivity of up to 5×10^{-3} cm/s. Tarefder et al. (2005) provide a range of hydraulic conductivity values for different conventional asphalt mix designs. Most values are on the order of 10^{-5} cm/s. Hassan et al. (2008) report hydraulic conductivity values for conventional hot mix asphalt on the order of 10^{-6} cm/s. Finally, Wiles and Sharp (2008) investigate what they call the secondary permeability of impervious cover. This refers to the hydraulic conductivity of cracks, fractures, and construction joints in conventional pavements. They report a range of hydraulic conductivity values from 10^{-3} cm/s to 10^{-6} cm/s. Therefore, the hydraulic conductivity of conventional pavements can range over several orders of magnitude. However, the hydraulic conductivity of PFC will be shown to be on the order of 1 cm/s on average, with a minimum hydraulic conductivity of 0.02 cm/s. Since the average value is multiple orders of magnitude greater than for conventional pavements, the assumption of a completely impervious underlying boundary is sufficient for the purposes of this research study.

2.5 Contribution of Research Study

The research study and results described in this dissertation will help to expand the current understanding and measurement of the hydraulic properties of PFC. This will be accomplished by the development of both a laboratory and field hydraulic conductivity measurement tests. Current methods for measurement of PFC hydraulic conductivity are well defined only for one-dimensional flow. In order to measure the in-situ hydraulic conductivity, a two-dimensional flow test in cylindrical coordinates must be conducted due to the relatively small thickness of the PFC layer (roughly 50 mm). Previous work avoided this complication by attempting to numerically model the flow conditions. However, the results of this model do not accurately represent the flow conditions which occur during a field test.

The use of a two-dimensional measurement test creates additional complications in that the flow paths are diverging. Therefore, the hydraulic gradient and specific discharge of the flow cannot be directly measured for use in the Forchheimer equation. Previous work avoided this problem by calculating an average hydraulic gradient. This research study will instead apply a modified Forchheimer equation for the overall flow conditions in which the hydraulic gradient and specific discharge do not need to be measured. This model is described in Section 3.3.2. The use of the modified Forchheimer equation allows for accurate measurement of the hydraulic characteristics describing the two-dimensional flow through PFC.

In order to properly relate the modified Forchheimer coefficients for the overall flow conditions to the true Forchheimer coefficients, the use of a numerical model is needed. This research study has developed a finite difference numerical model from which a relationship between the modified Forchheimer coefficients and true coefficients is simulated based on the geometry of the test setup. Using this information, we are able to determine the actual hydraulic conductivity of the PFC layer. Previous research has attempted to make approximations when calculating the hydraulic conductivity for two-dimensional flow.

Finally, four years worth of data for the hydraulic properties of PFC have been collected at three different roadways around Austin, TX. Statistical analyses of these data will determine whether the porosity and hydraulic conductivity have changed over time and between each roadway location. Comparison of these potential changes with stormwater quality monitoring data being collected at two of the roadway locations will help to determine when a reduction in hydraulic conductivity will adversely impact the water quality benefits of PFC. This will provide a guideline for when maintenance/cleaning of the PFC layer is required, or possibly when replacement of the PFC layer is needed. Currently, no scientific guidelines exist that demonstrate how to properly maintain a PFC layer.

Chapter Three
Laboratory Experimentation

In order to properly measure the PFC hydraulic conductivity and gain a better understanding of the nonlinear flow properties of PFC, laboratory experimental tests must be conducted. This is accomplished through a series of constant head permeability tests. This chapter describes the extraction process of PFC core specimens which have been tested, and the laboratory methodology for determining core specimen porosity and Forchheimer coefficients.

3.1 PFC Core Specimen Extraction

3.1.1 Coring Process

Laboratory experiments to determine porosity and hydraulic conductivity were conducted on PFC core specimens taken from three roadways around Austin, TX. PFC core specimens can be extracted by saw-cutting the road surface. A typical core specimen consists of the approximately 50 mm thick layer of PFC on the surface together with the underlying thicker impermeable HMAC. Prior to any testing, the layer of HMAC must be removed from the PFC layer. The coring process was organized by Gary Lantrip of TxDOT. Two TxDOT crash trucks were utilized to divert traffic from the travel lane in which the coring was taking place. This helped to avoid traffic accidents and protect the workers during the coring process. Additional details on the coring process are provided by Candaele (2008).

The cylindrical core specimens are extracted by a drill press attached to a truck. The drill press is operated by a subcontractor and is shown in Figure 3.1. During the coring process and removal of the HMAC layer, water is continuously applied to the saw blades in order to reduce any increases in temperature due to cutting friction. Therefore, temperature effects on the asphalt binder material are not expected to be significant. However, the addition of water may have an impact on the transport of fine particles created by the cutting process as well as the fine particles previously trapped in the void space of the PFC. Fine particles can either be washed out of the void space with the water, or can be drawn into the void space due to capillary forces. Visual inspection of the core specimens show that fine particles are washed out of the PFC during the coring processes. This suggests the core specimen has been disturbed and may create error between the core specimens and the in-situ PFC layer. Such disturbances cannot be avoided but are expected to be minor.

Figure 3.1 – Drill press used for core extraction

In March 2007, a total of nine 15.2 cm diameter cores were extracted from north Loop 360, east FM 1431, and north RR 620. Porosity and hydraulic conductivity tests were conducted by Candaele (2008). In February 2008, twelve 20.3 cm diameter PFC core specimens were extracted near the same sites. The change in core diameter was done to determine whether the core size had a significant effect on the resulting porosity or hydraulic conductivity measurements. In February 2009, an additional twelve 20.3 cm diameter cores were extracted. However, for this extraction, cores were taken from south RR 620 roughly 1.6 km away from the previous extraction site. The change in extraction site was made in order to take core specimens near a new stormwater quality monitoring site that had been recently installed. Finally, in February 2010, an additional nine 15.2 cm diameter cores were extracted. Six core specimens were taken from Loop 360 and three cores were taken from south RR 620. No cores were extracted from FM 1431 due to the recent realignment of the road and abandonment of the previous coring location. Figure 3.2 shows a typical 20.3 cm diameter PFC core specimen immediately after extraction.

Figure 3.2 – Extracted PFC core with porous layer and impermeable base

3.1.2 Loop 360 Site

The PFC overlay on Loop 360 was installed in October 2004. The average annual daily traffic count for the year 2005 was 48,000 vehicles per day (CAMPO, 2009). The coring location at Loop 360 is on the northbound lane, north of the intersection with Lakewood Drive. Three cores were extracted from the travel lane in 2007. In 2008, 2009, and 2010, three cores were extracted from the travel lane and an additional three cores were extracted from the roadway shoulder. All cores were extracted just north of the bridge over Bull Creek. Figure 3.3 shows the relative location of the core extraction site, which has a latitude of 30° 22’ 22” North (N) and longitude of 97° 47’ 03” West (W). There are two stormwater quality monitoring sites near this location. Stanard (2008) and Frasier (2009) discuss the water quality results obtained at this location.

Figure 3.3 – Loop 360 core extraction site (courtesy: Google Earth)

3.1.3 FM 1431 Site

The PFC overlay on FM 1431 was installed in February 2004. The average annual daily traffic count for the year 2005 was 18,200 vehicles per day (CAMPO, 2009). The coring location on FM 1431 is on the eastbound lane just east of the intersection with Hur Industrial Boulevard. Three cores were extracted from the travel lane in each of the three study years at this site (2007, 2008, and 2009). As previously mentioned, no cores were extracted in 2010 due to realignment of the roadway and abandonment of the previous coring location. There is no roadway shoulder at this location. Figure 3.4 shows the relative location of the core extraction site, which has a latitude of 30° 31’ 00” N and longitude of 97° 52’ 20” W. The realignment of the roadway under construction can be seen in this figure.

Figure 3.4 – FM 1431 core extraction site (courtesy: Google Earth)

3.1.4 RR 620 Site

The PFC overlay on RR 620 was installed in June 2004. The average annual daily traffic count for the year 2005 was 32,000 vehicles per day (CAMPO, 2009). There are two coring locations on RR 620. The first location is for the cores extracted in 2007 and 2008, on the northbound travel lane just north of the intersection with O’Connor Drive. Figure 3.5 shows the relative location of the first coring site, which has a latitude of 30° 30’ 06” N and longitude of 97° 43’ 12” W. The second location is for the cores extracted in 2009 and 2010. A new stormwater monitoring site was installed near

Cornerwood Drive; therefore, the cores were extracted near this site to gain information on the PFC layer at that location. The second site is roughly 1.6 km south of the first site, and is located just north of the intersection with Cornerwood Drive in the southbound travel lane. Figure 3.6 shows the relative location of the second coring site, which has a latitude of 30° 29’ 18” N and longitude of 97° 43’ 48” W.

Figure 3.5 – First RR 620 core extraction site (courtesy: Google Earth)

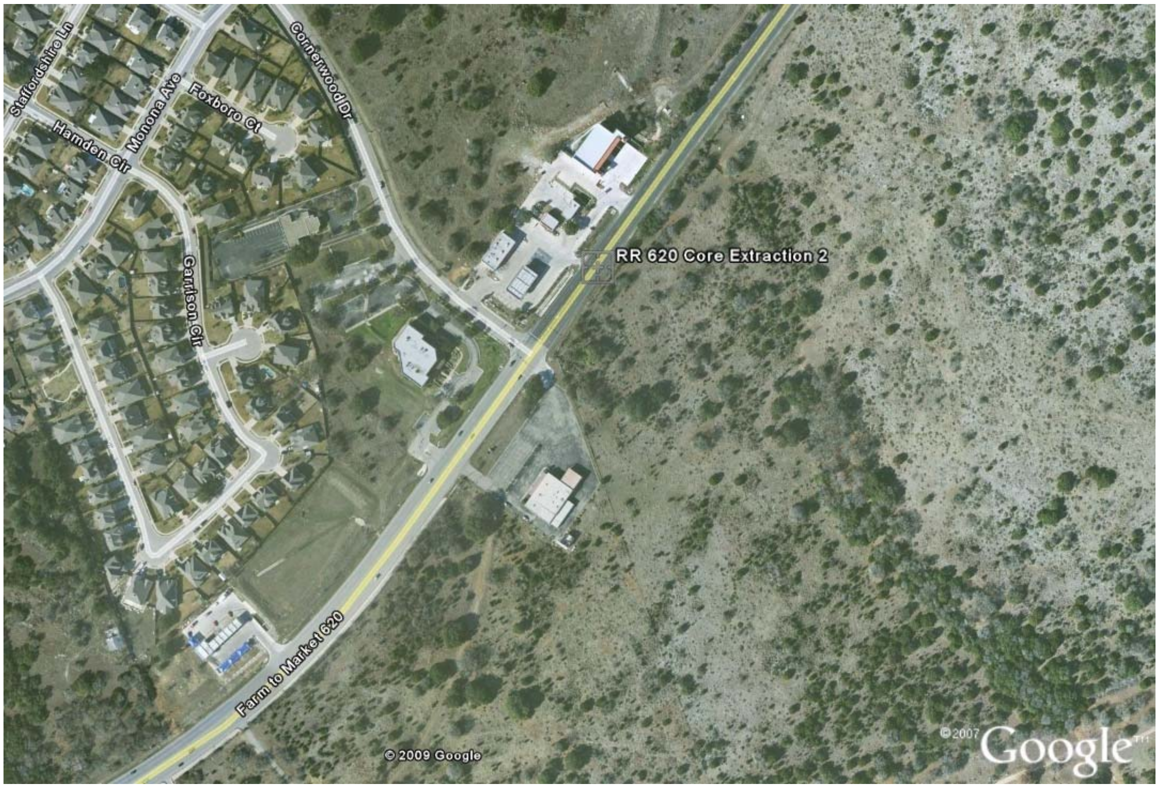

Figure 3.6 – Second RR 620 core extraction site (courtesy: Google Earth)

3.1.5 Core Specimen Naming System

The cores are distinguished from one another by a three character naming system. The first character in the core name corresponds to the site, or roadway, from which the core was extracted. Site 1 corresponds to Loop 360, site 2 is FM 1431, and site 3 is RR 620. The second character refers to the core location along that site. For each site, the core locations are relatively close to each other, and each site had three core locations. For the cores extracted in March 2007, the core locations are given capital letters (A, B, or C); for the cores extracted in February 2008, the core locations are given numbers (1, 2, or 3); for the cores extracted in February 2009, the core locations are given Roman numerals (i, ii, or iii); and for the cores extracted in February 2010, the core locations are given lower case letters (a, b, or c). Finally, the third character in the core name refers to whether that core was extracted from the travel lane (T) or shoulder (S). Only Loop 360 (site 1) has a large enough shoulder from which to extract cores, and only the 2008, 2009, and 2010 cores were taken from both the travel lane and the shoulder. For example, core 2-A-T is a core from FM 1431 (site 2), the first core location (A) which was from the travel lane (T). Since the core location is a letter (A), this is a core extracted in 2007. Core 1-2-S is from Loop 360 (site 1), the second core location (2), from the shoulder (S). Since the core location is a number (2), this is a core extracted in 2008. Core 3-iii-T is from RR 620 (site 3), the third core location (iii), from the travel lane (T). Since the core location is a Roman numeral (iii), this is a core extracted in 2009. Finally, core 1-a-T is from Loop 360 (site 1), the first core location (a), from the travel lane (T) in the year 2010.

3.2 Porosity Measurements

Porosity measurements were conducted at the TxDOT Asphalt Laboratory in Cedar Park, TX. Preparation included cutting the impermeable HMAC base material from the bottom of the core specimen so that the entire core consists of only PFC material. Therefore, the thickness of the core may be slightly less than the actual PFC thickness in-situ. Candaele (2008) determined the porosity for the 2007 cores using a submerged unit weight water displacement method (Regimand and James, 2004) and a destructive image analysis method. Both methods gave very similar results. In the image analysis method, fluorescent epoxy is injected into the pore space of the specimen. The epoxy is allowed to harden and the core is sliced vertically. Each slice is scanned, and computer software is used to count the number of pixels representing the epoxy and the number of pixels representing the PFC aggregate. With these two values, the porosity can be determined. This method is a destructive method and does not allow for further testing on the core specimens. Therefore, the submerged unit weight method is preferred as it is non-destructive. Candaele (2008) gives additional details on each of these methods.

Due to the favorable agreement between porosity values obtained from each method for the first set of cores, only the submerged unit weight method was used for the subsequent core specimens. There are several steps necessary to determine the porosity from the submerged unit weight method. Once the impermeable base is removed from the specimen, the PFC core is vacuum sealed in a plastic bag as shown in Figure 3.7.

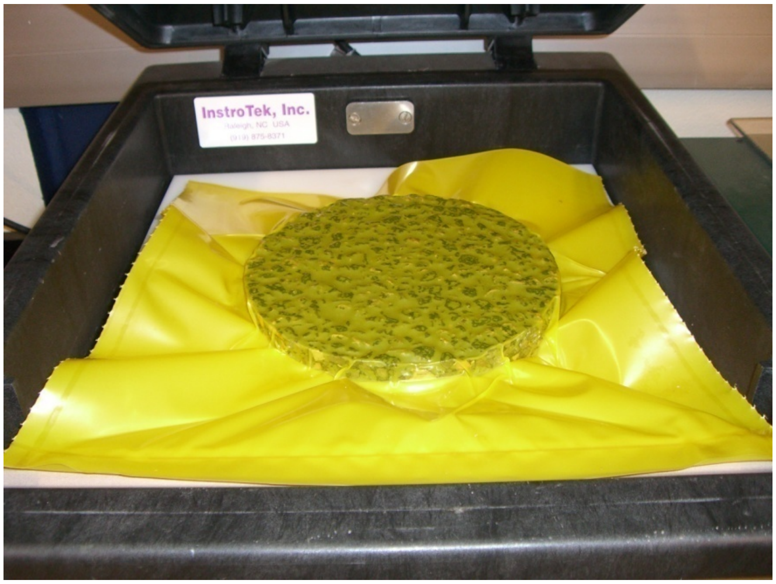

Figure 3.7 – PFC core vacuum sealed in plastic bag for porosity measurement

The submerged weight of the vacuum sealed core specimen is measured, and then the core is removed from the bag and the submerged weight of only the core is measured. Finally, the core is allowed to oven dry overnight and the dry weight of the core is measured. With these three measurements, the total volume of the core and volume of the solids be calculated using the following equations:

$$V_t = \frac{W_b + W_s - W_{sub,total}}{\rho} - V_b \tag{3.1}$$

$$V_s = \frac{W_s - W_{sub,solid}}{\rho} \tag{3.2}$$

In Equations (3.1) and (3.2), V_t is the total volume of the core (solid volume plus void volume), V_s is the volume of the solids in the specimen, W_b is the weight of the plastic bag, V_b is the volume of the plastic bag, W_s is the oven dry weight of the solids, $W_{sub,total}$ is the submerged weight of the core vacuum sealed in the bag, $W_{sub,solid}$ is the submerged weight of only the core specimen, and ρ is the density of water. The effective porosity can then be calculated as:

$$n_e = \frac{V_t - V_s}{V_t} \tag{3.3}$$

Tables 3.1 through 3.4 give the porosity measurements of the PFC core specimens for each of the past four years. In addition, the radius of the core, R_c, and the thickness of the core specimen, b_c, are included. Chapter Six provides a statistical analysis of these data to determine the changes in porosity both in time and at different locations.

Table 3.1 – Porosity of 2007 core specimens (source: Candaele, 2008)

Core ID	Porosity, n_e (%)	R_c (cm)	b_c (cm)
1-A-T	22.78	7.51	4.45
1-B-T	21.64	7.54	3.74
1-C-T	20.36[a]	N/A	N/A
2-A-T	23.17	7.52	3.56
2-B-T	20.51	7.52	4.08
2-C-T	20.98[a]	N/A	N/A
3-A-T	20.30[a]	N/A	N/A
3-B-T	19.44	7.54	4.02
3-C-T	19.55	7.54	3.95

[a] Porosity determined from destructive image analysis method.

Table 3.2 – Porosity of 2008 core specimens

Core ID	Porosity, n_e (%)	R_c (cm)	b_c (cm)
1-1-T	22.97	10.92	4.66
1-1-S	21.68	10.96	3.99
1-2-T	22.77	10.97	4.81
1-2-S	20.28	10.91	3.75
1-3-T	18.54	10.95	4.08
1-3-S	21.52	10.92	3.50
2-1-T	15.77	10.93	3.25
2-2-T	16.62	10.89	3.53
2-3-T	16.18	10.90	3.05
3-1-T	12.38	10.91	3.41
3-2-T	12.82	10.88	2.79
3-3-T	14.50	10.93	3.54

Table 3.3 – Porosity of 2009 core specimens

Core ID	Porosity, n_e (%)	R_c (cm)	b_c (cm)
1-i-T	17.00	10.92	4.24
1-i-S	20.49	10.92	3.47
1-ii-T	18.14	10.92	4.34
1-ii-S	19.20	10.92	3.18
1-iii-T	18.78	10.97	4.51
1-iii-S	19.74	10.92	3.27
2-i-T	15.57	10.93	3.24
2-ii-T	16.23	10.90	3.39
2-iii-T	15.90	10.93	3.44
3-i-T	12.96	10.93	3.68
3-ii-T	13.45	10.91	3.86
3-iii-T	17.96	10.92	3.76

Table 3.4 – Porosity of 2010 core specimens

Core ID	Porosity, n_e (%)	R_c (cm)	b_c (cm)
1-a-T	18.25	7.616	4.709
1-a-S	20.96	7.603	3.825
1-b-T	22.67	7.639	4.599
1-b-S	19.95	7.511	3.980
1-c-T	16.60	7.521	4.860
1-c-S	19.69	7.522	3.870
3-a-T	13.34	7.507	4.214
3-b-T	13.60	7.512	4.109
3-c-T	13.95	7.533	4.190

3.3 Laboratory Measurements

3.3.1 Laboratory Setup and Constant Head Test Procedure

Measurement of the hydraulic conductivity of the PFC core specimens is problematic for two reasons: the two-dimensional flow paths which occur in PFC and the nonlinear flow regime observed during testing. In most typical hydraulic conductivity measurements of porous media, the flow path is only in one dimension (vertical or horizontal), and the flow regime is typically linear such that Darcy's law applies. In the laboratory, a series of constant head tests are conducted to determine the hydraulic conductivity of each core specimen. The test apparatus and test procedure used to measure the hydraulic conductivity were developed for this research study and are described in detail by Candaele (2008). A preliminary method for determining the hydraulic conductivity is provided by Charbeneau et al. (in press). However, the methodology presented does not fully incorporate the nonlinear flow effects. A brief overview of the experimental setup is provided here. A constant head is established from a constant flow rate produced by a peristaltic pump to an inflow standpipe centered on the PFC core specimen. The standpipe has a radius of $R_s = 1.878$ cm for this setup. Water flows downward vertically at the inflow area and turns to exit the core radially at the circumference of the core. This creates a two-dimensional flow pattern in cylindrical coordinates. The reason for this unique flow setup is to mimic the flow conditions for the field test described in Chapter Four.

The testing procedure consists of placing a PFC core specimen between two pliable rubber membranes, each roughly one cm thick. Holes have been drilled into the membranes, where appropriate, to allow for an inflow boundary on the top surface at the location of a standpipe, and to allow for the measurement of hydraulic head at various radial distances from the center of the core both on the top surface and bottom surface of the core specimen. The rubber membranes and PFC core specimen are then placed between two metal plates which are tightened with threaded rods to compress the rubber membranes. This compression is applied to allow the membranes to enter the surface void space of the PFC core and create a no flow boundary on the upper and lower surfaces of the core. Similarly, the metal plates have appropriate holes drilled in them to allow water to enter the PFC core through a standpipe attached to the top plate, and tubes are attached to the radial hydraulic head measurement positions and connected to a slanted manometer board. The core, rubber membranes, and metal plates are placed in a Plexiglas tank and submerged in water. Figure 3.8 shows the experimental setup during testing and Figure 3.9 provides a schematic view of the setup with several important dimensions. R_c is the radius of the core specimen, b_c is the thickness of the core specimen, and h_s is the head in the standpipe measured from the constant water level in the tank. Therefore, h_s is actually the change in head throughout the core.

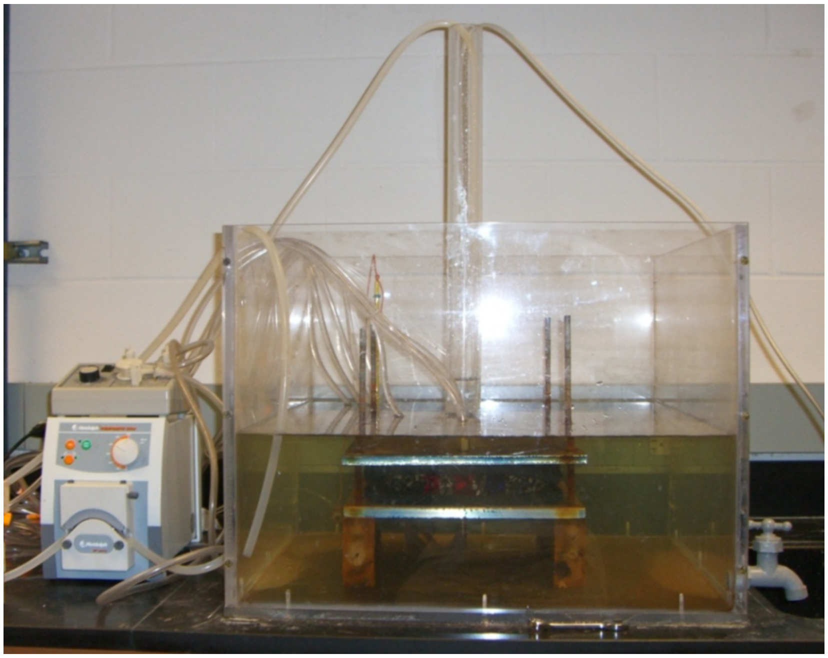

Figure 3.8 – Laboratory experimental setup

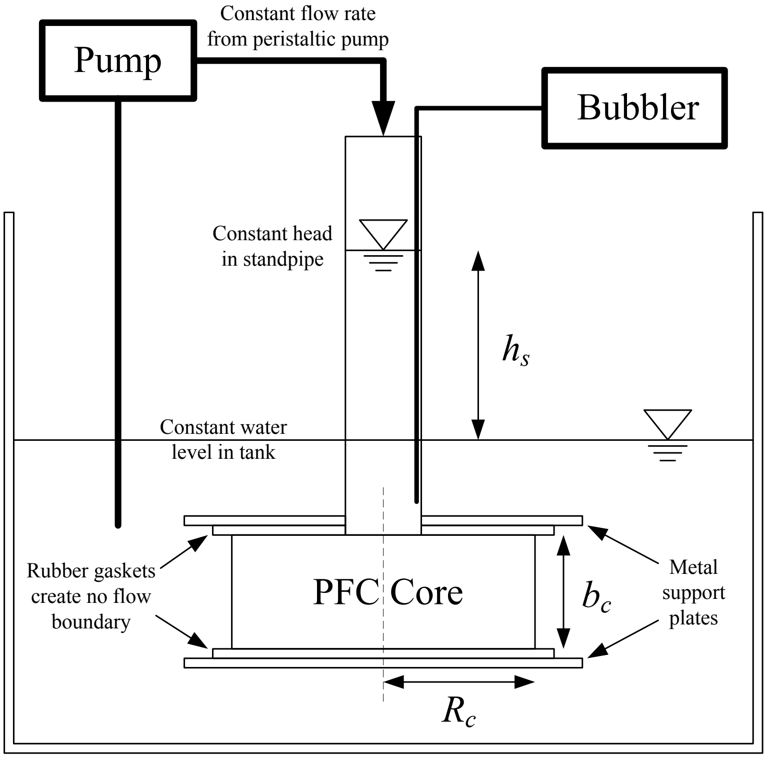

Figure 3.9 – Schematic of laboratory setup

Prior to testing, water is flushed through the core specimen in order to remove any air bubbles that may be present. The core is allowed to sit submerged overnight so that any additional air may leave the pore space. This will ideally create a saturated core specimen, which simplifies the mathematical equations derived below. In addition, the tubes on the manometer board must be flushed out to remove any air bubbles, which can only be accomplished by flushing the air bubbles into the core specimen. Therefore, the ability to create a completely saturated core specimen can be difficult.

Hydraulic conductivity testing consists of taking two measurements: volumetric flow rate and water depth in the standpipe. A constant flow rate is provided by one of two peristaltic pumps. The first pump (VWR mini-pump variable flow) is a low flow pump and can produce flow rates from 1.0 to 8.0 cm^3/s. The second pump (Heidolph pumpdrive 5106) can produce higher flow rates and has a range of flow from 2.0 to 40.0 cm^3/s. The volumetric flow rate is measured with a stopwatch and graduated cylinder.

The water depth in the standpipe is measured with an ISCO bubble flow meter (model #4230) shown in Figure 3.10. Prior to testing, the bubbler is set to a value of zero for the water depth in the tank. This establishes the hydraulic head on the outflow boundary as the datum.

Figure 3.10 – ISCO bubbler used to measure standpipe head

Prior to starting the pump and creating an inflow, the head at each radial position is measured on the slanted manometer board shown in Figure 3.11. This establishes the zero head elevation for each radial head position as well as the zero elevation at the standpipe. The peristaltic pump is turned on at a desired flow rate and steady state conditions are achieved. Typically, steady state is achieved in 15 minutes, but for PFC core specimens that appear to be considerably clogged with sediment, steady state can take considerably longer. Steady state is achieved when the reading on the ISCO bubbler does not change after roughly 10 minutes. At steady state, the bubble reading gives the head in the standpipe, and the manometer board gives the head reading at various radial positions on the top and bottom surface of the core specimen. The flow rate is then determined with a stopwatch and graduated cylinder. Both the head values and flow rate are measured twice and the average of the two is taken as the head and flow rate value for that test. This procedure completes one test and is repeated for a different flow rate until a curve of head in the standpipe as a function of flow rate is created.

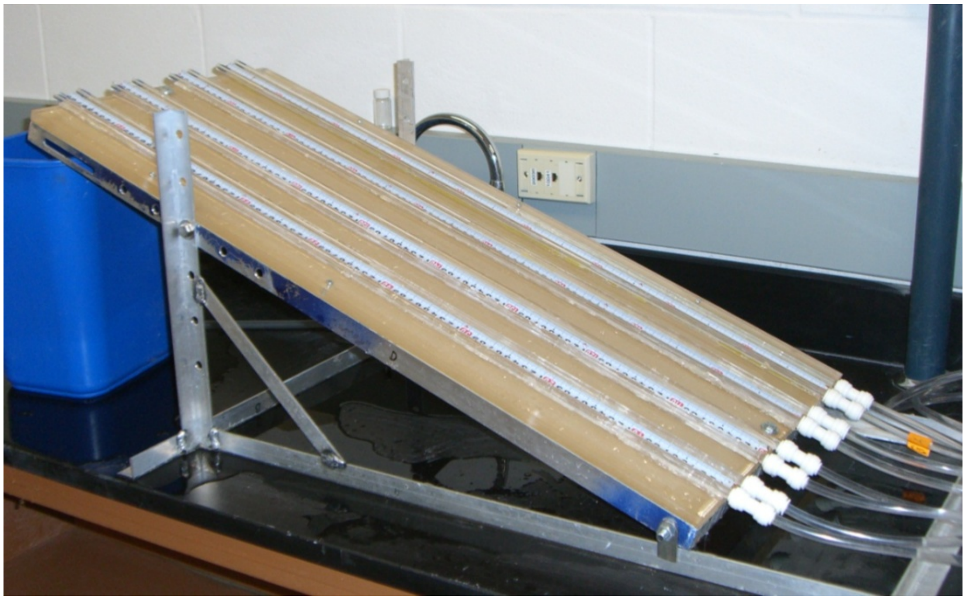

Figure 3.11 – Slanted manometer board for radial head measurements

3.3.2 Modified Forchheimer Equation

The data collected for a series of constant head tests gives the head in the standpipe as a function of flow rate. The data show that this relationship is nonlinear. Therefore, Darcy's law is not applicable and the use of the Forchheimer equation is required. However, the original Forchheimer equation relates the hydraulic gradient as a function of specific discharge. Neither the hydraulic gradient nor specific discharge can be measured precisely for this experimental setup due to the fact that the flow is two-dimensional and the streamlines within the core specimen are diverging. The use of a Forchheimer-type equation is necessary to analyze the data. Equation (3.4) gives the empirical modified Forchheimer equation used for the purposes of this research:

$$h_s = \alpha Q + \beta Q^2 \tag{3.4}$$

where h_s is the head on the standpipe, Q is the volumetric flow rate, and α [T/L^2] and β [T^2/L^5] are the modified Forchheimer coefficients. The modified Forchheimer equation replaces the hydraulic gradient in the original Forchheimer equation with the head in the standpipe, which is actually the change in head through the core specimen since the datum is taken as the head on the outflow boundary. The specific discharge in the original Forchheimer equation is replaced with the volumetric flow rate in the modified Forchheimer equation. These two changes result in a change to the two Forchheimer coefficients. The modified Forchheimer equation defines the nonlinear relationship for the global conditions of the core.

The volumetric flow rate is related to the specific discharge through $Q = Aq$. Q can be measured, but the area for flow changes as water moves through the core specimen. The inflow value of A is the area of the standpipe, πR_s^2. The outflow value of A is the circumference of the core times the thickness, $2\pi R_c b_c$. Therefore, A is not constant as flow passes through the core. Similarly, the hydraulic gradient for the overall core specimen is equal to the change in head, h_s, divided by the length over which this change occurs. However, the flow path length is also not constant for flow through the core. The shortest possible flow path length is $R_c - R_s$, which occurs at the upper no flow boundary. The longest flow length is $R_c + b_c$, which occurs at the lower no flow boundary. Since the flow path length and area are not known, these variables have been lumped into the modified Forchheimer coefficients. As will be shown in Chapter Five, the original Forchheimer coefficients can be related to the modified Forchheimer coefficients through the results of numerical simulations. Therefore, the modified Forchheimer equation is an empirical equation for the overall global conditions of the core specimen.

The use of Equation (3.4) to model the nonlinear flow through a PFC core specimen is useful and provides a good method for determining the modified Forchheimer coefficients. However, it is also useful to rearrange the modified Forchheimer Equation (3.4) to the following transformed form:

$$\frac{h_s}{R_c} = \frac{Q}{\xi}\left(1 + \frac{Q}{\eta}\right) \qquad (3.5)$$

The transformed modified Forchheimer equation represented in Equation (3.5) is useful because h_s/R_c represents an average hydraulic gradient through the core. Although this is not the actual hydraulic gradient, it does serve to nondimensionalize the equation. Furthermore, representing the nonlinear term as shown suggests that the value of Q/η can be compared to the value of one in order to determine whether the nonlinear effects are significant. The two transformed modified Forchheimer coefficients of Equation (3.5), ξ and η, can be compared to the two coefficients of Equation (3.4), α and β, through the following relationships:

$$\xi = \frac{R_c}{\alpha} \qquad (3.6)$$

$$\eta = \frac{\alpha}{\beta} \qquad (3.7)$$

In Equations (3.6) and (3.7), ξ has units of [L^3/T] and can be calculated from the core radius and the linear modified Forchheimer coefficient α through Equation (3.6). η also has units of [L^3/T] and is related to both the modified Forchheimer coefficients, α and β, through Equation (3.7). As discussed below, the use of Equation (3.4) as the modified Forchheimer equation is desirable for determination of the two coefficients from the experimental data. Once the two coefficients are determined, the use of Equation (3.5) as the transformed modified Forchheimer equation is desirable due to its nondimensional form, the units of ξ and η are the same as the flow rate, and the magnitude of Q/η can be compared to a value of one to determine the relative magnitude of the nonlinear effect.

The modified Forchheimer coefficients (α and β) can be determined experimentally from a series of constant head tests. Figure 3.12 shows a typical graph of h_s as a function of Q with the model fit for the modified Forchheimer Equation (3.4).

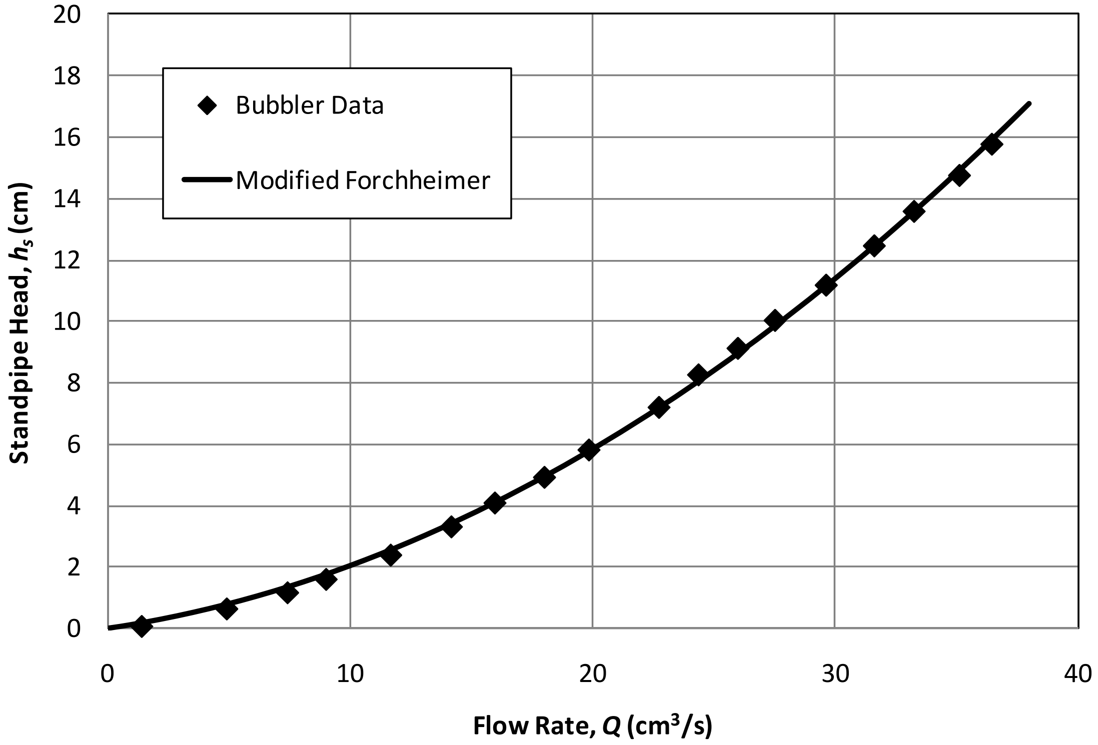

Figure 3.12 – Typical constant head data (Core 1-2-S)

The modified Forchheimer coefficients are determined by minimizing the standard error between the measured standpipe head data, h_{sd}, and the modeled standpipe head, h_{sm}, determined from the modified Forchheimer Equation (3.4). The standard error can be calculated as:

$$S.E. = \sqrt{\frac{1}{N}\sum_{i=1}^{N}\left(h_{sd} - h_{sm}\right)_i^2} \tag{3.8}$$

In Equation (3.8), *S.E.* is the standard error between the data and the modified Forchheimer equation for N observed data points. The standard error is minimized by simultaneously changing the value of α and β so that the model results closely match the observed data. This is accomplished using the Solver tool in Microsoft Excel. The use of Equation (3.4) as opposed to Equation (3.5) for calculating the standard error is due to the form of the equations. If Equation (3.5) is used, the Solver tool will minimize the standard error by simply increasing the value of η to be so large such that the nonlinear term is negligible. Therefore, Equation (3.4) is the most useful for determining the modified Forchheimer coefficients from the experimental data.

Although we can experimentally determine the modified Forchheimer coefficients (α and β or ξ and η), this gives us no indication of the values of the original Forchheimer coefficients (a and b or K and n) without further investigation. In order to address this issue and determine the true hydraulic conductivity, we must conduct numerical simulations of flow through the PFC core specimen as described in Chapter Five. For now, we will simply report the values of the modified Forchheimer coefficients and determined the hydraulic conductivity once the numerical model has been explained and results have been presented.

3.3.3 Falling Head Lab Test Procedure

Although a series of constant head tests is the preferred method for determining the modified Forchheimer coefficients, a falling head test can also be conducted in the laboratory. Comparison of the falling head test to the constant head test results is useful for determining whether the same nonlinear curve can be measured from both methods. This is a necessary concern as the field test for measuring in-situ hydraulic conductivity is based on the falling head principle.

In order to conduct the falling head test in the lab, the same test setup for the constant head tests is used with the core specimen submerged in water and compressed between the two rubber membranes. The water level in the tank is drained so that the surface of the water is near the top surface of the PFC core specimen. Therefore, this essentially means the top of the PFC surface is taken as the head datum. During a falling head test, the source head h_s varies with time. Assuming nonlinear flow conditions, the head-discharge relationship using the modified Forchheimer Equation (3.4) may be inverted to give Q as a function of h_s. Combined with the continuity equation for the water level in a standpipe with radius R_s one finds:

$$-\pi R_s^2 \frac{dh_s}{dt} = Q = \frac{\alpha}{2\beta}\left[\sqrt{1+\frac{4\beta h_s}{\alpha^2}}-1\right] \tag{3.9}$$

Equation (3.9) may be integrated to give the time for the standpipe head to decrease from the initial level $h_s(0)$ to an arbitrary level $h_s(t)$ as follows:

$$\frac{t}{\pi R_s^{\,2}\alpha} = \sqrt{1+\frac{4\beta h_s(0)}{\alpha^2}} - \sqrt{1+\frac{4\beta h_s(t)}{\alpha^2}} + \ln\left(\frac{\sqrt{1+4\beta h_s(0)/\alpha^2}-1}{\sqrt{1+4\beta h_s(t)/\alpha^2}-1}\right) \quad (3.10)$$

With Equation (3.10), three readings of time-depth pairs $[t, h_s(t)] = [0, h_s(0)]$, $[t_1, h_s(t_1)]$, and $[t_2, h_s(t_2)]$ are sufficient to determine the two unknown coefficients α and β, where the third time-depth measurement is used for an initial condition.

The constant head test, while more time-consuming, allows one to better define the entire head-discharge curve, and thus obtain a more reliable estimate of the hydraulic conductivity. That notwithstanding, the variation between the constant head and falling head tests is much less than the natural variation expected at field sites and among laboratory core specimens as described in Section 3.4.2. Both the constant head and falling head test methodologies provide useful and reproducible information on the hydraulic characteristics of PFC.

3.3.4 Establishment of No Flow Boundaries

One possible concern with this experimental test setup is whether the rubber membranes are actually creating a no flow boundary on the surface of the PFC core by simply compressing the core. When the core specimens are extracted, the specimen contains the PFC layer together with the underlying impervious asphalt. Prior to the porosity measurements, the impervious asphalt layer is removed. In order to test whether the rubber membranes are creating a no flow boundary, one of the remaining impervious asphalt layer specimens was placed in the test setup and compressed in an identical way as the PFC cores. A falling head test was conducted on the impervious core to determine if there is a significant amount of flow due to the presence of the rubber membranes. A period of roughly 24 hours was allowed to pass with water in the standpipe, and the water level dropped only by a couple of centimeters within that time. Therefore, it can be assumed that any flow that may occur due to the rubber membranes is negligible compared to the much larger flow rates through the PFC pore space. Furthermore, this test shows that simply compressing the core specimen with the arm strength of a typical engineering graduate student is sufficient to create the required no flow boundary, and no special tools are needed to compress the core under a greater load.

3.4 Lab Test Results

3.4.1 Constant Head Lab Results

The PFC core specimens extracted from the three different roadways in the years 2007, 2008, and 2009 were all tested in the laboratory using the series of constant head tests described in Section 3.3.1. From these tests, the modified Forchheimer coefficients were determined by minimizing the standard error between the constant head data and the modified Forchheimer Equation (3.4). The collected data used to determine the modified Forchheimer coefficients are provided in Appendix B. Tables 3.5 through 3.7 give the modified Forchheimer coefficients and resulting standard error for each of the core specimens tested.

Table 3.5 – Modified Forchheimer coefficients of 2007 core specimen (source: Candaele, 2008)

Core ID	α (s/cm^2)	β (s^2/cm^5)	ξ (cm^3/s)	η (cm^3/s)	*S.E.* (cm)
1-A-T	0.7016	0.0143	10.74	49.07	0.5860
1-B-T	0.0477	0.0028	158.06	16.98	0.1253
2-A-T	0.1883	0.0093	39.98	20.26	0.2118
2-B-T	0.4035	0.0154	18.63	26.18	0.3604
3-B-T	0.2965	0.0390	25.45	7.61	0.4659
3-C-T	0.2860	0.0141	26.52	20.28	0.3330

Table 3.6 – Modified Forchheimer coefficients of 2008 core specimens

Core ID	α (s/cm^2)	β (s^2/cm^5)	ξ (cm^3/s)	η (cm^3/s)	*S.E.* (cm)
1-1-T	0.1520	0.0092	71.88	16.51	0.3578
1-1-S	0.0551	0.0052	198.93	10.53	0.0459
1-2-T	0.1454	0.0115	75.42	12.64	0.1188
1-2-S	0.1172	0.0088	93.11	13.36	0.1226
1-3-T	0.0916	0.0066	119.57	13.97	0.1039
1-3-S	0.0735	0.0050	148.70	14.73	0.0405
2-1-T	0.2892	0.0188	37.80	15.39	0.3171
2-2-T	0.1392	0.0103	78.25	13.56	0.1175
2-3-T	0.2985	0.0187	36.54	15.92	0.2313
3-1-T	2.4007	0.2887	4.55	8.31	0.7898
3-2-T	3.0288	0.7882	3.59	3.84	0.1884
3-3-T	0.5850	0.0699	18.69	8.37	0.5957

Table 3.7 – Modified Forchheimer coefficients of 2009 core specimens

Core ID	α (s/cm^2)	β (s^2/cm^5)	ξ (cm^3/s)	η (cm^3/s)	*S.E.* (cm)
1-i-T	0.0686	0.0082	159.21	8.35	0.0807
1-i-S	0.0468	0.0039	233.50	11.96	0.0527
1-ii-T	0.2245	0.0151	48.62	14.89	0.3434
1-ii-S	0.0655	0.0074	166.53	8.89	0.1528
1-iii-T	0.0924	0.0053	118.77	17.45	0.0634
1-iii-S	0.1434	0.0141	76.17	10.21	0.1731
2-i-T	0.7067	0.204	15.46	34.58	1.3659
2-ii-T	0.3092	0.0097	35.26	31.78	0.3686
2-iii-T	0.1356	0.0090	80.58	15.08	0.1174
3-i-T	1.2954	0.1283	8.44	10.10	0.9058
3-ii-T	0.7192	0.0539	15.17	13.35	0.5381
3-iii-T	0.5424	0.0761	20.13	7.13	0.4604

As previously mentioned, these values give no indication of the hydraulic conductivity without further numerical modeling. However, it is interesting to note some general trends. One would expect that the linear modified Forchheimer coefficient would be related to the hydraulic conductivity. A large hydraulic conductivity is expected to occur for small values of α and large values of ξ. The data suggest that in general, the Loop 360 cores have a larger hydraulic conductivity than the cores from FM 1431 and RR 620. Further investigation of these relationships is provided in Chapter Six.

The nonlinear modified Forchheimer coefficient, particularly the η coefficient, can be used to determine when nonlinear flow effects are significant. As previously mentioned, if the value Q/η is large compared to a value of one, then the nonlinear flow effects cannot be ignored. Therefore, the larger the value of η, the more likely that Q/η will be small and nonlinear flow effects will be negligible. In general, the value of η is on the order of 10 cm^3/s, meaning that if the flow rate approaches a value of 10 cm^3/s, the nonlinear flow effects will become significant. It is interesting to note from Figure 3.12

that for flow rates less than roughly 10 cm^3/s, the experimental data could be fairly closely approximated with a linear relationship.

In addition to determining the modified Forchheimer coefficients by minimizing the standard error, we can also conduct a multiple linear regression on the model in order to obtain the two coefficients. The resulting values of α and β are the same for both methods, but the regression provides additional information that is worth noting. The p-values for each coefficient are very small, suggesting that the model is statistically significant. The regression results also provide 95% confidence intervals for both coefficients to give an indication of the precision of each coefficient. For the linear coefficient, the 95% confidence interval is roughly plus/minus 10% of the actual value. For the nonlinear coefficient, the 95% confidence interval is roughly 5% of the actual value. The relatively small confidence intervals, together with the small p-values, suggest this is an appropriate model to use in order to represent the experimental data.

3.4.2 Falling Head Lab Results

Several of the 2008 and 2009 core specimens were also tested in the laboratory using the falling head approach. The falling head test was conducted simply for verification that both methods would produce similar results. In general, it was assumed that the series of constant head tests will produce more reliable results.

The same core specimen (1-2-S) shown in Figure 3.12 was also tested using the falling head approach. The initial, intermediate, and final head values are as follows: $h_s(0) = 40.6$ cm, $h_s(t_1) = 20.3$ cm, and $h_s(t_2) = 2.54$ cm. The average of three sets of time measurements are taken with results (plus/minus one standard deviation): $t_1 = 4.04 \pm 0.10$ sec and $t_2 = 11.41 \pm 0.21$ sec. Using the mean time values in Equation (3.10), one finds $\alpha = 0.153$ s/cm^2 and $\beta = 0.00675$ s^2/cm^5. Similarly, α and β can be determined using the plus/minus one standard deviation to determine the variability in the falling head results. Figure 3.13 shows the curve of h_s versus Q for the averaged falling head test as well as its uncertainty from plus/minus one standard deviation together with the constant head test results. Good agreement exists between the constant head and falling head tests, suggesting that both methods are acceptable for determining the modified Forchheimer coefficients.

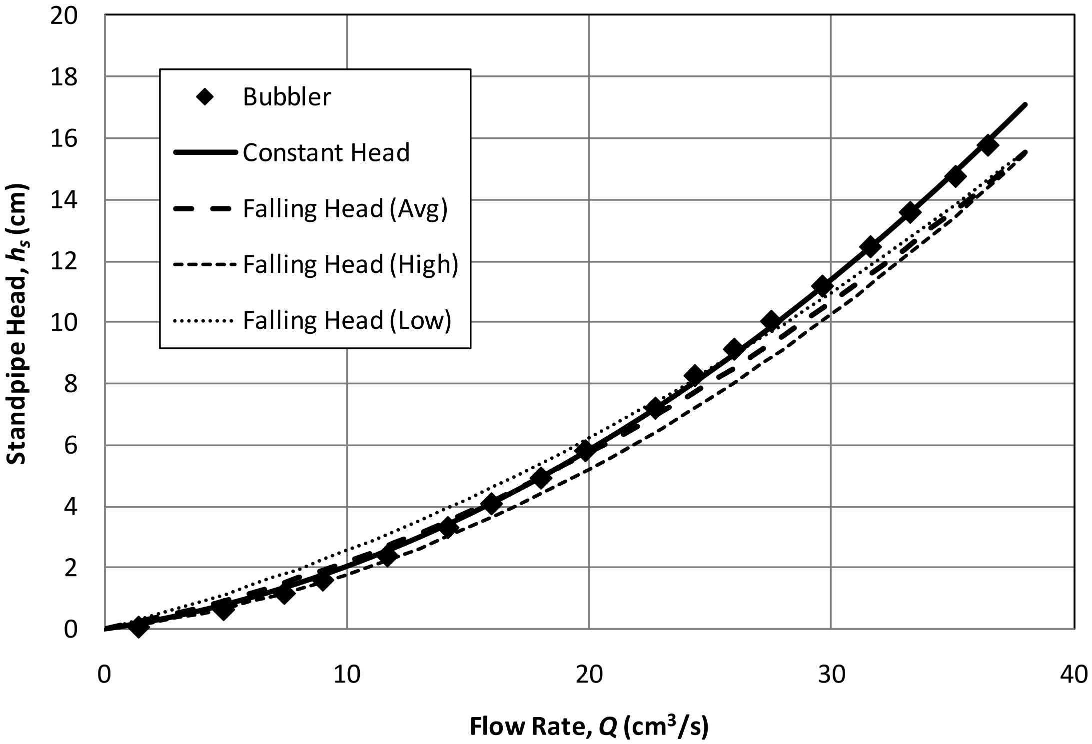

Figure 3.13 – Falling head test results (Core 1-2-S)

Table 3.8 provides the modified Forchheimer coefficients for the select cores tested using the falling head approach. In addition, the percent difference (*P.D.*) of the modified Forchheimer coefficients from the falling head test when compared to the constant head tests is provided in order to give an indication of the error that may be involved with the falling head test.

Table 3.8 – Modified Forchheimer coefficients for falling head tests on 2008 and 2009 core specimens

Core ID	α (s/cm^2)	β (s^2/cm^5)	ξ (cm^3/s)	η (cm^3/s)	*P.D.* in α	*P.D.* in β
1-1-S	0.1505	0.0050	72.50	30.35	-173.2	5.2
1-2-T	0.1480	0.0135	74.13	10.94	-1.7	-17.6
1-2-S	0.1188	0.0110	91.86	10.84	-1.4	-25.0
2-1-T	0.4161	0.0516	26.27	8.06	-43.9	-174.6
2-i-T	0.4057	0.0405	26.94	10.01	42.6	-98.2
2-iii-T	0.1873	0.0064	58.33	29.38	-38.1	29.1
3-i-T	0.9443	0.1799	11.57	5.25	27.1	-40.3
3-ii-T	0.5112	0.0715	21.34	7.15	28.9	-32.8
3-iii-T	0.5413	0.0836	20.17	6.47	0.2	-9.9

The same general trends observed in the constant head tests are seen here as well. Furthermore, there can be some large differences between the constant head and falling head tests. Many of the falling head tests are within acceptable levels of error when compared to the constant head tests, but there are several cases where the percent difference is very large. For this reason, the series of constant head tests is preferred in the laboratory.

In addition, all of the 2010 core specimens were tested only using the falling head approach. Although the constant head test method is the preferred method for determining the modified Forchheimer coefficients of a core specimen, the 2010 cores were not tested using the constant head method due to time constraints. Table 3.9 provides the modified Forchheimer coefficients for the 2010 core specimens using the falling head approach.

Table 3.9 – Modified Forchheimer coefficients for falling head tests on 2010 core specimens

Core ID	α (s/cm^2)	β (s^2/cm^5)	ξ (cm^3/s)	η (cm^3/s)
1-a-T	0.2997	0.0576	25.41	5.20
1-a-S	0.0868	0.0038	87.54	22.86
1-b-T	0.0524	0.0049	145.88	10.78
1-b-S	0.0750	0.0030	100.13	25.09
1-c-T	0.1804	0.0176	41.69	10.23
1-c-S	0.0737	0.0022	102.02	33.13
3-a-T	0.5464	0.1627	13.74	3.36
3-b-T	5.7616	3.0130	1.30	1.91
3-c-T	1.2329	0.6265	6.11	1.97

The linear modified Forchheimer coefficients for Loop 360 core specimens are greater than those from RR 620, again suggesting a greater hydraulic conductivity on Loop 360. Furthermore, in general, the nonlinear coefficient η is smaller for RR 620. All core specimens have a significant nonlinear effect, but the cores from RR 620 are significant at smaller flow rates due to the smaller η coefficients.

Chapter Four

Field Experimentation

In order to properly measure the in-situ hydraulic conductivity of PFC, field experimental tests must be conducted. This is accomplished through a falling head permeability test. In-situ hydraulic conductivity measurements are necessary to properly determine the extent of clogging the PFC layer has experienced. As the PFC layer becomes clogged over time, it is expected that the porosity and hydraulic conductivity will decrease and drainage benefits of the PFC will be lost. Therefore, a well defined field test is necessary to determine whether the drainage benefits of PFC will persist in the future. This chapter describes a new field test apparatus developed specifically for this research study as well as the test procedure for determining the in-situ modified Forchheimer coefficients.

4.1 Need for Improved Field Test

A field test method in the State of Texas currently exists for measuring the drainage capacity of PFC, and is described in detail by TxDOT (2004a). The current TxDOT method measures the time it takes to drain 27.9 cm of water from a 15.2 cm diameter pipe into the PFC layer. Plumbers putty is used to seal the interface between the pipe and the PFC surface. The current TxDOT test apparatus is shown in Figure 4.1. Although this test is useful for determining adequate compaction of the PFC layer between passes of the compaction vehicle during the construction process, it gives no indication of the hydraulic conductivity of the PFC layer. TxDOT provides a guideline of 20 sec as the minimum drainage capacity for newly constructed PFC layers. Based on the dimensions of the TxDOT test apparatus, a drainage time of 20 sec corresponds to an average minimum flow rate of 255 cm^3/s.

Figure 4.1 – Current TxDOT PFC drainage capacity test

Although the current TxDOT method can be used to compare the relative drainage capacity of a PFC layer, it cannot provide the actual hydraulic conductivity. One of the major reasons this is not possible is because as the water flows out of the pipe and into the PFC, the water immediately resurfaces after it moves out from under the plumbers putty. This results in very little actual porous media flow during the test, and so there is not adequate information from which to determine the hydraulic conductivity. Other traditional permeameters, such as a double-ring infiltrometer, typically assume vertical flow paths into the porous media. Although these devices work well for natural soils, they are not effective for PFC due to the impervious boundary roughly 5 cm or less from the surface. Because of the presence of this boundary, the method for determining the hydraulic conductivity from traditional permeameters is no longer valid. Therefore, there is a need for a new test apparatus from which to measure the hydraulic conductivity of PFC that accounts for two specific flow features, namely forcing water to flow through the PFC layer and accounting for the underlying impervious boundary near the surface.

A new field test apparatus developed at CRWR has been designed and constructed specifically for this research study which forces water to flow through the PFC layer; analysis of the results take into account the underlying impervious boundary. The new field test apparatus is shown in Figure 4.2. This apparatus consists of a solid metal base plate of radius R_c = 22.9 cm. A standpipe is centered on the plate with a radius R_s = 5.1 cm. A layer of vacuum grease (Dow Corning high vacuum grease) is placed on the bottom side of the base plate and is allowed to enter the surface void space of the PFC in order to create a no flow boundary along the surface of the plate. This helps to eliminate any flow that may occur between the PFC surface and the base plate surface. Water flows vertically into the PFC layer from the standpipe and turns to flow radially away from the standpipe and out from under the base plate. As water flows out from under the base plate, surface runoff tends to occur. This test apparatus mimics the boundary conditions imposed on the core specimens in the laboratory and can therefore be analyzed in the same way.

Figure 4.2 – CRWR field test apparatus

4.2 Field Measurements

4.2.1 Falling Head Test Procedure

The results of the laboratory experiments are used to determine the modified Forchheimer coefficients for a PFC core specimen. Although the laboratory method is effective in determining these coefficients, it is not ideal due to the destructive nature of the coring process and time restraints associated with conducting a series of constant head tests. Therefore, a need exists for a nondestructive field test in which the modified Forchheimer coefficients can be easily measured in-situ. This can be accomplished with a falling head test in the field, as opposed to a series of constant head tests in the lab. A falling head test in the field is necessary due to the large flow rates and large volume of water required for constant head field tests. The falling head test is conducted using the new CRWR test apparatus described above. As mentioned in Section 3.3.3, during a single falling head test, three time-depth measurements are taken. These three measurements are used to determine the two modified Forchheimer coefficients, with the third measurement used for the initial condition. The use of Equation (3.10) in Section 3.3.3 is used to determine the two modified Forchheimer coefficients and is repeated here for convenience.

$$\frac{t}{\pi R_s{}^2 \alpha} = \sqrt{1 + \frac{4\beta h_s(0)}{\alpha^2}} - \sqrt{1 + \frac{4\beta h_s(t)}{\alpha^2}} + \ln\left(\frac{\sqrt{1 + 4\beta h_s(0)/\alpha^2} - 1}{\sqrt{1 + 4\beta h_s(t)/\alpha^2} - 1} \right) \quad (4.1)$$

A similar test procedure as described in Section 3.3.3 is used in the field. Charbeneau et al. (in press) also describe the test methodology needed to conduct the field test. The following outlines the necessary materials needed to conduct the field test as well as a step-by-step procedure to properly obtain the required measurements.

The following materials are needed to conduct the falling head field test:

- *Proposed CRWR field test apparatus*: used to channel water into the PFC surface and create radial flow without surface runoff; the standpipe should be graduated in divisions of 0.3 cm (see Figure 4.2).
- *Stopwatch*: used to record the time for water to drain in divisions of 0.01 sec; must have a split function to record an intermediate time during the test.
- *Vacuum grease*: used to seal the PFC surface under the base plate of the test apparatus; Dow Corning silicon high vacuum grease works well, and typically 200 to 230 mL (one and a half tubes) is sufficient to cover the base plate surface during dry conditions.
- *Water*: roughly 45 L of water is sufficient to conduct one falling head test.

The following steps represent the CRWR test procedure for determining the in-situ modified Forchheimer coefficients:

1) Select an area of the existing PFC surface to test. Remove any debris on the surface and choose a sufficiently flat area so that the base plate of the test

apparatus can sit flat on the roadway surface and create a good seal with the PFC.

2) Place roughly 200 to 230 mL of vacuum grease on the underneath side of the base plate. Spread the vacuum grease by hand to create a uniform distribution.
3) Place the test apparatus onto the PFC pavement surface. Use enough force (typically standing on the base plate is sufficient) to create a water-tight seal between the base plate and the pavement surface such that the vacuum grease enters the surface voids of the PFC.
4) Flush an initial volume of water though the test apparatus to saturate the pore space. Typically about 19 L of water is necessary for sufficient saturation.
5) Fill the test apparatus with water to the top of the standpipe.
6) Start the timing device when the water level reaches the marking of 36.6 cm on the standpipe. This corresponds to a water depth of 40.4 cm above the PFC surface.
7) Use the split function on the timing device when the water level reaches the marking of 18.3 cm on the standpipe. This corresponds to a water depth of 22.1 cm above the PFC surface.
8) Stop the timing device when the water level reaches the marking of 0.0 cm on the standpipe. This corresponds to a water level of 3.8 cm above the PFC surface.
9) Record the three time-depth measurements.
10) Repeat steps 5 through 9 until a total of three falling head tests are completed. Average the three time measurements to get the average time-depth measurement necessary to calculate the modified Forchheimer coefficients using Equation (4.1).

An additional concern with the field test is the existing moisture content of the roadway itself, particularly after recent rainfall events. It is assumed that the pore space in the PFC layer is saturated for testing conditions. This suggests that if there was a recent rainfall event and the PFC layer had not fully dried then the assumption of saturated conditions would be more likely. However, experience has shown that when the PFC surface is moist, the vacuum grease does not create a good bond with the PFC surface. After rainfall events, there is a possibility that the testing apparatus may float during the test due to the poor bond. Therefore, a larger amount of vacuum grease may be needed in order to create the upper no flow boundary, and standing on the device during testing is recommended to avoid the possibility of floating. The test can be conducted properly after rainfall events, but additional care is needed in order to ensure that the upper no flow boundary is created. When the test is completed and the test apparatus is moved, the vacuum grease should cause the apparatus to stick to the PFC surface. If the apparatus did not stick to the surface when removed, then more vacuum grease should be added and the test procedure should be repeated.

4.2.2 Investigation of Saturated Pore Space

One of the assumptions in the theoretical development of the test process is that the pore space must be completely saturated. Due to the slope of the roadway in the field, water is constantly flowing down gradient toward the roadway shoulder by gravity. This suggests that the pore space may not be entirely saturated despite the initial volume of water allowed to drain through the test apparatus prior to testing. In the event that the pore space is not completely saturated, the hydraulic conductivity measurement would most likely result in an artificially high hydraulic conductivity. This increase in hydraulic conductivity is a result of some of the water acting to fill the pore space of the PFC.

An initial volume of 19 L of water is allowed to flow into the PFC layer prior to testing in order to saturate the pore space. In order to determine whether saturated conditions are actually achieved by the initial drainage prior to conducting the falling head test, a diffuser was built which allows water to drip into the PFC layer upslope from the test location. The diffuser consists of a 1.5 meter (m) long piece of PVC pipe attached to a 189 L water supply tank. The diffuser and water supply tank are shown in Figures 4.3 and 4.4, respectively. The diffuser has nine 0.64 cm diameter holes drilled through the PVC, and are spaced 15.2 cm apart and allow water to drip out. The flow rate from the diffuser can be controlled by a valve attached upstream of the diffuser. Prior to using the diffuser, an initial falling head test is conducted using the test procedure described above. Then 75.7 L of water is dripped into the PFC over a time of 15 minutes. With this volume of water in the pore space, it appears that the pores have become completely saturated. A second falling head test is conducted resulting in the same modified Forchheimer coefficients within the experimental error, verifying that saturated conditions are achieved with only the initial drainage volume of 19 L. This confirms our assumption of saturated conditions.

Figure 4.3 – Testing prior to using diffuser upslope

Figure 4.4 – 189 L water supply tank

4.2.3 Comparison with Constant Head Field Test

Although a falling head test is preferred in the field, a limited number of constant head tests were measured in the field as well. A falling head test serves to theoretically represent an infinite number of constant head tests. In order to determine whether a series of constant head tests is equivalent to a falling head test, several constant head tests were attempted in the field. The conduction of these tests requires a large amount of water due to the ease of flow through the PFC as well as the time required to reach steady state conditions. The head is measured as a constant in the standpipe, and the flow rate is measured with a stopwatch and graduated bucket. In addition, it is difficult to obtain precise measurements due to the large flow rates needed. Figure 4.5 shows a constant head field test with water flowing by gravity from the water supply tank, which must be continuously refilled with water from smaller buckets during the test in order to maintain a constant water level in the tank. The constant water level in the tank is necessary to obtain a constant flow rate.

Figure 4.5 – Constant head field test

Four constant head tests were conducted in the field, followed by one falling head test. The results are shown in Figure 4.6. The modified Forchheimer coefficients can be determined by fitting a curve to the four constant head tests by minimizing the standard error similar to the method used for the laboratory constant head data. There is good consistency between the constant head and falling head data, though more constant head measurements are necessary, especially at small discharge values, in order to better estimate the linear modified Forchheimer coefficient α. The similar shape between the constant head and falling head test results suggest that the falling head test serves as a good comparison to a series of constant head tests. However, the difference between the two curves can be attributed to the uncertainty associated with each of the constant head tests. The large flow rates needed to conduct a constant head test in the field make it difficult to obtain a constant flow rate and accurately measure that rate. In addition, obtaining steady state conditions are not guaranteed in the field. Furthermore, the large flow rates sustained during the constant head test may have flushed particles out of the flow paths in the PFC pore space, which will alter the Forchheimer coefficients.

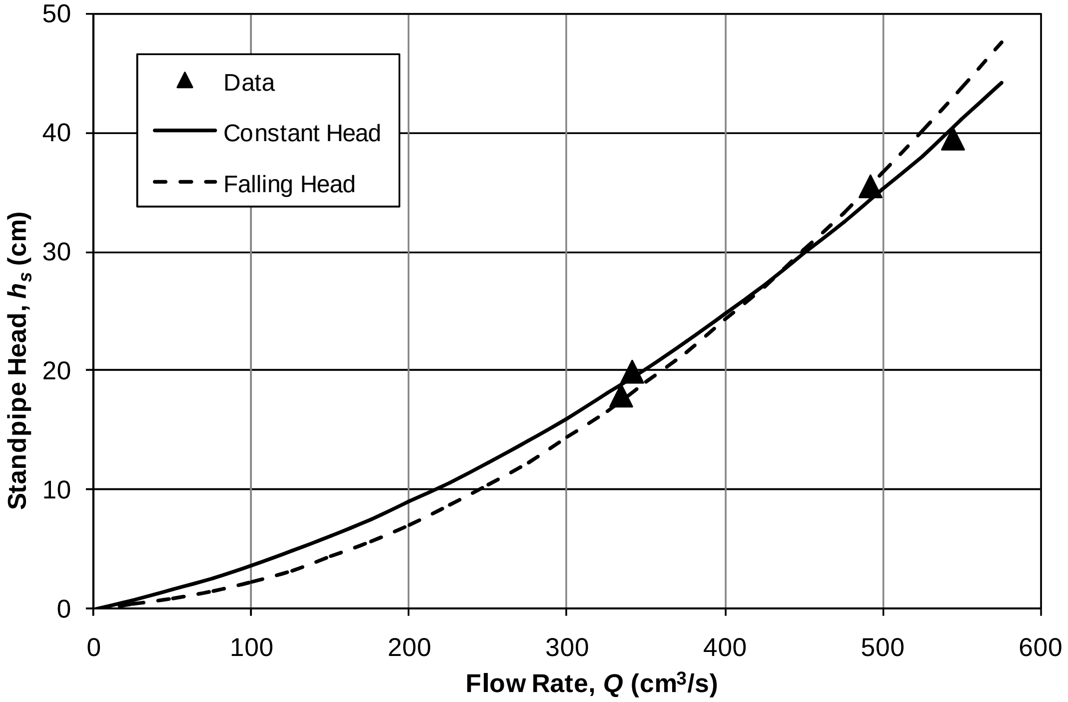

Figure 4.6 – Comparison between constant and falling head field tests

4.2.4 Effect of Roadway Slope

The final assumption that was investigated in this research study is the impact of gravity on the flow conditions due to the effect of the roadway slope. The longitudinal slope and cross slope of the roadway surface create a constant conveyance of water through the PFC overlay due to gravity alone. Therefore, gravity may have an effect on the field conditions, which would most likely result in an artificially high hydraulic conductivity measurement. This is because water will be transported through the porous media by the established head in the standpipe as well as by gravity. Since gravity is not included in any of the falling head equations, the transport of water by gravity would be attributed to the head difference, resulting in a high hydraulic conductivity estimate.

This is addressed by considering the following equation for the change in head through the test apparatus, i.e. the change in head from the inflow area to the outflow area:

$$h_s(\theta) = h_s + sR_c \cos(\theta) \tag{4.2}$$

In Equation (4.2), $\theta = 0$ corresponds to the downslope direction and s is the slope of the roadway; h_s is the change in head as before, but now corresponds specifically for a flat surface, i.e. $\theta = \pi/2$. Now, if we assume each flow path leading from the standpipe is independent, then the incremental discharge in the θ-direction can be given as:

$$\delta Q(\theta) = \frac{\alpha}{2\beta}\left[\sqrt{1 + \frac{4\beta(h_s + sR_c \cos(\theta))}{\alpha^2}} - 1\right]\delta\theta \tag{4.3}$$

Equation (4.3) gives the incremental discharge $\delta Q(\theta)$ as a function of the change in head. The total discharge from the standpipe can be found by integrating Equation (4.3) as follows:

$$Q(h_s, s) = \frac{1}{\pi}\int_0^\pi \frac{\alpha}{2\beta}\left[\sqrt{1 + \frac{4\beta(h_s + sR_c \cos(\theta))}{\alpha^2}} - 1\right]d\theta \tag{4.4}$$

Equation (4.4) can be solved numerically with a simple finite difference code. Of primary interest is the impact of the roadway slope for the smallest head value measured during testing. At the end of the falling head test, the final time measurement is taken for a value of $h_s = 3.8$ cm, and it should be expected that gravity will have the largest impact on the flow rate for this change in head. Table 4.1 calculates the flow rate from Equation (4.4) for multiple values of the roadway slope and then determines the percent error produced by the roadway slope when compared to zero slope. The modified Forchheimer coefficients used are $\alpha = 0.0204$ s/cm^2 and $\beta = 1.57\times10^{-4}$ s^2/cm^5, as determined from a falling head test conducted on Loop 360.

Table 4.1 – Numerical results for effect of roadway slope

Slope, *s* (cm/cm)	*Q* (cm^3/s)	Percent Error (%)
0.00	104.00	0.00
0.02	103.89	0.11
0.04	103.56	0.43
0.06	102.98	0.98
0.08	102.16	1.78

As can be seen in Table 4.1, the effect of the roadway slope is less than one percent error for slopes less than 6%. On the roadways for which the field test has been conducted, the roadway slope is roughly 4%, which will result in a percent error of roughly half a percent. Therefore, it can be assumed that the roadway slope has very little impact on the falling head test results, and Equation (4.1) can be used without any modification to calculate the modified Forchheimer coefficients.

4.2.5 Establishment of No Flow Boundary

The two main assumptions made in analyzing the falling head test are saturated pore space and the upper and lower no flow boundary conditions. The assumption of saturated pore space is addressed in Section 4.2.2. The lower no flow boundary is assumed to be created due to the underlying impervious pavement surface and cannot be verified through testing. However, there is no reason to believe that the lower no flow boundary is not established. Therefore, the main concern is whether the upper no flow boundary is properly established between the PFC surface and the metal base plate. Vacuum grease is used to create this no flow surface. As mentioned in Section 4.2.1, the vacuum grease will cause the metal base plate to stick to the surface if properly used. In this event, it is assumed that a good bond was obtained during testing and the no flow boundary was subsequently created. In order to confirm the creation of a no flow boundary, the test apparatus was used on conventional impervious asphalt and impervious concrete surfaces. The same test procedure outlined above was used on these two surfaces in order to determine whether there was significant flow between the impervious surfaces and the metal base plate. The falling head test was conducted and on the concrete surface, the total drainage time was nearly 11 minutes; on the asphalt surface, the total drainage time was nearly 30 minutes. Therefore, although this does not create a perfect no flow boundary, the flow is small enough that it can be considered negligible. When compared to the longest drainage time observed in the field on PFC, this drainage accounts for less than 5% error. Furthermore, this test helped to confirm that roughly 200 to 230 mL of vacuum grease is sufficient to create the no flow boundary under dry testing conditions.

4.3 Field Test Results

4.3.1 TxDOT Field Test Results

The current TxDOT field test described in Section 4.1 does not give any indication of the hydraulic conductivity of the PFC, but instead reports the drainage time for the falling head test. TxDOT guidance suggests that the typical drainage time is normally less than 20 sec for newly constructed PFC mixtures. Several TxDOT falling head tests have been conducted in the field during the core extraction process, and the TxDOT results are reported in Table 4.2 below.

Table 4.2 – TxDOT field test results

Roadway	Location	Date	Drainage Time (sec)
Loop 360	Shoulder	6-29-08	17.84
Loop 360	Shoulder	6-29-08	19.81
Loop 360	Shoulder	2-2-09	14.28
Loop 360	Travel Lane	2-2-09	16.45
Loop 360	Shoulder	2-5-10	12.62
Loop 360	Travel Lane	2-5-10	19.82
FM 1431	Travel Lane	2-2-09	112.61
RR 620	Travel Lane	2-2-09	69.73
RR 620	Travel Lane	2-5-10	44.98

The results from the TxDOT field test suggest that Loop 360 has retained relatively good drainage capacity throughout its life. None of the drainage times exceed 20 sec for all Loop 360 tests. However, for both FM 1431 and RR 620, drainage times were significantly greater than the 20 sec guideline, suggesting that these two roadways have experienced significant clogging. Although this test provides information on the drainage capacity of the PFC, it does not indicate whether the drainage capacity is sufficient for providing proper drainage benefits. The minimum average flow rate which is considered acceptable under the TxDOT procedure is 255 cm^3/s. This average flow rate will be compared to average flow rates determined from the CRWR test procedure in the following section.

4.3.2 CRWR Field Test Results

In order to better measure the in-situ hydraulic conductivity of PFC, the new CRWR field test described in Section 4.2.1 can be used to determine the modified Forchheimer coefficients, which give an indication of the hydraulic conductivity as described in Chapter Five. Table 4.3 below provides the results of the CRWR field falling head test. The middle and final times are reported with plus/minus one standard deviation together with the resulting modified Forchheimer coefficients calculated using Equation (4.1).

Table 4.3 – CRWR field test results

Roadway	Location	Date	t_1 (sec)	t_2 (sec)	α (s/cm^2)	β (s^2/cm^5)
Loop 360	Shoulder	6-29-08	3.92±0.14	11.12±0.22	0.0204	1.57×10^{-4}
Loop 360	Shoulder	6-29-08	4.28±0.13	12.36±0.30	0.0254	1.81×10^{-4}
Loop 360	Shoulder	9-25-08	4.07±0.18	11.75±0.16	0.0238	1.65×10^{-4}
Loop 360	Shoulder	9-25-08	4.17±0.19	11.90±0.41	0.0216	1.80×10^{-4}
Loop 360	Shoulder	11-9-08	3.88±0.15	10.63±0.01	0.0093	1.84×10^{-4}
Loop 360	Shoulder	11-23-08	3.27±0.00	9.05±0.05	0.0100	1.26×10^{-4}
Loop 360	Shoulder	2-2-09	4.46±0.14	12.88±0.21	0.0262	1.97×10^{-4}
Loop 360	Travel Lane	2-2-09	4.30±0.22	12.17±0.46	0.0197	2.00×10^{-4}
Loop 360	Shoulder	2-5-10	3.97±0.11	11.33±0.14	0.0206	1.64×10^{-4}
Loop 360	Travel Lane	2-5-10	3.47±0.19	10.11±0.16	0.0223	1.15×10^{-4}
FM 1431	Travel Lane	2-2-09	17.35±1.15	52.16±3.13	0.1430	2.50×10^{-3}
RR 620	Travel Lane	2-2-09	9.17±0.02	25.86±0.40	0.0403	9.17×10^{-4}
RR 620	Travel Lane	2-5-10	10.89±0.30	32.12±0.19	0.0784	1.07×10^{-3}

The results of the new field test also show that FM 1431 and RR 620 are more clogged than Loop 360 due to the longer drainage times. In addition, it appears that the modified nonlinear Forchheimer coefficients are significantly smaller than what was determined from the constant head laboratory tests on the core specimens report in Section 3.4.1. This can be attributed to the larger testing apparatus used in the field. The numerical model described in Chapter Five will show that we expect smaller coefficients as the standpipe and/or core radii increase.

On Loop 360 there are several hydraulic conductivity tests that were conducted with both the TxDOT and CRWR field tests at the same location. A correlation was attempted to relate the two results for these paired tests; however, no relationship could be found between the two tests. The final drainage time and average flow rate during the test were analyzed for comparison, but again no relationships were found. Therefore, test results from the TxDOT test cannot be used to estimate the results of the CRWR test in order to obtain a value for the hydraulic conductivity.

A final assessment of the field data is to compare the average flow rates obtained from the CRWR test to the minimum recommended flow rate based on the TxDOT guideline of 255 cm^3/s. As with the TxDOT field test results, both FM 1431 and RR 620 had smaller average flow rates when conducted with the CRWR field test. However, on Loop 360, half of the test results from the CRWR test have average flow rates less than the minimum suggested TxDOT guideline. Therefore, although the TxDOT test showed that the flow rates observed on Loop 360 were greater than the minimum suggested flow rate, the CRWR test shows that half of the flow rates are smaller than the guideline flow rate. The CRWR field tests result in very similar in-situ hydraulic conductivity values, signifying that the TxDOT guideline is not applicable for other testing devices.

4.3.3 Sensitivity of Time Measurement

The use of a stopwatch for measuring time during the falling head test in the field is useful as it provides a simple measuring device that is inexpensive and readily available. However, the use of such a device can result in some discrepancy due to possible human error. For this reason, it is recommended that the time measurements from three falling head tests be averaged in order to reduce any human error. To determine the uncertainty which can result from human error, a sensitivity analysis on the time measurements is provided here. Sensitivity is quantified by incrementally increasing or decreasing the actual time measurements observed in the field and determining the resulting change to the modified Forchheimer coefficients calculated from Equation (4.1).

A falling head field test conducted on Loop 360 has the following averaged time-depth measurements with plus/minus one standard deviation: $h_s(t_0) = 40.4$ cm, $h_s(t_1) = 22.1$ cm, $h_s(t_2) = 3.8$ cm, $t_0 = 0$ sec, $t_1 = 3.89 \pm 0.14$ sec, and $t_2 = 11.12 \pm 0.22$ sec. This results in the following modified Forchheimer coefficients: $\alpha = 0.0204$ s/cm^2 and $\beta = 1.57\times10^{-4}$ s^2/cm^5. The sensitivity analysis will be conducted by either increasing or decreasing the two time measurements by $\Delta t = 0.1$ sec or 0.2 sec and determining the resulting percent change of the modified Forchheimer coefficients when compared to the above reported values.

Figures 4.7 and 4.8 show the sensitivity on the linear and nonlinear modified Forchheimer coefficients, respectively. The four curves correspond to changes to the middle time (t_1), final time (t_2), both times in the same direction (both times increased or decreased), and both times in the opposite direction (middle time increased with final time decreased and vice versa). Clearly small changes in the time measurements can result in large changes to the calculated modified Forchheimer coefficients. The sensitivity to the linear coefficient is greater than that of the nonlinear coefficient, which is unfortunate because it is the linear coefficient that will be used to determine the in-situ hydraulic conductivity. However, the field tests conducted to date have resulted in very reliable and repeatable data when the average of three time measurements is used. Therefore, when conducted properly, the proposed field test is considered reliable. The in-situ hydraulic conductivity data reported in Section 5.5.5 show very little variability, suggesting sensitivity in time measurements is not a major source of error.

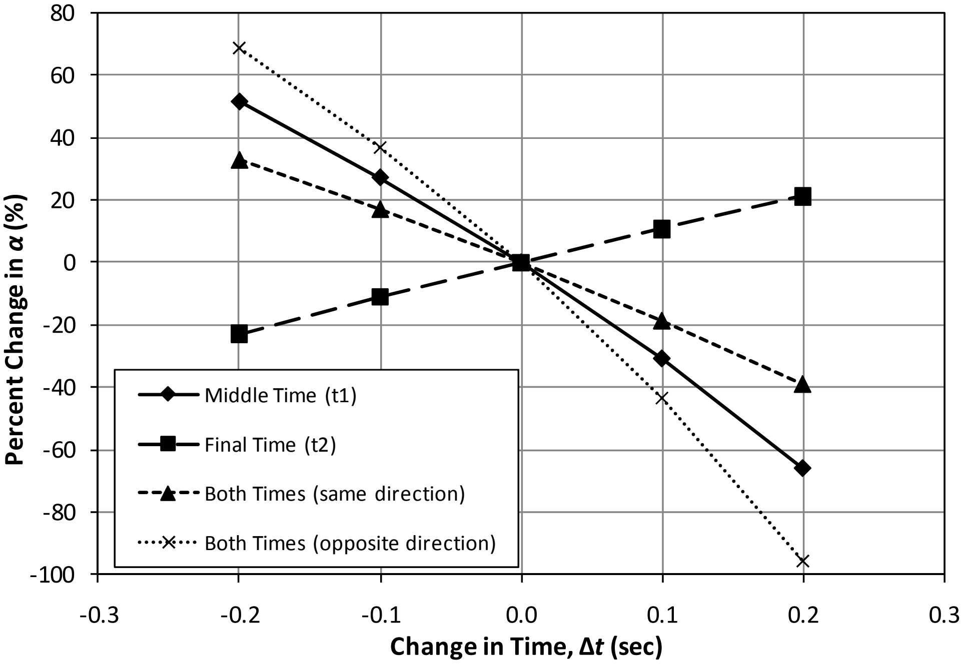

Figure 4.7 – Time sensitivity of linear modified Forchheimer coefficient

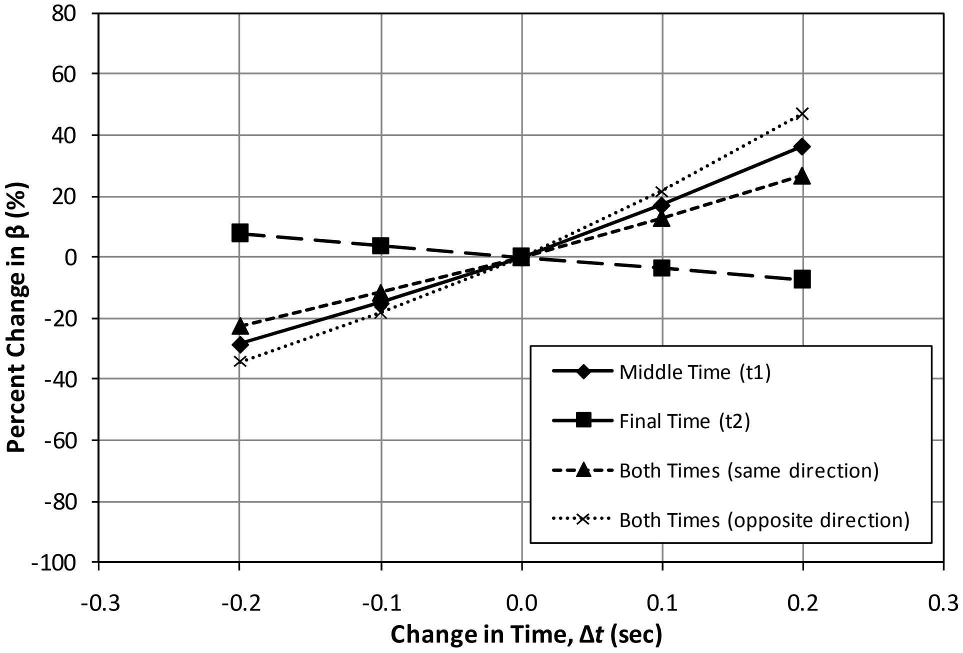

Figure 4.8 – Time sensitivity of nonlinear modified Forchheimer coefficient

It should be noted that the above sensitivity analysis was conducted on data obtained from Loop 360, which has the best drainage properties of all three roadways and will therefore have the largest sensitivity to small changes in time. The sensitivity analysis can be conducted on the other roadways with larger drainage times and it can be shown that for FM 1431, for example, the change in modified Forchheimer coefficients is less than ±10% error. Consequently, the larger the drainage times, the less sensitive the result is to small changes in the time measurements. As shown in Section 4.3.2, the larger drainage times tend to have more variability than the shorter times, which suggests that although the time measurements can be very sensitive to small changes in time, in general, we would not expect to see significant errors from our field measurements. This simply provides a method to quantify the possible uncertainty in the measurements.

4.3.4 Comparison to Video Results

In an effort to determine how accurate the field test results are at fully defining the falling head test by only reporting three time-depth measurements, a video of the falling head test was recorded. From the video, multiple points can be measured instead of the suggested three points during the test. A graph of head versus time can be accurately determined from the video. This curve can then be compared to the corresponding times calculated from Equation (4.1) for each of the head values using the modified Forchheimer coefficients determined from the average of three falling head tests. The goal is to show that the three time-depth measurements taken during the falling head test are sufficient to fully characterize the results of the falling head test.

Two videos were taken of the falling head test at Loop 360 and RR 620 on February 5, 2010. Prior to taking these videos, the falling head test procedure defined in Section 4.2.1 was conducted in order to determine the modified Forchheimer coefficients. Figures 4.9 and 4.10 show the curves of standpipe head versus time for RR 620 and Loop 360, respectively.

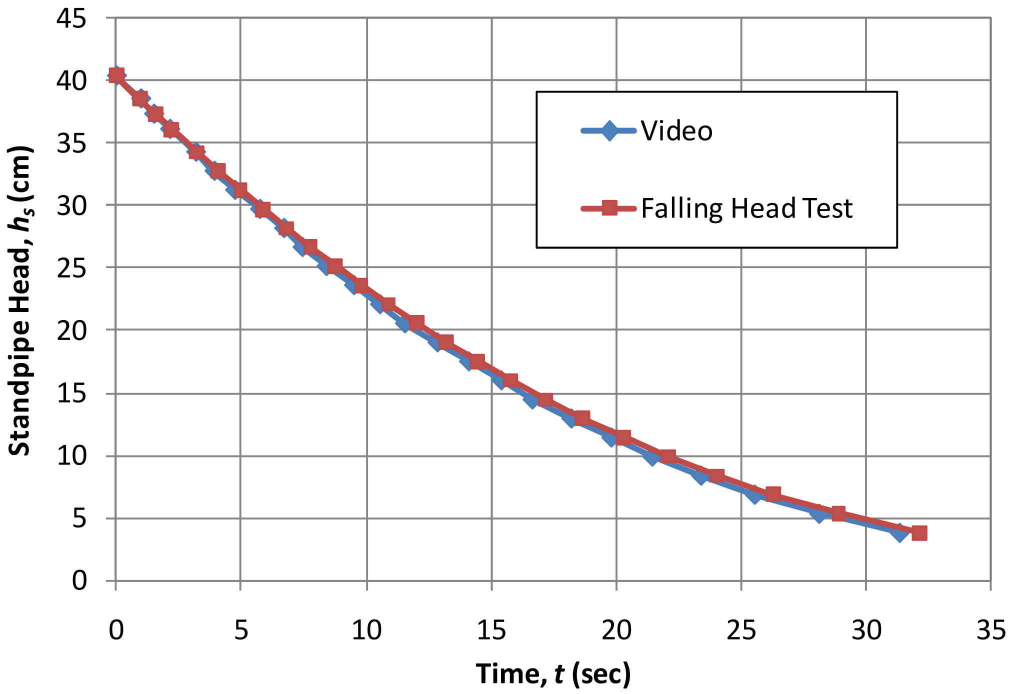

Figure 4.9 – Comparison of falling head test to video on RR 620

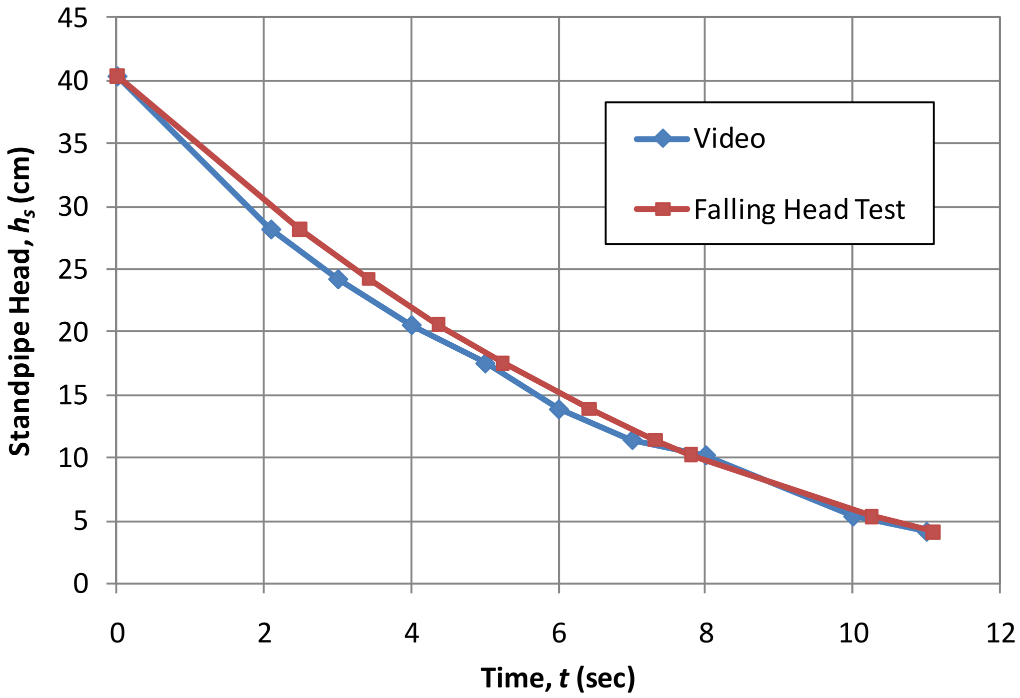

Figure 4.10 – Comparison of falling head test to video on Loop 360

The hydraulic conductivity on RR 620 is much lower than Loop 360, resulting in a longer time scale on RR 620 and the head in the standpipe decreasing at a slower rate. Because of this, it was easier to view the change in head on RR 620 from the video. On Loop 360, not only was the standpipe head falling faster, but the video was not zoomed in enough in order to accurately determine the change in time for less than a second. Because of the inability to decipher the change in time for less than a second, the “Video” curve in Figure 4.10 is not smooth. However, both videos produce a curve very similar to what was observed from the falling head test using Equation (4.1). Furthermore, the standard error can be calculated between the two curves in order to quantify the error involved in the falling head test. The standard error corresponds to the difference between the observed time in the video compared to the calculated time from the falling head test. The standard error on RR 620 for this test is 0.43 sec; the standard error on Loop 360 is 0.31 sec. Both tests produce reliable results, and this comparison shows that simply taking three time-depth measurements for the falling head test is sufficient to fully characterize the results of the falling head test.

Chapter Five

Numerical Modeling

5.1 Purpose of Numerical Model

Experimental studies have shown that under the large hydraulic gradients imposed during testing conditions, flow through PFC exhibits a nonlinear flow relationship which can be modeled using the Forchheimer equation. However, due to the two-dimensional flow paths observed in both lab tests of PFC core specimens and field tests, the use of a modified Forchheimer equation for the global conditions of the PFC was introduced. Experimental testing will result in determination of the two modified Forchheimer coefficients (α and β or ξ and η), but give no indication of the original Forchheimer coefficients (a and b or K and n). In order to determine a relationship between the modified and original Forchheimer coefficients, a numerical model is needed. The proposed numerical model solves the continuity equation in two-dimensional cylindrical coordinates using a finite difference scheme.

The purpose of this numerical model is to solve the continuity equation using the original Forchheimer equation for various assumed values of a and b. The result will give the head distribution through a core specimen for a specified value of the head on the standpipe, h_s. With this head distribution, the flow rate Q through the core specimen can be calculated based on the outflow hydraulic gradient. Simulating multiple values of h_s and calculating the corresponding flow rate will create a curve of h_s versus Q. From this curve the values of the modified Forchheimer coefficients can be determined by regression. Therefore, the inputs to the model are the core geometry (R_s, R_c, and b_c), the original Forchheimer coefficients (a and b), and the head on the standpipe (h_s). The output from the model is the flow rate (Q) and ultimately the modified Forchheimer coefficients (α and β) when multiple values of h_s are simulated. Essentially, this numerical model is analogous to the constant head tests conducted in the laboratory. The goal of the model is to relate the original Forchheimer coefficients to the modified Forchheimer coefficients so that we are able to determine the hydraulic conductivity from the modified Forchheimer coefficients. The numerical model was written in FORTRAN using a finite difference scheme. The FORTRAN code is provided in Appendix A.

5.2 Modeling of Linear Flow

Prior to modeling the Forchheimer equation we will investigate a simpler case for linear flow through a PFC core specimen using Darcy's law. The modeling of the linear case is beneficial in order to compare to the nonlinear case and therefore determine where the nonlinear effects have the greatest impact on the head distribution through the core, as well as to test whether the nonlinear solution approaches the linear solution for small values of h_s or b. The method shown below is similar in approach to that presented by Charbeneau et al. (in press). However, the nonlinear effects will be fully incorporated by the numerical model developed for the present research study, which is an improvement over the Charbeneau et al. approach.

5.2.1 Approximate Analytical Solution

As previously mentioned, the PFC core specimen is cylindrical with a radius of R_c and thickness b_c. The coordinate system can be taken as cylindrical coordinates with the origin centered on the top surface of the core and the vertical z-direction positive downward. The flow during a constant head test has vertical flow from the standpipe with radius R_s centered on the top of the specimen and radial flow along the edges of the core radius R_c. The setup is shown schematically in Figure 5.1. The established head in the standpipe, h_s, is uniform over the source disk $0 \le r \le R_s,\ z = 0$. The constant head along the outflow boundary is taken as the datum, so that $h = 0$ on $r = R_c,\ 0 \le z \le b_c$.

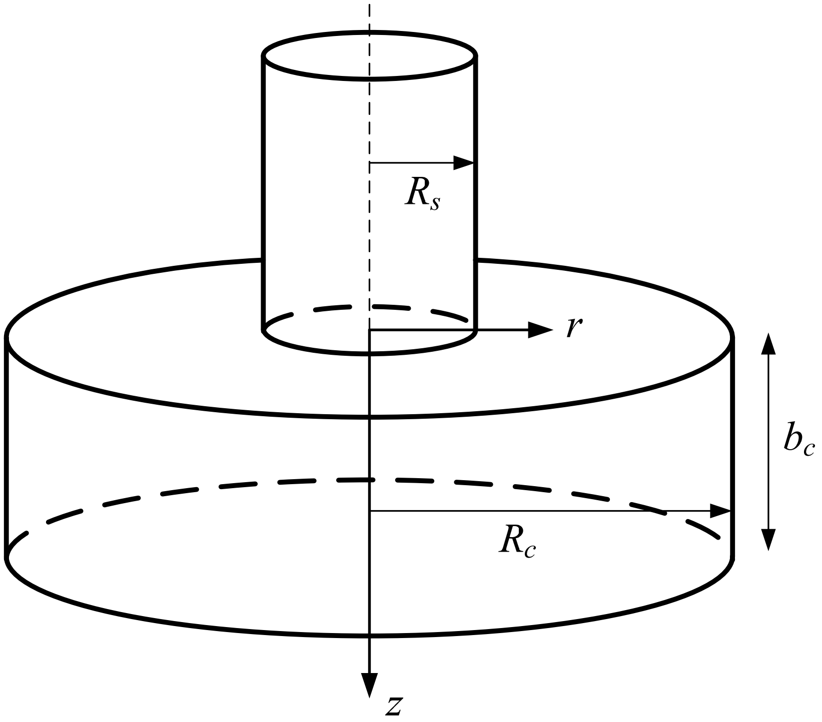

Figure 5.1 – Coordinate system and core dimensions

As mentioned in Section 2.1, flow through most typical porous media generally follows Darcy's law, so this linear relationship will be examined for the time being as a first approximation to the nonlinear case. Darcy's law as a vector function is given as:

$$\vec{q} = -K\vec{I} \tag{5.1}$$

For the PFC core setup described above, Equation (5.1) can be used in the continuity equation in cylindrical coordinates to determine the governing equation for Darcy flow. In two-dimensional cylindrical coordinates, the continuity equation can be written as:

$$\frac{1}{r}\frac{\partial}{\partial r}\left(r\vec{q}_r\right) + \frac{\partial \vec{q}_z}{\partial z} = 0 \tag{5.2}$$

And with the substitution of Darcy's law:

$$\frac{1}{r}\frac{\partial}{\partial r}\left(rK_r\vec{I}_r\right) + \frac{\partial K_z\vec{I}_z}{\partial z} = 0 \tag{5.3}$$

The general continuity equation assumes a constant fluid density, as well as no flow in the θ-direction. Assuming an isotropic hydraulic conductivity, $K_r = K_z = K$, and substituting the change in head for each hydraulic gradient results in the governing two-dimensional continuity equation for an isotropic hydraulic conductivity using Darcy's law:

$$\frac{1}{r}\frac{\partial}{\partial r}\left(r\frac{\partial h}{\partial r}\right)+\frac{\partial^2 h}{\partial z^2}=0 \tag{5.4}$$

The continuity equation in cylindrical coordinates for linear flow has been solved analytically by Carslaw and Jaeger (1959, pg. 215) through the use of Bessel functions. The Carslaw and Jaeger solution is for an infinite medium and has the following solution:

$$h^*(r,z)=\frac{2}{\pi}h_s\sin^{-1}\left(\frac{2R_s}{\sqrt{(r-R_s)^2+z^2}+\sqrt{(r+R_s)^2+z^2}}\right) \tag{5.5}$$

In Equation (5.5) the head $h^*(r,z)$ represents the head distribution with boundary conditions that apply to an infinite core (R_c and b_c approach infinity). However, the boundary conditions for the laboratory core specimens used in this research study are finite. Therefore, the applicable boundary conditions for the experimental setup are as follows:

$$h(r,z)=h_s(t) \qquad \left[0\le r\le R_s;\ z=0\right] \tag{5.6}$$

$$\frac{\partial h(r,z)}{\partial z}=0 \qquad \left[R_s<r\le R_c;\ z=0\right] \tag{5.7}$$

$$h(r,z)=0 \qquad \left[r=R_c;\ 0\le z\le b_c\right] \tag{5.8}$$

$$\frac{\partial h(r,z)}{\partial z}=0 \qquad \left[0\le r\le R_c;\ z=b_c\right] \tag{5.9}$$

The first boundary condition, Equation (5.6), states that the head on the source disk is equal to the head in the standpipe, which can change as a function of time. For testing purposes, the head on the standpipe is allowed to reach steady state such that it is a constant with respect to time. Equation (5.7) defines a no flow boundary on the top surface of the core for a radius greater than the radius of the standpipe. Equation (5.8) is the constant head at the outflow boundary, which is taken as the datum and set to a value of zero. Equation (5.9) defines a no flow boundary along the entire bottom surface of the core.

The volumetric flow rate can be determined from the head distribution through the following relation based on a linear flow relationship:

$$Q = -2\pi K_z \int_0^{R_s} r \frac{\partial h(r,0)}{\partial z} dr = -2\pi R_c K_r \int_0^{b_c} \frac{\partial h(R_c, z)}{\partial r} dz \tag{5.10}$$

The first part of Equation (5.10) calculates the flow rate that occurs across the inflow boundary, while the second part of the equation is the flow rate across the outflow boundary. The flow rate is not necessarily uniform over either the inflow or outflow boundary, but both equations should result in the same value to maintain continuity when Darcy's law is applicable.

Carslaw and Jaeger (1959) provide the solution to Equation (5.10) using the flow across the inflow boundary as follows:

$$Q = 4Kh_s R_s \tag{5.11}$$

Equation (5.11) has assumed an isotropic porous medium such that K_z is replaced with the generic hydraulic conductivity, K.

In order to determine the flow rate from the outflow boundary in Equation (5.10), a different approach is necessary. The effects of the finite vertical and radial dimensions are approximately addressed through the introduction of a linear shape factor F in Equation (5.11), which is changed to:

$$Q = 4Kh_s R_s F \tag{5.12}$$

Setting Equation (5.12) equal to the second part of Equation (5.10) shows that the linear shape factor is defined by:

$$F = -\frac{\pi}{2} \frac{R_c}{R_s} \frac{1}{h_s} \int_0^{b_c} \frac{\partial h(R_c, z)}{\partial r} dz \tag{5.13}$$

The practical issue becomes how to evaluate Equation (5.13) while taking into account the finite size of the PFC core specimen. The effects of the finite vertical dimension of the core are approximately addressed using the method of images in order to establish the no flow boundary conditions. However, the addition of each image (or image pair) alters the head both across the inflow and outflow boundaries. Head values are calculated using:

$$h(r,z;N_i) = \frac{2}{\pi} h_s \sum_{j=-N_i}^{N_i} \sin^{-1}\left(\frac{2R_s}{\sqrt{(r-R_s)^2 + (z+2jb_c)^2} + \sqrt{(r+R_s)^2 + (z+2jb_c)^2}} \right) \quad (5.14)$$

In Equation (5.14), $h(r,z;N_i)$ is the approximate solution to the Darcy continuity equation using the method of images, is a function of the *r*- and *z*-directions, and also depends on the number of image pairs, N_i. The image $j = 0$ corresponds to the basic solution given by Equation (5.5). The image $j = 1$ corresponds to a source disk located a distance $z = 2b_c$ below the surface ($z = 0$). This image attempts to make the plane $z = b_c$ a no flow boundary according to Equation (5.9); however, it causes an upward gradient across the $z = 0$ surface. The image $j = -1$ attempts to cancel this upward gradient, etc. This image solution satisfies the continuity Equation (5.4), and as the number of images is increased, the no flow boundary conditions are more closely met. The question remains of how well this approximate solution can satisfy the constant uniform head conditions along the inflow and outflow boundaries.

The effects of the finite radial dimension of the core can be addressed by nondimensionalizing the head distribution $h(r,z;N_i)$ for a unit head difference given the variable $H_u(r,z;N_i)$. This is accomplished by nondimensionalizing with respect to the head difference between the inflow and outflow areas. For the inflow area, the approximate head value can be described as the head at the location of mid-area within the standpipe. This mid-area location occurs at $r = R_s/\sqrt{2}$, $z = 0$. The head at the outflow boundary is given as $\bar{h}_b(r = R_c, b_c; N_i)$:

$$\bar{h}_b(r = R_c, b_c; N_i) = \frac{1}{b_c} \int_0^{b_c} h(R_c, z; N_i)\, dz \quad (5.15)$$

Therefore, the normalized unit head difference, H_u, can be calculated as:

$$H_u(r,z;N_i) = \frac{h(r,z;N_i) - \bar{h}_b(R_c, b_c; N_i)}{h(R_s/\sqrt{2}, 0; N_i) - \bar{h}_b(R_c, b_c; N_i)} \quad (5.16)$$

This results in a head distribution with a value of one at the standpipe inflow area and a value of zero at the outflow boundary. The contours of the head along the core are shown in Figures 5.2 and 5.3. These figures are normalized to the core radius, R_c, with Figure 5.2 having a vertical dimension of $b_c/R_c = 1$ and Figure 5.3 having $b_c/R_c = 0.5$. The inflow boundary for both figures occurs for $r/R_c < 0.25$, $z/b_c = 0$. The inflow is initially entirely vertical flow. The outflow boundary occurs at $r/R_c = 1$, and is purely radial. Furthermore, the comparison of the two figures shows that for a smaller relative core thickness, the head distribution becomes purely radial at a much faster rate.

The actual head distribution is equal to the head on the standpipe times the unit head distribution:

$$h(r,z;N_i) = h_s H_u(r,z;N_i) \tag{5.17}$$

Because this is a linear problem, the head can be nondimensionalized in this manner and the use of Equation (5.17) is appropriate. This will not be the case for nonlinear flow as shown in Section 5.3.7.

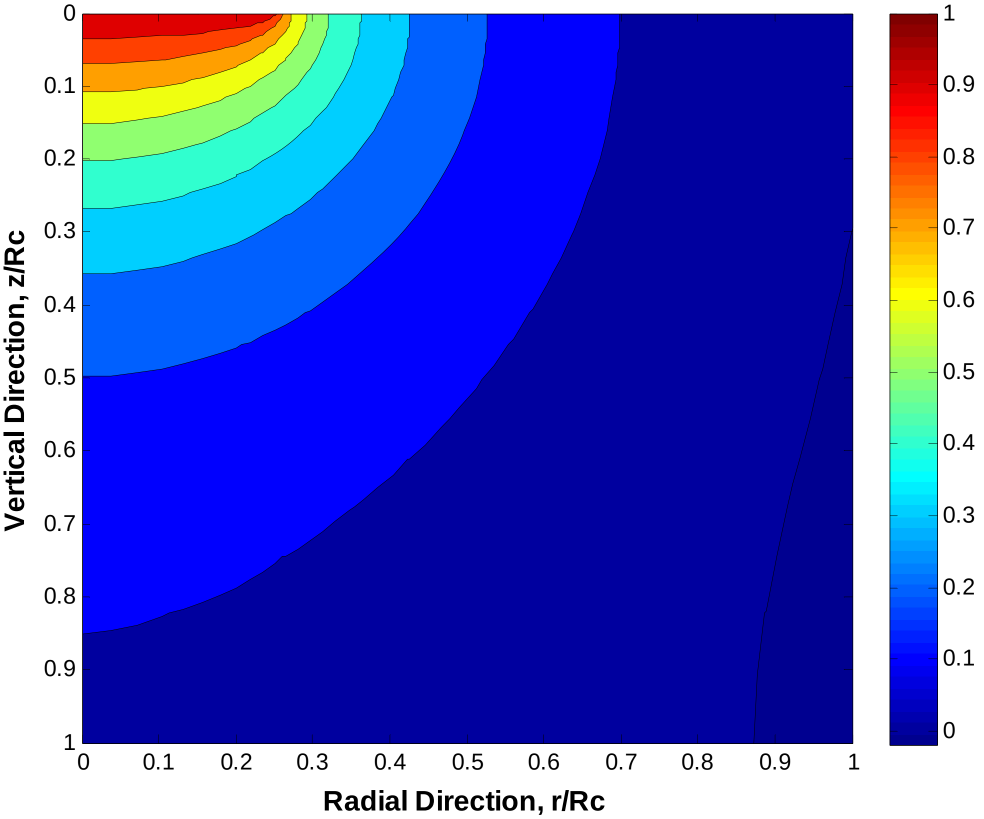

Figure 5.2 – Contour plot of normalized unit head distribution for linear flow using method of images analytic solution with R_s/R_c = 0.25 and b_c/R_c = 1

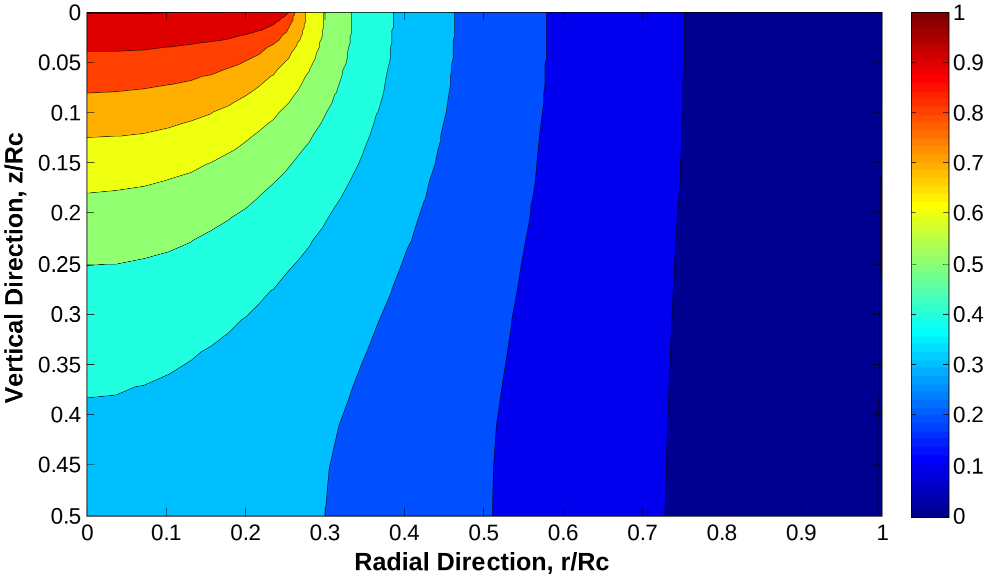

Figure 5.3 – Contour plot of normalized unit head distribution for linear flow using method of images analytic solution with $R_s/R_c = 0.25$ and $b_c/R_c = 0.5$

The method of images used in the solution shown in Equation (5.14) and the normalized solution in Equation (5.16) is used to create the no flow boundary at the top and bottom of the PFC core. However, this method has an impact on the constant head boundaries at the inflow and outflow areas. For the inflow area, the solution with $N_i = 0$ provides the exact constant head required by the boundary condition in Equation (5.6). As the value of N_i is increased, the head is no longer constant along this inflow boundary. On the other hand, for the outflow area, the solution with $N_i = 0$ does not provide a constant head at the outflow boundary as specified in Equation (5.8). As the value of N_i increases, the head approaches the required constant head at the outflow boundary. To summarize, as the number of images is increased, the solution better approximates the two no flow boundaries and the outflow constant head boundary, yet deviates from the required constant head inflow boundary.

The unit head difference approximate solution is evaluated in Figure 5.4. Figure 5.4(a) shows the calculated radial distribution of head across the inflow boundary for an example with $R_s/R_c = 0.25$ and $b_c/R_c = 0.5$, which is the same head distribution shown in

Figure 5.3. The solution without images ($N_i = 0$) exactly satisfies the boundary condition across the inflow surface. Addition of image pairs result in an increase in head at the center of the source area and a corresponding decrease in head near the boundary of the inflow area. However, with just a few images, the overall error is less than one-half percent from the unit value imposed. The use of $r = R_s \big/ \sqrt{2}$ for determining the head on the inflow boundary is the location where $H_u = 1$ in Figure 5.4(a) with the addition of image pairs. Figure 5.4(b) shows the head distribution across the outflow boundary. Addition of source images improves the approximate solution accuracy for a constant head along this boundary, with use of only a few images giving a solution within about 0.1 percent accuracy. The overall solution behavior is shown in Figure 5.4(c) with $N_i = 100$. This figure shows the vertical head distribution at different radial stations from the center of the specimen to the edge. The first two stations are within the source zone such that the head at the upper boundary is unity. The vertical gradient beneath the source region is greater towards the sides of the inflow boundary than in the middle of the inflow boundary. The radial gradient is largest along the upper no flow boundary, but the radial gradient becomes fairly uniform near the outflow boundary. Both vertical and horizontal flow components are important.

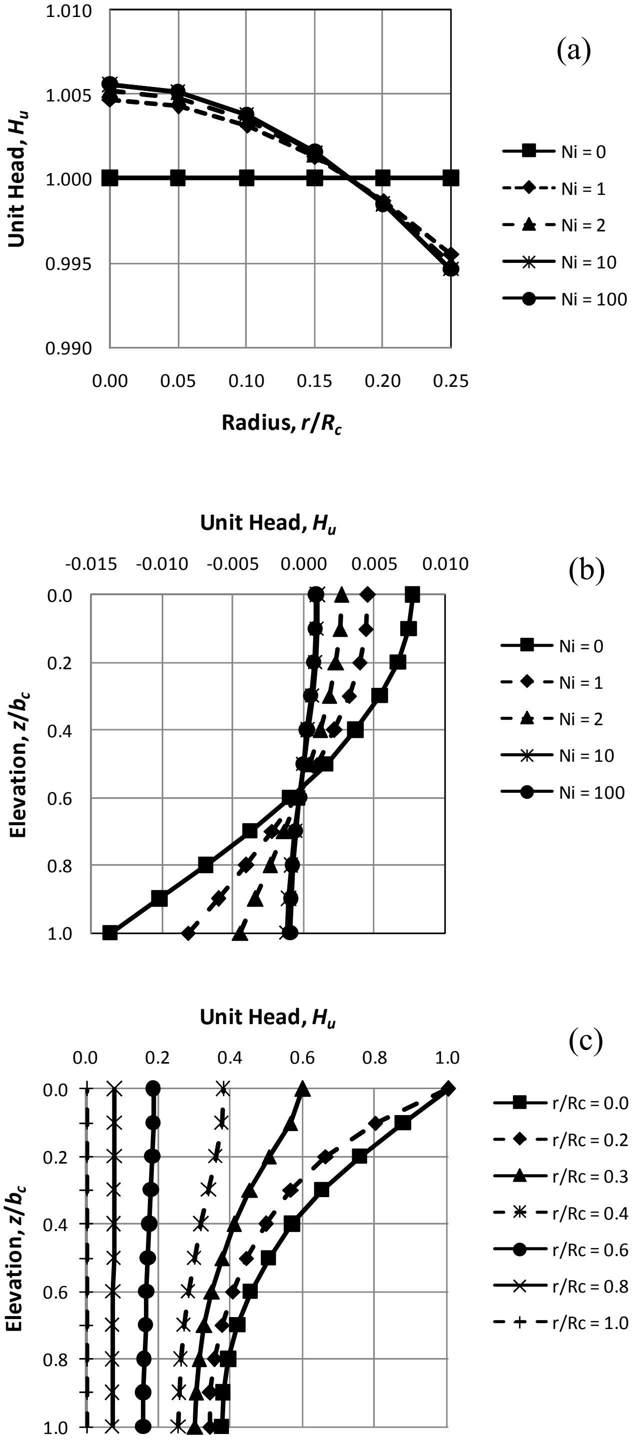

Figure 5.4 – Normalized unit head difference solution using method of images: (a) inflow boundary, (b) outflow boundary, (c) overall solution behavior for $N_i = 100$

The shape factor definition from Equation (5.13) and the approximate image solution from Equation (5.14) show that the linear shape factor is a function of the size of the core (specimen volume) and the radius of the standpipe under linear flow conditions. This may be expressed and calculated through a dimensionless form:

$$F = F\left(\frac{R_s}{R_c}, \frac{b_c}{R_c}\right) \tag{5.18}$$

The shape factor typically has a magnitude near unity for the linear flow conditions. For example, with the geometry used to calculate results shown in Figure 5.4, one can calculate $F(0.25,0.5) = 1.08$. Values for the shape factor F are presented in Table 5.1 for varying R_s/R_c and b_c/R_c. F is designated as a linear shape factor because it is determined from an approximate solution using the method of images of the linear Darcy-type flow equation. The linear shape factor cannot be used once nonlinear flow effects are taken into account.

Table 5.1 – Linear shape factor values using method of images

R_s/R_c \ b_c/R_c	**0.20**	**0.25**	**0.30**	**0.35**	**0.40**	**0.45**	**0.50**	**0.55**	**0.60**
0.05	0.911	0.956	0.985	1.004	1.017	1.027	1.034	1.039	1.042
0.10	0.826	0.900	0.950	0.985	1.010	1.029	1.042	1.052	1.060
0.15	0.765	0.856	0.922	0.970	1.006	1.032	1.052	1.067	1.079
0.20	0.722	0.824	0.901	0.960	1.005	1.039	1.065	1.084	1.100
0.25	0.693	0.802	0.888	0.955	1.008	1.048	1.080	1.104	1.123
0.30	0.675	0.789	0.882	0.956	1.015	1.062	1.099	1.127	1.150
0.35	0.666	0.784	0.883	0.963	1.028	1.080	1.122	1.155	1.181
0.40	0.664	0.787	0.891	0.977	1.047	1.104	1.150	1.186	1.216
0.45	0.670	0.797	0.906	0.997	1.072	1.134	1.184	1.224	1.256
0.50	0.682	0.814	0.928	1.024	1.104	1.170	1.224	1.268	1.303

If flow through the PFC core specimen experienced linear flow, the hydraulic conductivity could be determined from Equation (5.12) once a relationship between h_s and Q is determined. The use of this equation takes into account flow in two-dimensional cylindrical coordinates as well as the core geometry. However, this solution only applies to linear flow which follows Darcy's law. Therefore, although this is a valid solution, it does not apply to the nonlinear flow relationship observed in PFC. It is useful to provide an analytic solution in order to gain an understanding of how flow moves through the PFC core specimen which can be used to validate the more advanced numerical models which are described below.

5.2.2 Overview of Linear Numerical Model

The previous section describes an approximate analytical solution for two-dimensional linear flow through a core specimen using Darcy's law. The solution gives the head distribution throughout the core and the hydraulic conductivity can be calculated based on the relationship between the head on the standpipe h_s and the flow rate Q, as well as the core dimensions. A finite difference numerical model can be used to solve for the head distribution through the core with more precise inflow and outflow boundary conditions. The method of images used in the approximate analytical solution does not accurately meet the inflow and outflow boundary conditions. Therefore, a finite difference solution to the two-dimensional flow can be used to precisely meet these boundary conditions.

The finite difference model solves the same continuity equation given in Equation (5.4) with boundary conditions provided in Equations (5.6) through (5.9). Furthermore, since the flow problem is symmetric about the center of the core, only half of the flow domain needs to be modeled. Symmetry introduces an additional boundary condition:

$$\frac{\partial h(r,z)}{\partial r} = 0 \qquad \left[r = 0;\ 0 \le z \le b_c\right] \tag{5.19}$$

Equation (5.19) states that the change in head in the radial direction is zero at the center of the core. Therefore, there is no radial flow across the center of the core. The finite difference model solves the continuity equation together with the five boundary conditions.

The following subsections describe the grid generation used in the finite difference model, the method used to address the singularity at $r = 0$ in the continuity equation, the differencing scheme used to approximate the partial differential equation, and finally some results for the linear head distribution through the core specimen.

5.2.3 Grid Generation

The numerical model uses a finite difference scheme to solve the partial differential continuity equation in two-dimensional cylindrical coordinates. The finite difference grid used to solve this equation is described in detail in this section. Of particular interest in this finite difference model is to accurately model the core specimen geometry. Therefore, the grid must have nodes located precisely at the locations of the boundary conditions. This forces a node to be created at the center of the core $r = 0$. In addition, the boundary conditions change at the location of the standpipe radius, so a node must exist precisely at $r = R_s$. Finally, the core radius and core thickness also must be modeled correctly. As a result, the domain of the grid extends in the r-direction until $r = R_c$ and in the z-direction until $z = b_c$.

The largest hydraulic gradients are located directly under the standpipe. As the flow moves away from the standpipe, the gradients decrease in the vertical direction due to the no flow boundary. Also, as flow exits the core, the gradients are smaller due to the diverging nature of the flow. Because the highest gradients are located immediately under the standpipe, it is beneficial to refine the grid in this area. This is accomplished in the vertical direction by using an expansion ratio. The expansion ratio in the vertical direction is denoted as r_{ez}, and a vertical expansion ratio of $r_{ez} = 1.1$ is used for this finite difference scheme. This means that the difference between nodes is 10% larger than the previous difference for increasing z.

As previously mentioned, it is necessary to precisely model the radius of the standpipe. Therefore, a node is created at $r = R_s$, in addition to nodes at $r = 0$ and $r = R_c$.

The nodes placed between these three points are also spaced with an expansion factor. The number of elements is explicitly stated for $0 \le r \le R_s$ and for $R_s \le r \le R_c$. Instead of using constant spacing in each of these domains, an expansion ratio is used in order to maintain the second order scheme described in Section 5.2.5 (Ferziger and Peric, 2002). Two separate expansion ratios are necessary in the radial direction: r_{er1} is the expansion ratio from $r = R_s$ to $r = 0$, and r_{er2} is the expansion ratio from $r = R_s$ to $r = R_c$.

The expansion ratios are calculated based on the initial element size around $r = R_s$. The radial elements on either side of the node at $r = R_s$ have a specified spacing of $\Delta r = 0.15$ cm. Both radial expansion ratios are calculated by this initial spacing and the remaining length of the domain (either R_s or $R_c - R_s$ depending on the direction in question). The initial spacing is given as:

$$\Delta r = \frac{L(1 - r_{er})}{1 - r_{er}^{n_i}} \tag{5.20}$$

L in Equation (5.20) is either R_s or $R_c - R_s$ depending on the direction in question, n_i is the number of elements in that direction, and r_{er} is either r_{er1} or r_{er2} depending on the direction. The only unknown in Equation (5.20) is r_{er} and it can be determined from a Newton-Raphson method (c.f. Ferziger and Peric, 2002). The Newton-Raphson method uses the function $f(r_{er})$ and its derivative $f'(r_{er})$ to extend a tangent line at the current guess of r_{er} until it crosses zero, and uses that location as the second guess of r_{er}. The method is repeated until the change in r_{er} values is very small. The function and its derivative used for this root-finding technique are:

$$f(r_{er}) = \frac{1 - r_{er}}{1 - r_{er}^{n_i}} - \frac{\Delta r}{L} \tag{5.21}$$

$$\frac{\partial f(r_{er})}{\partial r_{er}} = f'(r_{er}) = -\frac{r_{er}^{n_i}(n_i - 1) - r_{er}^{n_i - 1} n_i + 1}{\left(r_{er}^{n_i} - 1\right)^2} \tag{5.22}$$

The change in r_{er} values is designated as dr_{er} and is equal to:

$$dr_{er} = \frac{-f(r_{er})}{f'(r_{er})} \tag{5.23}$$

The initial guess value of r_{er} used is 1.1. This value can then be used in $f(r_{er})$ and $f'(r_{er})$ to determine dr_{er}, from which the second guess value can be determined. The process is repeated until dr_{er} becomes nearly zero. At this point, the root to Equation (5.20) has been found.

A typical grid generated from this numerical model is shown in Figure 5.5. The domain of this grid is $R_c = 10.922$ cm and $b_c = 3.468$ cm. This is the typical domain of a PFC core specimen and $R_s = 1.878$ cm, which is the same value used during experimental testing. This grid has 40 elements in the z-direction, 10 elements for $r \leq R_s$, 30 elements for $R_s \leq r \leq R_c$, and the following expansion ratios: $r_{ez} = 1.1$, $r_{er1} = 1.049$, and $r_{er2} = 1.044$.

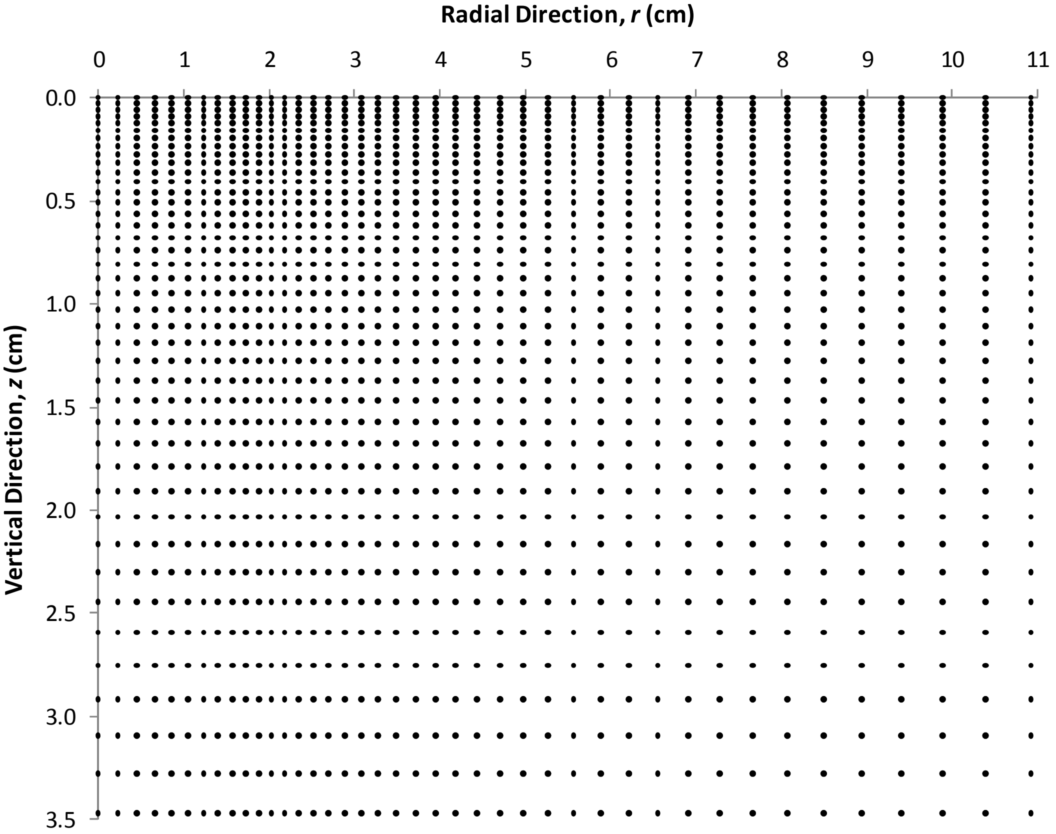

Figure 5.5 – Typical grid generation

5.2.4 Singularity Removal for Linear Model

The continuity equation in cylindrical coordinates as written in Equation (5.4) has a singularity at $r = 0$. In other words, the equation cannot be solved for $r = 0$ due to the $1/r$ term approaching infinity. Therefore, this singularity must be removed in order to properly model the equation at $r = 0$. In order to accomplish this we can follow a similar procedure outlined by Smith (1965, pg. 44). The continuity equation written in Equation (5.4) can be expanded as follows:

$$\frac{1}{r}\frac{\partial h}{\partial r}+\frac{\partial^2 h}{\partial r^2}+\frac{\partial^2 h}{\partial z^2}=0 \tag{5.24}$$

The singularity exists in the first term only and results in a value of 0/0 for $r = 0$ due to the symmetry boundary condition in Equation (5.19).

As described by Smith (1965), the first derivative can be expanded using a Maclaurin expansion to obtain:

$$\frac{\partial h(r,z)}{\partial r}=\frac{\partial h(0,z)}{\partial r}+r\frac{\partial^2 h(0,z)}{\partial r^2}+\frac{r^2}{2}\frac{\partial^3 h(0,z)}{\partial r^3}+\ldots \tag{5.25}$$

The first term on the right hand side of Equation (5.25) is equal to zero due to the symmetry boundary condition. If we drop the higher order terms, we can approximate the first derivative as:

$$\frac{\partial h(r,z)}{\partial r}\approx r\frac{\partial^2 h(0,z)}{\partial r^2} \tag{5.26}$$

Putting the above equation into the continuity Equation (5.24) and canceling the r terms gives the following continuity equation for $r = 0$:

$$2\frac{\partial^2 h}{\partial r^2}+\frac{\partial^2 h}{\partial z^2}=0 \tag{5.27}$$

The use of Equation (5.27) removes the singularity at $r = 0$ and can be used in the finite difference model to determine the head at the center of the core.

5.2.5 Linear Model Differencing Scheme

The differencing scheme used to solve the partial differential equation is a second order, five point central difference scheme (CDS). The computational node is shown in

Figure 5.6 for node *i,j* where *i* represents the radial direction and *j* represents the vertical direction. Node *i,j* is located at radial location r_i and vertical location z_j.

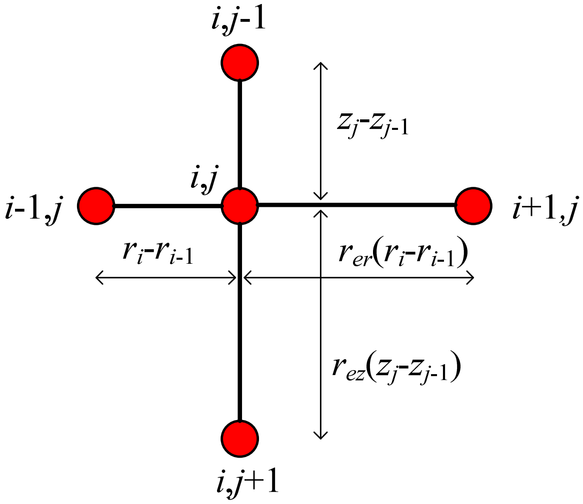

Figure 5.6 – Computational node schematic for linear model

The equation being solved for the linear solution is the two-dimensional continuity equation in cylindrical coordinates. However, the Crank-Nicolson method will be used to solve the equation in pseudo-time. This is essentially the time dependent solution, except the hydraulic conductivity has been removed from the equation. Therefore, the equation being solved for the linear solution is:

$$\frac{\partial h}{\partial t} = \frac{1}{r}\frac{\partial h}{\partial r} + \frac{\partial^2 h}{\partial r^2} + \frac{\partial^2 h}{\partial z^2} \tag{5.28}$$

Equation (5.28) can be discretized using the computation node discussed above. The three terms on the right hand side are approximated using the equations presented below with a CDS. Due to the use of an expansion ratio, the approximation depends on the location of the computational node. However, as described by Ferziger and Peric (2002), the CDS with the use of an expansion ratio results in a second order approximation.

$$\left.\frac{1}{r}\frac{\partial h}{\partial r}\right|_{i,j} \approx \frac{1}{r_i}\frac{h_{i+1,j}\left(r_i - r_{i-1}\right)^2 + h_{i,j}\left[\left(r_{i+1} - r_i\right)^2 - \left(r_i - r_{i-1}\right)^2\right] - h_{i-1,j}\left(r_{i+1} - r_i\right)^2}{\left(r_{i+1} - r_{i-1}\right)\left(r_{i+1} - r_i\right)\left(r_i - r_{i-1}\right)} \tag{5.29}$$

$$\left.\frac{\partial^2 h}{\partial r^2}\right|_{i,j} \approx 2\frac{h_{i+1,j}\left(r_i - r_{i-1}\right) - h_{i,j}\left(r_{i+1} - r_{i-1}\right) + h_{i-1,j}\left(r_{i+1} - r_i\right)}{\left(r_{i+1} - r_{i-1}\right)\left(r_{i+1} - r_i\right)\left(r_i - r_{i-1}\right)} \tag{5.30}$$

$$\left.\frac{\partial^2 h}{\partial z^2}\right|_{i,j} \approx 2\frac{h_{i,j+1}\left(z_j - z_{j-1}\right) - h_{i,j}\left(z_{j+1} - z_{j-1}\right) + h_{i,j-1}\left(z_{j+1} - z_j\right)}{\left(z_{j+1} - z_{j-1}\right)\left(z_{j+1} - z_j\right)\left(z_j - z_{j-1}\right)} \tag{5.31}$$

The Crank-Nicolson method is an implicit method used to approximate the time derivative for the head distribution at time level n+1 from the average of the head distributions at time levels n and n+1. The time derivative is approximated as follows:

$$\left.\frac{\partial h}{\partial t}\right|_{i,j} \approx \frac{h_{i,j}^{\ \ n+1} - h_{i,j}^{\ \ n}}{\Delta t} \approx \frac{1}{2}\left\{-\right\}^{n+1} + \frac{1}{2}\left\{-\right\}^{n} \tag{5.32}$$

Equation (5.32) is the Crank-Nicolson approximation of the time derivative where the terms in braces {-} refer to the three terms on the right hand side (RHS) approximated using Equations (5.29) through (5.31) at time levels n and n+1. A similar approach is used at the center of the core for $r = 0$. However, instead, the equation being solved is described in Equation (5.27). Only a slight modification is necessary to the discretization scheme in order to solve this equation at the centerline. The initial condition for the head distribution is taken as 10^{-6} throughout the entire core except at the inflow and outflow boundaries.

The result of the Crank-Nicolson method is an implicit system of equations which must be solved as a system of linear equations in matrix form. A penta-diagonal matrix is formed from this system of equations as shown in Figure 5.7 where E, W, P, S, and N are the coefficients associated with the east node, west node, computational node, south node, and north node, respectively. These coefficients can be determined from the approximations of the derivatives in Equations (5.29) through (5.31). The matrix of coefficients is multiplied times the vector of unknown head values at time level n+1. The RHS is a vector of known head values times the corresponding coefficients. The system of equations can be easily solved with a banded LU decomposition solver. The time step used in this model is Δt = 0.01 sec and the computational time needed to reach steady state conditions is on the order of one minute.

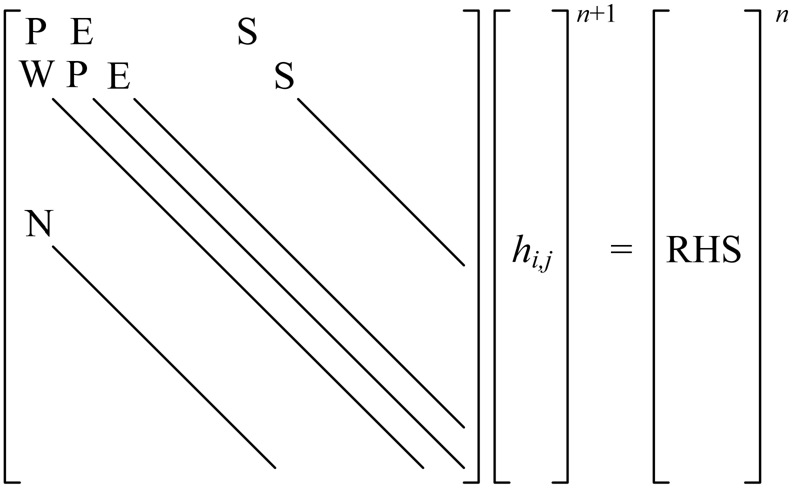

Figure 5.7 – System of linear equations

Using the described Crank-Nicolson method, the penta-diagonal matrix has a bandwidth equal to the number of elements in the radial direction. The five coefficients corresponding to the interior node calculations can be determined as:

$$\mathrm{E} = -\frac{\Delta t\left(r_i - r_{i-1}\right)^2 + 2\Delta t r_i\left(r_i - r_{i-1}\right)}{2r_i\left(r_{i+1} - r_{i-1}\right)\left(r_{i+1} - r_i\right)\left(r_i - r_{i-1}\right)} \tag{5.33}$$

$$\mathrm{W} = \frac{\Delta t\left(r_{i+1} - r_i\right)^2 - 2\Delta t r_i\left(r_{i+1} - r_i\right)}{2r_i\left(r_{i+1} - r_{i-1}\right)\left(r_{i+1} - r_i\right)\left(r_i - r_{i-1}\right)} \tag{5.34}$$

$$\begin{aligned}\mathrm{P} = 1 - \frac{\Delta t\left[\left(r_{i+1} - r_i\right)^2 - \left(r_i - r_{i-1}\right)^2\right] + 2\Delta t r_i\left(r_{i+1} - r_{i-1}\right)}{2r_i\left(r_{i+1} - r_{i-1}\right)\left(r_{i+1} - r_i\right)\left(r_i - r_{i-1}\right)} + \\ + \frac{\Delta t\left(z_{j+1} - z_{j-1}\right)}{\left(z_{j+1} - z_{j-1}\right)\left(z_{j+1} - z_j\right)\left(z_j - z_{j-1}\right)}\end{aligned} \tag{5.35}$$

$$\mathrm{S} = -\frac{\Delta t\left(z_j - z_{j-1}\right)}{\left(z_{j+1} - z_{j-1}\right)\left(z_{j+1} - z_j\right)\left(z_j - z_{j-1}\right)} \tag{5.36}$$

$$\mathrm{N} = -\frac{\Delta t\left(z_{j+1} - z_j\right)}{\left(z_{j+1} - z_{j-1}\right)\left(z_{j+1} - z_j\right)\left(z_j - z_{j-1}\right)} \tag{5.37}$$

$$\mathrm{RHS}^n = -\mathrm{E}h_{i+1,j}{}^n - \mathrm{W}h_{i-1,j}{}^n + \left(2 - \mathrm{P}\right)h_{i,j}{}^n - \mathrm{S}h_{i,j+1}{}^n - \mathrm{N}h_{i,j-1}{}^n \tag{5.38}$$

Slight modifications to the above coefficients are needed for the nodes on the boundaries due to the various boundary conditions. It is interesting to note that the above coefficients do not depend on the value of hydraulic conductivity. Furthermore, the head distribution is unchanged for the same nondimensional core geometry (R_s/R_c and b_c/R_c) and a normalized head value. This is useful because it allows for scaling of the head distribution if the core geometry is known. This will not be the case for nonlinear flow, as shown in Section 5.3.7.

Steady-state is achieved based on the value of the maximum relative change in head at each node. Therefore, the convergence criterion is determined from the L_∞-norm. The L_∞-norm is given as:

$$L_\infty = \max_{i,j}\left|\frac{h_{i,j}^{\;n+1} - h_{i,j}^{\;n}}{h_{i,j}^{\;n+1}}\right| < \varepsilon \tag{5.39}$$

Convergence is achieved when the L_∞-norm is less than $\varepsilon = 10^{-6}$. The Crank-Nicolson method is unconditionally stable meaning that the selection of Δt will not result in an unstable solution.

As previously mentioned, the input to the model is the core geometry (R_s, R_c, and b_c), the standpipe head (h_s), and the hydraulic conductivity ($1/a$). Once the continuity equation is solved and the head distribution through the core determined, the flow rate can be calculated based on the outflow gradient. The flow rate is found from $Q = qA$, where $q = I/a$ from Darcy's law and $A = 2\pi R_c dz$. The result is the second part of Equation (5.10). The flow rate can be approximated from the head distribution as follows:

$$Q = \frac{2\pi R_c}{a}\sum_{j=1}^{n_z-1}\frac{h_{n_r-1,j} - h_{n_r,j}}{R_c - r_{n_r-1}}\left(\frac{r_{ez}\left(z_j - z_{j-1}\right) + z_{j+1} - z_j}{r_{ez}+1}\right) \tag{5.40}$$

Equation (5.40) gives the approximation of the flow rate for all internal nodes. A slight modification to the above equation is needed for the two nodes on the edge of the domain. n_z is the number of elements in the vertical direction and n_r is the number of elements in the radial direction.

5.2.6 Linear Numerical Model Results

The linear numerical model using the above described discretization scheme and Crank-Nicolson method can be used to solve for the head distribution through a core specimen with a given core geometry. The grid refinement analysis presented in Section 5.4.1 suggests a domain of 40×40 elements as used here will produce accurate results. Figure 5.8 shows the normalized head distribution for a core with $R_s = 2.5$ cm, $R_c = 10$ cm, and $b_c = 5$ cm. This head distribution is comparable to the method of images solution shown in Figure 5.3.

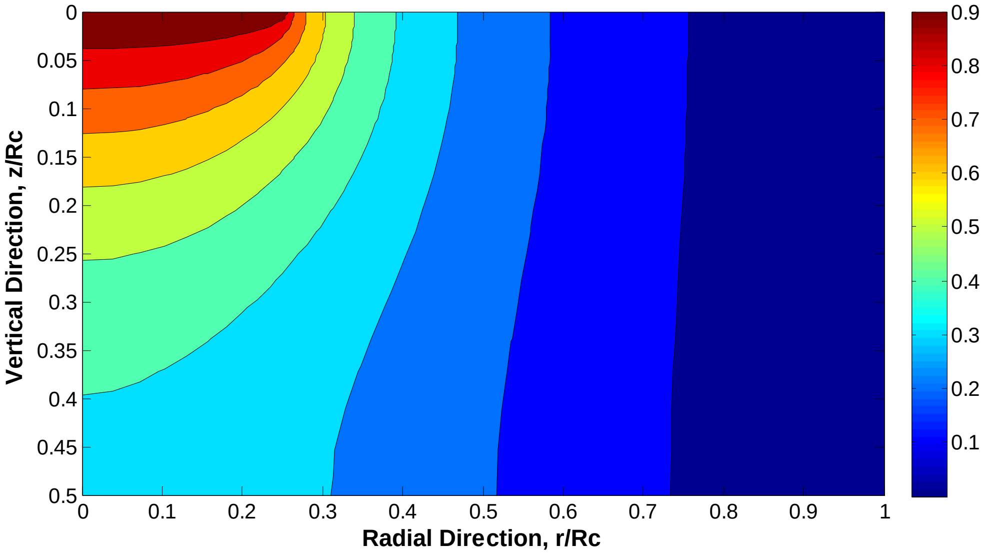

Figure 5.8 – Contour plot of normalized unit head distribution for linear flow using Darcy numerical model solution with $R_s/R_c = 0.25$ and $b_c/R_c = 0.5$

The boundary conditions, particularly the inflow and outflow known head boundaries, are more accurately represented for the linear numerical model. A comparison between the method of images solution and the linear numerical model solution can be conducted by calculating the difference between the head values at each node. The relative difference, or percent difference, is not desirable for this comparison because the method of images solutions calculates very small head values near the outflow boundary which cause the percent difference values to increase drastically. Therefore, a contour plot of the method of images head minus the linear numerical model head is shown in Figure 5.9. Clearly, the largest difference between the two models is near the location of the standpipe. At this location, the boundary conditions change from a known head boundary to a no flow boundary. For this reason, the grid used is refined near the standpipe location as mentioned in Section 5.2.3 using the expansion ratios.

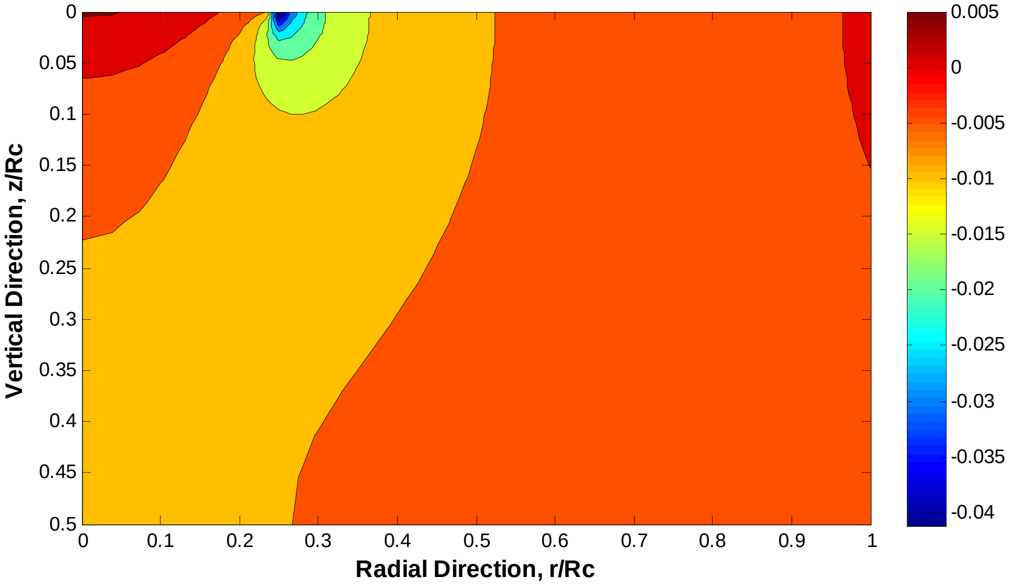

Figure 5.9 – Contour plot of head difference between method of images solution and linear numerical model solution with R_s/R_c = 0.25 and b_c/R_c = 0.5

Finally, a comparison of the outflow rates for both the method of images solution and the linear numerical model solution can be compared. The outflow rate can be determined in one of two ways: from the Carslaw and Jaeger equation modified for a finite core geometry using the linear shape factor as described in Equation (5.12), or from the outflow hydraulic gradient as determined from the head distribution assuming purely radial flow as described in Equation (5.40). For the method of images solution, the two outflow rates are approximately the same, to within less than one percent error. The reason for this slight difference is due to the minimal error in the boundary conditions of the method of images solution. For the linear numerical model based on Darcy's law, the two outflow rates are exactly the same. There is a small error between the method of images flow rate and linear numerical model flow rate, again due to the improper boundary conditions of the method of images. Figure 5.10 shows the standpipe head as a function of flow rate for both solutions using a core geometry of R_s = 2.5 cm, R_c = 10 cm, and b_c = 5 cm. Two values of the hydraulic conductivity are specified to determine the flow rates: K = 1 cm/s and K = 0.5 cm/s.

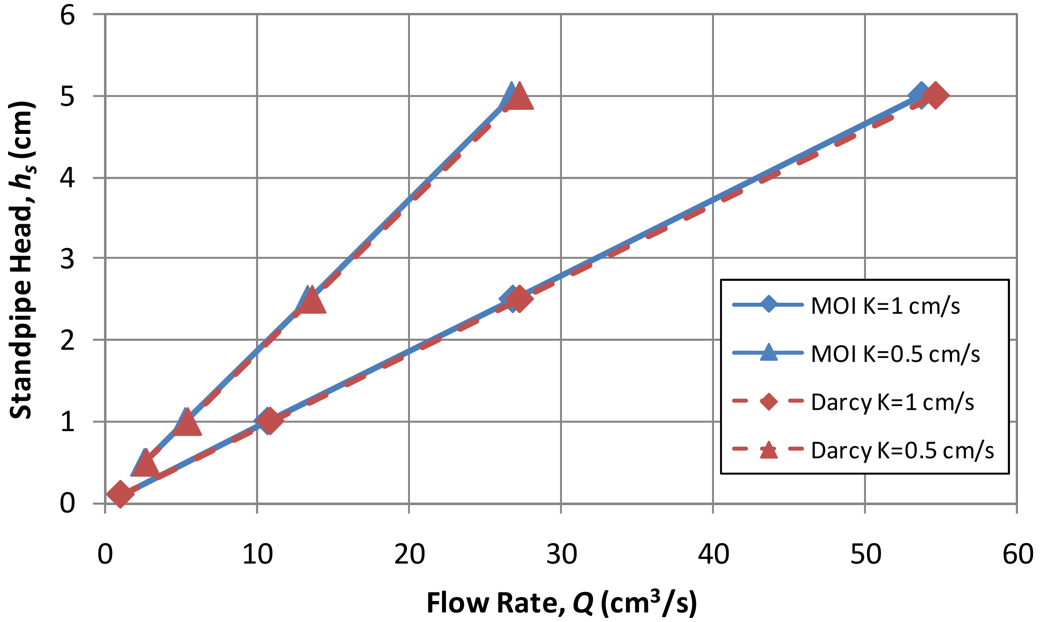

Figure 5.10 – Comparison of flow rates determined from method of images and linear numerical model solutions with R_s/R_c = 0.25 and b_c/R_c = 0.5

Clearly, the calculated flow rates for both solutions are approximately the same, meaning our linear numerical model produces the results we would expect. Furthermore, the relationship between the standpipe head and flow rate is linear, also as anticipated. The two hydraulic conductivity values shown in Figure 5.10 also behave as predicted. Specifically, the slopes of the lines are a function of 1/K. The line corresponding to K = 0.5 cm/s is exactly twice the slope of the line for K = 1 cm/s.

5.3 Modeling of Nonlinear Flow

5.3.1 Overview of Nonlinear Numerical Model

Section 5.2.5 describes the finite difference model that was created to solve the linear flow problem using Darcy's law. Although this model provides information on the general head distribution through the core, it is not applicable for flow through a PFC core. Experimental tests have shown a nonlinear relationship through PFC core specimens which can be modeled with the Forchheimer equation. The objective of the nonlinear numerical model is the same as before: to solve the two-dimensional continuity equation in cylindrical coordinates. However, now instead of using Darcy's law to determine the fluid specific discharge in the continuity Equation (5.2), the Forchheimer equation must be used. The specific discharge as given by the Forchheimer equation is:

$$q = \frac{a}{2b}\left[\sqrt{1+\frac{4b}{a^2}I} - 1\right] \tag{5.41}$$

Equation (5.41) is the specific discharge as determined from the nonlinear Forchheimer equation. Similar to the linear case using Darcy's law, the specific discharge is input into the continuity equation in order to get a partial differential equation in terms of head. As shown in the following subsection, the resulting equation does not have the proper invariance properties to simply substitute Equation (5.41) into the continuity equation and solve. Therefore, a more advanced approach is needed to properly model the continuity equation using the Forchheimer equation.

The nonlinear numerical model has the same domain as the linear model; namely, the radius of the core specimen and the thickness of the PFC layer. Due to symmetry it is only necessary to model half of the core. The same boundary conditions apply in the nonlinear flow case as were used in the linear model. The five boundary conditions are given in Equations (5.6) through (5.9) and the symmetry boundary condition Equation (5.19). The objective of the nonlinear model is to input the core geometry (R_s, R_c, and b_c) for a known standpipe head (h_s) and assumed porous media properties (a and b), and calculate the outflow rate (Q). For multiple values of h_s, a curve of h_s versus Q can be created which will be nonlinear. From this curve the two modified Forchheimer coefficients (α and β) can be determined and compared to laboratory results. With the assumed values of the original Forchheimer coefficients, the values of the modified Forchheimer coefficients can be calculated. This relationship can be used to estimate the original Forchheimer coefficients from the known modified Forchheimer coefficients obtained through experimental testing. Because the finite difference model is based on the original Forchheimer equation, an assumed value of the original Forchheimer coefficients must be made.

The finite difference model used to solve the continuity equation based on the Forchheimer equation requires a grid to approximate the partial differential equation. The same grid generation described in Section 5.2.3 for the linear model is used for the nonlinear model as well. As previously mentioned, this grid creates a node at the location of the standpipe in order to properly model the standpipe radius boundary. Expansion ratios are used in all directions in order to have a fine mesh on the upper core surface near the standpipe.

5.3.2 Invariance Properties of Forchheimer Equation

The Forchheimer equation does not have the proper invariance properties to be used in two-dimensional cylindrical coordinates without some additional investigation. As mentioned in Section 2.2.1 the Forchheimer equation has been used in two-dimensional flow problems, but the quadratic term is typically taken as the magnitude of the specific discharge times its vector. The source of the invariance problems is outlined below, followed by the suggested method for avoiding the problem and the proper approach used in the numerical model.

The Forchheimer equation is given as:

$$I = aq + bq^2 \tag{5.42}$$

from which the specific discharge is given in Equation (5.41). For two-dimensional flow in cylindrical coordinates, there is flow in both the radial and vertical directions. The hydraulic gradient in the radial and vertical directions, respectively, is given as:

$$I_r = aq_r + bq_r^{\,2} \tag{5.43}$$

$$I_z = aq_z + bq_z^{\,2} \tag{5.44}$$

In Equations (5.43) and (5.44), I_r is the radial hydraulic gradient and q_r is the radial specific discharge, and similarly for I_z and q_z. For two-dimensional flow, the local hydraulic gradient is the sum of the squares of the radial and vertical gradients, which can be found using Equations (5.43) and (5.44):

$$I = \sqrt{I_r^{\,2} + I_z^{\,2}} = \sqrt{(aq_r)^2 + 2abq_r^{\,3} + \left(bq_r^{\,2}\right)^2 + (aq_z)^2 + 2abq_z^{\,3} + \left(bq_z^{\,2}\right)^2} \tag{5.45}$$

Similarly, the local specific discharge is the sum of the squares of the radial and vertical specific discharges. The radial and vertical specific discharges are found using Equation (5.41) with the appropriate direction for *q* and *I*. The local specific discharge is:

$$q = \sqrt{q_r^{\,2} + q_z^{\,2}} = \frac{a}{b}\sqrt{1 + \frac{b}{a^2}(I_r + I_z) - 0.5\sqrt{1 + \frac{4bI_r}{a^2}} + 0.5\sqrt{1 + \frac{4bI_z}{a^2}}} \tag{5.46}$$

If the local hydraulic gradient and local specific discharge given in Equations (5.45) and (5.46) are substituted into the Forchheimer Equation (5.42), an identity is not achieved which illustrates the source of the invariance problem. Therefore, using the specific discharge in Equation (5.41) in the continuity equation is not sufficient because the equation cannot be rotated to another system of coordinates and maintain the same value. This requires further investigation to create another representation of the Forchheimer equation which is rotational.

5.3.3 Governing Continuity Equation for Forchheimer Flow

For the linear Darcy's law, the hydraulic conductivity is considered the slope of the linear relationship. For the nonlinear case, the hydraulic conductivity is considered the slope of the nonlinear relationship for a zero specific discharge. As the specific discharge increases, the slope increases as well resulting in the nonlinear relationship. We can consider the slope (which is a function of specific discharge) to be an effective Forchheimer hydraulic conductivity, which is not a constant and is given the symbol K_F. Using this approach, the Forchheimer equation can be rewritten in vector notation as:

$$\vec{q} = K_F \vec{I} \tag{5.47}$$

where the scalar effective Forchheimer hydraulic conductivity is:

$$K_F = \frac{a}{2bI}\left[\sqrt{1+\frac{4b}{a^2}I} - 1\right] \qquad (5.48)$$

Equation (5.47) is a rotational vector representation of the Forchheimer equation and can be modeled in any coordinate system. However, for low Reynolds number (small hydraulic gradient), this equation does not approximate Darcy's law. Therefore, we need to find a representation of the Forchheimer specific discharge that represents Darcy's law as the hydraulic gradient approaches zero. This can be accomplished by looking at the ratio of the Forchheimer specific discharge in Equation (5.41) to the Darcy specific discharge in Equation (5.1), where $K = 1/a$:

$$\frac{q_F}{q_D} = \frac{K_F I}{KI} = \frac{a^2}{2bI}\left[\sqrt{1+\frac{4b}{a^2}I} - 1\right] = \Phi(r, z) \qquad (5.49)$$

$\Phi(r,z)$ in Equation (5.49) is a dimensionless quantity called the hydraulic conductivity ratio, and is the ratio of the effective Forchheimer hydraulic conductivity to the true Darcy hydraulic conductivity. The true hydraulic conductivity ($K = 1/a$) is a constant for Darcy flow, but the effective Forchheimer hydraulic conductivity is not constant and depends on the magnitude of the hydraulic gradient. In cylindrical coordinates, the hydraulic gradient depends on both the *r*- and *z*-directions, so that the hydraulic conductivity ratio is a function of both directions.

The Forchheimer specific discharge can now be determined from Equation (5.49) as follows:

$$\vec{q} = K_F \vec{I} = K\Phi\vec{I} \qquad (5.50)$$

Equation (5.50) is rotational for any system of coordinates, K is a constant that can either be isotropic or anisotropic, and Φ is a scalar which depends on the magnitude of the hydraulic gradient and is a function of both the *r*- and *z*-directions. Using Equation (5.50) in the continuity equation is the proper method to model nonlinear flow in two-dimensions. Additional investigation of the hydraulic conductivity ratio is required to ensure that the Forchheimer equation approaches Darcy's law for low hydraulic gradients and is discussed in the next subsection.

The objective of the nonlinear numerical model is to solve the continuity equation now using Equation (5.50) for the specific discharge. Plugging this into the continuity Equation (5.2) gives:

$$\frac{1}{r}\frac{\partial}{\partial r}\left(rK\Phi I_r\right)+\frac{\partial}{\partial z}\left(K\Phi I_z\right)=0 \tag{5.51}$$

Since *K* is assumed to be a constant, it can be taken out of the derivatives and dropped out of the equation for the isotropic case. Representing the gradients as the change in head for the corresponding direction, Equation (5.51) can be rewritten as:

$$\Phi\left(\frac{1}{r}\frac{\partial h}{\partial r}+\frac{\partial^2 h}{\partial r^2}+\frac{\partial^2 h}{\partial z^2}\right)+\frac{\partial \Phi}{\partial r}\frac{\partial h}{\partial r}+\frac{\partial \Phi}{\partial z}\frac{\partial h}{\partial z}=0 \tag{5.52}$$

Equation (5.52) is the governing partial differential equation for the head distribution for two-dimensional Forchheimer flow in cylindrical coordinates. Notice that the term in parentheses is the continuity equation for Darcy flow multiplied by the scalar hydraulic conductivity ratio. However, this term is not equal to zero (as in Darcy flow) because the head distribution does not match that produced by Darcy flow. The finite difference model will solve Equation (5.52) in order to determine the head distribution through the core.

5.3.4 Analysis of Hydraulic Conductivity Ratio

Now that the Forchheimer equation has been rewritten with proper invariance properties, we must determine whether this form of the Forchheimer equation approaches Darcy's law for small hydraulic gradients. This can be accomplished by taking the limit of the hydraulic conductivity ratio as the hydraulic gradient approaches zero. It can be shown that this limit is:

$$\lim_{I\to 0}\Phi=\lim_{I\to 0}\frac{a^2}{2bI}\left[\sqrt{1+\frac{4b}{a^2}I}-1\right]=1 \tag{5.53}$$

Therefore, the limit of the Forchheimer Equation (5.50) is:

$$\lim_{I\to 0}\vec{q}=\lim_{I\to 0}K\Phi\vec{I}=K\vec{I} \tag{5.54}$$

This is equivalent to Darcy's law, satisfying the requirement that the Forchheimer equation approaches Darcy's law for small hydraulic gradients.

A graphical approach can be used to show that the hydraulic conductivity ratio approaches a value of one for low hydraulic gradients. Using Equation (5.49) with a = 0.3 s/cm and b = 0.2 s^2/cm^2 results in Figure 5.11. This shows that for low hydraulic gradient (or low Re), the hydraulic conductivity ratio approaches a value of one, representing Darcy flow.

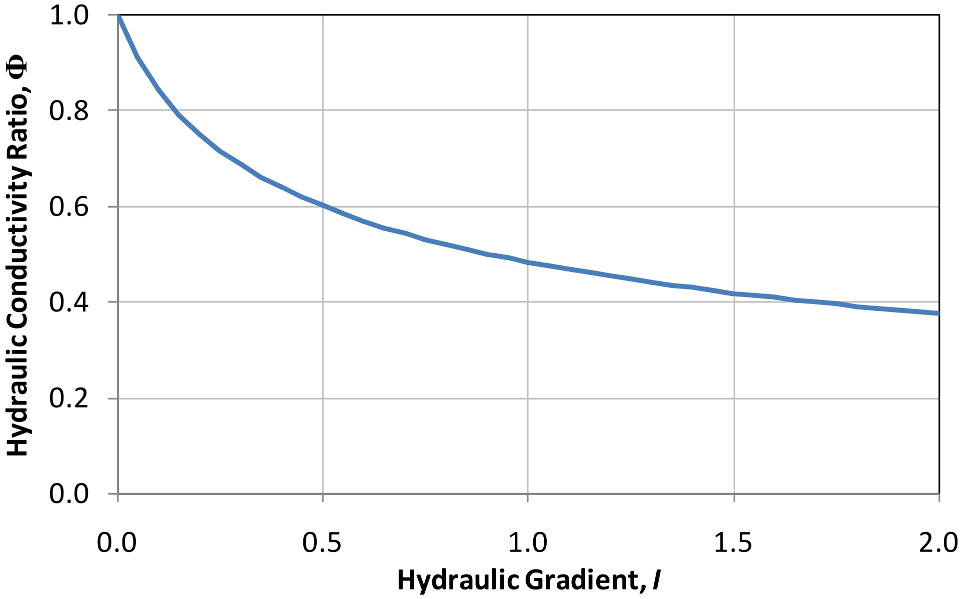

Figure 5.11 – Hydraulic conductivity ratio Φ as a function of hydraulic gradient

The hydraulic conductivity ratio is a scalar which is a function of both the r- and z-directions so that the hydraulic gradient used to calculate Φ is the local gradient given as the sum of the squares of the gradient in both directions. Φ can be found as follows:

$$\Phi(r,z) = \frac{a^2}{2b\sqrt{\left[I_r(r,z)\right]^2 + \left[I_z(r,z)\right]^2}}\left[\sqrt{1+\frac{4b}{a^2}\sqrt{\left[I_r(r,z)\right]^2+\left[I_z(r,z)\right]^2}}-1\right] \qquad (5.55)$$

where I_r and I_z are the partial derivates of the head in the r- and z-directions, respectively.

5.3.5 Singularity Removal for Nonlinear Model

The nonlinear model also has a singularity at $r = 0$ in the governing Equation (5.52). In order to remove the singularity, a similar approach to that used in Section 5.2.4 is needed. The first radial derivative can be approximated as before:

$$\frac{\partial h(r,z)}{\partial r} \approx r\frac{\partial^2 h(0,z)}{\partial r^2} \tag{5.56}$$

Substituting this into Equation (5.52) and recalling that the first radial derivative at $r = 0$ is equal to zero results in the following partial differential equation:

$$\Phi\left(2\frac{\partial^2 h}{\partial r^2} + \frac{\partial^2 h}{\partial z^2}\right) + \frac{\partial \Phi}{\partial z}\frac{\partial h}{\partial z} = 0 \tag{5.57}$$

Equation (5.57) is the governing partial differential equation for nonlinear flow at $r = 0$.

5.3.6 Nonlinear Model Differencing Scheme

The differencing scheme used to solve the governing nonlinear partial differential equation is the same as for the linear case: a second-order, five point CDS using the computational node in Figure 5.12. However, due to the addition of the hydraulic conductivity ratio, additional nodes are needed in order to properly determine Φ as it depends on additional nodes to find the hydraulic gradient. The suggested computational node for the nonlinear model is shown in Figure 5.12.

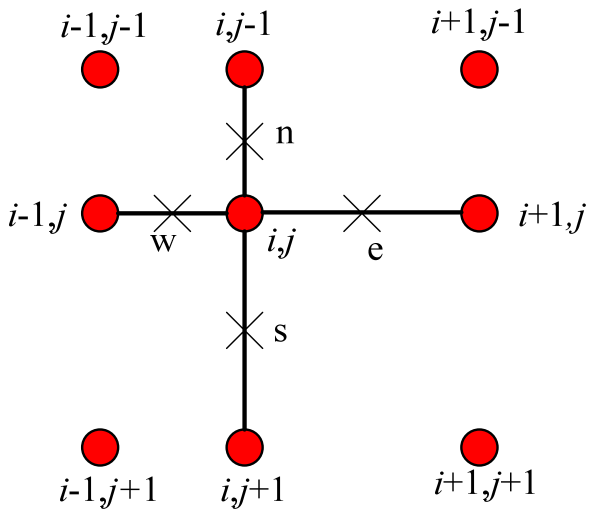

Figure 5.12 – Computational node schematic for nonlinear model

The simplest way to model the governing partial differential equation is in the following form:

$$\frac{1}{r}\frac{\partial}{\partial r}\left(r\Phi\frac{\partial h}{\partial r}\right)+\frac{\partial}{\partial z}\left(\Phi\frac{\partial h}{\partial z}\right)=0 \tag{5.58}$$

The terms in parentheses in Equation (5.58) can be taken as a new variable and the first derivative can be approximated at the half nodes shown in Figure 5.12 and designated as e, w, s, and n. The first derivative is approximated using the same method as before, described by Equation (5.29). However, instead of using $h_{i\text{-}1,j}$ and $h_{i+1,j}$, we will use h_{w} and h_{e}, which can be found as the average of $h_{i,j}$ and $h_{i\text{-}1,j}$ or $h_{i+1,j}$. Using the half node method requires an approximation for Φ at each half node location. Since Φ is determined based on the magnitude of the local hydraulic gradient, the four additional nodes are needed. For example, in order to approximate Φ_{w}, both the radial and vertical hydraulic gradients are needed. The radial hydraulic gradient is determined from $h_{i\text{-}1,j}$ and $h_{i,j}$, while the vertical hydraulic gradient is determined from the average of the two surrounding hydraulic gradients. The first vertical gradient is approximated using $h_{i\text{-}1,j\text{-}1}$, $h_{i\text{-}1,j}$, and $h_{i\text{-}1,j+1}$, and the second vertical gradient is approximated using $h_{i,j\text{-}1}$, $h_{i,j}$, and $h_{i,j+1}$. A similar approach is needed to find the hydraulic conductivity ratio at the other three half nodes.

The solution of the resulting approximation to the partial differential equation is found using the Gauss-Seidel iterative method (c.f. Smith, 1965). Time is not considered for this case due to the nonlinear nature of the problem. Therefore, the Gauss-Seidel iterative method is useful for simply finding the steady state solution. This method uses a known value of the head to calculate a new value of the head for a given node. That new value is then used to update the following node value and the solution is updated across the grid. Of particular interest is the initial guess at the head distribution needed to start the iterative process. For the nonlinear model, the initial guess used is the head distribution obtained from the linear model. Therefore, our initial guess is the solution for Darcy's law presented in Section 5.2.6, and is used to iterate upon in order to solve the continuity equation based on the Forchheimer equation. The Gauss-Seidel method is relatively quick at determining a solution, and the iteration is stopped based on the relative change in head at each node. The same convergence criterion described in Equation (5.39) is used for the nonlinear case. The L_∞-norm is used to determine convergence so that the relative change in head at all nodes is less than $\varepsilon = 10^{-6}$ when a solution is found. Computational time to run the model is on the order of approximately two minutes.

The Gauss-Seidel iterative method updates the current head value at a node of interest based on the surrounding nodes. Due to the numbering scheme used, the updated value (n+1) is calculated based on the updated values for the western and northern nodes, and the previous values (n) for the eastern and southern nodes. This is represented in Equation (5.59) below with the following coefficient values determined from the differencing scheme:

$$h_{i,j}{}^{n+1} = \frac{-1}{\mathrm{P}}\left(\mathrm{E}h_{i+1,j}{}^{n} + \mathrm{W}h_{i-1,j}{}^{n+1} + \mathrm{S}h_{i,j+1}{}^{n} + \mathrm{N}h_{i,j-1}{}^{n+1}\right) \tag{5.59}$$

where

$$\mathrm{E} = \frac{\Phi_{\mathrm{e}}\left(r_{i+1}+r_i\right)\left(r_i-r_{i-1}\right)^2}{r_i\left(r_{i+1}-r_{i-1}\right)\left(r_{i+1}-r_i\right)^2\left(r_i-r_{i-1}\right)} + \frac{2\Phi_{i,j}\left(r_i-r_{i-1}\right)^2\left[\left(r_{i+1}-r_i\right)^2-\left(r_i-r_{i-1}\right)^2\right]}{\left[\left(r_{i+1}-r_{i-1}\right)\left(r_{i+1}-r_i\right)\left(r_i-r_{i-1}\right)\right]^2} \tag{5.60}$$

$$\mathrm{W} = \frac{\Phi_{\mathrm{w}}\left(r_{i-1}+r_i\right)\left(r_{i+1}-r_i\right)^2}{r_i\left(r_{i+1}-r_{i-1}\right)\left(r_{i+1}-r_i\right)\left(r_i-r_{i-1}\right)^2} - \frac{2\Phi_{i,j}\left(r_{i+1}-r_i\right)^2\left[\left(r_{i+1}-r_i\right)^2-\left(r_i-r_{i-1}\right)^2\right]}{\left[\left(r_{i+1}-r_{i-1}\right)\left(r_{i+1}-r_i\right)\left(r_i-r_{i-1}\right)\right]^2} \tag{5.61}$$

$$\begin{aligned}\mathrm{P} = {} & \frac{2\Phi_{i,j}\left[\left(z_{j+1}-z_j\right)^2-\left(z_j-z_{j-1}\right)^2\right]^2}{\left[\left(z_{j+1}-z_{j-1}\right)\left(z_{j+1}-z_j\right)\left(z_j-z_{j-1}\right)\right]^2} - \frac{2\Phi_{\mathrm{s}}\left(z_j-z_{j-1}\right)^3+2\Phi_{\mathrm{n}}\left(z_{j+1}-z_j\right)^3}{\left(z_{j+1}-z_{j-1}\right)\left(z_{j+1}-z_j\right)^2\left(z_j-z_{j-1}\right)^2} + \\ & + \frac{2\Phi_{i,j}\left[\left(r_{i+1}-r_i\right)^2-\left(r_i-r_{i-1}\right)^2\right]^2}{\left[\left(r_{i+1}-r_{i-1}\right)\left(r_{i+1}-r_i\right)\left(r_i-r_{i-1}\right)\right]^2} + \\ & - \frac{\Phi_{\mathrm{e}}\left(r_{i+1}+r_i\right)\left(r_i-r_{i-1}\right)^3+\Phi_{\mathrm{w}}\left(r_{i-1}+r_i\right)\left(r_{i+1}-r_i\right)^3}{r_i\left(r_{i+1}-r_{i-1}\right)\left(r_{i+1}-r_i\right)^2\left(r_i-r_{i-1}\right)^2}\end{aligned} \tag{5.64}$$

$$\mathrm{S} = \frac{2\Phi_{\mathrm{s}}\left(z_j-z_{j-1}\right)^2}{\left(z_{j+1}-z_{j-1}\right)\left(z_{j+1}-z_j\right)^2\left(z_j-z_{j-1}\right)} + \frac{2\Phi_{i,j}\left(z_j-z_{j-1}\right)^2\left[\left(z_{j+1}-z_j\right)^2-\left(z_j-z_{j-1}\right)^2\right]}{\left[\left(z_{j+1}-z_{j-1}\right)\left(z_{j+1}-z_j\right)\left(z_j-z_{j-1}\right)\right]^2} \tag{5.63}$$

$$\mathrm{N} = \frac{2\Phi_{\mathrm{n}}\left(z_{j+1}-z_j\right)^2}{\left(z_{j+1}-z_{j-1}\right)\left(z_{j+1}-z_j\right)\left(z_j-z_{j-1}\right)^2} - \frac{2\Phi_{i,j}\left(z_{j+1}-z_j\right)^2\left[\left(z_{j+1}-z_j\right)^2-\left(z_j-z_{j-1}\right)^2\right]}{\left[\left(z_{j+1}-z_{j-1}\right)\left(z_{j+1}-z_j\right)\left(z_j-z_{j-1}\right)\right]^2} \tag{5.64}$$

When solving the system of equations using the Gauss-Seidel iterative method, the hydraulic conductivity ratio Φ remains at the previous iterative value. Therefore, Φ is not updated as the calculations proceed through the grid. The reason for lagging the calculation of Φ is that it depends on the hydraulic gradient at a point. So on one side of the computational node, the head value will be updated, but on the other side, the head will not be updated. Therefore, this would give an incorrect value of Φ since it depends on both values of the head. The lagging behind for Φ does not appear to produce any additional error or result in a significant increase in computational time.

It is interesting to note that the Forchheimer coefficients are included in the Φ term as shown in Equation (5.55). The nondimensional ratio b/a^2 is needed to calculate Φ, so the head distribution should be the same for a constant core geometry and any combination of b and a such that the b/a^2 ratio remains constant. Therefore, although the head distribution cannot be normalized for a unit head as in the linear case, the head distribution is a function of only one nondimensional parameter: b/a^2.

As before, the input to the model is the core geometry (R_s, R_c, and b_c), the standpipe head (h_s), and the original Forchheimer coefficients (a and b). Once the continuity equation is solved and the nonlinear head distribution through the core is determined, the flow rate can be calculated based on the outflow gradient. The flow rate is found from $Q = qA$, where $A = 2\pi R_c dz$ and q is found from the Forchheimer equation given in Equation (5.41). The outflow rate can be approximated from the head distribution for all internal nodes as follows:

$$Q = \frac{\pi R_c a}{b} \sum_{j=1}^{n_z - 1} \left[\sqrt{1 + \frac{4b}{a^2} \frac{h_{n_r - 1, j} - h_{n_r, j}}{R_c - r_{n_r - 1}}} - 1 \right] \left(\frac{r_{ez}\left(z_j - z_{j-1}\right) + z_{j+1} - z_j}{r_{ez} + 1} \right) \quad (5.65)$$

Equation (5.65) gives the approximation of the flow rate for all internal nodes. A slight modification to the above equation is needed for the two nodes on the edge of the domain. n_z is the number of elements in the vertical direction and n_r is the number of elements in the radial direction.

5.3.7 Nonlinear Numerical Model Results

The nonlinear numerical model using the above described discretization scheme and Gauss-Seidel iterative method can be used to solve for the head distribution through a core specimen with a given core geometry. The grid refinement analysis presented in Section 5.4.1 suggests a domain of 40×40 elements as used here will produce accurate results. Figure 5.13 shows the unit head distribution for a core with R_s = 2.5 cm, R_c = 10 cm, b_c = 5 cm, a = 1 s/cm, and b = 10 s^2/cm^2. This head distribution is comparable to the linear numerical model solution shown in Figure 5.8. It should be noted that although this figure is presented with the vertical and radial directions normalized to the core radius, the nonlinear solution does not scale in this way. As shown below, the nonlinear head distribution cannot be normalized. The following figures are presented in this way solely for comparison purposes to the linear numerical model results.

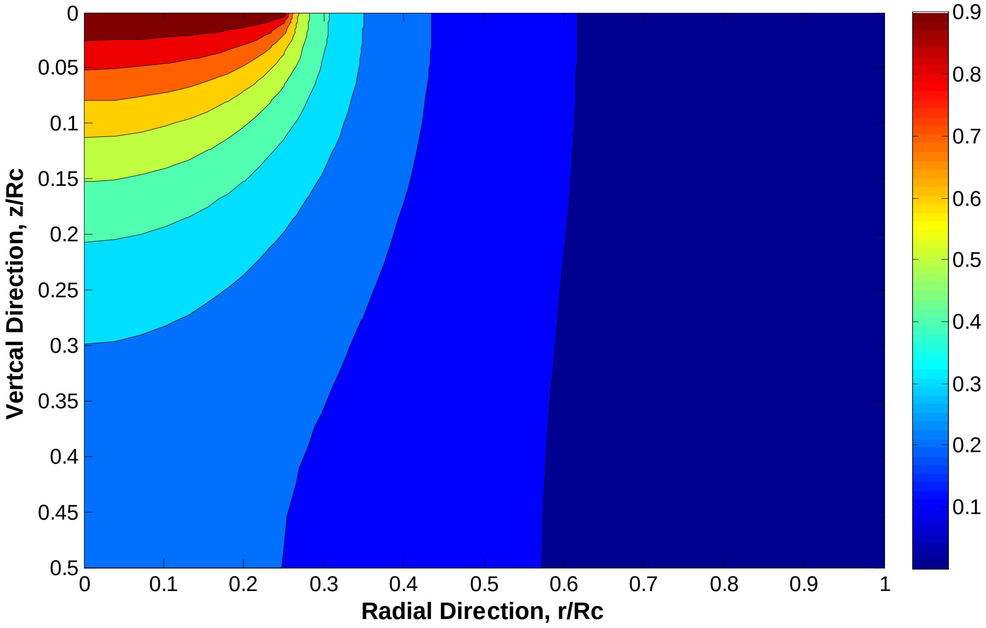

Figure 5.13 – Contour plot of unit head distribution for nonlinear flow using Forchheimer numerical model solution with R_s/R_c = 0.25 and b_c/R_c = 0.5

A comparison between the linear numerical model and nonlinear numerical model solutions can be conducted by calculating the percent difference between the head values at each node. A contour plot of the linear numerical model head minus the nonlinear numerical model head divided by the linear head is shown in Figure 5.14 expressed as a percent. The largest percent difference between the two models is near the outflow boundary. At this location, the head values are very nearly zero. The general trend in percent difference follows the contour plot for the head distribution, with the exception of zero percent difference at the known outflow boundary. For this core geometry, the nonlinear head distribution can be up to 45% lower than the linear head distribution.

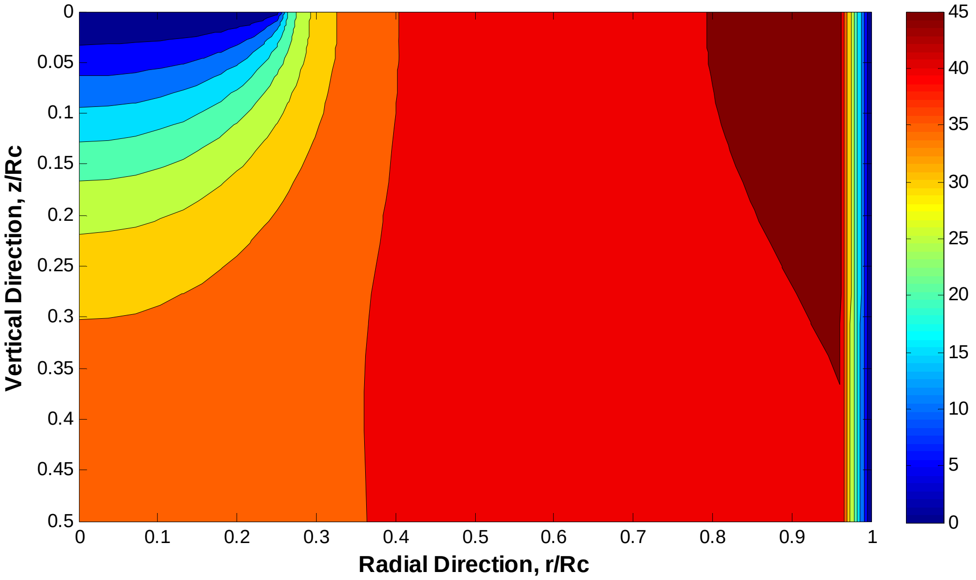

Figure 5.14 – Contour plot of percent difference between unit head distribution for linear and nonlinear numerical model solutions with $R_s/R_c = 0.25$ and $b_c/R_c = 0.5$

The outflow rate can be determined for both the linear and nonlinear numerical models from Equations (5.40) and (5.65), respectively. A graph of the two models shows that the nonlinear flow rate approaches the linear flow rate as the flow rate decreases. This characteristic is discussed in more detail in the next section. Figure 5.15 shows how the nonlinear flow rate approaches the linear flow rate for the above core geometry with $a = 1$ s/cm and $b = 1$ s^2/cm^2. The nonlinear numerical model results show that the relationship between h_s and Q can be fully defined using the quadratic modified Forchheimer equation.

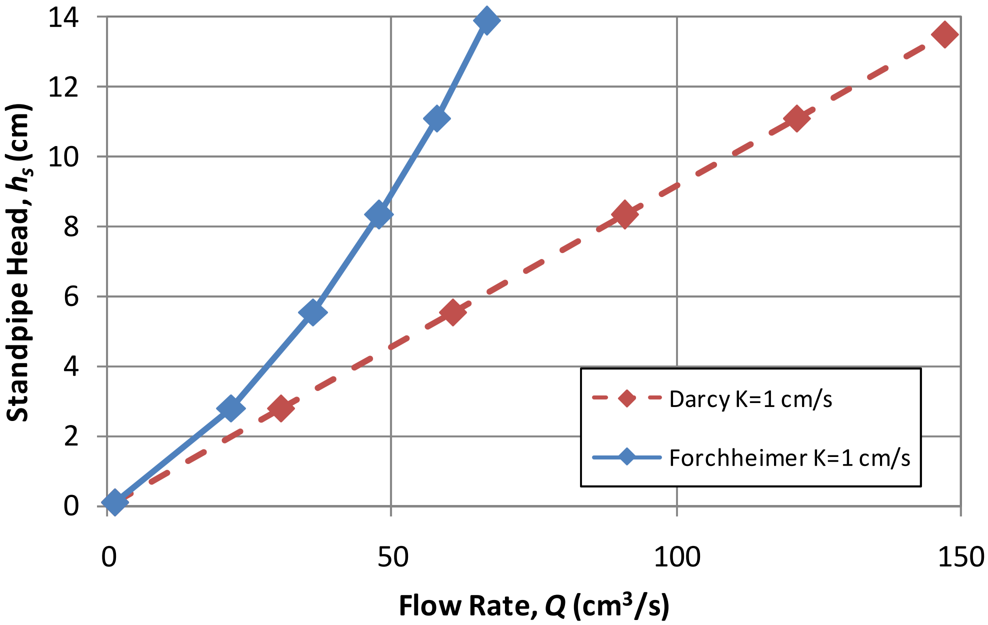

Figure 5.15 – Comparison of flow rates determined from linear and nonlinear numerical model solutions with $R_s/R_c = 0.25$ and $b_c/R_c = 0.5$

In addition to comparing the nonlinear flow rate to the linear flow rate for the same hydraulic conductivity, it is also interesting to compare two nonlinear flow rates with the same hydraulic conductivity but different nonlinear terms. Figure 5.16 shows the same core geometry as in Figure 5.15, but now the nonlinear term has been changed from $b = 1$ s^2/cm^2 to 10 s^2/cm^2. As expected, the greater nonlinear term results in more curvature in the flow rate relationship. Furthermore, the modified linear Forchheimer coefficient α is the same for both curves because a is the same.

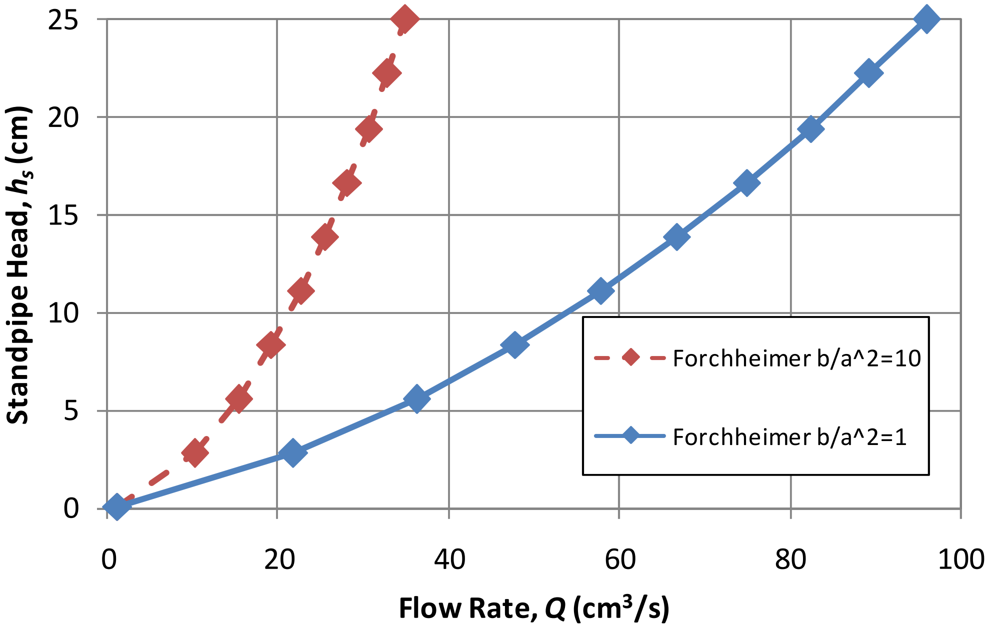

Figure 5.16 – Comparison of flow rates determined from nonlinear numerical model solutions with $R_s/R_c = 0.25$, $b_c/R_c = 0.5$, $a = 1$ s/cm, and $b = 1$ or 10 s^2/cm^2

As previously mentioned, the nonlinear numerical model cannot be represented in a nondimensional way, meaning the head distribution is not the same for a normalized unit head and normalized vertical and radial dimensions. To illustrate this point, we can graph the head distribution along the radial direction for a constant vertical coordinate for various values of h_s. Figure 5.17 shows the head distribution along the top and bottom surfaces of a PFC core with $R_s = 2.5$ cm, $R_c = 10$ cm, $b_c = 5$ cm, $a = 1$ s/cm, and $b = 10$ s^2/cm^2. The head distribution is normalized to the standpipe head. As seen in the figure, the head distributions do not collapse to a single line as in the linear case. For this reason, the nonlinear flow case cannot be nondimensionalized with respect to the standpipe head.

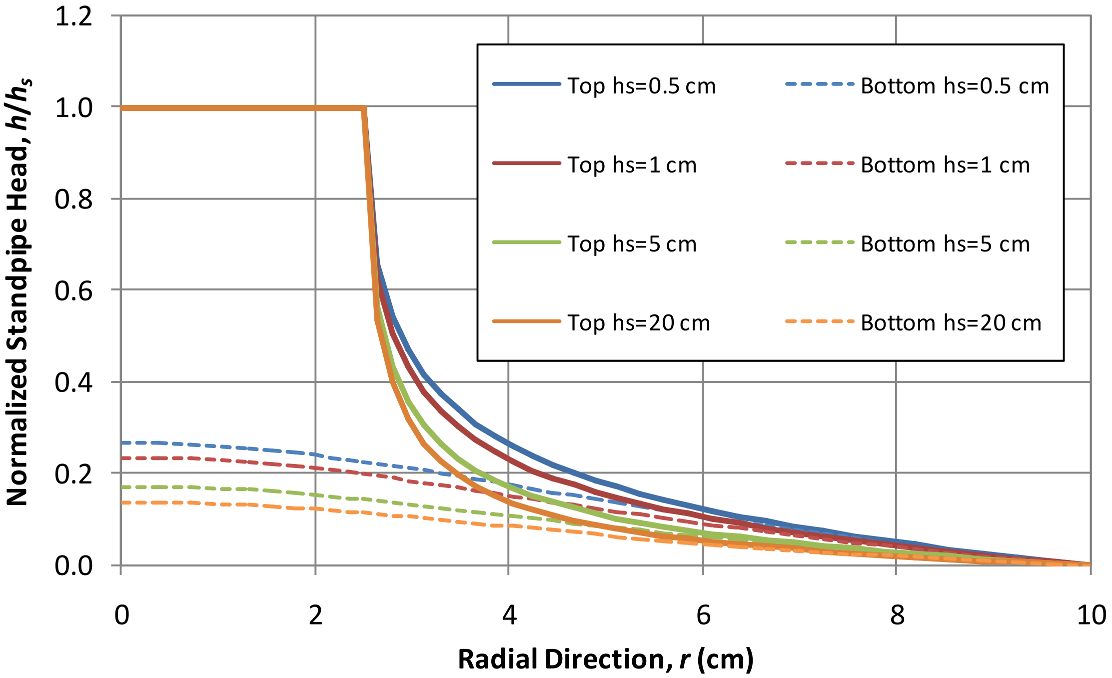

Figure 5.17 – Lack of nondimensionalization for nonlinear numerical model

The final result to investigate is the value of the hydraulic conductivity ratio Φ, determined from the nonlinear numerical model. Φ can be calculated at each node once the nonlinear head distribution is determined. A typical distribution of the hydraulic conductivity ratio is shown in Figure 5.18, with R_s = 2.5 cm, R_c = 10 cm, b_c = 5 cm, a = 1 s/cm, b = 10 s^2/cm^2, and h_s = 1 cm.

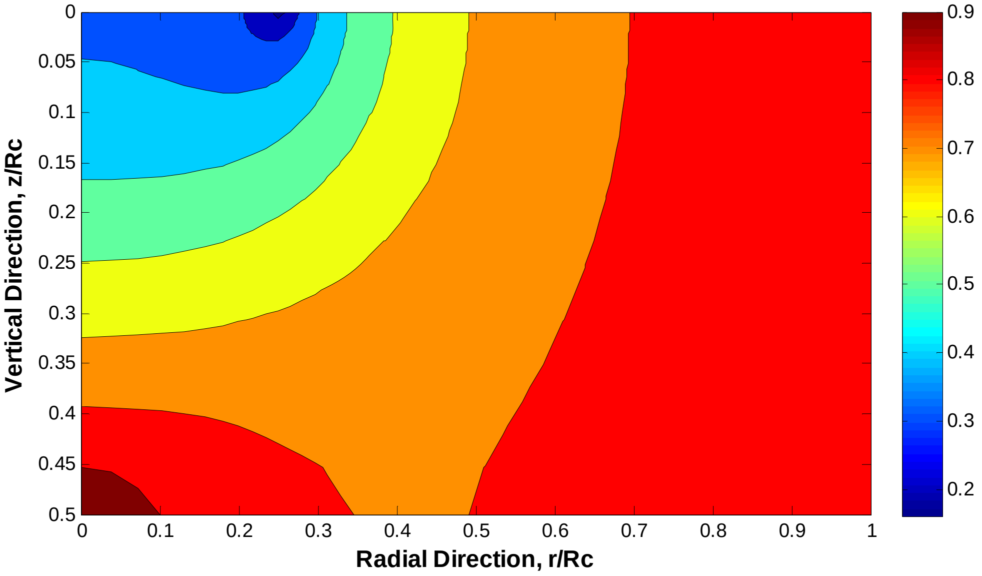

Figure 5.18 – Distribution of hydraulic conductivity ratio Φ

The smaller values of Φ correspond to where the nonlinear effect is greatest. As Φ approaches a value of one, it is expected that the nonlinear hydraulic conductivity approaches the true value of the hydraulic conductivity (for the linear case). Therefore, we can see that Φ is smallest near the location of the standpipe and under the inflow boundary, and generally typically increases towards the outflow boundary. This result is expected because as the flow reaches the outflow boundary, the specific discharge is decreasing and the Forchheimer equation is approaching Darcy's law. The largest value of Φ actually occurs at the center of the core on the lower boundary. At this location, there is both a no flow boundary in the radial direction (due to symmetry) and a no flow boundary in the vertical direction. Because of this, we expect to see virtually no flow and the Forchheimer equation should be approximately equal to Darcy's law. This distribution gives an idea of where, within the core, the nonlinear effects are dominant. It should be noted that this distribution of Φ is for h_s = 1 cm. As h_s increases, the distribution of Φ will have a similar shape, but the values will decrease, meaning the nonlinear effects are more dominant and cover more of the domain.

5.4 Model Characteristics

5.4.1 Grid Refinement

The goal of the numerical model used in this research study is primarily to determine the outflow rate for a given core geometry, original Forchheimer coefficients, and standpipe head. Therefore, grid refinement is based on a comparison of outflow rate as the number of elements in the grid increases. Because the grid is based on an expansion ratio, it is difficult to compare head values at various locations within the core specimen since the nodes are not calculated at the same radial and vertical positions as the number of elements increases. For this reason, an overall model result, in this case outflow rate, is used for grid refinement purposes. Figure 5.19 shows the grid refinement results.

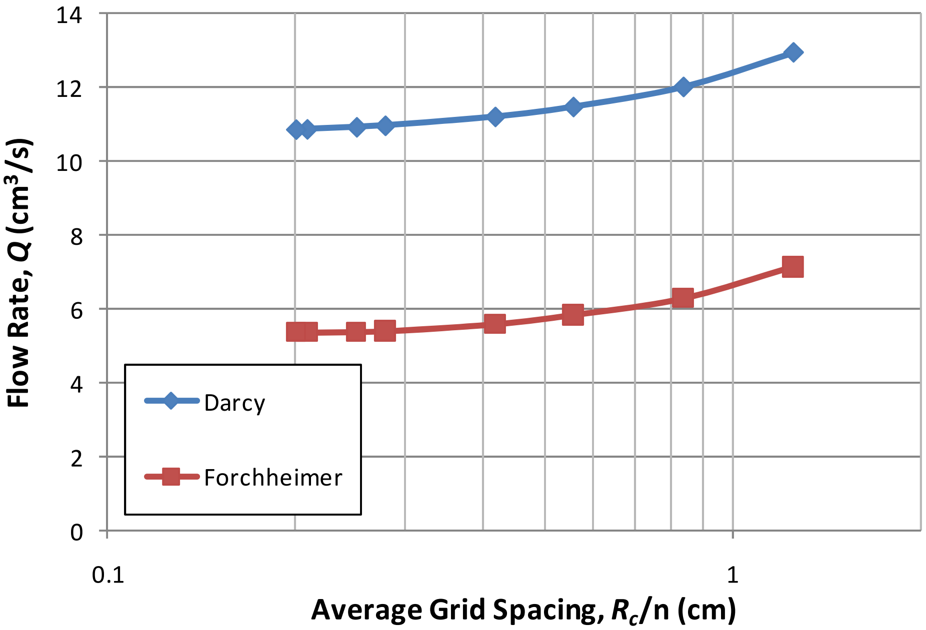

Figure 5.19 – Grid refinement for outflow rate

The model inputs used to investigate the grid refinement are as follows: $R_s = 2.5$ cm, $R_c = 10$ cm, $b_c = 5$ cm, $a = 1$ s/cm, $b = 10$ s^2/cm^2, and $h_s = 1$ cm. The outflow rate is graphed as a function of average grid spacing. Due to the expansion ratio, the average grid spacing does not represent the actual grid spacing, but is instead the core radius divided by the number of elements in the radial direction. The domain of the model has the same number of elements in both the radial and vertical directions.

The maximum number of elements for which the model will successfully converge in a reasonable amount of time is 50 elements in both the radial and vertical directions, for a total of 2,500 elements. This was conducted using an Intel Core 2 Duo CPU at 2.2 GHz with 3.5 GB of RAM. When the number of elements is decreased to 36 elements, the percent error in flow rate is less than one percent. The model results described in the previous sections used 40 elements in each direction, for a total of 1,600 elements, or 1,681 nodes. This number of elements results in a percent error in the flow rate of 0.6% for the linear model and 0.3% for the nonlinear model. The smaller percent error for the nonlinear model is desirable since we are primarily interested in the nonlinear results. Not only does a model using 40 elements produce accurate results, but computation times are also relatively small. The typical computation time to run the model for a given value of standpipe head is on the order of approximately two minutes.

Another typical concern in grid refinement is the observed convergence rate of the model. Since a CDS was used for model development, it is expected that the convergence rate should be approximately second-order. This can be tested by using the Richardson extrapolation method (Ferziger and Peric, 2002). The convergence rate *p* can be found by comparing the head values at similar nodes with differing number of elements:

$$p = \frac{\log\left(\dfrac{h_{2n} - h_{4n}}{h_n - h_{2n}}\right)}{\log(2)} \tag{5.66}$$

Equation (5.66) estimates the convergence rate of the model by comparing the head value as determined from grids with *n*, 2*n*, and 4*n* elements. For this analysis, $n = 12$ so that grids of 12×12, 24×24, and 48×48 elements were analyzed. Due to the model grid generation based on expansion ratios, the locations of the nodes change as the number of elements increases. Therefore, the only nodes that are constant for all three grids are at the following locations: $r = 0$, $z = b_c = 5$ cm and $r = R_s = 2.5$ cm, $z = b_c = 5$ cm. The convergence rate was calculated for these two nodes for both the linear head distribution and nonlinear head distribution. For the linear head distribution, $p = 1.74$ at both nodes; for the nonlinear head distribution, $p = 1.89$ at both nodes. Both these values are relatively close to the theoretical convergence rate of $p = 2$. Therefore, it can be assumed that the model is achieving nearly the desired convergence rate.

5.4.2 Nonlinear Solution Limits

One of the primary reasons for choosing the Forchheimer equation to model the nonlinear flow effects observed in PFC is that the Forchheimer equation should approach Darcy's law for either low hydraulic gradients or small values of the nonlinear Forchheimer coefficient. These two limiting cases were investigated in order to determine if the nonlinear model is working properly. Figure 5.20 shows the maximum percent difference between the linear and nonlinear head distributions as a function of standpipe head. The core dimensions used for this analysis are $R_s = 2.5$ cm, $R_c = 10$ cm, and $b_c = 5$ cm. For different core dimensions, the curves will shift, but the same general trends are observed.

As the standpipe head decreases, the percent difference between the two models decreases as well, so that the nonlinear head distribution approaches the linear head distribution as desired. Furthermore, as mentioned in Section 5.3.6, the nonlinear head distribution is solely a function of the value of the nondimensional parameter b/a^2. So the different curves correspond to different relative magnitudes of this nondimensional parameter. Finally, for smaller values of b/a^2, the nonlinear head distribution approaches the linear head distribution at a greater rate. This is expected because as the nonlinear Forchheimer coefficient decreases, one would expect the resulting nonlinear head distribution to approach the linear head distribution.

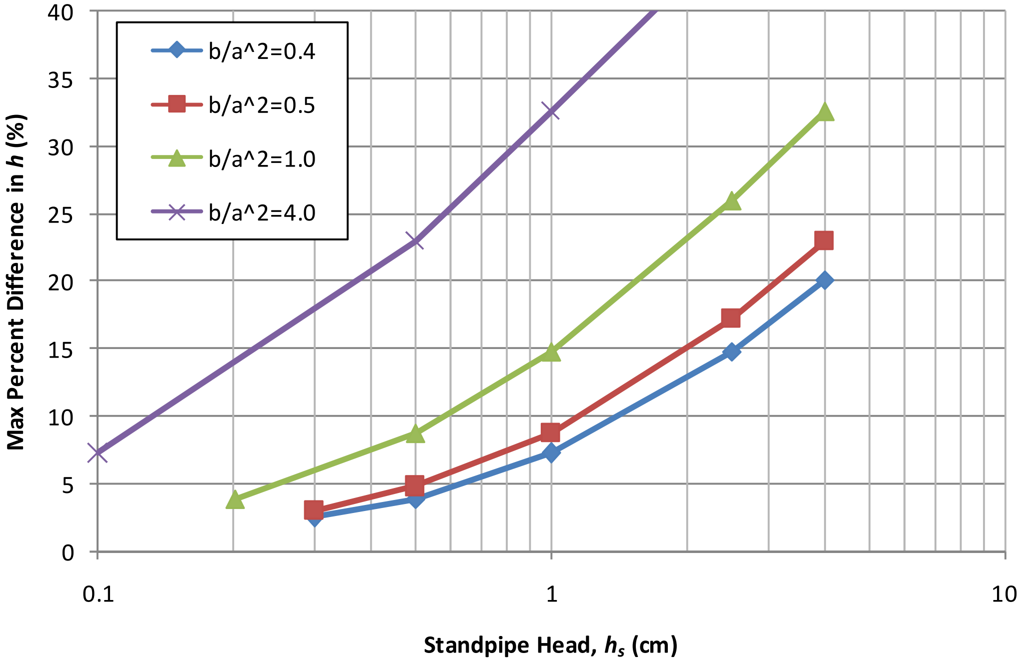

Figure 5.20 – Maximum percent difference in head distribution between linear and nonlinear models versus standpipe head for varying magnitudes of nonlinear effect

Another way to investigate how the nonlinear model approaches the linear model is by examining the outflow rate. Figure 5.21 is a similar graph to that shown in Figure 5.20 and shows the percent difference between the linear outflow rate and nonlinear outflow rate. Again, as the standpipe head and/or nonlinear effect decrease, the nonlinear outflow rate approaches the linear outflow rate as expected. A positive percent difference in flow rate is observed when the linear flow rate is greater than the nonlinear flow rate. This means that for the same standpipe head, the nonlinear model will produce a smaller flow rate.

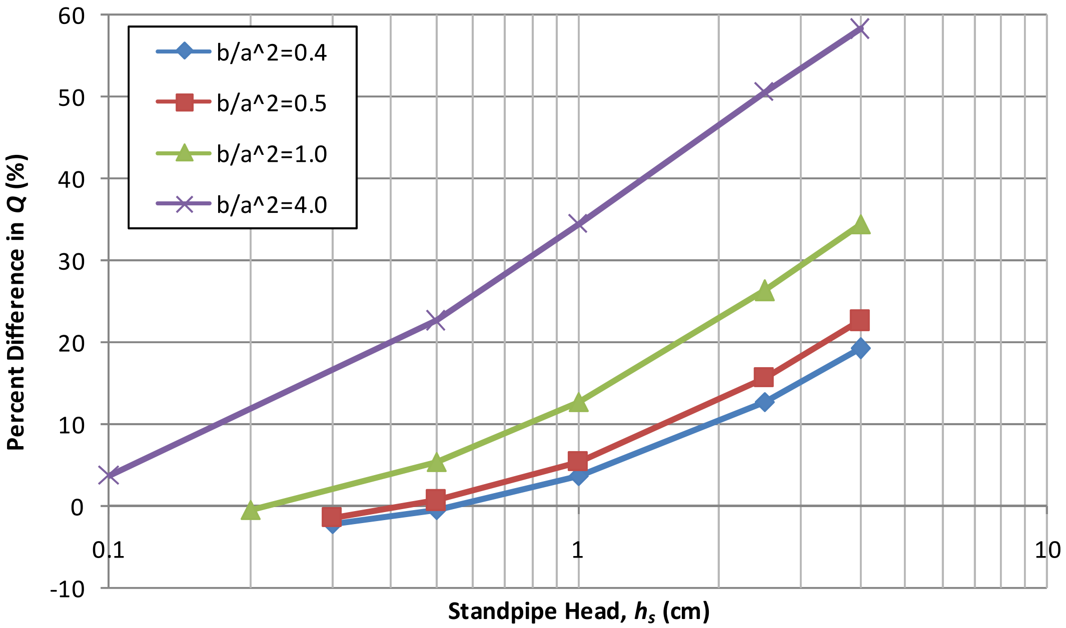

Figure 5.21 – Percent difference in outflow rate between linear and nonlinear models versus standpipe head for varying magnitudes of nonlinear effect

As with the change in percent difference for the head distribution, the percent difference in flow rate is solely dependent on the value of b/a^2. This result does not seem immediately obvious because the flow rate is not constant for a given value of b/a^2 (as shown in Equation (5.65)). However, the ratio of the linear flow rate to the nonlinear flow rate (Equation (5.40) divided by Equation (5.65)) is a function of b/a^2. Therefore, this ratio governs the relative magnitudes of the two flow rates such that the curves in Figure 5.21 can also be characterized by the magnitude of the nonlinear effect.

One final method to determine whether the nonlinear numerical model is behaving as we would expect is to compare the results to the Thiem equation for linear flow to a well. The Thiem equation is a solution for steady flow to a well in a confined aquifer for purely radial flow. Although the nonlinear numerical model applies to two-dimensional (vertical and radial) flow, we can compare the model results to the Thiem equation by using a core geometry with $R_s << R_c$ and $b_c << R_c$. In this case, we would expect to see radial flow in the majority of the domain (see comparison of Figures 5.2

and 5.3). Due to the upper and lower no flow boundaries imposed in the numerical model, flow through the PFC core resembles flow through a confined aquifer.

In general, the Thiem equation provides a solution for the head difference between two points as a function of the pumping flow rate out of the well, the transmissivity of the aquifer (hydraulic conductivity times aquifer thickness), and the radial position of the two points being compared. The Thiem equation is given as:

$$h_2 - h_1 = \frac{Q}{2\pi K b_c} \ln\left(\frac{r_2}{r_1}\right) \tag{5.67}$$

Equation (5.67) compares the head at radial positions r_1 and r_2 from the center of the pumping well. For comparison to the nonlinear numerical model, we will take $r_1 = R_c$ and $r_2 = R_s$ so that $h_1 = 0$ and $h_2 = h_s$. The flow rate must be negative because the Thiem equation is for a pumping well, whereas in our model, the addition of water on the standpipe can be considered an injection well. Therefore, the form of the Thiem equation used for comparison purposes is:

$$h_s = \frac{-Q}{2\pi K b_c} \ln\left(\frac{R_s}{R_c}\right) \tag{5.68}$$

The Thiem equation can be compared to the modified Forchheimer equation for a small nonlinear term. We have already shown that the Forchheimer solution approaches the Darcy solution for low hydraulic gradient and/or specific discharge. Therefore, we would expect in that case that the modified Forchheimer equation will approach the Thiem Equation (5.68). In this limit, the linear modified Forchheimer coefficient could be approximated by:

$$\alpha \approx -\frac{1}{2\pi K b_c} \ln\left(\frac{R_s}{R_c}\right) \tag{5.69}$$

In order to make the comparison, the following core geometry was modeled: R_s = 2.5 cm, R_c = 25 cm, b_c = 2.5 cm, and b = 1 s^2/cm^2; a varies from 1 s/cm to 7 s/cm. The nonlinear numerical model is run and the resulting α value is obtained for each value of a. Figure 5.22 shows a graph of the obtained α value from the numerical model compared to the expected α value obtained from the Thiem equation as given in Equation (5.69).

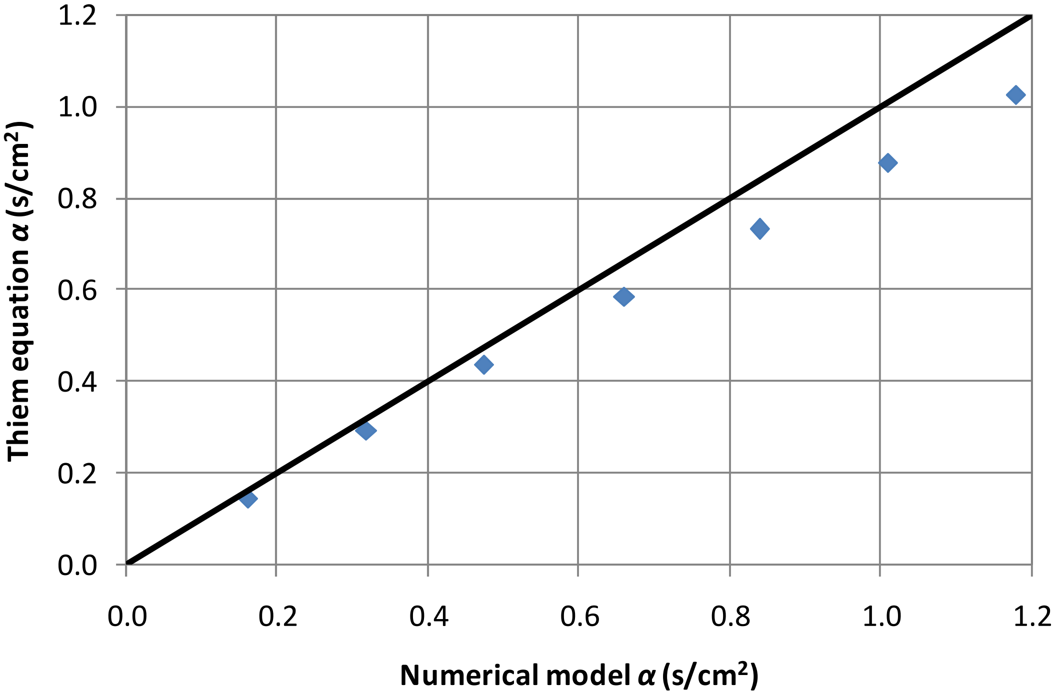

Figure 5.22 – Comparison of nonlinear numerical model with Thiem equation

As the numerical data points approach the 1:1 line shown in Figure 5.22, the α value is approaching the value predicted by the Thiem equation, suggesting that the nonlinear numerical model is behaving as we would expect a confined aquifer to respond. The minimum percent difference between the numerical model α and the Thiem equation α is 7% for the data shown above. This analysis again confirms our assumption that the Forchheimer equation should approach Darcy flow results.

5.5 Impact of Core Specimen Geometry

5.5.1 Methodology for Investigating Impact of Core Geometry

The nonlinear numerical model requires the following inputs: core geometry (R_s, R_c, and b_c), original Forchheimer coefficients (a and b), and standpipe head (h_s). From these inputs, the outflow rate Q is determined and a curve of h_s versus Q is developed for multiple values of h_s. From this curve, the two modified Forchheimer coefficients (α and

β) can be determined using a simple regression equation. This allows for a relationship between the modified Forchheimer coefficients and the original Forchheimer coefficients. As shown in the following subsections, the modified and original Forchheimer coefficients are linearly related. Therefore, in order to determine the impact of the core geometry on these linear relationships, a range of core dimensions were simulated. Four values each of R_s, R_c, and b_c were simulated for a total of 64 total combinations. For each core geometry combination, a total of 10 values of a and b were simulated to determine the relationship between the modified and original Forchheimer coefficients. For each combination of a and b, 10 values of h_s were simulated in order to determine the two modified Forchheimer coefficients from regression. Therefore, a total of 6,400 model simulations were conducted in order to investigate the impact of core geometry. The values tested were R_s = 1.5, 2, 2.5, and 3 cm; R_c = 7.5, 10, 15, and 20 cm; and b_c = 2.5, 3.25, 4, and 5 cm. The core specimens collected have a thickness that ranges from 2.8 to 4.8 cm, and radii of roughly 7.5 and 10.9 cm. The standpipe radius used during testing is 1.9 cm. Therefore, it is expected that the range of simulated core dimensions should include the range of core specimens that were extracted from the roadways. Finally, additional simulations will be determined specifically for the CRWR field test apparatus used to measure in-situ hydraulic conductivity because the field test apparatus has core dimensions that lie outside the above mentioned range of core dimensions.

There are two versions of the Forchheimer equation that are of interest. The original Forchheimer equation can be written in one of two ways:

$$I = aq + bq^2 \tag{5.70}$$

$$I = \frac{q}{K}\left(1 + \frac{q}{n}\right) \tag{5.71}$$

where the linear terms are related by $a = 1/K$ and the nonlinear terms are related by $n = a/b$. The modified Forchheimer equation can also be written in one of two ways:

$$h_s = \alpha Q + \beta Q^2 \tag{5.72}$$

$$\frac{h_s}{R_c} = \frac{Q}{\xi}\left(1 + \frac{Q}{\eta}\right) \tag{5.73}$$

where the linear terms are related by $\xi = R_c/\alpha$ and the nonlinear terms are related by $\eta = \alpha/\beta$. These relationships are important in the following regression results to ensure that a conversion between the two forms of the Forchheimer equation exists.

5.5.2 Regression of Linear Forchheimer Coefficients

The linear Forchheimer coefficients (a and α) are expected to be linearly related to each other. This relationship cannot be determined analytically and depends on the core geometry. For a core with dimensions R_s = 2.5 cm, R_c = 10 cm, and b_c = 5 cm, Figure 5.23 shows the resulting relationship between a and α. The two linear Forchheimer coefficients are linearly related, and the relationship is perfectly correlated from the numerical simulations.

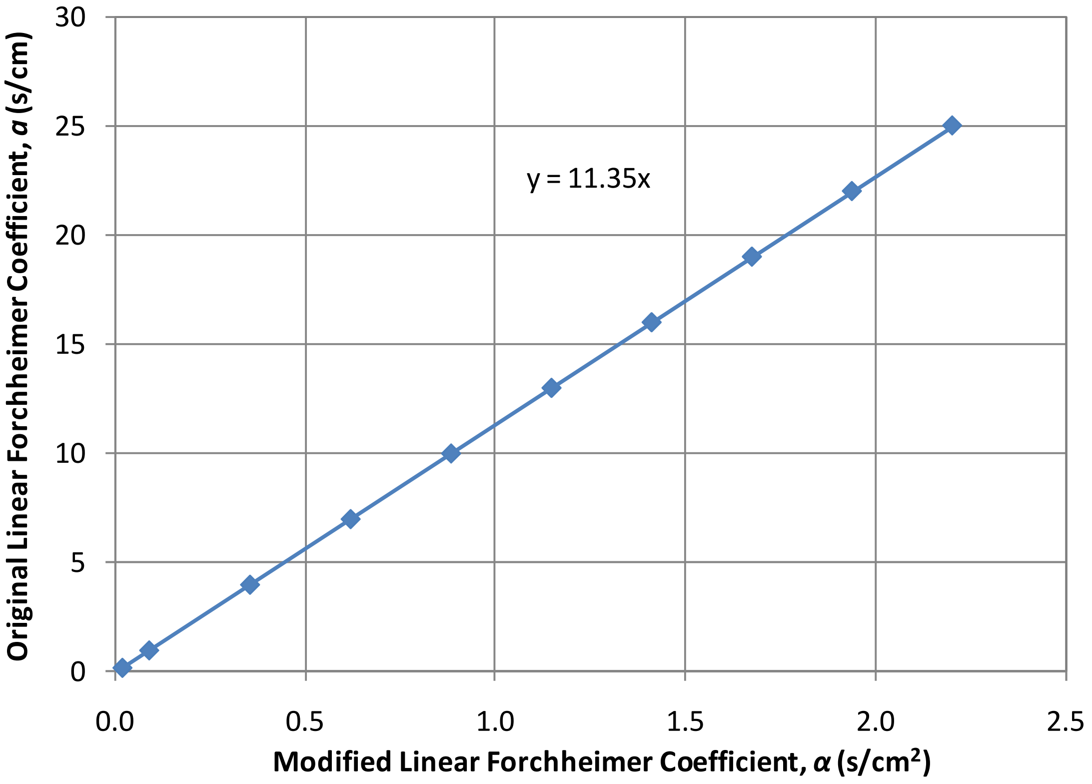

Figure 5.23 – Relationship between modified and original linear Forchheimer coefficient for R_s/R_c = 0.25 and b_c/R_c = 0.5

It can be shown that as any of the three core dimensions change, the slope of the line will shift. But in general, the following relationship exists between the two linear Forchheimer coefficients:

$$a = c_1(R_s, R_c, b_c)\alpha \tag{5.74}$$

Equation (5.74) says that the original linear Forchheimer coefficient is linearly related to the modified linear Forchheimer coefficient, where the slope of that relationship c_1 is a function of the core dimensions. The slope c_1 has units of [L]. Using the 64 core geometry combinations described above, the following regression equation was developed for the linear Forchheimer coefficients:

$$a \approx 5.8R_s\left(\frac{b_c}{R_c}\right)^{0.33}\alpha \tag{5.75}$$

Equation (5.75) assumes that the slope c_1 of the line relating a to α depends on a power relationship for the three core dimensions. In addition, the grouping of the three core dimensions results in a combination with units of [L]. Therefore, the constant 5.8 is dimensionless and the above equation can be used under any system of units.

The accuracy of the approximation for determining the slope c_1 can be addressed by graphing the slope obtained from Equation (5.75) as a function of the slope obtained from the numerical model. If the regression equation gives a good approximation to the numerical results, the data will plot as a straight line with unit slope. Figure 5.24 shows the comparison between c_1 obtained from regression to c_1 obtained from the numerical simulations. The standard error between the two values of c_1 is 0.422 cm. The average percent difference from the regression equation is nearly 4%, but the maximum percent difference is nearly 18%. This suggests that for the majority of the core dimensions tested, the regression equation produces a very good approximation.

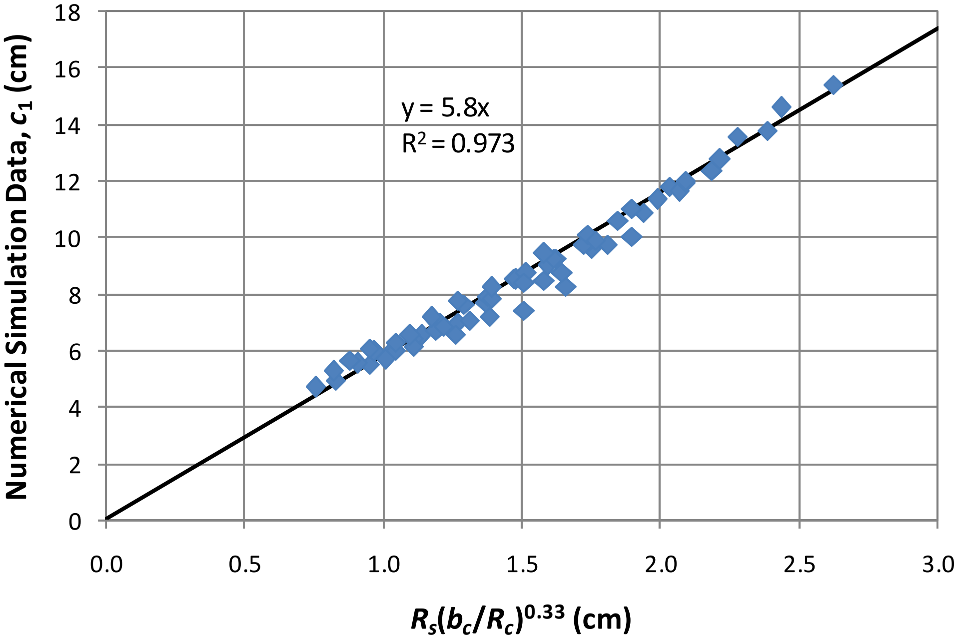

Figure 5.24 – Regression results for c_1 (cm)

As mentioned in Section 5.5.1, we can express the Forchheimer equation in one of two ways. Looking at the transformed form of the equation, we would expect a linear relationship between the transformed coefficients K and ξ. This equation can be written in a general form as:

$$K = c_3(R_s, R_c, b_c)\xi \tag{5.76}$$

The slope c_3 in Equation (5.76) has units of [1/L^2]. (Note: The symbol c_3 is used here because c_2 is reserved for the slope relating to the nonlinear coefficients. Slopes c_1 and c_2 will correspond to the first form of the Forchheimer equation, and slopes c_3 and c_4 correspond to the transformed form of the equation.) Conducting a power law regression on the core dimensions results in the following relationship:

$$K \approx \frac{0.175}{R_s R_c^{0.67} b_c^{0.33}}\xi \tag{5.77}$$

The power terms on each of the core dimensions in Equation (5.77) can be determined from the powers obtained in Equation (5.75) due to the conversions between the two forms of the Forchheimer equation. Therefore, only the constant 0.175 was changed in order to find the correct regression equation. Again, the powers on the core dimensions result in units of [1/L^2] so that the constant 0.175 is dimensionless.

Figure 5.25 shows a plot of the value of the slope c_3 obtained from the numerical simulation to that obtained from the regression Equation (5.77). The resulting standard error is 5.8×10^{-4} 1/cm^2, with an average percent difference of 4.5%, and a maximum percent difference of nearly 17%. Therefore, we see very good agreement from the regression equation and the numerical modeling results, suggesting that the regression equation provides a good approximation to the numerical model.

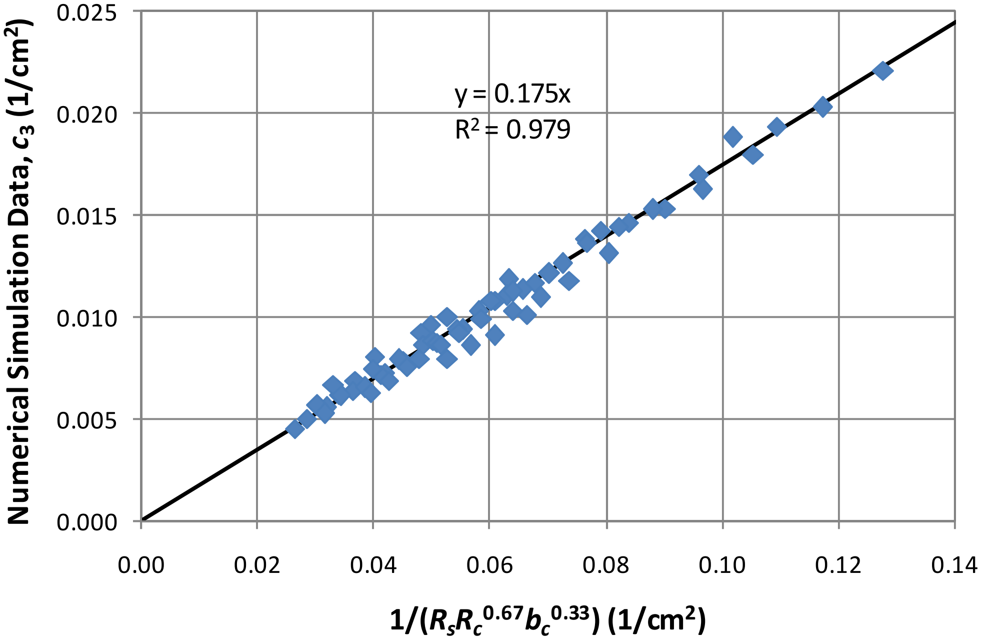

Figure 5.25 – Regression results for c_3 (1/cm^2)

One last comment should be made on the choice of a power law regression equation and the resulting errors from these equations. The power law produces desirable results in that the regression equation can be nondimensionalized and used with respect to any system of dimensions. However, errors are produced from this method. For example, we can take a closer look at the slope c_1 and specifically on the power term for the dimension R_s. Equation (5.75) says that the power term on R_s for slope c_1 has a value of one. One way of looking at the error produced by this value is to do a power law regression analysis on the four values of R_s simulated while keeping R_c and b_c constant. The results of this analysis are shown in Figure 5.26.

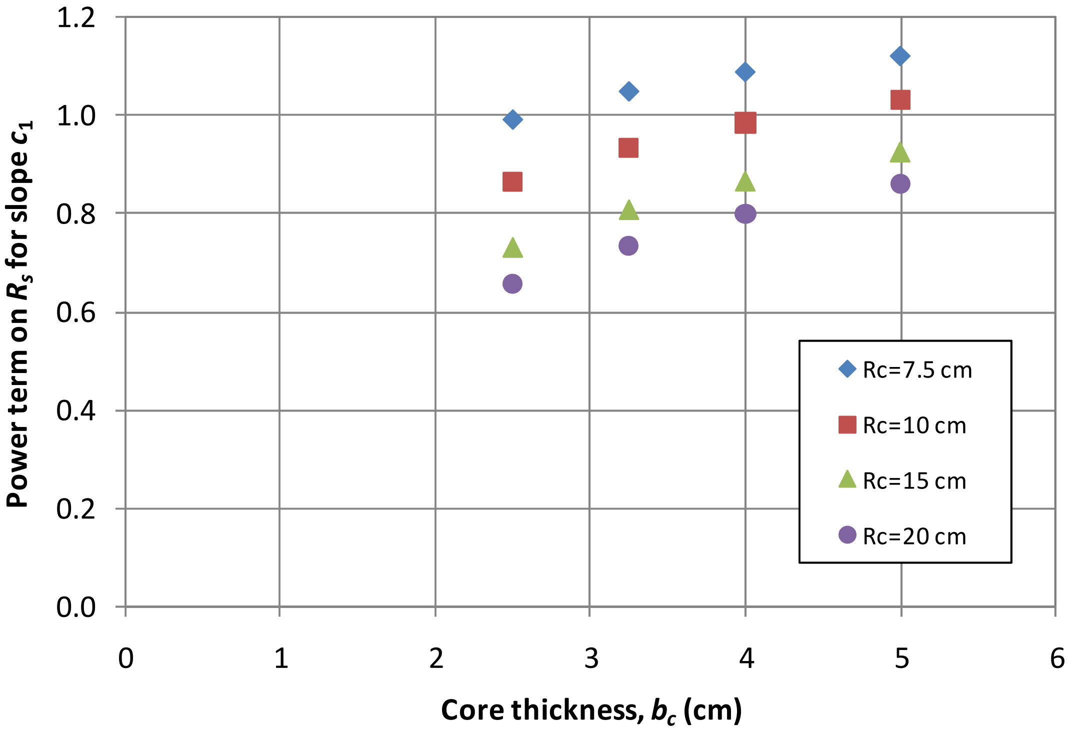

Figure 5.26 – Analysis of power law term as function of core dimensions

Figure 5.26 shows that the power on the R_s term is not a constant value of one, but instead changes with the values of R_c and b_c. For this reason, the power law regression will result in error. Due to the trends seen in Figure 5.26, perhaps a more complex regression could be conducted so that the power on one core dimension are functions of the other two core dimensions. However, the complexity of such a model would negate the benefit of having a simple approximation between the original and modified Forchheimer coefficients. Furthermore, the errors produced by the proposed power law relation are typically minimal for most core geometries. These trends can be observed for all the power terms determined from the regression equation and will result in greater errors when conducting regression equations for the nonlinear coefficients.

5.5.3 Regression of Nonlinear Modified Forchheimer Coefficients

The nonlinear Forchheimer coefficients (b and β) are also expected to be linearly related to each other. This relationship cannot be determined analytically and depends on the core geometry. For a core with dimensions $R_s = 2.5$ cm, $R_c = 10$ cm, and $b_c = 5$ cm, Figure 5.27 shows the resulting relationship between b and β. The two nonlinear Forchheimer coefficients are linearly related, and the relationship is perfectly correlated from the numerical simulations.

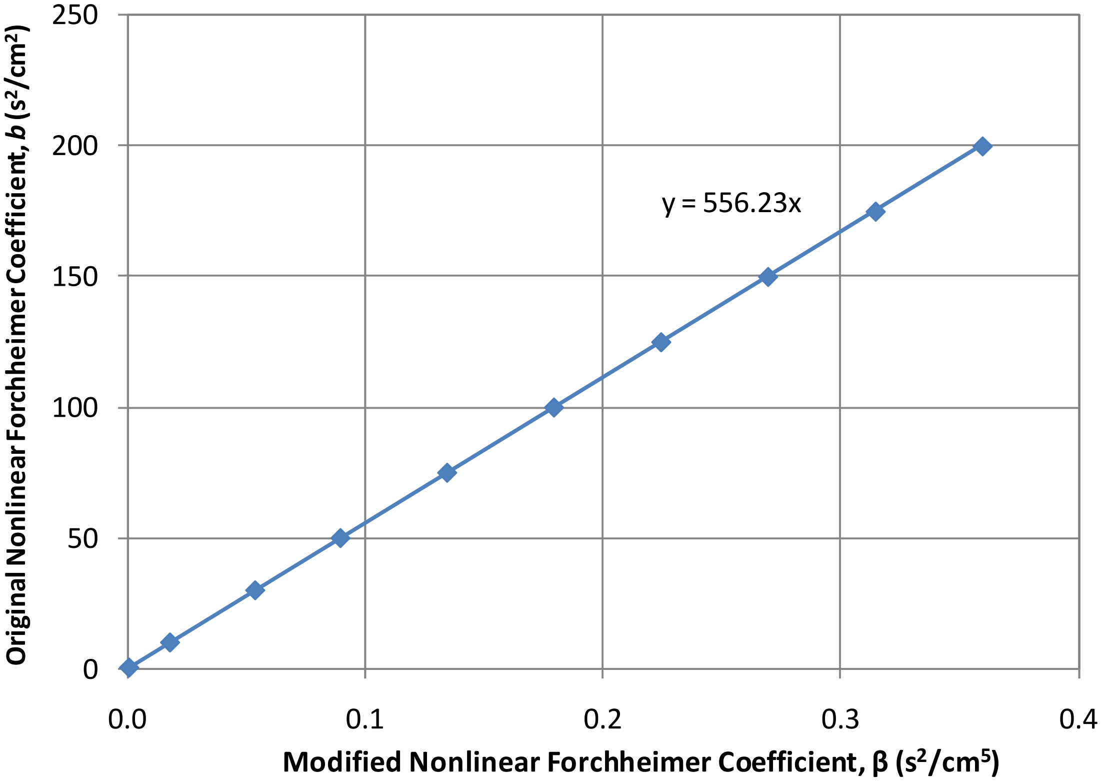

Figure 5.27 – Relationship between modified and original nonlinear Forchheimer coefficient for $R_s/R_c = 0.25$ and $b_c/R_c = 0.5$

The following relationship exists between the two nonlinear Forchheimer coefficients:

$$b = c_2\left(R_s, R_c, b_c\right)\beta \tag{5.78}$$

Equation (5.78) says that the original nonlinear Forchheimer coefficient is linearly related to the modified nonlinear Forchheimer coefficient, where the slope of that relationship c_2 is a function of the core dimensions and has units of [L^3]. The following regression equation was developed for the nonlinear Forchheimer coefficients:

$$b \approx 18.6 {R_s}^{2.5} \left(R_c b_c \right)^{0.25} \beta \tag{5.79}$$

Equation (5.79) makes the same assumptions of a power law relation as before. In addition, the grouping of the three core dimensions results in a combination with units of [L^3] so that the constant 18.6 is dimensionless and the above equation can be used under any system of units.

The accuracy of the approximation for determining the slope c_2 is addressed by graphing the slope obtained from Equation (5.79) as a function of the slope obtained from the numerical model. Figure 5.28 shows this comparison. The standard error between the two values of c_2 is 67 cm^3. This value is much larger than the standard error reported for the linear coefficients in part due to the significantly larger values of c_2. The average percent difference from the regression equation is 9%, and the maximum percent difference is 25%. This suggests that for the nonlinear coefficient, there is much more uncertainty involved in the regression equation. The cause of this uncertainty follows the error as shown in Figure 5.26. For the nonlinear coefficients, the change in power terms with respect to each dimension varies to a greater extent, causing more error. This is a concern, and a more complex model could be developed to reduce this error. However, as shown in the following sections, the error involved when compared to experimental data is within an acceptable range. In addition, the precise value of the nonlinear coefficient is of secondary concern. The nonlinear coefficient is used primarily to determine when and where nonlinear effects are significant. For the purposes of measuring the hydraulic conductivity of PFC, nonlinear effects will always be significant. Therefore, the precise value of the nonlinear coefficient will not provide any significant information and only an acceptable estimate is needed.

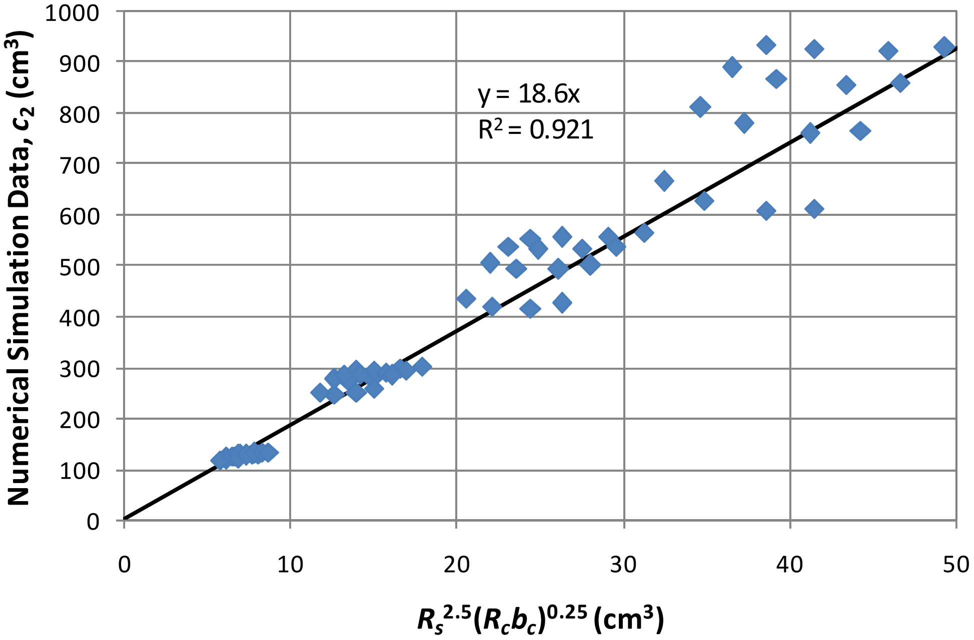

Figure 5.28 – Regression results for c_2 (cm^3)

Looking at the transformed form of the Forchheimer equation, we would expect a linear relationship between the transformed coefficients n and η. This equation can be written in a general form as:

$$n = c_4(R_s, R_c, b_c)\eta \tag{5.80}$$

The slope c_4 in Equation (5.80) has units of [1/L^2]. Conducting a power law regression on the core dimensions results in the following relationship:

$$n \approx \frac{0.3 b_c^{\ 0.08}}{R_s^{\ 1.5} R_c^{\ 0.58}} \eta \tag{5.81}$$

The power terms on each of the core dimensions in Equation (5.81) can be determined from the powers obtained in Equations (5.75) and (5.79) due to the conversions between the two forms of the Forchheimer equation. Therefore, only the constant 0.3 was changed in order to find the correct regression equation. Again, the powers on the core dimensions result in units of [1/L^2] so that the constant 0.3 is dimensionless.

Figure 5.29 shows a plot of the value of the slope c_4 obtained from the numerical simulation to that obtained from the regression Equation (5.81). The resulting standard error is 4.2×10^{-3} 1/cm^2, with an average percent difference of 11%, and a maximum percent difference of 30%. The standard error is very small due to the small values of c_4. The percent difference is considerably larger than that obtained for the linear coefficients. As previously mentioned, this is of lesser concern and as shown in the following section, the regression equation produces acceptable results.

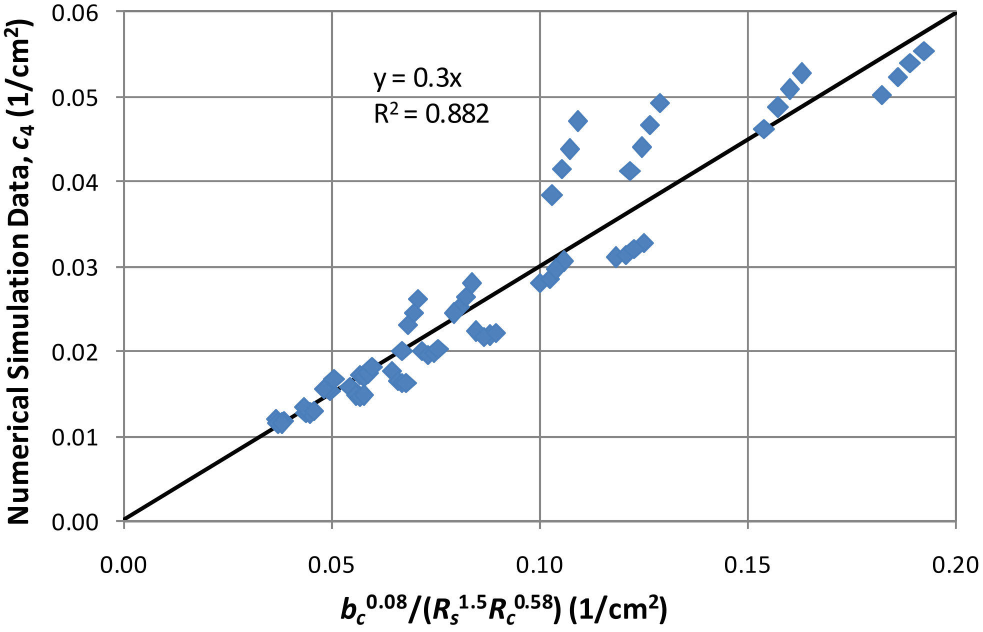

Figure 5.29 – Regression results for c_4 (1/cm^2)

5.5.4 Determination of Hydraulic Conductivity for Core Specimens

Now that we have established a method to relate the original Forchheimer coefficients (a and b) to the modified Forchheimer coefficients (α and β), we can estimate the original coefficients from the measured modified coefficients reported in Section 3.4. Tables 5.2 through 5.5 report the estimated original Forchheimer coefficients ($K = 1/a$ and b) obtained from Equations (5.75) and (5.79) for each core specimens tested in the laboratory. In addition, the resulting modified Forchheimer coefficients obtained from the nonlinear numerical model for the estimated original coefficients are provided. Finally, the percent difference (*P.D.*) in the modified Forchheimer coefficients obtained from the model when compared to the coefficients obtained from laboratory testing is reported. This is the final step necessary in obtaining the hydraulic conductivity for each core specimen.

Table 5.2 – Results of numerical simulations for 2007 core specimens

Core ID	**K (cm/s)**	**b (s^2/cm^2)**	**α (s/cm^2)**	**β (s^2/cm^5)**	***P.D.* in α**	***P.D.* in β**
1-A-T	0.180	2.785	0.7036	0.0125	0.29	-12.84
1-B-T	2.427	0.584	0.0485	0.0024	1.67	-13.35
2-A-T	0.668	1.812	0.1906	0.0080	1.21	-14.38
2-B-T	0.308	3.034	0.4062	0.0132	0.67	-14.16
3-B-T	0.455	7.206	0.3069	0.0344	3.52	-11.74
3-C-T	0.457	2.679	0.2916	0.0122	1.96	-13.19

Table 5.3 – Results of numerical simulations for 2008 core specimens

Core ID	**K (cm/s)**	**b (s^2/cm^2)**	**α (s/cm^2)**	**β (s^2/cm^5)**	***P.D.* in α**	***P.D.* in β**
1-1-T	0.801	2.216	0.1530	0.0090	0.66	-2.14
1-1-S	2.328	1.213	0.0547	0.0050	-0.69	-4.22
1-2-T	0.829	2.797	0.1466	0.0113	0.79	-1.39
1-2-S	1.115	2.000	0.1168	0.0083	-0.28	-5.11
1-3-T	1.389	1.529	0.0912	0.0063	-0.36	-4.03
1-3-S	1.820	1.118	0.0734	0.0047	-0.13	-5.59
2-1-T	0.474	4.136	0.2907	0.0176	0.55	-6.07
2-2-T	0.957	2.306	0.1390	0.0097	-0.14	-5.61
2-3-T	0.468	4.060	0.3008	0.0176	0.77	-5.83
3-1-T	0.056	64.297	02.3938	0.2735	-0.29	-5.29
3-2-T	0.048	166.832	3.0816	0.7476	1.74	-5.15
3-3-T	0.228	15.720	0.5850	0.0660	0.01	-5.54

Table 5.4 – Results of numerical simulations for 2009 core specimens

Core ID	*K* (cm/s)	*b* (s^2/cm^2)	*α* (s/cm^2)	*β* (s^2/cm^5)	*P.D.* in *α*	*P.D.* in *β*
1-i-T	1.831	1.932	0.0683	0.0079	-0.39	-3.50
1-i-S	2.868	0.875	0.0467	0.0037	-0.17	-5.63
1-ii-T	0.555	3.567	0.2250	0.0146	0.19	-3.33
1-ii-S	2.106	1.613	0.0657	0.0069	0.30	-5.88
1-iii-T	1.334	1.266	0.0927	0.0052	0.29	-2.59
1-iii-S	0.954	3.096	0.1437	0.0132	0.22	-5.87
2-i-T	0.194	4.496	0.7066	0.0193	-0.01	-5.34
2-ii-T	0.437	2.162	0.3090	0.0092	-0.05	-5.69
2-iii-T	0.992	2.007	0.1356	0.0085	0.02	-5.75
3-i-T	0.102	29.132	1.2910	0.1217	-0.34	-5.12
3-ii-T	0.180	12.368	0.7167	0.0513	-0.36	-4.70
3-iii-T	0.241	17.371	0.5413	0.0722	-0.19	-5.14

Table 5.5 – Results of numerical simulations for 2010 core specimens

Core ID	*K* (cm/s)	*b* (s^2/cm^2)	*α* (s/cm^2)	*β* (s^2/cm^5)	*P.D.* in *α*	*P.D.* in *β*
1-a-T	0.359	12.721	0.3139	0.0521	4.74	-9.68
1-a-S	1.327	0.795	0.0884	0.0033	1.82	-12.97
1-b-T	2.074	1.067	0.0545	0.0044	4.17	-10.02
1-b-S	1.510	0.630	0.0767	0.0026	2.21	-12.76
1-c-T	0.588	3.909	0.1903	0.0160	5.46	-9.31
1-c-S	1.551	0.466	0.0752	0.0019	1.96	-13.03
3-a-T	0.203	34.789	0.5626	0.1433	2.97	-11.90
3-b-T	0.019	640.386	5.8899	2.6548	2.23	-11.89
3-c-T	0.090	133.903	1.2685	0.5518	2.88	-11.92

From Tables 5.2 through 5.5, we now have a value of the hydraulic conductivity for each core specimen. It is necessary to investigate the error associated with this value of hydraulic conductivity. This is addressed in the comparison between modified Forchheimer coefficients obtained in the lab and from the numerical model. The linear modified Forchheimer coefficient α obtained from the numerical model is at most 3.5% greater than the value obtained in the lab (Core 3-B-T). The majority of the core specimens have a percent difference in the linear modified Forchheimer coefficient of less than one percent. Therefore, the regression equations used to estimate the original linear Forchheimer coefficients are producing very reliable estimates.

The nonlinear modified Forchheimer coefficient has a much greater error associated with it. The maximum percent difference in β is roughly 14% (Core 2-A-T). The smaller diameter cores which were extracted in 2007 and 2010 tend to result in a larger percent difference in the nonlinear term, on the order of over 10% error. This begins to show the limitations of the regression equations presented in Section 5.5.3 for the nonlinear coefficients. However, for the larger diameter cores, the nonlinear term has a percent error of typically less than 5%. In general, the regression equations used to estimate the original nonlinear Forchheimer coefficients result in more error to the experimental data. This is of minimal concern because the nonlinear term is typically only necessary to determine when nonlinear effects can be ignored. Clearly, for the hydraulic conductivity test methodology developed for this research study, nonlinear effects will never be negligible. Therefore, we have no need to be extremely precise in our estimates of the nonlinear Forchheimer coefficient.

The above estimates for the original Forchheimer coefficients (a and b) were made using regression Equations (5.75) and (5.79). Similarly, we can use estimates for the transformed original Forchheimer coefficients (K and n) using regression Equations (5.77) and (5.81) in order to determine the percent difference between the modeled and measured modified Forchheimer coefficients. The purpose of this analysis is to determine which set of regression equations provides a more accurate estimate of the measured modified Forchheimer coefficients. Using either set of regression equations results in roughly the same percent difference in the calculated modified Forchheimer coefficients. For example, the percent different in α when determined using the regression equation for a ranges from -0.69% to 5.46%; whereas the percent difference using the regression equation for K ranges from -2.26% to 3.97%. Therefore, although these values shift slightly, the overall range of percent difference for both equations is roughly 6.2%. Similarly, for the nonlinear coefficients, the range of percent difference in β when determined using the equation for b is 15.7%; whereas, the range using the equation for n is 13.3%. Again, both sets of regression equations result in nominally the same precision to the measured lab or field data.

5.5.5 Determination of Hydraulic Conductivity for Field Test Apparatus

The dimensions of the CRWR field test apparatus extend beyond the limitations of the dimensions discussed in the previous sections due to the large standpipe and core radii. For this reason, a regression equation was developed specifically for the dimensions of the CRWR field test apparatus with varying PFC thicknesses. The CRWR field test apparatus has dimensions R_s = 5.08 cm and R_c = 22.86 cm. The resulting regression equations based on six different core thicknesses ranging from 2.5 to 5 cm are as follows:

$$a = 5b_c^{0.75}\alpha \qquad (5.82)$$

$$b = 482b_c^{1.25}\beta \qquad (5.83)$$

$$K = 8.8\times10^{-3}b_c^{-0.75}\xi \qquad (5.84)$$

$$n = 0.01b_c^{-0.5}\eta \qquad (5.85)$$

These four regression equations apply specifically to the CRWR test apparatus and cannot be used for any other values of R_s or R_c. Furthermore, the constants in Equations (5.82) through (5.85) have units associated with them so that the dimensions used must be expressed in cm.

The above regression equations were used for the CRWR field test results obtained to determine the in-situ hydraulic conductivity and reported in Section 4.3.2. The PFC thickness used in the regression equations above is the average PFC thickness from all core specimens extracted for each roadway. For Loop 360, the average thickness is 4.013 cm; for FM 1431, the average thickness is 3.228 cm; and for RR 620, the average thickness is 3.499 cm. Although these thicknesses are not precisely what exist in the field, it should give a good approximation to the actual thickness. The results are reported in Table 5.6 below. The field test location and date are provided together with the hydraulic conductivity and nonlinear Forchheimer coefficient obtained from the regression equations. The resulting percent difference (*P.D.*) in the modified Forchheimer equations when compared to the values measured in the field are provided as well.

Table 5.6 – Results of numerical simulations for CRWR field test

Roadway	**Location**	**Date**	***K*** **(cm/s)**	***b*** **(s^2/cm^2)**	***P.D.*** **in α**	***P.D.*** **in β**
Loop 360	Shoulder	6-29-08	3.46	0.429	0.65	-3.07
Loop 360	Shoulder	6-29-08	2.78	0.495	0.50	-2.87
Loop 360	Shoulder	9-25-08	2.96	0.451	0.64	-3.05
Loop 360	Shoulder	9-25-08	3.26	0.493	0.72	-3.03
Loop 360	Shoulder	11-9-08	7.61	0.505	0.11	-2.83
Loop 360	Shoulder	11-23-08	7.07	0.346	-0.01	-2.92
Loop 360	Shoulder	2-2-09	2.69	0.541	0.65	-2.95
Loop 360	Travel Lane	2-2-09	3.59	0.547	0.58	-2.99
Loop 360	Shoulder	2-5-10	3.43	0.448	0.90	-3.06
Loop 360	Travel Lane	2-5-10	3.16	0.314	0.37	-2.97
FM 1431	Travel Lane	2-2-09	0.58	5.209	-1.09	-3.38
RR 620	Travel Lane	2-2-09	1.94	2.115	-0.30	-4.05
RR 620	Travel Lane	2-5-10	1.00	2.462	-0.31	-4.08

The average percent difference in the modified linear Forchheimer coefficient is typically less than one percent, whereas the percent difference in the nonlinear coefficient is roughly three percent. These results are much more accurate because the regression equations were developed for only one changing core dimension (b_c). The average hydraulic conductivity on Loop 360 is roughly 3 cm/s. This is of the same order of magnitude obtained for the core specimens extracted from Loop 360. The core specimens have much more variability than the field data, which is the reason for conducting the field test in order to remove this variability. There were two field tests on Loop 360 with significantly larger hydraulic conductivity of roughly 7 cm/s. These two tests were conducted immediately after the constant head field tests described in Section 4.2.3. The large, sustained flow rates used during the constant head tests may have flushed some trapped sediment out of the pore space and/or caused a poor seal from the vacuum grease, resulting in an artificially large value of hydraulic conductivity.

The resulting hydraulic conductivity obtained on FM 1431 matches well with the value obtained in the laboratory. The hydraulic conductivity obtained on RR 620 appears to be slightly larger than what was obtained in the laboratory. There is no explanation for this variability, and further testing may be needed in order to verify these results. As mentioned in Section 2.2.4, Kelkar (2000) suggests that the nonlinear Forchheimer coefficient is typically larger when observed in the field than in the laboratory. A comparison of the experimental results presented above show that the field data do not result in significantly greater nonlinear coefficients. Therefore, the claim made by Kelkar (2000) does not apply to this experimental data set.

In order to determine the uncertainty associated with using the average core specimen thickness as the roadway thickness in the above analysis, we can compare the estimates for the original Forchheimer coefficients using plus/minus one standard deviation of the core specimen thickness. For Loop 360, the average thickness plus and minus one standard deviation is 4.588 cm and 3.438 cm, respectively. The larger thickness provides the following estimates: K = 3.13 cm/s and b = 0.507 s^2/cm^2 with a percent difference in α of 1.78% and β of 0.43%. The smaller thickness provides the following estimates: K = 3.89 cm/s and b = 0.354 s^2/cm^2 with a percent difference in α of -0.25% and β of -4.08%. Therefore, using plus/minus one standard deviation in the PFC thickness provides minimal error in the results. The percent difference in the modified

Forchheimer coefficients are of the same order of magnitude as before, suggesting that small changes in the PFC thickness are not expected to result in large errors.

In addition to the regression results obtained for the CRWR field test described above, a regression was also conducted for the field test described by Tan et al. (2002). Their field test has the following dimensions: R_s = 7.5 cm and R_c = 25 cm. A range of PFC thicknesses were simulated to determine the following regression equations in order to estimate the original Forchheimer coefficients:

$$a = 6.5 b_c^{0.75} \alpha \tag{5.86}$$

$$b = 680 b_c^{1.5} \beta \tag{5.87}$$

$$K = 6.2 \times 10^{-3} b_c^{-0.75} \xi \tag{5.88}$$

$$n = 0.01 b_c^{-0.75} \eta \tag{5.89}$$

The above equations are specific to the field test used by Tan et al. (2002), and the constants have units associated with them. Therefore, these equations can only be used for the Tan et al. field test when R_s and R_c are expressed in cm. Slightly different relationships are obtained for the Tan et al. field test when compared to the CRWR field test. This is due to the varying dimensions of the test apparatus. Unfortunately, Tan et al. do not provide their falling head data in such a way that these equations can be compared with their experimental results. Therefore, a comparison between the proposed regression equations and the method used by Tan et al. cannot be conducted.

Chapter Six

Analysis of Hydraulic Properties

6.1 Statistical Objective and Data

The purpose for accurately measuring the hydraulic properties of PFC is to ultimately be able to determine when the benefits associated with driver safety and improved water quality will no longer persist. Because the pore space of PFC becomes clogged with sediment over time, it is expected that the porosity and hydraulic conductivity will decrease over time as a result. If the pore space becomes too clogged with sediment, it is expected that the benefits of the PFC will degrade. Measuring the in-situ hydraulic conductivity should be an indicator as to whether or not the PFC is adequately allowing for the drainage of stormwater runoff. Therefore, analyzing the trends in hydraulic properties should give an indication as to how these properties are changing.

The objectives of the following statistical analyses are to determine whether the hydraulic properties – porosity and hydraulic conductivity – are changing over time and between each roadway location. The two data sets that will be analyzed are the core specimen porosity and laboratory hydraulic conductivity. Measurement of the porosity is described in detail in Chapter Three. Measurement of hydraulic conductivity is determined based on laboratory evaluation of the modified Forchheimer coefficients (described in Chapter Three) and numerical modeling results to convert the modified coefficients to the hydraulic conductivity (described in Chapter Five). Figures 6.1 and 6.2 show the raw data for the porosity and hydraulic conductivity, respectively. The statistical tests we will use compare the average of each set with the overall average. Therefore, in these figures, the colored horizontal lines correspond to the average value of each roadway for each year. The thick dashed lines correspond to the overall average for each year, regardless of location. Finally, the thin dotted line gives the overall average of the hydraulic property regardless of year or location. This helps to give an indication of the relative differences in averages.

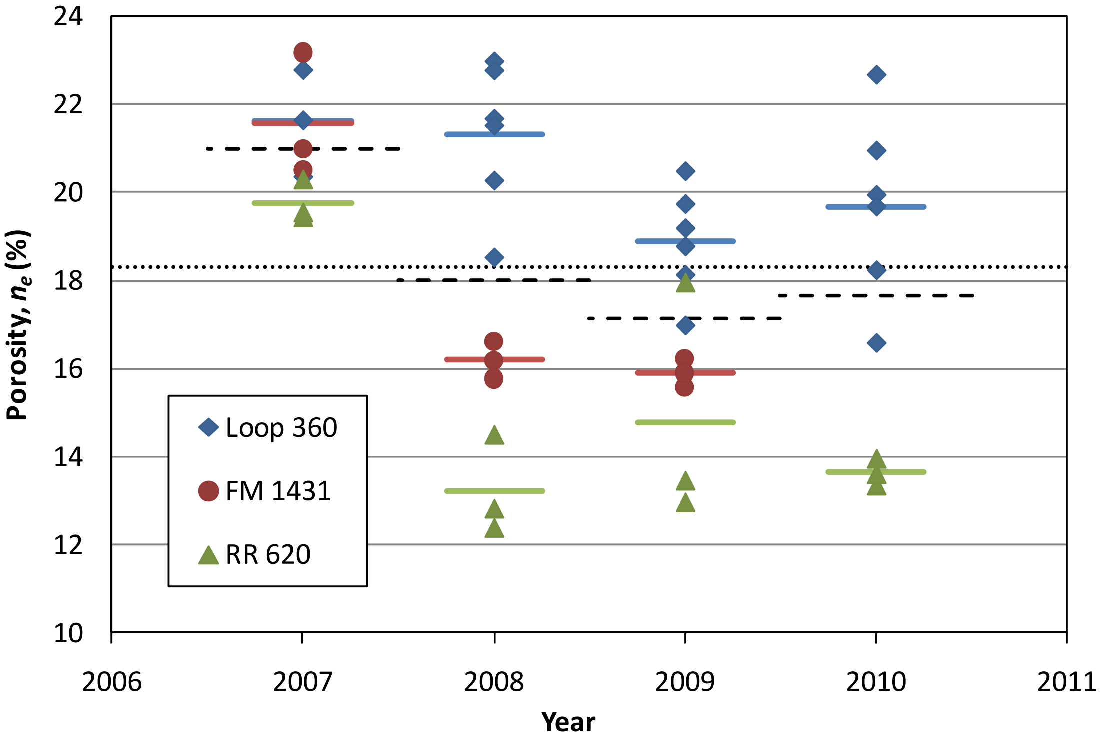

Figure 6.1 – Raw porosity data (averages indicated by lines)

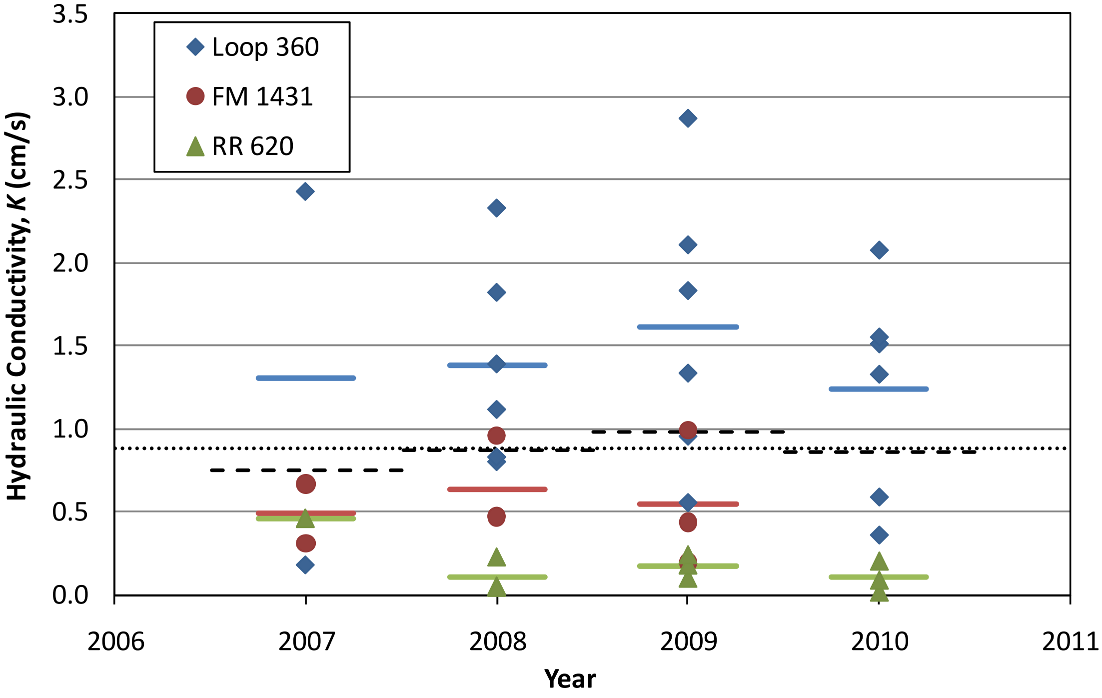

Figure 6.2 – Raw hydraulic conductivity data (averages indicated by lines)

In order to gain a clearer view of how the hydraulic properties are changing over time, Figures 6.3 and 6.4 show the average of porosity and hydraulic conductivity, respectively, for each year and each location. The error bars show plus/minus one standard deviation of the data. Based on Figure 6.3, we would expect that the porosity has decreased over time for each roadway and the variability in the porosity is not very large. Figure 6.4 suggests that the hydraulic conductivity has remained relatively constant over time for each roadway but the variability in hydraulic conductivity is much larger. The statistical tests described below will be used to determine whether the observed trends based on the data are statistically significant.

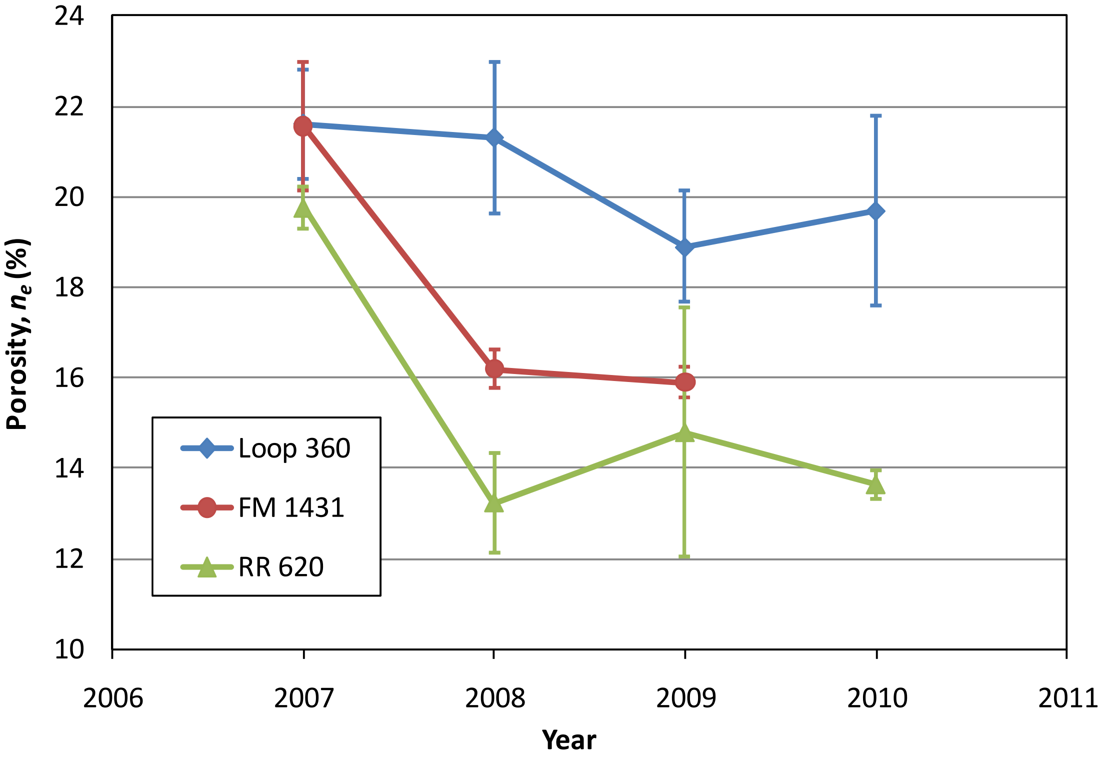

Figure 6.3 – Averaged porosity data

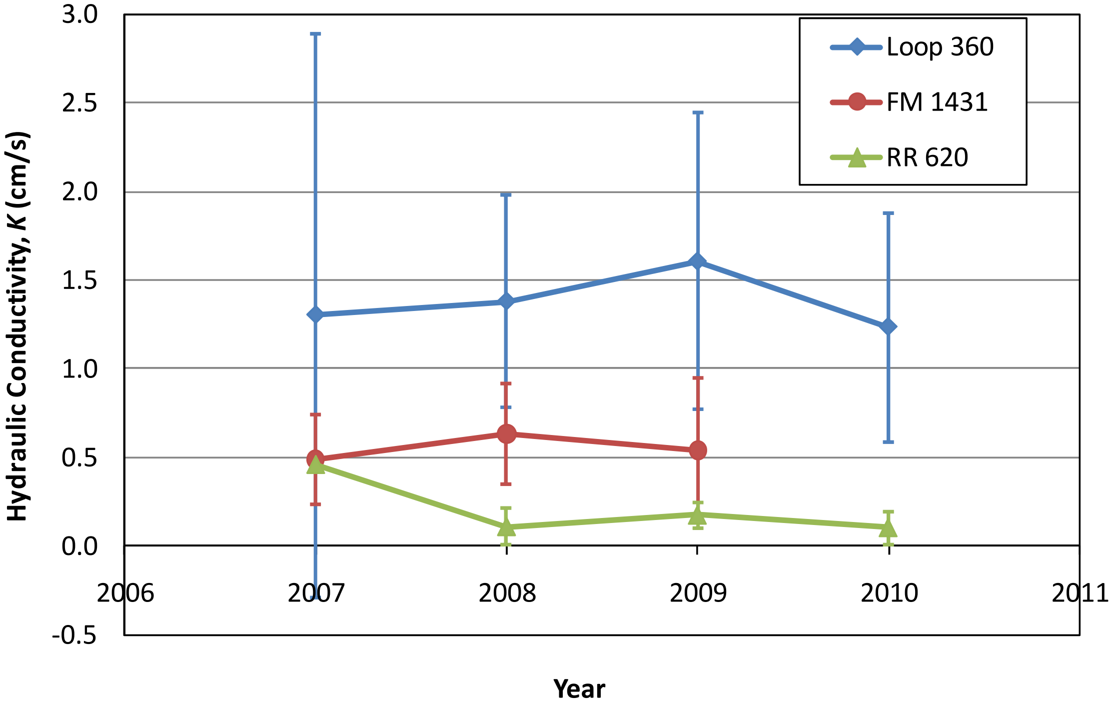

Figure 6.4 – Averaged hydraulic conductivity data

Another interesting way to look at the raw data is to compare the hydraulic conductivity as a function of porosity. Ideally there would be some relationship between these two drainage properties so that it is possible to predict one property from the other. Figure 6.5 shows these two properties graphed together for each roadway. There does not appear to be any correlation between these two properties. In general, as the porosity increases, the hydraulic conductivity increases as well. The large variability in this relationship means we cannot use one property to predict the other with any degree of confidence. For this reason, the two properties must be analyzed separately.

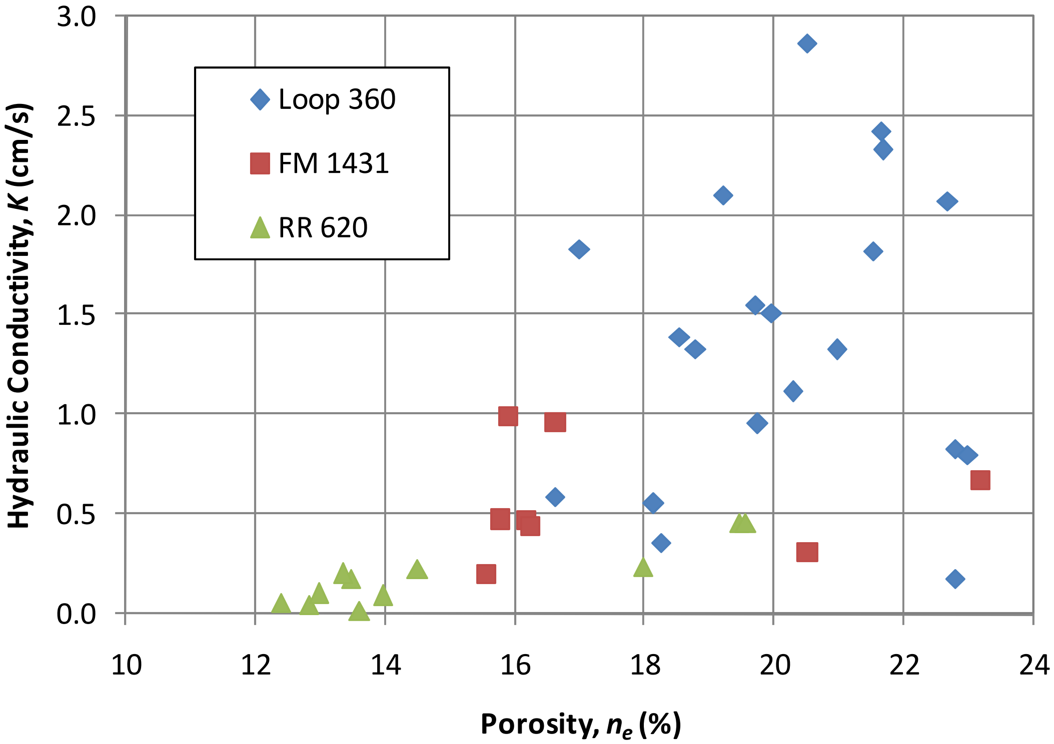

Figure 6.5 – Comparison of hydraulic conductivity and porosity data

6.2 Nonparametric Statistical Test Descriptions

In order to accomplish the above objective of this statistical analysis, we must use an appropriate statistical test. Only three or six core specimens were extracted at each roadway location for a given year. Therefore, the individual data sets we are interested in comparing are relatively small. This means we cannot make any assumptions about the distribution of the data, and we cannot use a large sample approximation. Due to this constraint, we must use an exact nonparametric statistical test. In order to compare groups of data (three or more groups), we can use the Kruskal-Wallis test. If we want to compare pairs of data we can use the Mann-Whitney test. Both of these tests determine statistics based on the ranks of the data and do not make any assumptions about the distribution of the data. If we had a large number of core specimens and could prove that the data were normally distributed, we would use the more common parametric ANOVA (analysis of variance) test and Students *t*-test, respectively, instead of the nonparametric tests.

6.2.1 Kruskal-Wallis Test

The Kruskal-Wallis test is used to determine whether three or more groups of data (either the three roadway locations for a given year or three years for a given roadway location) are statistically similar. This is the nonparametric equivalent to the ANOVA test. The Kruskal-Wallis test ranks the data and performs a nonparametric test on the ranks of the data. No assumptions are made about the distribution of the data. The null hypothesis of the Kruskal-Wallis test is: H_0 = all three groups of data have identical distributions. The alternative hypothesis is: H_a = at least one group differs in its distribution.

Helsel and Hirsch (2002) define the Kruskal-Wallis test statistic as follows:

$$K_W = \frac{12}{N(N+1)} \sum_{j=1}^{3} n_j \left[R_j - \frac{N+1}{2} \right]^2 \qquad (6.1)$$

In Equation (6.1), K_W is the Kruskal-Wallis test statistic, N is the total number of data points, n_j is the number of data points in group j, and R_j is the average of the ranks for group j. R_j is defined as follows:

$$R_j = \frac{1}{n_j} \sum_{i=1}^{n_j} R_{ij} \qquad (6.2)$$

In Equation (6.2), R_{ij} is the rank of the i^{th} data value in group j. Equation (6.1) gives the exact test statistic when there are no ties in the data. If ties occur, a correction must be made, but for the porosity and hydraulic conductivity data we will analyze, no ties will exist.

The test statistic can be compared to a table of critical K_W values in order to determine the decision on the null hypothesis for a significance level α'. If the calculated test statistic K_{Wcalc} value is greater than or equal to the critical statistic $K_{W\alpha'}$ obtained from the table for the given sample sizes and significance level α', then the null hypothesis is rejected at that significance level and the groups cannot be shown to have identical distributions. In this event, the test gives no indication of which group differs from the others. In order to determine which group is different from the others, the Mann-Whitney test must be conducted.

6.2.2 Mann-Whitney Test

The Mann-Whitney test is also typically referred to as the Wilcoxon test or rank sum test. It is an exact nonparametric test that compares the ranks of only two data groups. This is the nonparametric equivalent of the Students *t*-test. Again, no assumptions are made about the distribution of the data sets. The null hypothesis of the Mann-Whitney test is: H_0 = the means of the two groups are the same. The alternative hypothesis is: H_a = the means of the two groups are not equal. Due to the statement of the alternative hypothesis, we must consider a two tailed test.

Conover (1980) defines the Mann-Whitney test statistic as follows:

$$T = \sum_{i=1}^{n} R_i \tag{6.3}$$

In Equation (6.3), T is calculated for the smaller of the two groups with n data points. The larger of the two groups has m data points, for a total of $N = n + m$ data points when combined. Therefore, T is the sum of the ranks of each data point in the small group, R_i. If ties occur in the data, a correction must be made, but we will have no ties for the porosity and hydraulic conductivity data.

The test statistic can be compared to a table of critical values in order to determine the decision on the null hypothesis for a significance level α'. Because we are using a two sided test, we must look at the critical test statistic at level $\alpha'/2$. If the calculated test statistic T_{calc} is less than or equal to the critical test statistic $T_{\alpha'/2}$ obtained from the table for the given sample sizes and significance level α', then the null hypothesis is rejected at that significance level and the groups cannot be shown to have identical means. In this event, the test suggests that the two group means are not equal, but does not give any indication of which mean is larger than the other. This can, in general, be determined based on the value of the means.

6.2.3 Critical Test Statistics

Tables 6.1 and 6.2 give the critical test statistics for the Kruskal-Wallis test and Mann-Whitney test, respectively. A significance level of $\alpha' = 0.05$ is used to make the decision on the null hypothesis. Table 6.1 gives the critical values of $K_{W\alpha'}$ based on the number of data values in each group. These critical values were taken from Kanji (2006) or Conover (1980) and only the critical values for the group sizes relevant for these data sets are provided.

Table 6.1 – Critical test statistics for Kruskal-Wallis test

n_1	n_2	n_3	$K_{W0.05}$
2	2	2	4.571
2	3	3	5.361
2	6	6	5.410
3	3	3	5.600
3	3	6	5.615
3	6	6	5.625

Table 6.2 gives the critical values of $T_{\alpha'/2}$ based on the number of data points in each group. These critical values were taken from Kanji (2006) or Conover (1980) and only the critical values relevant for the group sizes needed for these data are provided. Since we are using a two sided test, the test statistic is taken at a significance level of $\alpha'/2 = 0.025$, or $\alpha' = 0.05$.

Table 6.2 – Critical test statistics for Mann-Whitney test

n	m	$T_{0.025}$
2	2	3.0
2	3	3.0
2	6	3.0
3	3	6.0
3	6	8.0
6	6	27.0
6	9	32.0
9	9	62.0

6.3 Statistical Test Results on Porosity

6.3.1 Porosity Data Grouped by Year

The first step in analyzing the hydraulic data is to use the Kruskal-Wallis test on the porosity data grouped by year. Each year will be investigated independently and the porosity data for each of the three roadways will be compared for a given year. If the Kruskal-Wallis test shows that there is a difference in porosity for one of the years, we will reject the null hypothesis. In this event, we can conduct the Mann-Whitney test to determine which group (roadway) is different from the others.

Table 6.3 provides the calculated Kruskal-Wallis test statistic for the porosity data grouped by year, together with the critical Kruskal-Wallis test statistic (obtained from Table 6.1) at a significance level of $\alpha' = 0.05$ and the decision on the null hypothesis. We will reject the null hypothesis for $K_{Wcalc} \geq K_{W0.05}$ meaning one of the three groups is different from the others. The core specimens extracted in the year 2010 are not included here as cores were extracted from only two roadways.

Table 6.3 – Kruskal-Wallis test results for porosity data grouped by year

Year	K_{Wcalc}	$K_{W0.05}$	Decision
2007	5.422	5.600	Do Not Reject H_0
2008	9.346	5.615	Reject H_0
2009	7.462	5.615	Reject H_0

For the porosity data in 2007, we do not have sufficient evidence to reject the null hypothesis at a significance level of 0.05. This means that the data suggest that the porosity at each of the three roadways have identical distributions for the year 2007. This result is a desirable outcome as it says that the porosity at all three roadways is roughly the same when we started collecting core specimens. Therefore, all three roadways are starting at essentially the same porosity when the first core specimens were collected.

For the porosity data in 2008 and 2009, we reject the null hypothesis, meaning that at least one of the three roadways has a different porosity than the others. Based on visual inspection of our porosity data, this result is to be expected since there are significant changes in the data. If we would like to determine which road has a different porosity than the others, we must conduct the Mann-Whitney test. These results are summarized in Tables 6.4 and 6.5 for the 2008 and 2009 porosity data, respectively. We will reject the null hypothesis for $T_{calc} \le T_{0.025}$. Table 6.6 shows the Mann-Whitney test results for the 2010 porosity data collected only at Loop 360 and RR 620.

Table 6.4 – Mann-Whitney test results for 2008 porosity data

Roadways	T_{calc}	$T_{0.025}$	Decision
Loop 360 & FM 1431	6.0	8.0	Reject H_0
Loop 360 & RR 620	6.0	8.0	Reject H_0
FM 1431 & RR 620	6.0	6.0	Reject H_0

Table 6.5 – Mann-Whitney test results for 2009 porosity data

Roadways	T_{calc}	$T_{0.025}$	Decision
Loop 360 & FM 1431	6.0	8.0	Reject H_0
Loop 360 & RR 620	7.0	8.0	Reject H_0
FM 1431 & RR 620	9.0	6.0	Do Not Reject H_0

Table 6.6 – Mann-Whitney test results for 2010 porosity data

Roadways	T_{calc}	$T_{0.025}$	Decision
Loop 360 & RR 620	6.0	8.0	Reject H_0

For the year 2008, the Mann-Whitney test suggests that all three roadways have different porosity from each other. However, for 2009, the Mann-Whitney test suggests that FM 1431 and RR 620 have the same porosity. This is due in part to the large variability we observed in the RR 620 porosity data. Due to this large variability, the Mann-Whitney test cannot distinguish between the porosity at these two roadways, so we cannot reject the null hypothesis. Furthermore, for the year 2010, the Mann-Whitney test suggests that the porosity at the two roadways where cores were extracted are different from each other.

This analysis allows for a comparison of porosity data between roadways for each given year core specimens were extracted. Essentially, this tells us that the porosity (or changes in porosity) at a given roadway do not necessarily follow the same trends observed at another roadway. This should be expected due to the varying traffic volumes, rainfall events, and various other factors that are different at each of the three roadways. Furthermore, parametric tests can be conducted on these data (either the ANOVA test or Students *t*-test) which provide the same decisions on the null hypothesis as determined from the nonparametric tests described above at a significance level of 0.05. Therefore, although it is more appropriate to use a nonparametric test due to the small sample size, the corresponding parametric tests provide support for the same decisions on the null hypothesis.

6.3.2 Porosity Data Grouped by Location

We can repeat the above analysis for the data grouped by each roadway in order to determine how the porosity at a roadway changes in time. The results of the Kruskal-Wallis test are shown in Table 6.7 below. For Loop 360 and RR 620, there are four years worth of data; whereas for FM 1431 there are three years worth of data. However, due to difficulties in determining the critical test statistics for four or more groups, only the first three years worth of data (from 2007 to 2009) are analyzed. All four years worth of data for Loop 360 and RR 620 will be analyzed by using the parametric ANOVA test.

Table 6.7 – Kruskal-Wallis test results for porosity data from 2007 to 2009 grouped by roadway

Roadway	K_{Wcalc}	$K_{W0.05}$	**Decision**
Loop 360	6.225	5.625	Reject H_0
FM 1431	5.600	5.600	Reject H_0
RR 620	5.956	5.600	Reject H_0

For each roadway, we reject the null hypothesis suggesting that the porosity at each roadway location is changing through time from the year 2007 to 2009, which we observed from the original data. Similarly, if we conduct the ANOVA test on these data, we obtain the same decisions on the null hypothesis at a significance level of 0.05. In order to analyze all four years worth of porosity data from Loop 360 and RR 620, we are restricted to using the ANOVA test. The results of that test are provided in Table 6.8. The p-value is provided, and the decision is made based on the magnitude of the p-value relative to the significance level. If the p-value is greater than the significance level, we do not reject the null hypothesis, meaning the test suggests all four years worth of porosity data are the same.

Table 6.8 – ANOVA test results for porosity data from 2007 to 2010 grouped by roadway

Roadway	p-value	Decision
Loop 360	0.058	Do Not Reject H_0
RR 620	0.003	Reject H_0

Table 6.8 suggests that the porosity on Loop 360 is constant over time, whereas the porosity on RR 620 is changing over time. This matches our decision for RR 620 for the first three years worth of data. However, for Loop 360, this contradicts our decision determined from the first three years worth of data and reported in Table 6.7. There are several reasons for this discrepancy. First, the parametric ANOVA test is not expected to be as precise as the Kruskal-Wallis test due the small number of data samples. Second, we cannot determine if the data are normally distributed, as required by the ANOVA test. Finally, the calculated p-value of 0.058 is very nearly equal to our significance level of 0.05. This test suggests that we are 94.2% confident that the porosity data on Loop 360 are changing over time. Due to the assumptions made in using the ANOVA test, perhaps it is appropriate to increase the significance level to 0.10 for the parametric test. In this case, we will reject the null hypothesis for the Loop 360 data suggesting the porosity changes over time, which agrees with our initial test findings for the nonparametric Kruskal-Wallis test.

From the Kruskal-Wallis test results and ANOVA test results provided above, we determined that the porosity has changed over time at each roadway. If we would like to determine which year has porosity different from the other years, we must conduct the Mann-Whitney test. The results for Loop 360, FM 1431, and RR 620 are shown in Tables 6.9, 6.10, and 6.11, respectively.

Table 6.9 – Mann-Whitney test results for Loop 360 porosity data

Years	T_{calc}	$T_{0.025}$	Decision
2007 & 2008	16.0	8.0	Do Not Reject H_0
2008 & 2009	26.0	27.0	Reject H_0
2009 & 2010	34.0	27.0	Do Not Reject H_0

Table 6.10 – Mann-Whitney test results for FM 1431 porosity data

Years	T_{calc}	$T_{0.025}$	Decision
2007 & 2008	6.0	6.0	Reject H_0
2008 & 2009	9.0	6.0	Do Not Reject H_0

Table 6.11 – Mann-Whitney test results for RR 620 porosity data

Years	T_{calc}	$T_{0.025}$	Decision
2007 & 2008	6.0	6.0	Reject H_0
2008 & 2009	8.0	6.0	Do Not Reject H_0
2009 & 2010	10.0	6.0	Do Not Reject H_0

From the above Mann-Whitney test results, we can make the following observations based on our decisions on the null hypothesis. On Loop 360, the porosity data remains constant from 2007 to 2008, decreases in 2009, and remains constant in 2010. For FM 1431, the porosity initially decreases from 2007 to 2008 but then remains constant from 2008 to 2009. Similarly, on RR 620, the porosity initially decreases from 2007 to 2008, but then remains constant for the years 2009 and 2010. These are the general trends we would expect from our raw data, and confirm our decisions obtained from the Kruskal-Wallis test above. This now provides a decision based on a statistical test to confirm our initial guesses. In addition, the RR 620 data appear to increase from 2008 to 2009 (based on Figure 6.3), but our Mann-Whitney test does not support this change in porosity due to the large variability in the 2009 data.

6.3.3 Travel Lane versus Shoulder Porosity

One final test to conduct in this research study has to deal with porosity in the travel lane versus porosity on the roadway shoulder. Loop 360 has a large enough shoulder so that core specimens can be extracted from both the travel lane and shoulder. However, only cores extracted in 2008, 2009, and 2010 were obtained from both locations; the 2007 cores were only extracted from the travel lane. Several researchers (c.f. Isenring et al., 1990; Van Heystraeten and Moraux, 1990; Berbee et al., 1999; and Pagotto et al., 2000) suggest that the pumping action of tires in the travel lane will help to remove trapped sediment in the PFC pore space, thereby increasing the porosity and hydraulic conductivity. This is also a concern in terms of design speed on a roadway with a PFC overlay. Typically, a larger design speed (80 km/hr) is considered more desirable due to this assumed pumping action of the tires which will help maintain adequate porosity. In order to test whether our data support this claim, we can use our two statistical tests to make a decision on whether the porosity in the travel lane is larger than the porosity in the shoulder. Figure 6.6 presents the porosity data from Loop 360 divided by travel lane or shoulder. These data are taken from the original data presented in Figure 6.1.

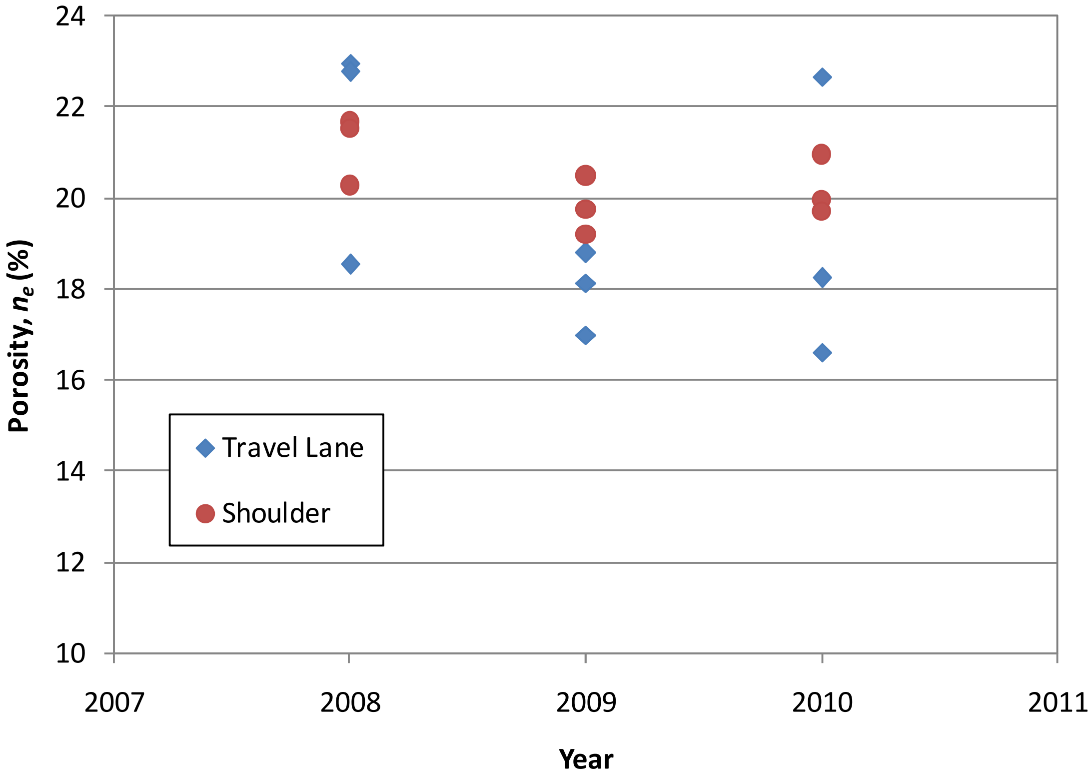

Figure 6.6 – Travel lane versus shoulder porosity data on Loop 360

We will start by analyzing the porosity data in the travel lane. Because we only have porosity data in the shoulder for the last three years worth of data, we will only analyze these three years of data for the travel lane as well (2008 to 2010). For the Kruskal-Wallis test, we obtain $K_{Wcalc} = 3.289$, which when compared to $K_{W0.05} = 5.600$, we do not reject the null hypothesis. This suggests that the porosity in the travel lane has not changed over time for Loop 360 from 2008 to 2010 and might confirm our claim that the pumping action of tires helps to maintain porosity. This seems to contradict our findings in Table 6.7 which suggest that the porosity does change over time for Loop 360. However, we are now looking at a different data set, which has more relative variability due to the smaller number of data points, making it more difficult for the Kruskal-Wallis test to reject the null hypothesis. We can conduct a similar test on the three years of data for porosity in the shoulder also using the Kruskal-Wallis test. This test gives $K_{Wcalc} = 3.467$, which when compared to $K_{W0.05} = 5.600$, we do not reject the null hypothesis. Again, this seems to contradict the previous claim that the porosity in Loop 360 decreases from 2008 to 2010. However, we are again looking at a different data set with a smaller number of data points, meaning we have less confidence in our decision to reject the null hypothesis.

The above test results suggest that the porosity in the travel lane of Loop 360 has not changed with time over the years 2008 to 2010; similarly, the porosity in the shoulder of Loop 360 has not changed with time. We can now compare the porosity in the travel lane to the porosity in the shoulder using the Mann-Whitney test. The results of these data give $T_{calc} = 72.0$, which when compared to $T_{0.025} = 62.0$, we do not reject the null hypothesis. This suggests that for our limited data set, we cannot distinguish differences between the porosity in the travel lane and the shoulder. The average porosity in the travel lane from the three years of data is 19.52%, whereas the average porosity in the shoulder for the three years of data is 20.39%. This confirms that the two porosity values cannot be assumed to be different from one another. Therefore, this statistical decision does not support the claim suggesting the pumping action of tires helps to remove sediment from the pore space. However, due to the limited number of data available, there may not be sufficient information to make a reliable decision.

6.4 Statistical Test Results on Hydraulic Conductivity

6.4.1 Hydraulic Conductivity Data Grouped by Year

The same statistical analysis conducted on the porosity data shown above will be conducted on the hydraulic conductivity data of each core specimen. The hydraulic conductivity is obtained through laboratory testing to determine the modified Forchheimer coefficients. These data are then converted to the original Forchheimer coefficients through the use of numerical modeling, resulting in an accurate measurement of hydraulic conductivity, as reported in Section 5.5.4. Each year will be investigated independently and the hydraulic conductivity data for each of the three roadways will be compared for a given year. If the Kruskal-Wallis test shows that there is a difference in hydraulic conductivity for one of the years, we will reject the null hypothesis. In this event, we can conduct the Mann-Whitney test to determine which group is different from the others. For the year 2010, only the Mann-Whitney test will be conducted since core specimens were extracted at only two roadways.

Table 6.12 provides the calculated Kruskal-Wallis test statistic for the hydraulic conductivity data grouped by year, together with the critical Kruskal-Wallis test statistic (obtained from Table 6.1) at a significance level of α' = 0.05 and the decision on the null hypothesis. We will reject the null hypothesis for $K_{Wcalc} \geq K_{W0.05}$, meaning one of the three groups is different from the others.

Table 6.12 – Kruskal-Wallis test results for hydraulic conductivity data grouped by year

Year	K_{Wcalc}	$K_{W0.05}$	**Decision**
2007	0.000	4.571	Do Not Reject H_0
2008	8.115	5.615	Reject H_0
2009	7.603	5.615	Reject H_0

For the hydraulic conductivity data in 2007, we do not have sufficient evidence to reject the null hypothesis at a significance level of 0.05. This means that the data suggest that the hydraulic conductivity at each of the three roadways have identical distributions for the year 2007. This result is not necessarily expected due to the range of average hydraulic conductivity values at each roadway, but the variability within those averages is very large meaning we do not have sufficient evidence to reject the null hypothesis. This is the same result we determined from the porosity data for the year 2007.

For the hydraulic conductivity data in 2008 and 2009, we reject the null hypothesis meaning that at least one of the three roadways has a different hydraulic conductivity than the others. Based on visual inspection of our hydraulic conductivity data, this result is to be expected since there are significant differences in the data and the variability in the average data has decreased. If we would like to determine which road has a different hydraulic conductivity than the others, we must conduct the Mann-Whitney test. These results are summarized in Tables 6.13, 6.14, and 6.15 for the 2008, 2009, and 2010 hydraulic conductivity data, respectively. We will reject the null hypothesis for $T_{calc} \leq T_{0.025}$.

Table 6.13 – Mann-Whitney test results for 2008 hydraulic conductivity data

Roadways	T_{calc}	$T_{0.025}$	**Decision**
Loop 360 & FM 1431	8.0	8.0	Reject H_0
Loop 360 & RR 620	6.0	8.0	Reject H_0
FM 1431 & RR 620	6.0	6.0	Reject H_0

Table 6.14 – Mann-Whitney test results for 2009 hydraulic conductivity data

Roadways	T_{calc}	$T_{0.025}$	**Decision**
Loop 360 & FM 1431	8.0	8.0	Reject H_0
Loop 360 & RR 620	6.0	8.0	Reject H_0
FM 1431 & RR 620	7.0	6.0	Do Not Reject H_0

Table 6.15 – Mann-Whitney test results for 2010 hydraulic conductivity data

Roadways	T_{calc}	$T_{0.025}$	**Decision**
Loop 360 & RR 620	6.0	8.0	Reject H_0

For the year 2008, the Mann-Whitney test suggests that all three roadways have different hydraulic conductivities from each other. However, for 2009, the Mann-Whitney test suggests that FM 1431 and RR 620 have the same hydraulic conductivity. This is due in part to the large variability we observed in the FM 1431 hydraulic conductivity data. Due to this variability, the Mann-Whitney test cannot distinguish between the hydraulic conductivity at these two roadways, so we cannot reject the null hypothesis. For the year 2010, we reject the null hypothesis. As expected, the hydraulic conductivity at Loop 360 is greater than that at RR 620. It is interesting to note that the decisions made based on the statistical analysis for the hydraulic conductivity data grouped by year is virtually the same as the decisions made on the porosity data.

This analysis provides a comparison of the hydraulic conductivity data between roadways for a given year in order to determine any statistical differences in the data. In general, each roadway has a different hydraulic conductivity than the other roadways. As with the porosity data, this suggests that the magnitudes of the hydraulic conductivity data, as well as any changes, vary depending on roadway location. Of particular interest would be the initial hydraulic conductivity of each roadway immediately after construction of the PFC layer. There are large differences in hydraulic conductivity at each roadway which may be attributed to varying construction methods. Furthermore, as with the porosity data, the equivalent parametric statistical tests provide support for the decision on the null hypothesis as determined from the nonparametric tests.

6.4.2 Hydraulic Conductivity Data Grouped by Location

We can repeat the above analysis for the data grouped by each roadway in order to determine how the hydraulic conductivity at a roadway changes in time. The results of the Kruskal-Wallis test are shown in Table 6.16 below. For Loop 360 and RR 620, there are four years worth of data; whereas for FM 1431 there are three years worth of data. As previously mentioned, due to difficulties in determining accurate critical test statistics for four or more groups, only the first three years worth of data (from 2007 to 2009) are analyzed with the Kruskal-Wallis test. All four years worth of data for Loop 360 and RR 620 will be analyzed using the ANOVA test.

Table 6.16 – Kruskal-Wallis test results for hydraulic conductivity data from 2007 to 2009 grouped by roadway

Roadway	K_{Wcalc}	$K_{W0.05}$	Decision
Loop 360	0.267	5.410	Do Not Reject H_0
FM 1431	0.556	5.361	Do Not Reject H_0
RR 620	4.694	5.361	Do Not Reject H_0

For each roadway from 2007 to 2009, we do not reject the null hypothesis suggesting that the hydraulic conductivity at each roadway location is constant through time, which appears to be reasonable from the original data. Therefore, although we observed a decrease in porosity at each roadway over time, the hydraulic conductivity has not been decreasing over time from a statistical standpoint. Similarly, if we conduct the ANOVA test on these three years of data, for Loop 360 and FM 1431, we do not reject the null hypothesis. However, the ANOVA test suggests we reject the null hypothesis for RR 620 with a p-value of 0.011. This suggests that the hydraulic conductivity has changed from the year 2007 to 2009 and contradicts our decision based on the Kruskal-Wallis test. Due to the small sample size, it is expected that the nonparametric Kruskal-Wallis test provides the more accurate decision.

We can also use the ANOVA test in order to analyze the four years of hydraulic conductivity data for Loop 360 and RR 620. The decision of the ANOVA test and the corresponding p-value are provided in Table 6.17.

Table 6.17 – ANOVA test results for hydraulic conductivity data from 2007 to 2010 grouped by roadway

Roadway	p-value	Decision
Loop 360	0.868	Do Not Reject H_0
RR 620	0.008	Reject H_0

Table 6.17 suggests that the hydraulic conductivity on Loop 360 is constant over time, whereas the hydraulic conductivity on RR 620 is changing over time. This matches our decision on Loop 360 for the first three years worth of data. However, this contradicts our decision on RR 620 from the Kruskal-Wallis test.

In order to determine whether the hydraulic conductivity data on RR 620 is changing over time, we can conduct the Mann-Whitney test for all four years of data. Table 6.18 provides the analysis of the RR 620 data.

Table 6.18 – Mann-Whitney test results for RR 620 hydraulic conductivity data

Years	T_{calc}	$T_{0.025}$	Decision
2007 & 2008	6.0	3.0	Do Not Reject H_0
2008 & 2009	8.0	6.0	Do Not Reject H_0
2009 & 2010	8.0	6.0	Do Not Reject H_0

For the Mann-Whitney test, we do not reject the null hypothesis, meaning there is not sufficient evidence to determine whether there is a change in hydraulic conductivity. This suggests that the hydraulic conductivity data is constant on RR 620 from the year 2007 to 2010. This agrees with our Kruskal-Wallis test results, but contradicts the ANOVA test results. It is expected due to the small sample size and lack of ability to determine whether the data are normally distributed that the nonparametric tests would provide a more accurate decision on the null hypothesis. Therefore, it can be assumed that the hydraulic conductivity data on RR 620 is statistically constant over time, and there is not sufficient evidence to determine a change in hydraulic conductivity. The above statistical analysis suggests that the hydraulic conductivity at each roadway has remained constant over time. Although we observed a statistical decrease in porosity over time at each roadway, this does not correspond to a statistical decrease in hydraulic conductivity at this point in time. The main reason we cannot determine a statistical decrease in hydraulic conductivity over time is the much larger variability in hydraulic conductivity. Because of this variability, the statistical tests do not have enough information to determine a trend in the data.

6.4.3 Travel Lane versus Shoulder Hydraulic Conductivity

The final test to conduct on the hydraulic conductivity data is a comparison between the travel lane versus the roadway shoulder. In order to test whether our data support the claim that the pumping action of vehicle tires result in a greater hydraulic conductivity, we can use our two statistical tests to make a decision on whether the hydraulic conductivity in the travel lane is larger than in the shoulder. Figure 6.7 presents the hydraulic conductivity data from Loop 360 divided by travel lane or shoulder. These data are taken from the original data presented in Figure 6.2.

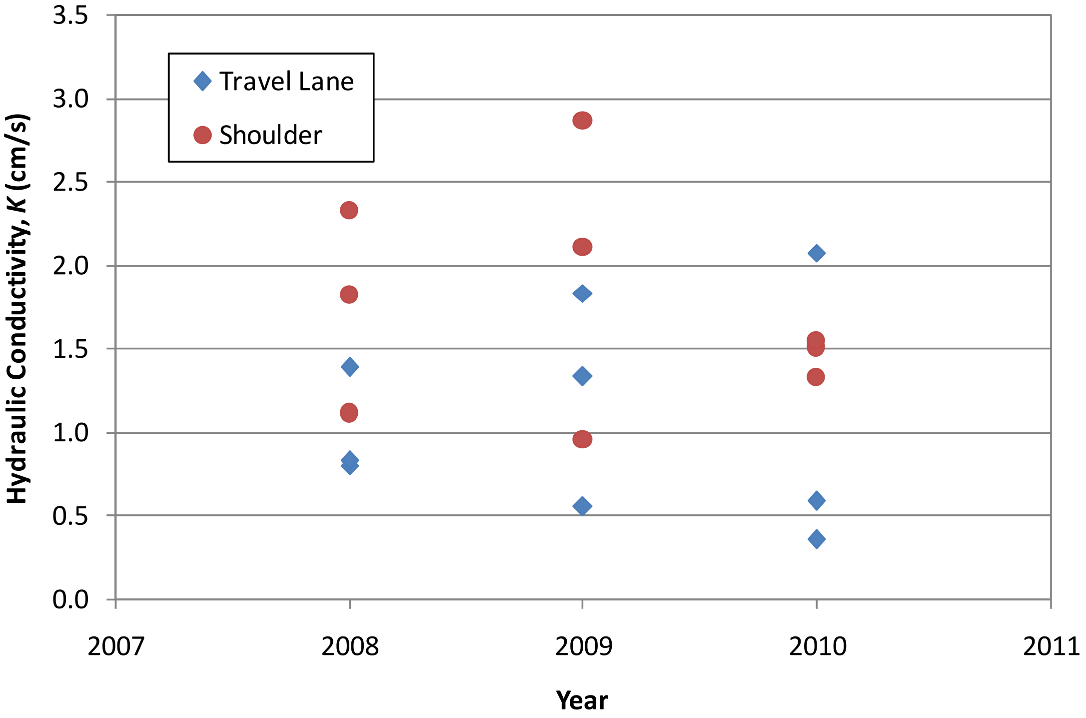

Figure 6.7 – Travel lane versus shoulder hydraulic conductivity data on Loop 360

We will start by analyzing the hydraulic conductivity data in the travel lane. Because we only have hydraulic conductivity data in the shoulder for the last three years (2008 to 2010), we will only analyze these three years worth of data in the travel lane. For the Kruskal-Wallis test, we obtain $K_{W_{calc}} = 0.267$, which when compared to $K_{W0.05} = 5.600$, we do not reject the null hypothesis. This suggests that the hydraulic conductivity in the travel lane has not changed over time for Loop 360. This agrees with our findings in Tables 6.16 and 6.17 which suggest that the hydraulic conductivity remains constant over time for Loop 360. We can conduct a similar test on the three years of data for hydraulic conductivity in the shoulder also using the Kruskal-Wallis test. This test gives $K_{W_{calc}} = 0.622$, which when compared to $K_{W0.05} = 5.600$, we do not reject the null hypothesis. Again, this agrees with the previous claim that the hydraulic conductivity at Loop 360 remains constant with time.

The above test results suggest that the hydraulic conductivity in the travel lane of Loop 360 has not changed with time. Similarly, the hydraulic conductivity in the shoulder of Loop 360 has not changed with time. We can now compare the hydraulic conductivity in the travel lane to the hydraulic conductivity in the shoulder using the Mann-Whitney test. The results of this data give $T_{calc} = 63.0$, which when compared to $T_{0.025} = 62.0$, we do not reject the null hypothesis. This suggests that for our limited data set, we cannot distinguish differences between the hydraulic conductivity in the travel lane and the shoulder. The average hydraulic conductivity in the travel lane from the last three years of data is 1.08 cm/s, whereas the average hydraulic conductivity in the shoulder for the three years of data is 1.73 cm/s. Although it appears the average hydraulic conductivity in the shoulder is greater than the average hydraulic conductivity in the travel lane, due to the variability in the data we do not have sufficient evidence to statistically distinguish between the two. Therefore, this decision does not support the claim suggesting the pumping action of tires helps to remove sediment from the pore space. However, due to the limited number of data available, there may not be sufficient information to make a reliable decision.

6.5 Experimental Forchheimer Coefficients Compared to Empirical Equations

Various studies have been conducted in the past which attempt to approximate the original Forchheimer coefficients (*a* and *b*) from properties of the fluid and porous medium. Although these empirical approximations typically work well for the material which was being studied, they do not translate to most other porous media that exhibit nonlinear flow. Sidiropoulou et al. (2007) provide a good overview of many of the empirical equations used to estimate the Forchheimer coefficients. These estimates typically depend on the porosity, particle diameter, and fluid properties being tested. Several of these empirical equations will be discussed here and compared to the experimental results obtained for this research study on PFC.

Ergun (1952) was one of the first researchers to develop equations to estimate the Forchheimer coefficients. These equations are based on the Kozeny-Carman model and give the following empirical relations:

$$a = \frac{150\mu(1-n_e)^2}{\rho g n_e^3 D_p^2} \tag{6.4}$$

$$b = \frac{1.75(1-n_e)}{g n_e^3 D_p} \tag{6.5}$$

Equations (6.4) and (6.5) estimate the Forchheimer coefficients based on the fluid viscosity μ and density ρ as well as the porous medium porosity n_e and particle diameter D_p. For the purposes of this comparison, the PFC particle diameter that will be used is the d_{50} diameter obtained from the particle size distribution used for mix design given in TxDOT (2004b).

Ward (1964) suggests the following empirical equations to estimate the Forchheimer coefficients:

$$a = \frac{360\mu}{\rho g D_p^2} \tag{6.6}$$

$$b = \frac{10.44}{g D_p} \tag{6.7}$$

Although the above relationships worked well for the porous media tested, the empirical Equations (6.6) and (6.7) are not functions of the porosity. Therefore, when compared to the PFC results, Ward's equations will not change when the PFC porosity changes. This is problematic because there is no way to measure D_p when the PFC porosity decreases. For comparisons with the PFC experimental data, it is expected that Ward's equations will not produce reliable estimates. For this reason, the empirical equations presented by Ward will not be compared to the PFC data.

Kovacs (1981) derived the following equations for spherical particles:

$$a = \frac{144\mu(1-n_e)^2}{\rho g n_e^{3} D_p^{2}} \tag{6.8}$$

$$b = \frac{2.4(1-n_e)}{g n_e^{3} D_p} \tag{6.9}$$

Equations (6.8) and (6.9) are very similar to the equations proposed by Ergun. Therefore, we would expect that these two sets of equations produce similar results.

Finally, Kadlec and Knight (1996) present the following equations:

$$a = \frac{255\mu(1-n_e)}{\rho g n_e^{3.7} D_p^{2}} \tag{6.10}$$

$$b = \frac{2(1-n_e)}{g n_e^{3} D_p} \tag{6.11}$$

Again, these equations are similar in form to those proposed by Ergun and Kovacs with slightly different exponential terms. As previously mentioned, the particle diameter used for the comparison is the d_{50} diameter obtained from the mix design for PFC. A sieve analysis on typical PFC mixtures suggests a diameter of 9.525 mm correspond to a range of percent passing particles. This range is from 35% to 60% passing. Therefore, the range of values for d_{50} is between 8.5 mm and 10.5 mm based on the resulting gradation curves. Using an average d_{50} of 9.5 mm for use as D_p in the equations above will provide a comparison to the empirical equations and the experimental values obtained for this research. It should be noted that due to the entrapment of sediment in the pore space, the actual average particle diameter cannot be determined.

Figures 6.8 and 6.9 show the measured PFC core specimen hydraulic conductivity and original nonlinear Forchheimer coefficient, respectively, as determined from the experimental data and numerical modeling compared to the empirical equations in the literature described above. If the empirical equations agree well with the experimental PFC data, then the resulting graph should fall on a 1:1 line. For the hydraulic conductivity data, the empirical equation proposed by Kadlec and Knight (1996) has the best agreement to the experimental data. Although the Kadlec and Knight equation does not fall directly on the 1:1 line shown in Figure 6.8, it does give a same order of magnitude estimate of the hydraulic conductivity. The empirical equations proposed by Ergun (1952) and Kovacs (1981) greatly overestimate the measured PFC hydraulic conductivity. However, as expected, these two empirical equations produce nearly the same estimates. In conclusion, the empirical equation proposed by Kadlec and Knight produce the same order of magnitude estimate of PFC hydraulic conductivity. The Ergun and Kovacs equations are not recommended for estimating PFC hydraulic conductivity as they overestimate the hydraulic conductivity.

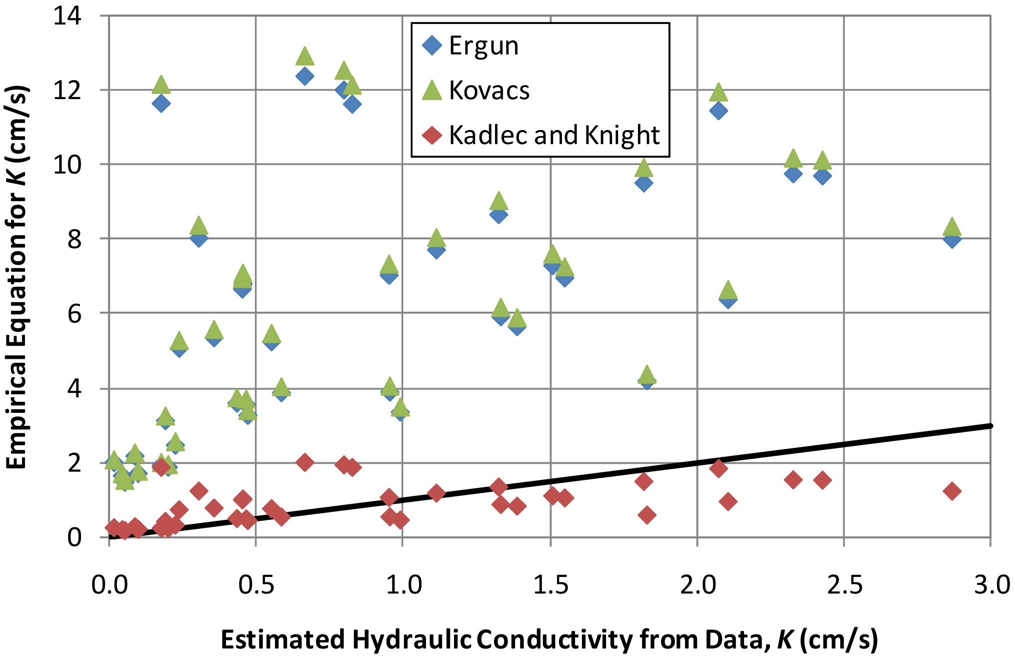

Figure 6.8 – Empirical equations for estimating hydraulic conductivity

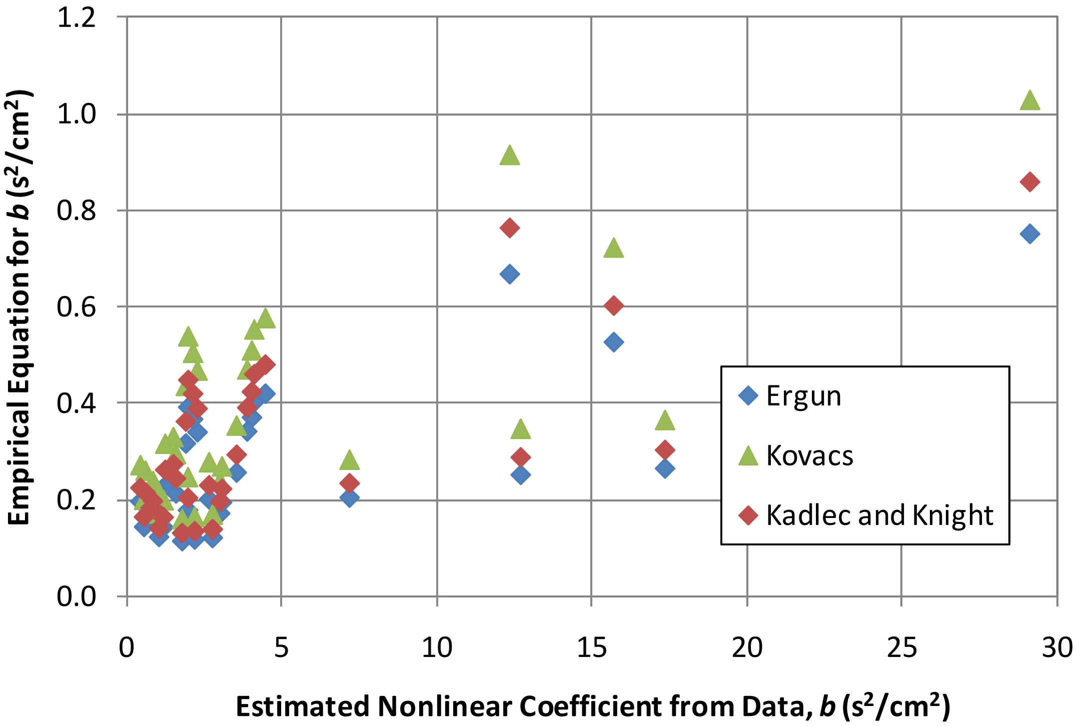

Figure 6.9 – Empirical equations for estimating nonlinear Forchheimer coefficient

Figure 6.9 shows the measured and empirical nonlinear Forchheimer coefficient. Clearly, the empirical equations drastically underestimate the nonlinear coefficient when compared to the measured data. Four measured values of *b* were so large that they were not included in the above graph. All three empirical equations shown here result in roughly the same estimate. Therefore, in general, these empirical equations for estimating the nonlinear coefficient do not apply to the measured PFC data.

6.6 Sediment Removal Estimate

One of the critical questions remaining about the water quality benefits of PFC is whether the PFC is actually removing pollutants from the stormwater runoff, or simply reducing the source of the pollutants from being washed off of vehicles due to the reduced splash and spray. The removal mechanism which results in an improvement in water quality can be examined by investigating the change in porosity over time together with the expected volume of sediment removed from the stormwater runoff. If the PFC overlay acts primarily as a filter in removing sediment, then the volume of sediment removed from the runoff will result in the observed decrease in porosity over time. On the other hand, if the PFC overlay is simply reducing the source of the sediment by not washing sediment off of cars, then the volume of sediment removed from the runoff will be greater than the volume of sediment needed to decrease the observed porosity.

In this analysis, sediment removal will be estimated as a mass of sediment per surface area of pavement. Two sediment removals will be estimated and then compared to one another. The first sediment removal estimate is based on the observed decrease in core specimen porosity over time. The mass of sediment per volume of PFC layer can be determined by multiplying the change in porosity times an assumed sediment density. This makes the assumption that all of the change in porosity is a result of trapped sediment volume. A sediment density of 2.65 g/cm^3 was used for this analysis. The sediment mass per unit area is determined by multiplying the sediment mass per volume times the average PFC thickness. The PFC thickness is determined from the thickness of the core specimens for all years. Table 6.19 provides the change in porosity and resulting sediment mass per area needed to cause that observed change in porosity from the 2007 cores to the 2010 cores. In general, several hundred milligrams (mg) of sediment per square centimeter surface area of pavement are needed to clog the PFC pore space and result in the observed decrease in porosity.

Table 6.19 – Sediment mass estimate for change in porosity

Roadway	Average Thickness (cm)	Decrease in Porosity (%)	Sediment Mass (mg/cm^2)
Loop 360	4.01	2.70	287
FM 1431	3.23	5.65	483
RR 620	3.50	6.53	606

In order to determine the estimated sediment mass per area that we would expect from water quality data, we must investigate the rainfall over the time period together with the average total suspended solids (TSS) concentration and TSS removal observed due to the use of PFC. The rainfall data we will use is specifically for a rain gage located near the core extraction site on Loop 360. Precipitation data was collected from the Lower Colorado River Authority (LCRA) Hydromet data set at the "Bull Creek at Loop 360, Austin" rain gage (LCRA, 2010). Previous research conducted on the water quality benefits of PFC (Stanard, 2008 and Frasier, 2009) measured the TSS concentration in the runoff from a conventional impervious asphalt surface as well as a PFC overlay. These results show that the TSS concentration from PFC runoff is approximately 90% less than from conventional pavement. The difference between the conventional TSS concentration and the PFC TSS concentration is the assumed volume of sediment trapped within the PFC, which causes a decrease in porosity. Therefore, with known values of rainfall depth, average TSS concentration from a conventional roadway, and TSS removal due to the PFC, we can determine the expected mass of sediment trapped per unit area of PFC.

The average TSS concentration from conventional pavement is roughly 135 mg/L as reported by Stanard (2008) and Frasier (2009). This is a general average and varies from storm event to storm event, but is useful for an approximation of the amount of sediment that may be trapped in the PFC pore space. If the PFC is assumed to remove 90% of this concentration according to water quality measurements, then the TSS concentration from a PFC surface is 14 mg/L, meaning 121 mg/L of TSS is expected to be retained within the PFC pore space. The average sediment retained per unit area can be determined by multiplying the TSS concentration times the rainfall for a given period of time. The cumulative rainfall since the first core extraction date to the fourth and final core extraction date is 243.1 cm (LCRA, 2010). This rainfall can be split based on core extraction dates. The rainfall between the first and second set of cores is 97.4 cm for the year 2007. The year 2008 had 42.6 cm of rain, and the year 2009 had 103.1 cm of rainfall. The cumulative rainfall amount times the assumed average TSS concentration retained within the PFC pore space (121 mg/L) results in an average sediment removal of 29.5 mg/cm^2. Clearly this value, when compared to the estimated sediment mass required to change the observed porosity reported in Table 6.19, is significantly less. Therefore, the 90% removal of TSS does not produce nearly enough mass of sediment needed to cause the observed decrease in porosity.

Part of the problem with estimating the trapped mass of sediment in the PFC pore space is that this method only considers the entrapment of sediment in water produced from rainfall runoff. Sediment may become trapped within the PFC pore space even when rainfall is not present. This entrapment of solids during dry conditions is what has caused the PFC porosity to decrease over time. The entrapment of particles during rainfall events most likely produces minimal decreases in porosity. Although the results of this analysis do not provide any definite information on the removal mechanism of suspended solids from runoff, it does show that the observed change in porosity accounts for much more trapped sediment than is expected from water quality data. If the opposite finding was observed, i.e. if the sediment mass from water quality data was greater than the change in porosity, then we could assume that PFC is simply reducing the source of pollutants from being washed off vehicles. Since this finding did not occur, we can at least assume that the PFC has the capacity to retain 90% of the TSS concentration within the stormwater runoff.

Chapter Seven
Conclusions

7.1 Summary of Problem

Permeable Friction Course (PFC) is an innovative roadway material that allows rainfall to drain within the pavement as opposed to across the surface. PFC is a layer of porous asphalt up to 50 mm thick overlain on a conventional impervious roadway surface so that the structural integrity of the entire roadway pavement system is not compromised. Water flows by gravity at the underlying impervious boundary to the roadway shoulder. The reduction of surface runoff improves driver safety by reducing splash and spray behind vehicles, improving visibility, reducing the chance of hydroplaning, and improving wet friction (i.e. decreasing stopping distance) when compared to conventional pavements. In addition, PFC is also used for its environmental benefits as it has been shown to improve the stormwater quality and reduce the concentration of pollutants typically observed in highway runoff. The Texas Commission on Environmental Quality (TCEQ) recently approved the use of PFC as a stormwater best management practice on uncurbed roads with a design speed of 80 km/hr or greater. However, over time, the pore space of the PFC layer becomes clogged with trapped sediment resulting in an expected decrease in hydraulic properties (porosity and hydraulic conductivity). This expected loss of drainage capacity over time suggests that the benefits of PFC may be lost at a faster rate than the structural deterioration of the pavement. Therefore, accurate measurement of the hydraulic properties of PFC is necessary in order to ensure proper drainage capacity and maintain the driver safety and stormwater quality benefits associated with the use of PFC. Specifically, a quick nondestructive field test is needed in order to measure the in-situ hydraulic conductivity at any given time so that the drainage capacity of the PFC layer can be assessed.

Hydraulic testing on PFC core specimens and roadway surfaces reveals a nonlinear flow relationship which can be characterized using the Forchheimer equation.

Nonlinear flow is created as a result of the large hydraulic conductivity and large pore space within the PFC layer as well as the large hydraulic gradients imposed on the core specimens during testing. The two-dimensional flow pattern imposed during testing creates an additional complication which can be addressed through numerical modeling. Due to the two-dimensional diverging flow paths, a modified Forchheimer equation for the global conditions of the core specimen must be used. The modified Forchheimer equation relates the change in head through the core specimen to the volumetric flow rate, as opposed to the original Forchheimer equation which relates the local hydraulic gradient and local specific discharge. The modified Forchheimer coefficients obtained from experimental testing are related to the original Forchheimer coefficients through a finite difference numerical model of Forchheimer flow in two-dimensional cylindrical coordinates. Proper modeling of the flow characteristics can relate the measurable PFC hydraulic characteristics to the hydraulic conductivity. This is accomplished with the introduction of a scalar hydraulic conductivity ratio which allows for proper modeling of the original Forchheimer equation in two dimensions. With an accurate measurement of hydraulic conductivity, the extent of clogging over the life of the pavement can be observed in order to determine when maintenance or replacement of the PFC layer, based on drainage capacity, is necessary. Measurement of in-situ hydraulic conductivity is useful as an indicator as to when the driver safety and water quality benefits of the PFC layer are expected to decrease.

7.2 Research Objective Conclusions

Four major research objectives are addressed in this dissertation and related research study. The first objective addresses laboratory testing on PFC core specimens in order to measure its hydraulic properties: porosity and hydraulic conductivity. The second objective develops a field test methodology for measurement of in-situ hydraulic conductivity. The third objective investigates a numerical model of the two-dimensional nonlinear flow problem necessary to relate the measureable hydraulic characteristics to the true hydraulic conductivity. The fourth objective uses nonparametric statistical tests to analyze the measured hydraulic properties of PFC over time and at different locations in order to determine any trends or changes in the data which may give an indication of when the benefits of PFC are expected to degrade due to clogging of the pore space by trapped sediment.

7.2.1 Conclusions for Evaluation of Hydraulic Properties in the Laboratory

The first research objective investigates laboratory testing on PFC core specimens extracted from three roadways (Loop 360, FM 1431, and RR 620) around Austin, Texas (TX) over the past four years (2007 to 2010) and provides a methodology for determining the porosity and hydraulic characteristics of flow through the core specimen. The extraction of core specimens is accomplished by saw-cutting the roadway surface, which results in a cylindrical core specimen. The PFC core specimen porosity is determined using either an image analysis method or a submerged unit weight method. The submerged unit weight method is preferred as this method leaves the core intact and allows for additional hydraulic testing to be conducted.

Hydraulic testing of PFC core specimens in the laboratory consists of a series of constant head permeability tests. The large hydraulic gradients imposed on the core specimen during testing, combined with the large pore volumes in the PFC cores, result in a nonlinear flow relationship which can be modeled using the Forchheimer equation. The Forchheimer equation was chosen to model the nonlinear effects due to its ability to approximate Darcy's law for low hydraulic gradients and/or low specific discharge. The upper and lower no flow boundary conditions imposed on the core specimen create a two-dimensional cylindrical flow pattern which results in an additional complication due to the inability to directly measure the hydraulic gradient or specific discharge. This problem can be addressed by investigating the global conditions of the core specimen through the use of a modified Forchheimer equation (see Equation (3.4)). The modified Forchheimer coefficients can be determined from the constant head tests but give no indication of the hydraulic conductivity.

The PFC core specimen hydraulic conductivity can be determined through the use of numerical modeling. The result is a well defined test procedure for determining the hydraulic characteristics of two-dimensional nonlinear flow through PFC core specimens, which is both repeatable and reliable. Data collected on PFC core specimens over four years is reported. Core porosity values range from roughly 12% to 23%. A series of laboratory constant head tests allow for the determination of two modified Forchheimer coefficients, α and β, with the following ranges: $\alpha = 0.05$ to $5.76\ \mathrm{s/cm^2}$ and $\beta = 0.002$ to $3.01\ \mathrm{s^2/cm^5}$. Furthermore, falling head tests can be conducted on the core specimens, which result in roughly the same modified Forchheimer coefficients as determined from the constant head tests. Through numerical modeling, the modified Forchheimer coefficients can be related to the original Forchheimer coefficients in order to accurately determine the core specimen isotropic hydraulic conductivity.

7.2.2 Conclusions for Evaluation of Hydraulic Conductivity in the Field

Field testing on the PFC roadway surface can be conducted with a falling head test methodology in order to determine the in-situ hydraulic characteristics, which is the goal of the second research objective. In-situ measurement of the hydraulic conductivity is necessary in order to ensure proper drainage capacity of the PFC layer. If the hydraulic conductivity decreases due to trapped sediment in the pore space, the driver safety and water quality benefits are expected to degrade. Therefore, periodic measurement of in-situ hydraulic conductivity is required. A field test apparatus has been developed at the Center for Research in Water Resources (CRWR) specifically for this research study which creates a similar test setup and boundary conditions used in the laboratory. The upper no flow boundary is created with silicon vacuum grease placed on a metal support base, and the lower no flow boundary is imposed by the underlying impervious roadway surface. These boundary conditions result in two-dimensional cylindrical flow and force water to flow within the PFC pore space as opposed to on the roadway surface. The global flow characteristics can also be modeled with the modified Forchheimer equation for the two-dimensional flow pattern observed in the field. The result of the second research objective not only proposes a well defined test procedure for determining the in-situ hydraulic conductivity, but also proposes a standard piece of equipment used for measurement purposes. This equipment is both simple in design and requires very little instrumentation for proper measurements. The use of a stopwatch with a split function is the only instrumentation needed in order to record the three time-depth measurements used to determine the modified Forchheimer coefficients, α and β, through Equation (4.1). Therefore, any field technician can easily use this field test to accurately determine the in-situ hydraulic conductivity of the PFC layer.

Upon completion of the falling head test, the modified Forchheimer coefficients can be determined which have the following ranges: $\alpha = 0.01$ to $0.14\ \mathrm{s/cm^2}$ and $\beta = 1.2\times10^{-4}$ to $2.5\times10^{-3}\ \mathrm{s^2/cm^5}$. The simple, nondestructive field test proposed here is needed due to the additional time and effort needed to conduct tests on core specimens in the laboratory. Furthermore, extraction of the core specimens for lab testing may disturb the PFC layer resulting in inaccurate hydraulic data. The in-situ field test is much quicker and does not disturb the PFC layer.

7.2.3 Conclusions for Numerical Modeling of Hydraulic Characteristics

The third research objective investigates numerical modeling of the continuity equation in two-dimensional cylindrical coordinates in order to relate the experimentally measured modified Forchheimer coefficients, α and β, to the original Forchheimer coefficients, $a = 1/K$ and b, for determination of the hydraulic conductivity of a PFC core specimen. Due to the nonlinear form of the Forchheimer equation in two dimensions, additional efforts must be made in order to properly model the flow. Previous research has not fully addressed nonlinear flow in two dimensions. Proper modeling of the flow is accomplished through the introduction of a new scalar hydraulic conductivity ratio in order to allow for appropriate invariance properties of the nonlinear equations. The numerical model uses a finite difference scheme to solve the continuity equation in two-dimensional cylindrical coordinates. Expansion ratios are used in both the vertical and radial directions in order to refine the grid near the inflow boundary, where the largest hydraulic gradients occur.

Input parameters to the numerical model are the core dimensions (R_s, R_c, and b_c), the original Forchheimer coefficients (a and b), and the standpipe head (h_s). Both linear and nonlinear solutions of the head distribution through a core specimen are provided. The linear case uses Darcy's law and is solved with an implicit Crank-Nicolson scheme. The linear numerical model results are compared to an approximate analytic solution provided by Carslaw and Jaeger (1959) in order to ensure the model is producing desirable results. The nonlinear case models the Forchheimer equation and uses the iterative Gauss-Seidel method where the initial head value used to iterate about is the solution to the linear model. With the nonlinear head distribution determined, the global flow characteristics can be calculated. The outflow rate is determined from the outflow hydraulic gradient, and the results are fit to the modified Forchheimer equation using a regression equation to determine α and β. In addition, the nonlinear model results approach the linear Darcy flow case for small values of standpipe head and/or small nonlinear coefficients. Therefore, the Forchheimer equation approximates Darcy's law for low hydraulic gradients or specific discharges. This feature of the Forchheimer equation is the basis for choosing this equation to model the nonlinear flow effects. The value of the scalar hydraulic conductivity ratio provides information as to the location in the core specimen in which nonlinear effects are significant. As expected the hydraulic conductivity ratio shows the large nonlinear effects occur directly under the standpipe at the inflow boundary.

The results of the nonlinear numerical model are used to determine a relationship between the modified and original Forchheimer coefficients for a variety of core geometries. The two linear coefficients, α and a, as well as the two nonlinear coefficients, β and b, are linearly related, where the slope of this relationship depends on the dimensions of the core specimen: R_s, R_c, and b_c. Regression equations using a power law model were developed from 64 numerical simulations of the core geometry and provide useful relationships for estimating the original Forchheimer coefficients based on the measured modified Forchheimer coefficients. Finally, regression equations developed specifically for the CRWR field test apparatus used in this research allow for accurate measurement of the in-situ hydraulic conductivity. These regression equations provide very accurate estimates of the linear Forchheimer coefficient, but produce slightly larger errors in the estimate of the nonlinear Forchheimer coefficient. The estimates of the original Forchheimer coefficients obtained from the regression equations can be used as inputs to the nonlinear numerical model in order to determine the corresponding modified Forchheimer coefficients. A comparison of the modified Forchheimer coefficients obtained from the numerical model and the coefficients obtained from experimental data result in errors within an acceptable range of uncertainty. This allows for an estimate of the hydraulic conductivity and nonlinear original Forchheimer coefficient based on the core geometry and measured modified Forchheimer coefficients from experimental data.

For the PFC core specimens tested in the laboratory, the hydraulic conductivity K and nonlinear Forchheimer coefficient b have the following ranges: $K = 0.02$ to 2.87 cm/s and $b = 0.47$ to 640 s^2/cm^2. The in-situ hydraulic conductivity determined using the CRWR field test result in the following range of hydraulic conductivity and nonlinear Forchheimer coefficient: $K = 0.6$ to 3.6 cm/s and $b = 0.31$ to 5.21 s^2/cm^2.

7.2.4 Conclusions for Analysis of Hydraulic Properties

With four years of porosity and hydraulic conductivity data collected at three roadway sites around Austin, TX, a statistical analysis of the data can be conducted to determine any trends or changes in the data as addressed in the fourth research objective. Nonparametric statistical tests must be conducted on the data due to the small sample size and inability to show the data are normally distributed. The two nonparametric tests used are the Kruskal-Wallis test and Mann-Whitney test. The results of these tests show there have been statistically significant observed decreases in porosity at each roadway location over time. This suggests that the pore space of the PFC is becoming clogged with trapped sediment. In addition, all three roadways have different porosity, suggesting that the varying traffic conditions, construction methods, and environmental or hydrologic conditions at each site affect the porosity of the PFC layer. However, despite the observed statistical decrease in porosity over time, there has been no observed statistically significant decrease in hydraulic conductivity over time. Although the porosity is decreasing due to trapped sediment, this is not yet causing a significant decrease in hydraulic conductivity over time. Each of the three roadways has a different hydraulic conductivity from the other roadways, but these values are not changing in time due primarily to the large variability in hydraulic conductivity data. Furthermore, water quality monitoring from two roadway locations conducted by other researchers has shown the persistence of improved stormwater quality when compared to conventional roadway surfaces. The measurement of hydraulic conductivity is used as an indicator of when these water quality benefits will decrease. Since there has not been an observed decrease in hydraulic conductivity over time and water quality monitoring shows continued improved stormwater runoff quality to date, an indication of when we expect to see a degradation in drainage benefits due to a decrease in hydraulic conductivity has not been observed.

An estimate of the volume of sediment trapped within the pore space is presented based on the volume of sediment needed to result in the observed decrease in porosity versus the volume of sediment removed from stormwater runoff. This estimate suggests that the removal of total suspended solids from stormwater runoff does not provide a large enough sediment volume to result in the observed decrease in porosity over time. Therefore, the majority of the observed decrease in porosity is due to dry deposition of sediment on the roadway surface between rainfall events. Finally, the measured original Forchheimer coefficients are compared to empirical equations presented in the literature in order to determine the applicability of the empirical equations for use with PFC. Only one empirical equation, presented by Kadlec and Knight (1996), for estimating the linear original Forchheimer coefficient produced reasonable results. Therefore, the Forchheimer coefficients presented in previous literature do not generally apply to use in PFC materials. In conclusion, nonparametric statistical tests conducted on the collected hydraulic data of PFC core specimens show that the measured porosity has decreased over time, but no changes in hydraulic conductivity have been observed to date.

The results of this dissertation and associated research study are summarized here. A well-defined methodology for measurement of porosity and hydraulic conductivity on PFC core specimens in the laboratory using a series of constant head tests is presented. Testing involves two-dimensional nonlinear cylindrical flow and is modeled with a modified Forchheimer equation. In order to measure the in-situ hydraulic conductivity, a field test apparatus has been developed using a falling head test with similar boundary conditions created in the laboratory. The field test methodology is both simple and nondestructive allowing for accurate measurement of the modified Forchheimer coefficients. Numerical modeling of the Forchheimer equation in two-dimensional cylindrical coordinates is accomplished through the introduction of a scalar hydraulic conductivity ratio. This allows for a relationship between the measured modified Forchheimer coefficients and the original Forchheimer coefficients to be determined. Regression equations developed on a range of core dimensions allows for an estimate of the original Forchheimer coefficients from measured experimental data. The results of the numerical model also show where nonlinear flow effects are dominate within the core specimen and provide an improved method of modeling nonlinear flow in two dimensions. Finally, a statistical analysis on the measured hydraulic data suggest a decrease in porosity over time due to the entrapment of sediment, but the measured hydraulic conductivity has remained constant through time.

7.3 Related Research and Future Work

Additional research is currently being conducted on other aspects of the use of PFC by researchers at The University of Texas at Austin. Stormwater quality monitoring of three PFC sites on two separate roadways has shown that the improved water quality produced by PFC has persisted for nearly six years of operation. This research has been the basis for the recent approval of PFC as a new stormwater best management practice by TCEQ in the State of Texas. It should be noted that no maintenance of the PFC layer has been conducted during this time. Both water quality and rainfall runoff data have been collected at one of the stormwater monitoring sites. These data show the measured inflow rate from rainfall together with the resulting outflow rate after the water passes through the PFC layer. Research is also currently being conducted in the development of a finite volume numerical model of the entire roadway surface. This model, named Permeable Friction Course Drainage Code (PERFCODE) and described by Eck (2010), couples subsurface porous media flow together with surface runoff. The goal of PERFCODE is to model a time varying rainfall event for a given roadway geometry in order to determine the water surface elevation within the PFC layer, as well as to observe if, when, and where surface runoff will occur. This code is useful for design purposes to determine the required PFC thickness needed to ensure surface runoff does not occur for a given roadway width and slope. The model can be validated with collected rainfall runoff data at the stormwater monitoring site. An important input to this model is the porosity and hydraulic conductivity of the PFC layer. The present research study defines the test methodology needed in order to determine these input parameters.

With respect to the current research study, improvements can be made by incorporating an anisotropic hydraulic conductivity. The current analysis assumes isotropic conditions and proves to work well for the data collected. However, an improvement to this method would be to allow for anisotropic conditions in the event that there is a significant impact due to these effects. Fully incorporating anisotropic effects would most likely have a minimal impact on the results due to the relatively thin PFC layers, but would be useful for other applications such as nonlinear modeling in aquifer systems. In addition, the finite difference numerical model could be improved by using a finite volume approach. This might provide an improvement in the flow rate calculations, but similar results and trends should be expected.

There are several areas in which future research can be conducted with respect to proper use of PFC. One such area is to investigate effective maintenance methods. Currently, the PFC layer is not cleaned at regular intervals. Although current research has shown the drainage benefits will persist without cleaning maintenance, there is a possibility that if the PFC layer becomes clogged, cleaning will be required. A second need for additional research is to determine the actual removal mechanisms with which PFC improves the stormwater quality. There has been debate over whether the PFC layer is acting as a filter in removing pollutants or simply reducing the source of pollutants from being washed from vehicles. Accurate measurement of both inflow and outflow pollutant concentrations will help determine the removal mechanisms which are taking place within the PFC layer. Additional research is needed in the winter maintenance practices of PFC as well as the impacts of freezing conditions on the PFC layer. Although questions remain about the practices and applications of PFC, it has proven to be effective in improving driving conditions during rainfall events, as well as improving stormwater quality runoff. For these reasons, PFC is an innovative roadway material that should be further investigated by researchers and practitioners in order to fully take advantage of these benefits.

Appendix A

Numerical Model Code

A.1 Module of Constants

```
!====================================================================================!
! \\\\\\\\\\\\\\\\\\\\\\\\\\\\                                  //////////////////////////// !
!                               BEGIN MODULE: CONSTANTS                              !
! ////////////////////////////                                  \\\\\\\\\\\\\\\\\\\\\\\\\\\\ !
!====================================================================================!

MODULE constants

  ! This module is used by the main program and subroutines.
  ! This module contains:
  !       PFC core dimensions
  !       Radial direction number of elements and initial step size
  !       Vertical direction number of elements and expansion ratio
  !       Time discretization size
  !       Original Forchheimer coefficients
  !       Convergence criteria values
  !       Other miscellaneous constants

  IMPLICIT NONE
  SAVE

  ! Define PFC core dimensions
  CHARACTER*7 :: CoreID = '1-i-S'        ! Core identification number
  REAL, PARAMETER :: Rs = 2.5            ! Standpipe radius (cm)
  REAL, PARAMETER :: Rc = 10.            ! Core radius (cm)
  REAL, PARAMETER :: bc = 5.             ! Core thickness (cm)
  REAL, PARAMETER :: hmax = 10.          ! Standpipe head (cm)

  ! Define discretization size
  INTEGER, PARAMETER :: nrs = 10            ! Number of elements under the standpipe in the radial direction
  INTEGER, PARAMETER :: nrc = 30            ! Number of elements outside the standpipe in the radial direction
  INTEGER, PARAMETER :: nr = nrs + nrc      ! Total number of elements in the radial direction
  REAL, PARAMETER :: dr = 0.15              ! Element step size at location of standpipe (cm)

  REAL, PARAMETER :: rez = 1.1              ! Expansion ratio for vertical spacing
  INTEGER, PARAMETER :: nz = 40             ! Number of elements in the vertical direction

  INTEGER, PARAMETER :: ntd = 99999         ! Maximum number of time steps for Darcy solution
  INTEGER, PARAMETER :: ntf = 99999         ! Maximum number of iterations for Forchheimer solution
  REAL, PARAMETER :: dtd = 1. / 100.        ! Time step size for Darcy solution

  ! Define original Forchheimer coefficients
  REAL, PARAMETER :: aa = 1.                ! Original linear Forchheimer coefficient (s/cm)
  REAL, PARAMETER :: bb = 10.               ! Original nonlinear Forchheimer coefficient (s2/cm2)
```

```
  ! Define other miscellaneous constants
  REAL, PARAMETER :: pi = 3.14159265359    ! Pi
  REAL, PARAMETER :: epsd = 1.e-6          ! Convergence criteria for Darcy solution
  REAL, PARAMETER :: epsf = 1.e-6          ! Convergence criteria for Forchheimer solution
  INTEGER, PARAMETER :: ni = 100           ! Number of image pairs used for method of images analytic solution

END MODULE constants

!==========================================================================================!
! \\\\\\\\\\\\\\\\\\\\\\\\\\\\                                   ///////////////////////////// !
!                                  END MODULE: CONSTANTS                                   !
! ////////////////////////////                                   \\\\\\\\\\\\\\\\\\\\\\\\\\\\\ !
!==========================================================================================!
```

A.2 Main Program

```
!==========================================================================================!
! \\\\\\\\\\\\\\\\\\\\\\\\\\\\\\                                 /////////////////////////////// !
!                                  BEGIN PROGRAM: MAIN                                     !
! //////////////////////////////                                 \\\\\\\\\\\\\\\\\\\\\\\\\\\\\\\ !
!==========================================================================================!

PROGRAM main

  ! This program uses the constants module.
  ! This program calls the following subroutines:
  !       S_MOIHead
  !       S_DarcyHead
  !       S_ForchHead
  !       S_PhiFunc

  USE constants
  IMPLICIT NONE

  ! Declare additional variables as needed
  CHARACTER*12 file10
  CHARACTER*14 file20
  CHARACTER*14 file30
  CHARACTER*12 file40
  CHARACTER*14 file50
  CHARACTER*8 date
  CHARACTER*10 time

  REAL, ALLOCATABLE :: radi(:)
  REAL, ALLOCATABLE :: vert(:)
  REAL, ALLOCATABLE :: moi(:,:)
  REAL, ALLOCATABLE :: hd(:,:)
  REAL, ALLOCATABLE :: hf3(:,:,:)
  REAL, ALLOCATABLE :: hf(:,:)
  REAL, ALLOCATABLE :: phi(:,:)
```

```
REAL rer1, rer2
REAL dz, dx
INTEGER i, j
INTEGER td, tf
REAL AQinL, AQoutL, DQinL, DQoutL, FQinL, FQoutL
REAL AQinN, AQoutN, DQinN, DQoutN, FQinN, FQoutN
REAL AQcjL, AQcjN, DQcjL, DQcjN, FQcjL, FQcjN
REAL AsfL, DsfL, FsfL
REAL AsfN, DsfN, FsfN

! Record the date and time of compilation
CALL date_and_time(date,time)

! Create .csv files for output
file10 = '3HeadMOI.csv'
file20 = '3HeadDarcy.csv'
file30 = '3HeadForch.csv'
file40 = '3PhiFunc.csv'
file50 = '3FlowRates.csv'

OPEN(10, FILE = file10, STATUS = 'unknown')
OPEN(20, FILE = file20, STATUS = 'unknown')
OPEN(30, FILE = file30, STATUS = 'unknown')
OPEN(40, FILE = file40, STATUS = 'unknown')
OPEN(50, FILE = file50, STATUS = 'unknown')

! Define direction vector dimensions
ALLOCATE (radi(0:nr))
ALLOCATE (vert(0:nz))

! Define array dimensions
ALLOCATE (moi(0:nr,0:nz))
ALLOCATE (hd(0:nr,0:nz))
ALLOCATE (hf3(0:nr,0:nz,0:ntf))
ALLOCATE (hf(0:nr,0:nz))
ALLOCATE (phi(0:nr,0:nz))


!==========================================================================================!
!                              DEFINE SPACE AND TIME VECTORS                               !
!==========================================================================================!

! Calculate initial step size based on expansion factor (cm)
IF (rez .EQ. 1.) THEN
  dz = bc / nz
ELSE
  dz = bc * (1. - rez) / (1. - rez ** nz)
END IF

! Calculate expansion ratio under standpipe
rer1 = 1.1
DO i = 1,25
  rer1 = rer1 + ((1. - rer1) / (1. - rer1 ** nrs) - dr / Rs) * &
```

```
     & (rer1 ** nrs - 1.) ** 2 / (rer1 ** nrs * (nrs - 1.) - rer1 ** (nrs - 1) * nrs + 1.)
END DO
! Calculate expansion ratio outside of standpipe
rer2 = 1.1
DO i = 1,25
  rer2 = rer2 + ((1. - rer2) / (1. - rer2 ** nrc) - dr / (Rc - Rs)) * &
     & (rer2 ** nrc - 1.) ** 2 / (rer2 ** nrc * (nrc - 1.) - rer2 ** (nrc - 1) * nrc + 1.)
END DO

! Define radius vector
radi(nrs) = Rs
DO i = nrs-1,1,-1
  radi(i) = radi(i+1) - dr * rer1 ** (nrs-1 - i)
END DO
DO i = nrs+1,nr
  radi(i) = radi(i-1) + dr * rer2 ** (i - (nrs+1))
END DO
radi(0) = 0.
radi(nr) = Rc

! Define vertical vector
vert(0) = 0.
DO j = 1,nz
  vert(j) = vert(j-1) + dz * rez ** (j-1)
END DO


!==================================================================================================!
!                        DETERMINE HEAD DISTRIBUTIONS SOLUTIONS USING SUBROUTINES                  !
!==================================================================================================!

! Use subroutine S_MOIHead to determine the analytic head distribution.
! The result will be stored in the moi array.
CALL S_MOIHead(radi, vert, moi)

  DO j = 0,nz
    DO i = 0,nr
      moi(i,j) = hmax * moi(i,j)
    END DO
  END DO

! Use subroutine S_DarcyHead to determine the Darcy head distribution.
! The result will be stored in the hd array.
CALL S_DarcyHead(radi, vert, hd, td)

  DO j = 0,nz
    DO i = 0,nr
      hd(i,j) = hmax * hd(i,j)
    END DO
  END DO

! Use subroutine S_ForchHead to determine the Forchheimer head distribution.
! The result will be stored in the hf array.
! The Darcy array is used as an input since this is used as the initial condition.
CALL S_ForchHead(radi, vert, hd, hf3, tf)
```

```
  ! Put the converged Forchheimer solution into a 2-D array
  DO j = 0,nz
    DO i = 0,nr
      hf(i,j) = hf3(i,j,tf)
    END DO
  END DO

! Use subroutine S_PhiFunc to determine the Phi function distribution.
! The result will be stored in the phi array.
CALL S_PhiFunc(radi, vert, hf, phi)


!==========================================================================================!
!                              CALCULATE SHAPE FACTORS FOR EACH SOLUTION                   !
!==========================================================================================!

! Use subroutine S_LinearSF to determine the linear shape factor for each solution.
CALL S_LinearSF(radi, vert, moi, AsfL)
CALL S_LinearSF(radi, vert, hd, DsfL)
CALL S_LinearSF(radi, vert, hf, FsfL)

! Use subroutine S_NonlinearSF to determine the nonlinear shape factor for each solution.
CALL S_NonlinearSF(radi, vert, moi, AsfN)
CALL S_NonlinearSF(radi, vert, hd, DsfN)
CALL S_NonlinearSF(radi, vert, hf, FsfN)


!==========================================================================================!
!                               CALCULATE FLOW RATES FOR EACH SOLUTION                     !
!==========================================================================================!

! Use subroutine S_LinearQout to determine the outflow rate using Darcy's Law.
CALL S_LinearQout(radi, vert, moi, AQoutL)
CALL S_LinearQout(radi, vert, hd, DQoutL)
CALL S_LinearQout(radi, vert, hf, FQoutL)

! Use subroutine S_NonlinearQout to determine the outflow rate using Forchheimer's Equation.
CALL S_NonlinearQout(radi, vert, moi, AQoutN)
CALL S_NonlinearQout(radi, vert, hd, DQoutN)
CALL S_NonlinearQout(radi, vert, hf, FQoutN)

! Calculate Carslaw and Jaeger flow rate from linear shape factor
AQcjL = 4. * Rs * AsfL / aa * hmax
DQcjL = 4. * Rs * DsfL / aa * hmax
FQcjL = 4. * Rs * FsfL / aa * hmax

! Calculate Carslaw and Jaeger flow rate from nonlinear shape factor
AQcjN = 4. * Rs * AsfN / aa * hmax
DQcjN = 4. * Rs * DsfN / aa * hmax
FQcjN = 4. * Rs * FsfN / aa * hmax
```

```
!=====================================================================================!
!                                 WRITE TO ANALYTIC HEAD SOLUTION FILE                                 !
!=====================================================================================!

! Write header to output file
WRITE (10,1001) date, time, file10, nrs, nr, nz, CoreID, Rs, bc, Rc, AsfL, AsfN, aa, bb, rer1, rer2, rez
1001 FORMAT ('Date,', a8, /, 'Time,', a10, /, /, 'Method of Images Analytic Solution', /, &
        & 'Filename,', a12, /, 'Nrs=,', i4, /, 'Nr=,', i4, / 'Nz=,', i4, /, /,       &
        & 'Core ID,', a7, /, 'Rs=,', f8.4, ',cm', /, 'bc=,', f8.4, ',cm', /, 'Rc=,',  &
        & f8.4, ',cm', /, 'hs=,1.0,cm', /, 'AsfL=,', f10.8, /, 'AsfN=,', f14.8,      &
        & /, 'aa=,', f7.4, ',s/cm', /, 'bb=,', f7.4, ',s2/cm2', /, 'rer1=,', f10.8, /,&
        & 'rer2=,', f10.8, /, 'rez=,', f10.8)

! Write Flow Rates
WRITE (10,1002) AQcjL, AQoutL, AQinL, AQcjN, AQoutN, AQinN
1002 FORMAT ('QcjL=,', f14.8, ',cm3/s', /, 'QoutL=,', f14.8, ',cm3/s', /,   &
        & 'QinL=,', f14.8, ',cm3/s', /, 'QcjN=,', f14.8, ',cm3/s', /,   &
        & 'QoutN=,', f14.8, ',cm3/s', /, 'QinN=,', f14.8, ',cm3/s')

! Write method of images analytic solution to output file
WRITE (10,1003) radi(:)
1003 FORMAT (/, ',', 1000(f13.6, ','))
DO j = 0,nz
  WRITE (10,1004) vert(j), moi(:,j)
  1004 FORMAT (f13.6, ',', 1000(f18.9, ','))
END DO


!=====================================================================================!
!                                   WRITE TO DARCY HEAD SOLUTION FILE                                   !
!=====================================================================================!

! Write header to output file
WRITE (20,2001) date, time, file20, nrs, nr, nz, dtd, REAL(td)*dtd, &
         & CoreID, Rs, bc, Rc, DsfL, DsfN, aa, bb, rer1, rer2, rez
2001 FORMAT ('Date,', a8, /, 'Time,', a10, /, /, 'Darcy Head Solution', /,              &
        & 'Filename,', a14, /, 'Nrs=,', i4, /, 'Nr=,', i4, /, 'Nz=,', i4, /,         &
        & 'Dt=,', f8.6, ',sec', /, 'Steady State=,', f10.5, ',sec', /, /,           &
        & 'Core ID,', a7, /, 'Rs=,', f8.4, ',cm', /, 'bc=,', f8.4, ',cm', /, 'Rc=,',  &
        & f8.4, ',cm', /, 'hs=,1.0,cm', /, 'DsfL=,', f10.8, /, 'DsfN=,', f14.8,      &
        & /, 'aa=,', f7.4, ',s/cm', /, 'bb=,', f7.4, ',s2/cm2', /, 'rer1=,', f10.8, /,&
        & 'rer2=,', f10.8, /, 'rez=,', f10.8)

! Write Flow Rates
WRITE (20,2002) DQcjL, DQoutL, DQinL, DQcjN, DQoutN, DQinN
2002 FORMAT ('QcjL=,', f14.8, ',cm3/s', /, 'QoutL=,', f14.8, ',cm3/s', /,   &
        & 'QinL=,', f14.8, ',cm3/s', /, 'QcjN=,', f14.8, ',cm3/s', /,   &
        & 'QoutN=,', f14.8, ',cm3/s', /, 'QinN=,', f14.8, ',cm3/s')

! Write Darcy head solution to output file
WRITE (20,2003) radi(:)
2003 FORMAT (/, ',', 1000(f13.6, ','))
DO j = 0,nz
  WRITE (20,2004) vert(j), hd(:,j)
  2004 FORMAT (f13.6, ',', 1000(f18.9, ','))
```

```
END DO


!======================================================================================!
!                              WRITE TO FORCHHEIMER HEAD SOLUTION FILE                                 !
!======================================================================================!

! Write header to output file
WRITE (30,3001) date, time, file30, nrs, nr, nz, tf,                              &
          & CoreID, Rs, bc, Rc, FsfL, FsfN, aa, bb, rer1, rer2, rez
3001 FORMAT ('Date,', a8, /, 'Time,', a10, /, /, 'Forchheimer Head Solution', /,         &
         & 'Filename,', a14, /, 'Nrs=,', i4, /, 'Nr=,', i4, / 'Nz=,', i4, /,          &
         & '# Iterations,', i6, /, /,                                        &
         & 'Core ID,', a7, /, 'Rs=,', f8.4, ',cm', /, 'bc=,', f8.4, ',cm', /, 'Rc=,',  &
         & f8.4, ',cm', /, 'hs=,1.0,cm', /, 'FsfL=,', f10.8, /, 'FsfN=,', f14.8,      &
         & /, 'aa=,', f7.4, ',s/cm', /, 'bb=,', f7.4, ',s2/cm2', /, 'rer1=,', f10.8, /,&
         & 'rer2=,', f10.8, /, 'rez=,', f10.8)

! Write Flow Rates
WRITE (30,3002) FQcjL, FQoutL, FQinL, FQcjN, FQoutN, FQinL
3002 FORMAT ('QcjL=,', f14.8, ',cm3/s', /, 'QoutL=,', f14.8, ',cm3/s', /,   &
         & 'QinL=,', f14.8, ',cm3/s', /, 'QcjN=,', f14.8, ',cm3/s', /,   &
         & 'QoutN=,', f14.8, ',cm3/s', /, 'QinN=,', f14.8, ',cm3/s')

! Write Forchheimer head solution to output file
WRITE (30,3003) radi(:)
3003 FORMAT (/, ',', 1000(f13.6, ','))
DO j = 0,nz
  WRITE (30,3004) vert(j), hf(:,j)
  3004 FORMAT (f13.6, ',', 1000(f18.9, ','))
END DO


!======================================================================================!
!                                        WRITE TO PHI FUNCTION FILE                                            !
!======================================================================================!

! Write header to output file
WRITE (40,4001) date, time, file40, nrs, nr, nz,                                  &
          & CoreID, Rs, bc, Rc, hmax, FsfL, FsfN, aa, bb, rer1, rer2, rez
4001 FORMAT ('Date,', a8, /, 'Time,', a10, /, /, 'Phi Function', /,                  &
         & 'Filename,', a12, /, 'Nrs=,', i4, /, 'Nr=,', i4, /, 'Nz=,', i4, /, /,      &
         & 'Core ID,', a7, /, 'Rs=,', f8.4, ',cm', /, 'bc=,', f8.4, ',cm', /, 'Rc=,',  &
         & f8.4, ',cm', /, 'hs=,', f7.4, ',cm', /, 'FsfL=,', f10.8, /, 'FsfN=,', f14.8,&
         & /, 'aa=,', f7.4, ',s/cm', /, 'bb=,', f7.4, ',s2/cm2', /, 'rer1=,', f10.8, /,&
         & 'rer2=,', f10.8, /, 'rez=,', f10.8)

! Write phi function to output file
WRITE (40,4002) radi(:)
4002 FORMAT (/, ',', 1000(f13.6, ','))
DO j = 0,nz
  WRITE (40,4003) vert(j), phi(:,j)
  4003 FORMAT (f13.6, ',', 1000(f18.9, ','))
END DO
```

```
  !==========================================================================================!
  !                                    WRITE TO FLOW RATE FILE                                !
  !==========================================================================================!

  ! Write header to output file
  WRITE (50,5001) date, time, file50, nrs, nr, nz,                              &
          & CoreID, Rs, bc, Rc, rer1, rer2, rez, hmax, aa, bb
  5001 FORMAT ('Date,', a8, /, 'Time,', a10, /, /, 'Flow Rates', /,                     &
         & 'Filename,', a14, /, 'Nrs=,', i4, /, 'Nr=,', i4, /, 'Nz=,', i4, /, /,      &
         & 'Core ID,', a7, /, 'Rs=,', f8.4, ',cm', /, 'bc=,', f8.4, ',cm', /, 'Rc=,',  &
         & f8.4, ',cm', /, 'rer1=,', f10.8, /, 'rer2=,', f10.8, /, 'rez=,', f10.8, /,  &
         & /, 'hs=,', f7.4, ',cm', /, 'aa=,', f7.4, ',s/cm', /, 'bb=,', f7.4, ',s2/cm2')

  ! Write linear flow rates to output file
  WRITE (50,5002) AQcjL, AQoutL, AQinL, DQcjL, DQoutL, DQinL, FQcjL, FQoutL, FQinL
  5002 FORMAT (/, 'Linear Flow Rates', /, 'AQcjL,', f14.8, /, 'AQoutL,', f14.8, /,          &
         & 'AQinL,', f14.8, /, /, 'DQcjL,', f14.8, /, 'DQoutL,', f14.8, /,             &
         & 'DQinL,', f14.8, /, /, 'FQcjL,', f14.8, /, 'FQoutL,', f14.8, /, 'FQinL,', f14.8)

  ! Write nonlinear flow rates to output file
  WRITE (50,5003) AQcjN, AQoutN, AQinN, DQcjN, DQoutN, DQinN, FQcjN, FQoutN, FQinN
  5003 FORMAT (/, 'Nonlinear Flow Rates', /, 'AQcjN,', f14.8, /, 'AQoutN,', f14.8, /,        &
         & 'AQinN,', f14.8, /, /, 'DQcjN,', f14.8, /, 'DQoutN,', f14.8, /,             &
         & 'DQinN,', f14.8, /, /, 'FQcjN,', f14.8, /, 'FQoutN,', f14.8, /, 'FQinN,', f14.8)

  ! Write shape factors to output file
  WRITE (50,5004) AsfL, DsfL, FsfL, AsfN, DsfN, FsfN
  5004 FORMAT (/, 'Linear Shape Factors', /, 'AsfL,', f10.8, /, 'DsfL,', f10.8, /,        &
         & 'FsfL,', f10.8, /, /, 'Nonlinear Shape Factors', /, 'AsfN,', f14.8, /,     &
         & 'DsfN,', f14.8, /, 'FsfN,', f14.8)


  CLOSE(10)
  CLOSE(20)
  CLOSE(30)
  CLOSE(40)
  CLOSE(50)

END PROGRAM main

!==========================================================================================!
! \\\\\\\\\\\\\\\\\\\\\\\\\\\\\\                                ////////////////////////////// !
!                                    END PROGRAM: MAIN                                     !
! //////////////////////////////                                \\\\\\\\\\\\\\\\\\\\\\\\\\\\\\ !
!==========================================================================================!
```

A.3 Subroutine to Determine Method of Images Solution

```
!==========================================================================================!
! \\\\\\\\\\\\\\\\\\\\\\\\\\                                        ////////////////////////// !
!                                  BEGIN SUBROUTINE: S_MOIHEAD                               !
! //////////////////////////                                        \\\\\\\\\\\\\\\\\\\\\\\\\\ !
!==========================================================================================!

! This subroutine calculates the head distribution based on the analytic method of images.
SUBROUTINE S_MOIHead(r, z, h)

  USE constants
  IMPLICIT NONE

  ! Define dummy variables
  REAL, DIMENSION(0:nr), INTENT(IN) :: r
  REAL, DIMENSION(0:nz), INTENT(IN) :: z
  REAL, DIMENSION(0:nr,0:nz), INTENT(OUT) :: h

  ! Define temporary variables
  INTEGER i, j, k
  REAL ha, hb
  REAL sum1, arg

  ! Define 'dimensional' method of images analytic solution
  DO i = 0,nr
    DO j = 0,nz
      sum1 = 0.
      DO k = -ni,ni
        sum1 = sum1 + ASIN(2. * Rs / (                          &
           &            SQRT((r(i) - Rs) ** 2. +         &
           &               (z(j) + 2. * k * bc) ** 2.) +  &
           &            SQRT((r(i) + Rs) ** 2. +         &
           &               (z(j) + 2. * k * bc) ** 2.)    &
           &            )                         &
           &       )
      END DO
      h(i,j) = 2. * sum1 / pi
    END DO
  END DO

  ! Define heads used for normalization of method of images analytic solution
  sum1 = 0.
  DO k = -ni,ni
    arg = 2. * Rs / (                                        &
       &       SQRT((Rs / SQRT(2.) - Rs) ** 2. + (2. * k * bc) ** 2.) + &
       &       SQRT((Rs / SQRT(2.) + Rs) ** 2. + (2. * k * bc) ** 2.)   &
       &       )
    sum1 = sum1 + ASIN(arg)
  END DO
  ha = 2. / pi * sum1

  sum1 = 0.
  DO j = 0,nz
    sum1 = sum1 + h(nr,j)
```

```
  END DO
  hb = sum1 / (nz + 1.)

  ! Define normalized unit method of images analytic solution
  DO i = 0,nr
    DO j = 0,nz
      h(i,j) = (h(i,j) - hb) / (ha - hb)
    END DO
  END DO

END SUBROUTINE S_MOIHead

!=======================================================================================!
! \\\\\\\\\\\\\\\\\\\\\\\\\\\                                  /////////////////////////// !
!                                  END SUBROUTINE: S_MOIHEAD                            !
! ///////////////////////////                                  \\\\\\\\\\\\\\\\\\\\\\\\\\\ !
!=======================================================================================!
```

A.4 Subroutine to Determine Darcy Solution

```
!=======================================================================================!
! \\\\\\\\\\\\\\\\\\\\\\\                                      /////////////////////////// !
!                               BEGIN SUBROUTINE: S_DARCYHEAD                           !
! ///////////////////////                                      \\\\\\\\\\\\\\\\\\\\\\\\\\\ !
!=======================================================================================!

! This subroutine calculates the head distribution of a finite difference scheme
!   for Darcy's Law using a Crank-Nicolson scheme with banded LU decomposition.
SUBROUTINE S_DarcyHead(r, z, h, t)

  USE constants
  IMPLICIT NONE

  ! Define dummy variables
  REAL, DIMENSION(0:nr), INTENT(IN) :: r
  REAL, DIMENSION(0:nz), INTENT(IN) :: z
  REAL, DIMENSION(0:nr,0:nz), INTENT(OUT) :: h
  INTEGER, INTENT(OUT) :: t

  ! Define temporary variables
  INTEGER i, j, k, m, ne
  REAL nn, ss, ww, ee, pp
  REAL maxdh
  REAL rrr, zzz
  REAL, ALLOCATABLE :: matA(:,:), RHS(:)

  ne = (nr+1) * (nz+1)
  ALLOCATE (matA(ne,ne), RHS(ne))
```

```
!==========================================================================================!
!                                    INITIAL AND BOUNDARY CONDITIONS                                      !
!==========================================================================================!

! Define Initial Condition
DO j = 0,nz
  DO i = 0,nr-1
    h(i,j) = 0.000001
  END DO
END DO

! Define Dirichlet Boundary Conditions
DO i = 0,nrs
  h(i,0) = 1.
END DO
DO j = 0,nz
  h(nr,j) = 0.
END DO

!==========================================================================================!
!                                    CREATE MATRIX A AND LU DECOMPOSE                                      !
!==========================================================================================!

! Inflow Boundary
DO j = 0,0
  DO i = 0,nrs
    k = i + 1 + j * (nr + 1)
    matA(k,k) = 1.
  END DO
END DO

! Outflow Boundary
DO j = 0,nz
  DO i = nr,nr
    k = i + 1 + j * (nr + 1)
    matA(k,k) = 1.
  END DO
END DO

! Upper No Flow Boundary   z(j-1) = -z(j+1)
DO j = 0,0
  DO i = nrs+1,nr-1
    k = i + 1 + j * (nr + 1)
    rrr = (r(i+1) - r(i-1)) * (r(i+1) - r(i)) * (r(i) - r(i-1))
    zzz = (z(j+1) + z(j+1)) * (z(j+1) - z(j)) * (z(j) + z(j+1))
    ee = -1. * dtd * (r(i) - r(i-1)) ** 2 / (2. * r(i) * rrr) - dtd * (r(i) - r(i-1)) / rrr
    ww = dtd * (r(i+1) - r(i)) ** 2 / (2. * r(i) * rrr) - dtd * (r(i+1) - r(i)) / rrr
    pp = 1. - dtd * ((r(i+1) - r(i)) ** 2 - (r(i) - r(i-1)) ** 2) / (2. * r(i) * rrr) + &
      & dtd * (r(i+1) - r(i-1)) / rrr + dtd * (z(j+1) + z(j+1)) / zzz
    ss = -1. * dtd * (z(j) + z(j+1)) / zzz
    nn = -1. * dtd * (z(j+1) - z(j)) / zzz

    matA(k,k+1) = ee
    matA(k,k-1) = ww
    matA(k,k) = pp
```

```
    matA(k,k+nr+1) = ss + nn
  END DO
END DO

! Lower No Flow Boundary   z(j+1) = 2*z(j) - z(j-1)
DO j = nz,nz
  DO i = 1,nr-1
    k = i + 1 + j * (nr + 1)
    rrr = (r(i+1) - r(i-1)) * (r(i+1) - r(i)) * (r(i) - r(i-1))
    zzz = (2. * z(j) - 2. * z(j-1)) * (z(j) - z(j-1)) * (z(j) - z(j-1))
    ee = -1. * dtd * (r(i) - r(i-1)) ** 2 / (2. * r(i) * rrr) - dtd * (r(i) - r(i-1)) / rrr
    ww = dtd * (r(i+1) - r(i)) ** 2 / (2. * r(i) * rrr) - dtd * (r(i+1) - r(i)) / rrr
    pp = 1. - dtd * ((r(i+1) - r(i)) ** 2 - (r(i) - r(i-1)) ** 2) / (2. * r(i) * rrr) + &
      & dtd * (r(i+1) - r(i-1)) / rrr + dtd * (2. * z(j) - 2. * z(j-1)) / zzz
    ss = -1. * dtd * (z(j) - z(j-1)) / zzz
    nn = -1. * dtd * (z(j) - z(j-1)) / zzz

    matA(k,k+1) = ee
    matA(k,k-1) = ww
    matA(k,k) = pp
    matA(k,k-nr-1) = nn + ss
  END DO
END DO

! Bottom Center Node   z(j+1) = 2*z(j) - z(j-1)   and   r(i-1) = -r(i+1)
DO j = nz,nz
  DO i = 0,0
    k = i + 1 + j * (nr + 1)
    rrr = (r(i+1) + r(i+1)) * (r(i+1) - r(i)) * (r(i) + r(i+1))
    zzz = (2. * z(j) - 2. * z(j-1)) * (z(j) - z(j-1)) * (z(j) - z(j-1))
    ee = -2. * dtd * (r(i) + r(i+1)) / rrr
    ww = -2. * dtd * (r(i+1) - r(i)) / rrr
    pp = 1. + 2. * dtd * (r(i+1) + r(i+1)) / rrr + dtd * (2. * z(j) - 2. * z(j-1)) / zzz
    ss = -1. * dtd * (z(j) - z(j-1)) / zzz
    nn = -1. * dtd * (z(j) - z(j-1)) / zzz

    matA(k,k+1) = ee + ww
    matA(k,k) = pp
    matA(k,k-nr-1) = nn + ss
  END DO
END DO

! Symmetry No Flow Boundary for r = 0   r(i-1) = -r(i+1)
DO j = 1,nz-1
  DO i = 0,0
    k = i + 1 + j * (nr + 1)
    rrr = (r(i+1) + r(i+1)) * (r(i+1) - r(i)) * (r(i) + r(i+1))
    zzz = (z(j+1) - z(j-1)) * (z(j+1) - z(j)) * (z(j) - z(j-1))
    ee = -2. * dtd * (r(i) + r(i+1)) / rrr
    ww = -2. * dtd * (r(i+1) - r(i)) / rrr
    pp = 1. + 2. * dtd * (r(i+1) + r(i+1)) / rrr + dtd * (z(j+1) - z(j-1)) / zzz
    ss = -1. * dtd * (z(j) - z(j-1)) / zzz
    nn = -1. * dtd * (z(j+1) - z(j)) / zzz
```

```
    matA(k,k+1) = ee + ww
    matA(k,k) = pp
    matA(k,k+nr+1) = ss
    matA(k,k-nr-1) = nn
  END DO
END DO

! Interior Nodes
DO j = 1,nz-1
  DO i = 1,nr-1
    k = i + 1 + j * (nr + 1)
    rrr = (r(i+1) - r(i-1)) * (r(i+1) - r(i)) * (r(i) - r(i-1))
    zzz = (z(j+1) - z(j-1)) * (z(j+1) - z(j)) * (z(j) - z(j-1))
    ee = -1. * dtd * (r(i) - r(i-1)) ** 2 / (2. * r(i) * rrr) - dtd * (r(i) - r(i-1)) / rrr
    ww = dtd * (r(i+1) - r(i)) ** 2 / (2. * r(i) * rrr) - dtd * (r(i+1) - r(i)) / rrr
    pp = 1. - dtd * ((r(i+1) - r(i)) ** 2 - (r(i) - r(i-1)) ** 2) / (2. * r(i) * rrr) + &
      & dtd * (r(i+1) - r(i-1)) / rrr + dtd * (z(j+1) - z(j-1)) / zzz
    ss = -1. * dtd * (z(j) - z(j-1)) / zzz
    nn = -1. * dtd * (z(j+1) - z(j)) / zzz

    matA(k,k+1) = ee
    matA(k,k-1) = ww
    matA(k,k) = pp
    matA(k,k+nr+1) = ss
    matA(k,k-nr-1) = nn
  END DO
END DO

! LU decomposition of banded matrix A
CALL S_LUDecomp(matA, ne)


!=====================================================================================!
!             SOLVE CRANK-NICOLSON METHOD IN TIME, DETERMINE WHEN STEADY STATE IS ACHIEVED          !
!=====================================================================================!

! Start solving using Crank-Nicolson method
DO m = 1,ntd

  ! Define RHS Vector
  RHS(:) = 0.

  ! Inflow Boundary
  DO j = 0,0
    DO i = 0,nrs
      k = i + 1 + j * (nr + 1)
      RHS(k) = h(i,j)
    END DO
  END DO

  ! Outflow Boundary
  DO j = 0,nz
    DO i = nr,nr
      k = i + 1 + j * (nr + 1)
      RHS(k) = h(i,j)
```

```
  END DO
END DO

! Upper No Flow Boundary   z(j-1) = -z(j+1)
DO j = 0,0
  DO i = nrs+1,nr-1
    k = i + 1 + j * (nr + 1)
    rrr = (r(i+1) - r(i-1)) * (r(i+1) - r(i)) * (r(i) - r(i-1))
    zzz = (z(j+1) + z(j+1)) * (z(j+1) - z(j)) * (z(j) + z(j+1))
    ee = dtd * (r(i) - r(i-1)) ** 2 / (2. * r(i) * rrr) + dtd * (r(i) - r(i-1)) / rrr
    ww = -1. * dtd * (r(i+1) - r(i)) ** 2 / (2. * r(i) * rrr) + dtd * (r(i+1) - r(i)) / rrr
    pp = 1. + dtd * ((r(i+1) - r(i)) ** 2 - (r(i) - r(i-1)) ** 2) / (2. * r(i) * rrr) - &
      & dtd * (r(i+1) - r(i-1)) / rrr - dtd * (z(j+1) + z(j+1)) / zzz
    ss = dtd * (z(j) + z(j+1)) / zzz
    nn = dtd * (z(j+1) - z(j)) / zzz

    RHS(k) = h(i+1,j) * ee + &
         & h(i-1,j) * ww + &
         & h(i,j) * pp +   &
         & h(i,j+1) * ss + &
         & h(i,j+1) * nn
  END DO
END DO

! Lower No Flow Boundary   z(j+1) = 2*z(j) - z(j-1)
DO j = nz,nz
  DO i = 1,nr-1
    k = i + 1 + j * (nr + 1)
    rrr = (r(i+1) - r(i-1)) * (r(i+1) - r(i)) * (r(i) - r(i-1))
    zzz = (2. * z(j) - 2. * z(j-1)) * (z(j) - z(j-1)) * (z(j) - z(j-1))
    ee = dtd * (r(i) - r(i-1)) ** 2 / (2. * r(i) * rrr) + dtd * (r(i) - r(i-1)) / rrr
    ww = -1. * dtd * (r(i+1) - r(i)) ** 2 / (2. * r(i) * rrr) + dtd * (r(i+1) - r(i)) / rrr
    pp = 1. + dtd * ((r(i+1) - r(i)) ** 2 - (r(i) - r(i-1)) ** 2) / (2. * r(i) * rrr) - &
      & dtd * (r(i+1) - r(i-1)) / rrr - dtd * (2. * z(j) - 2. * z(j-1)) / zzz
    ss = dtd * (z(j) - z(j-1)) / zzz
    nn = dtd * (z(j) - z(j-1)) / zzz

    RHS(k) = h(i+1,j) * ee + &
         & h(i-1,j) * ww + &
         & h(i,j) * pp +   &
         & h(i,j-1) * ss + &
         & h(i,j-1) * nn
  END DO
END DO

! Bottom Center Node   z(j+1) = 2*z(j) - z(j-1)   and   r(i-1) = -r(i+1)
DO j = nz,nz
  DO i = 0,0
    k = i + 1 + j * (nr + 1)
    rrr = (r(i+1) + r(i+1)) * (r(i+1) - r(i)) * (r(i) + r(i+1))
    zzz = (2. * z(j) - 2. * z(j-1)) * (z(j) - z(j-1)) * (z(j) - z(j-1))
    ee = 2. * dtd * (r(i) + r(i+1)) / rrr
    ww = 2. * dtd * (r(i+1) - r(i)) / rrr
    pp = 1. - 2. * dtd * (r(i+1) + r(i+1)) / rrr - dtd * (2. * z(j) - 2. * z(j-1)) / zzz
    ss = dtd * (z(j) - z(j-1)) / zzz
```

```
    nn = dtd * (z(j) - z(j-1)) / zzz

    RHS(k) = h(i+1,j) * ee + &
         & h(i+1,j) * ww + &
         & h(i,j) * pp +   &
         & h(i,j-1) * ss + &
         & h(i,j-1) * nn
  END DO
END DO

! Symmetry No Flow Boundary for r = 0   r(i-1) = -r(i+1)
DO j = 1,nz-1
  DO i = 0,0
    k = i + 1 + j * (nr + 1)
    rrr = (r(i+1) + r(i+1)) * (r(i+1) - r(i)) * (r(i) + r(i+1))
    zzz = (z(j+1) - z(j-1)) * (z(j+1) - z(j)) * (z(j) - z(j-1))
    ee = 2. * dtd * (r(i) + r(i+1)) / rrr
    ww = 2. * dtd * (r(i+1) - r(i)) / rrr
    pp = 1. - 2. * dtd * (r(i+1) + r(i+1)) / rrr - dtd * (z(j+1) - z(j-1)) / zzz
    ss = dtd * (z(j) - z(j-1)) / zzz
    nn = dtd * (z(j+1) - z(j)) / zzz

    RHS(k) = h(i+1,j) * ee + &
         & h(i+1,j) * ww + &
         & h(i,j) * pp +   &
         & h(i,j+1) * ss + &
         & h(i,j-1) * nn
  END DO
END DO

! Interior Nodes
DO j = 1,nz-1
  DO i = 1,nr-1
    k = i + 1 + j * (nr + 1)
    rrr = (r(i+1) - r(i-1)) * (r(i+1) - r(i)) * (r(i) - r(i-1))
    zzz = (z(j+1) - z(j-1)) * (z(j+1) - z(j)) * (z(j) - z(j-1))
    ee = dtd * (r(i) - r(i-1)) ** 2 / (2. * r(i) * rrr) + dtd * (r(i) - r(i-1)) / rrr
    ww = -1. * dtd * (r(i+1) - r(i)) ** 2 / (2. * r(i) * rrr) + dtd * (r(i+1) - r(i)) / rrr
    pp = 1. + dtd * ((r(i+1) - r(i)) ** 2 - (r(i) - r(i-1)) ** 2) / (2. * r(i) * rrr) - &
      & dtd * (r(i+1) - r(i-1)) / rrr - dtd * (z(j+1) - z(j-1)) / zzz
    ss = dtd * (z(j) - z(j-1)) / zzz
    nn = dtd * (z(j+1) - z(j)) / zzz

    RHS(k) = h(i+1,j) * ee + &
         & h(i-1,j) * ww + &
         & h(i,j) * pp +   &
         & h(i,j+1) * ss + &
         & h(i,j-1) * nn
  END DO
END DO

! Use LU decomposition for backsubsitition
CALL S_LUBkSub(matA, RHS, ne)
```

```
    ! Determine if dh/dt = 0
    maxdh = 0.
    DO j = 0,nz
      DO i = 0,nr-1
        k = i + 1 + j * (nr + 1)
        IF (ABS(maxdh) .LT. ABS((RHS(k) - h(i,j)) / RHS(k))) THEN
          maxdh = ABS((RHS(k) - h(i,j)) / RHS(k))
        END IF
      END DO
    END DO

    ! Put solution into head array
    DO j = 0,nz
      DO i = 0,nr
        k = i + 1 + j * (nr + 1)
        h(i,j) = RHS(k)
      END DO
    END DO

    WRITE (6,2101) m, maxdh
    2101 FORMAT (' m = ', i6, ' Darcy Maxdh = ', f9.7)

    t = m

    IF (m .LT. ntd) THEN
      IF (ABS(maxdh) .LT. epsd) THEN
        WRITE (6,*) 'Darcy steady state achieved!'
        EXIT
      END IF
    ELSE
      WRITE (6,2102) m
      2102 FORMAT (' !!!!WARNING!!!!', /, ' DARCY STEADY STATE NOT ACHIEVED IN ', i6, 'ITERATIONS!!!!!!!')
      PAUSE
    END IF
  END DO

END SUBROUTINE S_DarcyHead

!=========================================================================================!
! \\\\\\\\\\\\\\\\\\\\\\\\                                        ////////////////////////////  !
!                                   END SUBROUTINE: S_DARCYHEAD                                  !
! ////////////////////////                                        \\\\\\\\\\\\\\\\\\\\\\\\\\\\  !
!=========================================================================================!
```

A.5 Subroutine to Determine Forchheimer Solution

```
!==========================================================================================!
! \\\\\\\\\\\\\\\\\\\\\\\\                                            //////////////////////////// !
!                                 BEGIN SUBROUTINE: S_FORCHHEAD                                  !
! ////////////////////////                                            \\\\\\\\\\\\\\\\\\\\\\\\\\\\ !
!==========================================================================================!

! This subroutine calculates the head distribution of a finite difference scheme
!    for Forchheimer's Equation using a Gauss-Seidel iterative method.
SUBROUTINE S_ForchHead(r, z, hd, h, t)

  USE constants
  IMPLICIT NONE

  ! Define dummy variables
  REAL, DIMENSION(0:nr), INTENT(IN) :: r
  REAL, DIMENSION(0:nz), INTENT(IN) :: z
  REAL, DIMENSION(0:nr,0:nz), INTENT(IN) :: hd
  REAL, DIMENSION(0:nr,0:nz,0:ntf), INTENT(OUT) :: h
  INTEGER, INTENT(OUT) :: t

  ! Define temporary variables
  REAL, ALLOCATABLE :: hf(:,:)
  REAL, ALLOCATABLE :: hs(:)
  REAL, ALLOCATABLE :: Q(:)
  REAL, ALLOCATABLE :: SF(:)
  REAL Q2, Q3, Q4, hQ1, hQ2, alphar, betar
  INTEGER i, j, k, m, kmax
  REAL nn, ss, ee, pp, ww
  REAL gradN, gradS, gradE, gradW, gradP
  REAL phiN,  phiS,  phiE,  phiW,  phiP
  REAL maxdh, rrr, zzz
  CHARACTER*16 file60

  file60 = '3ForchRegres.csv'
  OPEN(60, FILE = file60, STATUS = 'unknown')

  kmax = 1
  ALLOCATE (hf(0:nr,0:nz))
  ALLOCATE (hs(kmax))
  ALLOCATE (Q(kmax))
  ALLOCATE (SF(kmax))

  ! Define head values that will be tested
  hs(1) = hmax

  ! For each head value determine the outflow rate
  DO k = 1,kmax

    ! Define Initial Condition as Darcy head distribution
    DO i = 0,nr
      DO j = 0,nz
        h(i,j,0) = hd(i,j)
      END DO
```

```
END DO

! Solve steady state solution using Gauss-Seidel iterative method
DO m = 1,ntf

  DO j = 0,nz
    DO i = 0,nr
      ! Inflow Boundary
      IF (j .EQ. 0) THEN
        IF (i .LE. nrs ) THEN
          h(i,j,m) = hs(k)
        END IF
      END IF

      ! Outflow Boundary
      IF (i .EQ. nr) THEN
        h(i,j,m) = 0.
      END IF

      ! Upper No Flow Boundary     z(j-1) = -z(j+1)
      !                            h(i,j-1) = h(i,j+1)
      IF (j .EQ. 0) THEN
        IF (i .GT. nrs) THEN
          IF (i .LT. nr) THEN
            rrr = (r(i+1) - r(i-1)) * (r(i+1) - r(i)) * (r(i) - r(i-1))
            zzz = (z(j+1) + z(j+1)) * (z(j+1) - z(j)) * (z(j) + z(j+1))
            gradE = SQRT(((h(i+1,j,m-1) - h(i,j,m-1)) / (r(i+1) - r(i))) ** 2 + &
                 & (((h(i+1,j+1,m-1) + h(i,j+1,m-1)) *                          &
                 &      (z(j) + z(j+1)) ** 2 +                                  &
                 & (h(i+1,j,m-1) + h(i,j,m-1)) *                                &
                 &      ((z(j+1) - z(j)) ** 2 - (z(j) + z(j+1)) ** 2) -         &
                 & (h(i+1,j+1,m-1) + h(i,j+1,m-1)) *                            &
                 &      (z(j+1) - z(j)) ** 2) / (2. * zzz)) ** 2)
            gradW = SQRT(((h(i,j,m-1) - h(i-1,j,m-1)) / (r(i) - r(i-1))) ** 2 + &
                 & (((h(i,j+1,m-1) + h(i-1,j+1,m-1)) *                          &
                 &      (z(j) + z(j+1)) ** 2 +                                  &
                 & (h(i,j,m-1) + h(i-1,j,m-1)) *                                &
                 &      ((z(j+1) - z(j)) ** 2 - (z(j) + z(j+1)) ** 2) -         &
                 & (h(i,j+1,m-1) + h(i-1,j+1,m-1)) *                            &
                 &      (z(j+1) - z(j)) ** 2) / (2. * zzz)) ** 2)
            gradP = SQRT(((h(i+1,j,m-1) * (r(i) - r(i-1)) ** 2 + h(i,j,m-1) *   &
                 & ((r(i+1) - r(i)) ** 2 - (r(i) - r(i-1)) ** 2) -              &
                 & h(i-1,j,m-1) * (r(i+1) - r(i)) ** 2) / rrr) ** 2 + &
                 & ((h(i,j+1,m-1) * (z(j) + z(j+1)) ** 2 + h(i,j,m-1) *         &
                 & ((z(j+1) - z(j)) ** 2 - (z(j) + z(j+1)) ** 2) -              &
                 & h(i,j+1,m-1) * (z(j+1) - z(j)) ** 2) / zzz) ** 2)
            gradS = SQRT(((h(i,j+1,m-1) - h(i,j,m-1)) / (z(j+1) - z(j))) ** 2 + &
                 & (((h(i+1,j+1,m-1) + h(i+1,j,m-1)) *                          &
                 &      (r(i) - r(i-1)) ** 2 +                                  &
                 & (h(i,j+1,m-1) + h(i,j,m-1)) *                                &
                 &      ((r(i+1) - r(i)) ** 2 - (r(i) - r(i-1)) ** 2) -         &
                 & (h(i-1,j+1,m-1) + h(i-1,j,m-1)) *                            &
                 &      (r(i+1) - r(i)) ** 2) / (2. * rrr)) ** 2)
            gradN = SQRT(((h(i,j,m-1) - h(i,j+1,m-1)) / (z(j) + z(j+1))) ** 2 + &
                 & (((h(i+1,j,m-1) + h(i+1,j+1,m-1)) *                          &
```

```
          &     (r(i) - r(i-1)) ** 2 +                        &
          & (h(i,j,m-1) + h(i,j+1,m-1)) *                        &
          &     ((r(i+1) - r(i)) ** 2 - (r(i) - r(i-1)) ** 2) -      &
          & (h(i-1,j,m-1) + h(i-1,j+1,m-1)) *                      &
          &     (r(i+1) - r(i)) ** 2) / (2. * rrr)) ** 2)
      phiE = aa ** 2 / (2. * bb * gradE) * (SQRT(1. + 4. * bb * gradE / aa ** 2) - 1.)
      phiW = aa ** 2 / (2. * bb * gradW) * (SQRT(1. + 4. * bb * gradW / aa ** 2) - 1.)
      phiP = aa ** 2 / (2. * bb * gradP) * (SQRT(1. + 4. * bb * gradP / aa ** 2) - 1.)
      phiS = aa ** 2 / (2. * bb * gradS) * (SQRT(1. + 4. * bb * gradS / aa ** 2) - 1.)
      phiN = aa ** 2 / (2. * bb * gradN) * (SQRT(1. + 4. * bb * gradN / aa ** 2) - 1.)

      ee = phiE * (r(i+1) + r(i)) * (r(i) - r(i-1)) ** 2 /                         &
        & (r(i) * (r(i+1) - r(i)) * rrr) + 2. * phiP * (r(i) - r(i-1)) ** 2 / (rrr ** 2) * &
        & ((r(i+1) - r(i)) ** 2 - (r(i) - r(i-1)) ** 2)
      ww = phiW * (r(i-1) + r(i)) * (r(i+1) - r(i)) ** 2 /                           &
        & (r(i) * (r(i) - r(i-1)) * rrr) - 2. * phiP * (r(i+1) - r(i)) ** 2 / (rrr ** 2) * &
        & ((r(i+1) - r(i)) ** 2 - (r(i) - r(i-1)) ** 2)
      pp = -1. * phiE * (r(i+1) + r(i)) * (r(i) - r(i-1)) ** 2 /                     &
        & (r(i) * (r(i+1) - r(i)) * rrr) - phiW * (r(i-1) + r(i)) * (r(i+1) - r(i)) ** 2 / &
        & (r(i) * (r(i) - r(i-1)) * rrr) + 2. * phiP / (rrr ** 2) *                  &
        & ((r(i+1) - r(i)) ** 2 - (r(i) - r(i-1)) ** 2) ** 2 -                     &
        & 2. * phiS * (z(j) + z(j+1)) ** 2 / ((z(j+1) - z(j)) * zzz) -                &
        & 2. * phiN * (z(j+1) - z(j)) ** 2 / ((z(j) + z(j+1)) * zzz) +                &
        & 2. * phiP / (zzz ** 2) * ((z(j+1) - z(j)) ** 2 - (z(j) + z(j+1)) ** 2) ** 2
      ss = 2. * phiS * (z(j) + z(j+1)) ** 2 / ((z(j+1) - z(j)) * zzz) +               &
        & 2. * phiP * (z(j) + z(j+1)) ** 2 / (zzz ** 2) *                           &
        & ((z(j+1) - z(j)) ** 2 - (z(j) + z(j+1)) ** 2)
      nn = 2. * phiN * (z(j+1) - z(j)) ** 2 / ((z(j) + z(j+1)) * zzz) -                &
        & 2. * phiP * (z(j+1) - z(j)) ** 2 / (zzz ** 2) *                           &
        & ((z(j+1) - z(j)) ** 2 - (z(j) + z(j+1)) ** 2)

      h(i,j,m) = -1. / pp * (       &
            & h(i+1,j,m-1) * ee + &
            & h(i-1,j,m  ) * ww + &
            & h(i,j+1,m-1) * ss + &
            & h(i,j+1,m-1) * nn)
    END IF
  END IF
END IF

! Lower No Flow Boundary     z(j+1) = 2*z(j) - z(j-1)
!                            h(i,j+1) = h(i,j-1)
IF (j .EQ. nz) THEN
  IF (i .GT. 0) THEN
    IF (i .LT. nr) THEN
        rrr = (r(i+1) - r(i-1)) * (r(i+1) - r(i)) * (r(i) - r(i-1))
        zzz = (2. * z(j) - 2. * z(j-1)) * (z(j) - z(j-1)) * (z(j) - z(j-1))
        gradE = SQRT(((h(i+1,j,m-1) - h(i,j,m-1)) / (r(i+1) - r(i))) ** 2 + &
            & (((h(i+1,j-1,m-1) + h(i,j-1,m-1)) *                    &
            &     (z(j) - z(j-1)) ** 2 +                        &
            & (h(i+1,j,m-1) + h(i,j,m-1)) *                       &
            &     ((z(j) - z(j-1)) ** 2 - (z(j) - z(j-1)) ** 2) -      &
            & (h(i+1,j-1,m-1) + h(i,j-1,m-1)) *                    &
            &     (z(j) - z(j-1)) ** 2) / (2. * zzz)) ** 2)
        gradW = SQRT(((h(i,j,m-1) - h(i-1,j,m-1)) / (r(i) - r(i-1))) ** 2 + &
```

```
    & (((h(i,j-1,m-1) + h(i-1,j-1,m-1)) *                     &
    &      (z(j) - z(j-1)) ** 2 +                            &
    & (h(i,j,m-1) + h(i-1,j,m-1)) *                          &
    &      ((z(j) - z(j-1)) ** 2 - (z(j) - z(j-1)) ** 2) -       &
    & (h(i,j-1,m-1) + h(i-1,j-1,m-1)) *                      &
    &      (z(j) - z(j-1)) ** 2) / (2. * zzz)) ** 2)
gradP = SQRT(((h(i+1,j,m-1) * (r(i) - r(i-1)) ** 2 + h(i,j,m-1) *   &
    & ((r(i+1) - r(i)) ** 2 - (r(i) - r(i-1)) ** 2) -           &
    & h(i-1,j,m-1) * (r(i+1) - r(i)) ** 2) / rrr) ** 2 + &
    & ((h(i,j-1,m-1) * (z(j) - z(j-1)) ** 2 + h(i,j,m-1) *       &
    & ((z(j) - z(j-1)) ** 2 - (z(j) - z(j-1)) ** 2) -           &
    & h(i,j-1,m-1) * (z(j) - z(j-1)) ** 2) / zzz) ** 2)
gradS = SQRT(((h(i,j-1,m-1) - h(i,j,m-1)) / (z(j) - z(j-1))) ** 2 + &
    & (((h(i+1,j-1,m-1) + h(i+1,j,m-1)) *                     &
    &      (r(i) - r(i-1)) ** 2 +                            &
    & (h(i,j-1,m-1) + h(i,j,m-1)) *                          &
    &      ((r(i+1) - r(i)) ** 2 - (r(i) - r(i-1)) ** 2) -       &
    & (h(i-1,j-1,m-1) + h(i-1,j,m-1)) *                      &
    &      (r(i+1) - r(i)) ** 2) / (2. * rrr)) ** 2)
gradN = SQRT(((h(i,j,m-1) - h(i,j-1,m-1)) / (z(j) - z(j-1))) ** 2 + &
    & (((h(i+1,j,m-1) + h(i+1,j-1,m-1)) *                     &
    &      (r(i) - r(i-1)) ** 2 +                            &
    & (h(i,j,m-1) + h(i,j-1,m-1)) *                          &
    &      ((r(i+1) - r(i)) ** 2 - (r(i) - r(i-1)) ** 2) -       &
    & (h(i-1,j,m-1) + h(i-1,j-1,m-1)) *                      &
    &      (r(i+1) - r(i)) ** 2) / (2. * rrr)) ** 2)
phiE = aa ** 2 / (2. * bb * gradE) * (SQRT(1. + 4. * bb * gradE / aa ** 2) - 1.)
phiW = aa ** 2 / (2. * bb * gradW) * (SQRT(1. + 4. * bb * gradW / aa ** 2) - 1.)
phiP = aa ** 2 / (2. * bb * gradP) * (SQRT(1. + 4. * bb * gradP / aa ** 2) - 1.)
phiS = aa ** 2 / (2. * bb * gradS) * (SQRT(1. + 4. * bb * gradS / aa ** 2) - 1.)
phiN = aa ** 2 / (2. * bb * gradN) * (SQRT(1. + 4. * bb * gradN / aa ** 2) - 1.)

ee = phiE * (r(i+1) + r(i)) * (r(i) - r(i-1)) ** 2 /                        &
  & (r(i) * (r(i+1) - r(i)) * rrr) + 2. * phiP * (r(i) - r(i-1)) ** 2 / (rrr ** 2) * &
  & ((r(i+1) - r(i)) ** 2 - (r(i) - r(i-1)) ** 2)
ww = phiW * (r(i-1) + r(i)) * (r(i+1) - r(i)) ** 2 /                       &
  & (r(i) * (r(i) - r(i-1)) * rrr) - 2. * phiP * (r(i+1) - r(i)) ** 2 / (rrr ** 2) * &
  & ((r(i+1) - r(i)) ** 2 - (r(i) - r(i-1)) ** 2)
pp = -1. * phiE * (r(i+1) + r(i)) * (r(i) - r(i-1)) ** 2 /                  &
  & (r(i) * (r(i+1) - r(i)) * rrr) - phiW * (r(i-1) + r(i)) * (r(i+1) - r(i)) ** 2 / &
  & (r(i) * (r(i) - r(i-1)) * rrr) + 2. * phiP / (rrr ** 2) *                &
  & ((r(i+1) - r(i)) ** 2 - (r(i) - r(i-1)) ** 2) ** 2 -                   &
  & 2. * phiS * (z(j) - z(j-1)) ** 2 / ((z(j) - z(j-1)) * zzz) -              &
  & 2. * phiN * (z(j) - z(j-1)) ** 2 / ((z(j) - z(j-1)) * zzz) +              &
  & 2. * phiP / (zzz ** 2) * ((z(j) - z(j-1)) ** 2 - (z(j) - z(j-1)) ** 2) ** 2
ss = 2. * phiS * (z(j) - z(j-1)) ** 2 / ((z(j) - z(j-1)) * zzz) +             &
  & 2. * phiP * (z(j) - z(j-1)) ** 2 / (zzz ** 2) *                        &
  & ((z(j) - z(j-1)) ** 2 - (z(j) - z(j-1)) ** 2)
nn = 2. * phiN * (z(j) - z(j-1)) ** 2 / ((z(j) - z(j-1)) * zzz) -             &
  & 2. * phiP * (z(j) - z(j-1)) ** 2 / (zzz ** 2) *                        &
  & ((z(j) - z(j-1)) ** 2 - (z(j) - z(j-1)) ** 2)

h(i,j,m) = -1. / pp * (       &
       & h(i+1,j,m-1) * ee + &
       & h(i-1,j,m  ) * ww + &
```

```
                   & h(i,j-1,m  ) * ss + &
                   & h(i,j-1,m  ) * nn)
        END IF
    END IF
END IF

! Bottom Center Node    z(j+1) = 2*z(j) - z(j-1)
!                       h(i,j+1) = h(i,j-1)
IF (j .EQ. nz) THEN
    IF (i .EQ. 0) THEN
        zzz = (2. * z(j) - 2. * z(j-1)) * (z(j) - z(j-1)) * (z(j) - z(j-1))
        gradS = SQRT(((h(i,j-1,m-1) - h(i,j,m-1)) / (z(j) - z(j-1))) ** 2)
        gradN = SQRT(((h(i,j,m-1) - h(i,j-1,m-1)) / (z(j) - z(j-1))) ** 2)
        phiP = 1.
        phiS = aa ** 2 / (2. * bb * gradS) * (SQRT(1. + 4. * bb * gradS / aa ** 2) - 1.)
        phiN = aa ** 2 / (2. * bb * gradN) * (SQRT(1. + 4. * bb * gradN / aa ** 2) - 1.)

        ee = 4. * phiP / (r(i+1) ** 2)
        pp = -4. * phiP / (r(i+1) ** 2) -                                    &
          & 2. * phiS * (z(j) - z(j-1)) ** 2 / ((z(j) - z(j-1)) * zzz) -              &
          & 2. * phiN * (z(j) - z(j-1)) ** 2 / ((z(j) - z(j-1)) * zzz) +              &
          & 2. * phiP / (zzz ** 2) * ((z(j) - z(j-1)) ** 2 - (z(j) - z(j-1)) ** 2) ** 2
        ss = 2. * phiS * (z(j) - z(j-1)) ** 2 / ((z(j) - z(j-1)) * zzz) +              &
          & 2. * phiP * (z(j) - z(j-1)) ** 2 / (zzz ** 2) *                          &
          &      ((z(j) - z(j-1)) ** 2 - (z(j) - z(j-1)) ** 2)
        nn = 2. * phiN * (z(j) - z(j-1)) ** 2 / ((z(j) - z(j-1)) * zzz) -              &
          & 2. * phiP * (z(j) - z(j-1)) ** 2 / (zzz ** 2) *                          &
          &      ((z(j) - z(j-1)) ** 2 - (z(j) - z(j-1)) ** 2)

        h(i,j,m) = -1. / pp * (       &
              & h(i+1,j,m-1) * ee + &
              & h(i,j-1,m  ) * ss + &
              & h(i,j-1,m  ) * nn)
    END IF
END IF

! Symmetry No Flow Boundary for r = 0
IF (i .EQ. 0) THEN
    IF (j .GT. 0) THEN
        IF (j .LT. nz) THEN
            zzz = (z(j+1) - z(j-1)) * (z(j+1) - z(j)) * (z(j) - z(j-1))
            gradP = SQRT(((h(i,j+1,m-1) * (z(j) - z(j-1)) ** 2 + h(i,j,m-1) * &
                 &      ((z(j+1) - z(j)) ** 2 - (z(j) - z(j-1)) ** 2) -      &
                 & h(i,j-1,m-1) * (z(j+1) - z(j)) ** 2) / zzz) ** 2)
            gradS = SQRT(((h(i,j+1,m-1) - h(i,j,m-1)) / (z(j+1) - z(j))) ** 2)
            gradN = SQRT(((h(i,j,m-1) - h(i,j-1,m-1)) / (z(j) - z(j-1))) ** 2)
            phiP = aa ** 2 / (2. * bb * gradP) * (SQRT(1. + 4. * bb * gradP / aa ** 2) - 1.)
            phiS = aa ** 2 / (2. * bb * gradS) * (SQRT(1. + 4. * bb * gradS / aa ** 2) - 1.)
            phiN = aa ** 2 / (2. * bb * gradN) * (SQRT(1. + 4. * bb * gradN / aa ** 2) - 1.)

            ee = 4. * phiP / (r(i+1) ** 2)
            pp = -4. * phiP / (r(i+1) ** 2) -                                    &
              & 2. * phiS * (z(j) - z(j-1)) ** 2 / ((z(j+1) - z(j)) * zzz) -              &
              & 2. * phiN * (z(j+1) - z(j)) ** 2 / ((z(j) - z(j-1)) * zzz) +              &
              & 2. * phiP / (zzz ** 2) * ((z(j+1) - z(j)) ** 2 - (z(j) - z(j-1)) ** 2) ** 2
```

```
      ss = 2. * phiS * (z(j) - z(j-1)) ** 2 / ((z(j+1) - z(j)) * zzz) +              &
        & 2. * phiP * (z(j) - z(j-1)) ** 2 / (zzz ** 2) *                          &
        &     ((z(j+1) - z(j)) ** 2 - (z(j) - z(j-1)) ** 2)
      nn = 2. * phiN * (z(j+1) - z(j)) ** 2 / ((z(j) - z(j-1)) * zzz) -              &
        & 2. * phiP * (z(j+1) - z(j)) ** 2 / (zzz ** 2) *                          &
        &     ((z(j+1) - z(j)) ** 2 - (z(j) - z(j-1)) ** 2)

      h(i,j,m) = -1. / pp * (       &
            & h(i+1,j,m-1) * ee + &
            & h(i,j+1,m-1) * ss + &
            & h(i,j-1,m  ) * nn)
    END IF
  END IF
END IF

! Interior Nodes
IF (i .GT. 0) THEN
  IF (i .LT. nr) THEN
    IF (j .GT. 0) THEN
      IF (j .LT. nz) THEN
        rrr = (r(i+1) - r(i-1)) * (r(i+1) - r(i)) * (r(i) - r(i-1))
        zzz = (z(j+1) - z(j-1)) * (z(j+1) - z(j)) * (z(j) - z(j-1))
        gradE = SQRT(((h(i+1,j,m-1) - h(i,j,m-1)) / (r(i+1) - r(i))) ** 2 + &
            & (((h(i+1,j+1,m-1) + h(i,j+1,m-1)) *                       &
            &     (z(j) - z(j-1)) ** 2 +                               &
            & (h(i+1,j,m-1) + h(i,j,m-1)) *                            &
            &     ((z(j+1) - z(j)) ** 2 - (z(j) - z(j-1)) ** 2) -       &
            & (h(i+1,j-1,m-1) + h(i,j-1,m-1)) *                        &
            &     (z(j+1) - z(j)) ** 2) / (2. * zzz)) ** 2)
        gradW = SQRT(((h(i,j,m-1) - h(i-1,j,m-1)) / (r(i) - r(i-1))) ** 2 + &
            & (((h(i,j+1,m-1) + h(i-1,j+1,m-1)) *                       &
            &     (z(j) - z(j-1)) ** 2 +                               &
            & (h(i,j,m-1) + h(i-1,j,m-1)) *                            &
            &     ((z(j+1) - z(j)) ** 2 - (z(j) - z(j-1)) ** 2) -       &
            & (h(i,j-1,m-1) + h(i-1,j-1,m-1)) *                        &
            &     (z(j+1) - z(j)) ** 2) / (2. * zzz)) ** 2)
        gradP = SQRT(((h(i+1,j,m-1) * (r(i) - r(i-1)) ** 2 + h(i,j,m-1) *   &
            & ((r(i+1) - r(i)) ** 2 - (r(i) - r(i-1)) ** 2) -           &
            & h(i-1,j,m-1) * (r(i+1) - r(i)) ** 2) / rrr) ** 2 + &
            & ((h(i,j+1,m-1) * (z(j) - z(j-1)) ** 2 + h(i,j,m-1) *       &
            & ((z(j+1) - z(j)) ** 2 - (z(j) - z(j-1)) ** 2) -           &
            & h(i,j-1,m-1) * (z(j+1) - z(j)) ** 2) / zzz) ** 2)
        gradS = SQRT(((h(i,j+1,m-1) - h(i,j,m-1)) / (z(j+1) - z(j))) ** 2 + &
            & (((h(i+1,j+1,m-1) + h(i+1,j,m-1)) *                       &
            &     (r(i) - r(i-1)) ** 2 +                               &
            & (h(i,j+1,m-1) + h(i,j,m-1)) *                            &
            &     ((r(i+1) - r(i)) ** 2 - (r(i) - r(i-1)) ** 2) -       &
            & (h(i-1,j+1,m-1) + h(i-1,j,m-1)) *                        &
            &     (r(i+1) - r(i)) ** 2) / (2. * rrr)) ** 2)
        gradN = SQRT(((h(i,j,m-1) - h(i,j-1,m-1)) / (z(j) - z(j-1))) ** 2 + &
            & (((h(i+1,j,m-1) + h(i+1,j-1,m-1)) *                       &
            &     (r(i) - r(i-1)) ** 2 +                               &
            & (h(i,j,m-1) + h(i,j-1,m-1)) *                            &
            &     ((r(i+1) - r(i)) ** 2 - (r(i) - r(i-1)) ** 2) -       &
            & (h(i-1,j,m-1) + h(i-1,j-1,m-1)) *                        &
```

```
                &     (r(i+1) - r(i)) ** 2) / (2. * rrr)) ** 2)
            phiE = aa ** 2 / (2. * bb * gradE) * (SQRT(1. + 4. * bb * gradE / aa ** 2) - 1.)
            phiW = aa ** 2 / (2. * bb * gradW) * (SQRT(1. + 4. * bb * gradW / aa ** 2) - 1.)
            phiP = aa ** 2 / (2. * bb * gradP) * (SQRT(1. + 4. * bb * gradP / aa ** 2) - 1.)
            phiS = aa ** 2 / (2. * bb * gradS) * (SQRT(1. + 4. * bb * gradS / aa ** 2) - 1.)
            phiN = aa ** 2 / (2. * bb * gradN) * (SQRT(1. + 4. * bb * gradN / aa ** 2) - 1.)

            ee = phiE * (r(i+1) + r(i)) * (r(i) - r(i-1)) ** 2 /                              &
              & (r(i) * (r(i+1) - r(i)) * rrr) + 2. * phiP * (r(i) - r(i-1)) ** 2 / (rrr ** 2) * &
              & ((r(i+1) - r(i)) ** 2 - (r(i) - r(i-1)) ** 2)
            ww = phiW * (r(i-1) + r(i)) * (r(i+1) - r(i)) ** 2 /                              &
              & (r(i) * (r(i) - r(i-1)) * rrr) - 2. * phiP * (r(i+1) - r(i)) ** 2 / (rrr ** 2) * &
              & ((r(i+1) - r(i)) ** 2 - (r(i) - r(i-1)) ** 2)
            pp = -1. * phiE * (r(i+1) + r(i)) * (r(i) - r(i-1)) ** 2 /                        &
              & (r(i) * (r(i+1) - r(i)) * rrr) - phiW * (r(i-1) + r(i)) * (r(i+1) - r(i)) ** 2 / &
              & (r(i) * (r(i) - r(i-1)) * rrr) + 2. * phiP / (rrr ** 2) *                      &
              & ((r(i+1) - r(i)) ** 2 - (r(i) - r(i-1)) ** 2) ** 2 -                           &
              & 2. * phiS * (z(j) - z(j-1)) ** 2 / ((z(j+1) - z(j)) * zzz) -                   &
              & 2. * phiN * (z(j+1) - z(j)) ** 2 / ((z(j) - z(j-1)) * zzz) +                   &
              & 2. * phiP / (zzz ** 2) * ((z(j+1) - z(j)) ** 2 - (z(j) - z(j-1)) ** 2) ** 2
            ss = 2. * phiS * (z(j) - z(j-1)) ** 2 / ((z(j+1) - z(j)) * zzz) +                  &
              & 2. * phiP * (z(j) - z(j-1)) ** 2 / (zzz ** 2) *                                &
              & ((z(j+1) - z(j)) ** 2 - (z(j) - z(j-1)) ** 2)
            nn = 2. * phiN * (z(j+1) - z(j)) ** 2 / ((z(j) - z(j-1)) * zzz) -                  &
              & 2. * phiP * (z(j+1) - z(j)) ** 2 / (zzz ** 2) *                                &
              & ((z(j+1) - z(j)) ** 2 - (z(j) - z(j-1)) ** 2)

            h(i,j,m) = -1. / pp * (       &
                  & h(i+1,j,m-1) * ee + &
                  & h(i-1,j,m  ) * ww + &
                  & h(i,j+1,m-1) * ss + &
                  & h(i,j-1,m  ) * nn)
          END IF
        END IF
      END IF
    END IF
  END DO
END DO

! Determine if dh/dt = 0
maxdh = 0.
DO j = 0,nz
  DO i = 0,nr-1
    IF (ABS(maxdh) .LT. ABS((h(i,j,m) - h(i,j,m-1)) / h(i,j,m))) THEN
      maxdh = ABS((h(i,j,m) - h(i,j,m-1)) / h(i,j,m))
    END IF
  END DO
END DO

WRITE (6,4103) k, m, maxdh
4103 FORMAT (' k = ', i2, ' m = ', i6, ' Forch Maxdh = ', f9.7)

t = m

IF (m .LT. ntf) THEN
```

```
        IF (ABS(maxdh) .LT. epsf) THEN
          WRITE (6,*) 'Forchheimer steady state achieved!'
          EXIT
        END IF
      ELSE
        WRITE (6,4104) m
        4104 FORMAT (' !!!!WARNING!!!!', /, ' FORCHHEIMER STEADY STATE NOT ACHIEVED IN ', i6, '
ITERATIONS!!!!!!!')
        PAUSE
      END IF
    END DO

    ! Put the converged Forchheimer solution into a 2-D array
    DO j = 0,nz
      DO i = 0,nr
        hf(i,j) = h(i,j,t)
      END DO
    END DO

    ! Determine Nonlinear Outflow Rate
    CALL S_NonlinearQout(r, z, hf, Q(k))
    ! Determine Nonlinear Shape Factor
    CALL S_NonlinearSF(r, z, hf, SF(k), hs(k))

  END DO  ! end of k loop

  ! Determine alpha and beta from regression of hs(k) versus Q(k)
  DO k = 0,kmax
    Q2 = Q2 + Q(k) ** 2
    Q3 = Q3 + Q(k) ** 3
    Q4 = Q4 + Q(k) ** 4
    hQ1 = hQ1 + hs(k) * Q(k)
    hQ2 = hQ2 + hs(k) * Q(k) ** 2
  END DO

  alphar = 1. / (Q2 * Q4 - Q3 ** 2) * (Q4 * hQ1 - Q3 * hQ2)
  betar = 1. / (Q2 * Q4 - Q3 ** 2) * (Q2 * hQ2 - Q3 * hQ1)


  !==========================================================================================!
  !                                WRITE TO REGRESSION FILE                                  !
  !==========================================================================================!

  ! Write header to output file
  WRITE (60,6101) file60, nrs, nr, nz, CoreID, Rs, bc, Rc, aa, bb
  6101 FORMAT (/, 'Forchheimer Regression', /, 'Filename,', a16, /, 'Nrs=,', i4, /,      &
          & 'Nr=,', i4, /, 'Nz=,', i4, /, /, 'Core ID,', a7, /, 'Rs=,', f8.4, ',cm', &
          & /, 'bc=,', f8.4, ',cm', /, 'Rc=,', f8.4, ',cm', /, /,                   &
          & 'aa=,', f14.8, ',s/cm', /, 'bb=,', f14.8, ',s2/cm2', /)

  ! Write regression summary
  WRITE (60,6103) Rs, Rc, bc, aa, bb, alphar, betar
  6103 FORMAT ('Rs (cm),Rc (cm),bc (cm),aa (s/cm),bb (s2/cm2),alpha (s/cm2),beta (s2/cm5)', /, &
          & f14.8, ',', f14.8, ',', f14.8, ',', f14.8, ',', f14.8, ',', f14.8, ',', f14.8, &
          & /, /, 'Q (cm3/s),hs (cm),SF')
```

```
  ! Write standpipe head, nonlinear outflow rate, nonlinear shape factor
  DO k = 1,kmax
    WRITE (60,6104) Q(k), hs(k), SF(k)
    6104 FORMAT (f15.10, ',', f15.10, ',', f15.10)
  END DO

  CLOSE (60)

END SUBROUTINE S_ForchHead

!==========================================================================================!
!  \\\\\\\\\\\\\\\\\\\\\\\\                                      ////////////////////////////  !
!                                  END SUBROUTINE: S_FORCHHEAD                               !
!  ////////////////////////                                      \\\\\\\\\\\\\\\\\\\\\\\\\\\\  !
!==========================================================================================!
```

A.6 Subroutine to Calculation Hydraulic Conductivity Ratio

```
!==========================================================================================!
!  \\\\\\\\\\\\\\\\\\\\\\\\                                      ////////////////////////////  !
!                                  BEGIN SUBROUTINE: S_PHIFUNC                               !
!  ////////////////////////                                      \\\\\\\\\\\\\\\\\\\\\\\\\\\\  !
!==========================================================================================!

! This subroutine calculates the phi function at each node using a second order finite
!    difference scheme.  At the boundaries, a second order upwind scheme is used.
SUBROUTINE S_PhiFunc(r, z, h, phi)

  USE constants
  IMPLICIT NONE

  ! Define dummy variables
  REAL, DIMENSION(0:nr), INTENT(IN) :: r
  REAL, DIMENSION(0:nz), INTENT(IN) :: z
  REAL, DIMENSION(0:nr,0:nz), INTENT(IN) :: h
  REAL, DIMENSION(0:nr,0:nz), INTENT(OUT) :: phi

  ! Define temporary variables
  REAL grad, rrr, zzz
  INTEGER i, j

  ! Upper Boundary
  DO j = 0,0
    DO i = 1,nr-1
      rrr = (r(i+1) - r(i-1)) * (r(i+1) - r(i)) * (r(i) - r(i-1))
      zzz = (z(j+2) - z(j)) * (z(j+2) - z(j+1)) * (z(j+1) - z(j))
      grad = SQRT(((h(i+1,j) * (r(i) - r(i-1)) ** 2 + h(i,j) * ((r(i+1) - r(i)) ** 2 - &
          &                 (r(i) - r(i-1)) ** 2) - h(i-1,j) * (r(i+1) - r(i)) ** 2) / rrr) ** 2 + &
          &     ((h(i,j) * ((z(j+1) - z(j)) ** 2 - (z(j+2) - z(j)) * (z(j+2) - z(j+1)) - (z(j+2) - z(j)) * (z(j+1) - z(j))) &
          &     + h(i,j+1) * ((z(j+2) - z(j)) * (z(j+2) - z(j+1)) + (z(j+2) - z(j)) * (z(j+1) - z(j))) - &
          &       h(i,j+2) * (z(j+1) - z(j)) ** 2) / zzz) ** 2)
```

```
    phi(i,j) = aa ** 2 / (2. * bb * grad) * &
          & (SQRT(1. + 4. * bb * grad / (aa ** 2)) - 1.)
  END DO
END DO

! Top Center Node
DO j = 0,0
  DO i = 0,0
    rrr = (r(i+2) - r(i)) * (r(i+2) - r(i+1)) * (r(i+1) - r(i))
    zzz = (z(j+2) - z(j)) * (z(j+2) - z(j+1)) * (z(j+1) - z(j))
    grad = SQRT(((h(i,j) * ((r(i+1) - r(i)) ** 2 - (r(i+2) - r(i)) * (r(i+2) - r(i+1)) - (r(i+2) - r(i)) * (r(i+1) - r(i))) &
        &     + h(i+1,j) * ((r(i+2) - r(i)) * (r(i+2) - r(i+1)) + (r(i+2) - r(i)) * (r(i+1) - r(i))) - &
        &       h(i+2,j) * (r(i+1) - r(i)) ** 2) / rrr) ** 2 + &
        &     ((h(i,j) * ((z(j+1) - z(j)) ** 2 - (z(j+2) - z(j)) * (z(j+2) - z(j+1)) - (z(j+2) - z(j)) * (z(j+1) - z(j))) &
        &     + h(i,j+1) * ((z(j+2) - z(j)) * (z(j+2) - z(j+1)) + (z(j+2) - z(j)) * (z(j+1) - z(j))) - &
        &       h(i,j+2) * (z(j+1) - z(j)) ** 2) / zzz) ** 2)
    phi(i,j) = aa ** 2 / (2. * bb * grad) * &
          & (SQRT(1. + 4. * bb * grad / (aa ** 2)) - 1.)
  END DO
END DO

! Outflow Boundary
DO j = 1,nz-1
  DO i = nr,nr
    rrr = (r(i-2) - r(i)) * (r(i-2) - r(i-1)) * (r(i-1) - r(i))
    zzz = (z(j+1) - z(j-1)) * (z(j+1) - z(j)) * (z(j) - z(j-1))
    grad = SQRT(((h(i,j) * ((r(i-1) - r(i)) ** 2 - (r(i-2) - r(i)) * (r(i-2) - r(i-1)) - (r(i-2) - r(i)) * (r(i-1) - r(i))) &
        &     + h(i-1,j) * ((r(i-2) - r(i)) * (r(i-2) - r(i-1)) + (r(i-2) - r(i)) * (r(i-1) - r(i))) - &
        &       h(i-2,j) * (r(i-1) - r(i)) ** 2) / rrr) ** 2 + &
        &     ((h(i,j+1) * (z(j) - z(j-1)) ** 2 + h(i,j) * ((z(j+1) - z(j)) ** 2 - &
        &                 (z(j) - z(j-1)) ** 2) - h(i,j-1) * (z(j+1) - z(j)) ** 2) / zzz) ** 2)
    phi(i,j) = aa ** 2 / (2. * bb * grad) * &
          & (SQRT(1. + 4. * bb * grad / (aa ** 2)) - 1.)
  END DO
END DO

! Top Radius Node
DO j = 0,0
  DO i = nr,nr
    rrr = (r(i-2) - r(i)) * (r(i-2) - r(i-1)) * (r(i-1) - r(i))
    zzz = (z(j+2) - z(j)) * (z(j+2) - z(j+1)) * (z(j+1) - z(j))
    grad = SQRT(((h(i,j) * ((r(i-1) - r(i)) ** 2 - (r(i-2) - r(i)) * (r(i-2) - r(i-1)) - (r(i-2) - r(i)) * (r(i-1) - r(i))) &
        &     + h(i-1,j) * ((r(i-2) - r(i)) * (r(i-2) - r(i-1)) + (r(i-2) - r(i)) * (r(i-1) - r(i))) - &
        &       h(i-2,j) * (r(i-1) - r(i)) ** 2) / rrr) ** 2 + &
        &     ((h(i,j) * ((z(j+1) - z(j)) ** 2 - (z(j+2) - z(j)) * (z(j+2) - z(j+1)) - (z(j+2) - z(j)) * (z(j+1) - z(j))) &
        &     + h(i,j+1) * ((z(j+2) - z(j)) * (z(j+2) - z(j+1)) + (z(j+2) - z(j)) * (z(j+1) - z(j))) - &
        &       h(i,j+2) * (z(j+1) - z(j)) ** 2) / zzz) ** 2)
    phi(i,j) = aa ** 2 / (2. * bb * grad) * &
          & (SQRT(1. + 4. * bb * grad / (aa ** 2)) - 1.)
  END DO
END DO

! Bottom Radius Node
DO j = nz,nz
  DO i = nr,nr
```

```
    rrr = (r(i-2) - r(i)) * (r(i-2) - r(i-1)) * (r(i-1) - r(i))
    zzz = (z(j-2) - z(j)) * (z(j-2) - z(j-1)) * (z(j-1) - z(j))
    grad = SQRT(((h(i,j) * ((r(i-1) - r(i)) ** 2 - (r(i-2) - r(i)) * (r(i-2) - r(i-1)) - (r(i-2) - r(i)) * (r(i-1) - r(i))) &
        &     + h(i-1,j) * ((r(i-2) - r(i)) * (r(i-2) - r(i-1)) + (r(i-2) - r(i)) * (r(i-1) - r(i))) - &
        &       h(i-2,j) * (r(i-1) - r(i)) ** 2) / rrr) ** 2 + &
        &     ((h(i,j) * ((z(j-1) - z(j)) ** 2 - (z(j-2) - z(j)) * (z(j-2) - z(j-1)) - (z(j-2) - z(j)) * (z(j-1) - z(j))) &
        &     + h(i,j-1) * ((z(j-2) - z(j)) * (z(j-2) - z(j-1)) + (z(j-2) - z(j)) * (z(j-1) - z(j))) - &
        &       h(i,j-2) * (z(j-1) - z(j)) ** 2) / zzz) ** 2)
    phi(i,j) = aa ** 2 / (2. * bb * grad) * &
          & (SQRT(1. + 4. * bb * grad / (aa ** 2)) - 1.)
  END DO
END DO

! Lower No Flow Boundary
DO j = nz,nz
  DO i = 1,nr-1
    rrr = (r(i+1) - r(i-1)) * (r(i+1) - r(i)) * (r(i) - r(i-1))
    zzz = (z(j-2) - z(j)) * (z(j-2) - z(j-1)) * (z(j-1) - z(j))
    grad = SQRT(((h(i+1,j) * (r(i) - r(i-1)) ** 2 + h(i,j) * ((r(i+1) - r(i)) ** 2 - &
        &                 (r(i) - r(i-1)) ** 2) - h(i-1,j) * (r(i+1) - r(i)) ** 2) / rrr) ** 2 + &
        &     ((h(i,j) * ((z(j-1) - z(j)) ** 2 - (z(j-2) - z(j)) * (z(j-2) - z(j-1)) - (z(j-2) - z(j)) * (z(j-1) - z(j))) &
        &     + h(i,j-1) * ((z(j-2) - z(j)) * (z(j-2) - z(j-1)) + (z(j-2) - z(j)) * (z(j-1) - z(j))) - &
        &       h(i,j-2) * (z(j-1) - z(j)) ** 2) / zzz) ** 2)
    phi(i,j) = aa ** 2 / (2. * bb * grad) * &
          & (SQRT(1. + 4. * bb * grad / (aa ** 2)) - 1.)
  END DO
END DO

! Bottom Center Node
DO j = nz,nz
  DO i = 0,0
    rrr = (r(i+2) - r(i)) * (r(i+2) - r(i+1)) * (r(i+1) - r(i))
    zzz = (z(j-2) - z(j)) * (z(j-2) - z(j-1)) * (z(j-1) - z(j))
    grad = SQRT(((h(i,j) * ((r(i+1) - r(i)) ** 2 - (r(i+2) - r(i)) * (r(i+2) - r(i+1)) - (r(i+2) - r(i)) * (r(i+1) - r(i))) &
        &     + h(i+1,j) * ((r(i+2) - r(i)) * (r(i+2) - r(i+1)) + (r(i+2) - r(i)) * (r(i+1) - r(i))) - &
        &       h(i+2,j) * (r(i+1) - r(i)) ** 2) / rrr) ** 2 + &
        &     ((h(i,j) * ((z(j-1) - z(j)) ** 2 - (z(j-2) - z(j)) * (z(j-2) - z(j-1)) - (z(j-2) - z(j)) * (z(j-1) - z(j))) &
        &     + h(i,j-1) * ((z(j-2) - z(j)) * (z(j-2) - z(j-1)) + (z(j-2) - z(j)) * (z(j-1) - z(j))) - &
        &       h(i,j-2) * (z(j-1) - z(j)) ** 2) / zzz) ** 2)
    phi(i,j) = aa ** 2 / (2. * bb * grad) * &
          & (SQRT(1. + 4. * bb * grad / (aa ** 2)) - 1.)
  END DO
END DO

! Symmetry No Flow Boundary for r = 0
DO j = 1,nz-1
  DO i = 0,0
    rrr = (r(i+2) - r(i)) * (r(i+2) - r(i+1)) * (r(i+1) - r(i))
    zzz = (z(j+1) - z(j-1)) * (z(j+1) - z(j)) * (z(j) - z(j-1))
    grad = SQRT(((h(i,j) * ((r(i+1) - r(i)) ** 2 - (r(i+2) - r(i)) * (r(i+2) - r(i+1)) - (r(i+2) - r(i)) * (r(i+1) - r(i))) &
        &     + h(i+1,j) * ((r(i+2) - r(i)) * (r(i+2) - r(i+1)) + (r(i+2) - r(i)) * (r(i+1) - r(i))) - &
        &       h(i+2,j) * (r(i+1) - r(i)) ** 2) / rrr) ** 2 + &
        &     ((h(i,j+1) * (z(j) - z(j-1)) ** 2 + h(i,j) * ((z(j+1) - z(j)) ** 2 - &
        &                 (z(j) - z(j-1)) ** 2) - h(i,j-1) * (z(j+1) - z(j)) ** 2) / zzz) ** 2)
    phi(i,j) = aa ** 2 / (2. * bb * grad) * &
```

```
            & (SQRT(1. + 4. * bb * grad / (aa ** 2)) - 1.)
    END DO
  END DO

  ! Interior Nodes
  DO j = 1,nz-1
    DO i = 1,nr-1
      rrr = (r(i+1) - r(i-1)) * (r(i+1) - r(i)) * (r(i) - r(i-1))
      zzz = (z(j+1) - z(j-1)) * (z(j+1) - z(j)) * (z(j) - z(j-1))
      grad = SQRT(((h(i+1,j) * (r(i) - r(i-1)) ** 2 + h(i,j) * ((r(i+1) - r(i)) ** 2 - &
          &                (r(i) - r(i-1)) ** 2) - h(i-1,j) * (r(i+1) - r(i)) ** 2) / rrr) ** 2 + &
          &     ((h(i,j+1) * (z(j) - z(j-1)) ** 2 + h(i,j) * ((z(j+1) - z(j)) ** 2 - &
          &                (z(j) - z(j-1)) ** 2) - h(i,j-1) * (z(j+1) - z(j)) ** 2) / zzz) ** 2)
      phi(i,j) = aa ** 2 / (2. * bb * grad) * &
            & (SQRT(1. + 4. * bb * grad / (aa ** 2)) - 1.)
    END DO
  END DO

END SUBROUTINE S_PhiFunc

!==================================================================================================!
! \\\\\\\\\\\\\\\\\\\\\\\\\                                                 ///////////////////////////// !
!                                         END SUBROUTINE: S_PHIFUNC                                          !
! /////////////////////////                                                 \\\\\\\\\\\\\\\\\\\\\\\\\\\\\ !
!==================================================================================================!
```

A.7 Subroutines to Determine Shape Factor

```
!==================================================================================================!
! \\\\\\\\\\\\\\\\\\\\                                                          ////////////////////////// !
!                                       BEGIN SUBROUTINE: S_LINEARSF                                          !
! ////////////////////                                                          \\\\\\\\\\\\\\\\\\\\\\\\\\ !
!==================================================================================================!

! This subroutine calculates the linear shape factor.
SUBROUTINE S_LinearSF(r, z, h, f)

  USE constants
  IMPLICIT NONE

  ! Define dummy variables
  REAL, DIMENSION(0:nr), INTENT(IN) :: r
  REAL, DIMENSION(0:nz), INTENT(IN) :: z
  REAL, DIMENSION(0:nr,0:nz), INTENT(IN) :: h
  REAL, INTENT(OUT) :: f

  ! Define temporary variables
  INTEGER j

  ! Top Node
  f = pi * Rc / (2. * Rs * h(0,0)) * z(1) / (rez + 1.) * &
   & (h(nr-1,0) - h(nr,0)) / (r(nr) - r(nr-1))
```

```
  ! Interior Nodes
  DO j = 1,nz-1
    f = f + pi * Rc / (2. * Rs * h(0,0)) * (h(nr-1,j) - h(nr,j)) / (r(nr) - r(nr-1)) * &
      & (rez * (z(j) - z(j-1)) + z(j+1) - z(j)) / (rez + 1.)
  END DO

  ! Bottom Node
  f = f + pi * Rc / (2. * Rs * h(0,0)) * (h(nr-1,nz) - h(nr,nz)) / (r(nr) - r(nr-1)) * &
   & rez * (z(nz) - z(nz-1)) / (rez + 1.)

END SUBROUTINE S_LinearSF

!========================================================================================!
! \\\\\\\\\\\\\\\\\\\\\\\\\                                          ///////////////////////////// !
!                                END SUBROUTINE: S_LINEARSF                                    !
! /////////////////////////                                          \\\\\\\\\\\\\\\\\\\\\\\\\\\\\ !
!========================================================================================!
```

A.8 Subroutine to Determine Outflow Rates

```
!========================================================================================!
! \\\\\\\\\\\\\\\\\\\\                                                  ////////////////////////// !
!                               BEGIN SUBROUTINE: S_LINEARQOUT                                  !
! ////////////////////                                                  \\\\\\\\\\\\\\\\\\\\\\\\\\ !
!========================================================================================!

! This subroutine calculates the outflow rate using Darcy's Law.
SUBROUTINE S_LinearQout(r, z, h, Q)

  USE constants
  IMPLICIT NONE

  ! Define dummy variables
  REAL, DIMENSION(0:nr), INTENT(IN) :: r
  REAL, DIMENSION(0:nz), INTENT(IN) :: z
  REAL, DIMENSION(0:nr,0:nz), INTENT(IN) :: h
  REAL, INTENT(OUT) :: Q

  ! Define temporary variables
  INTEGER j

  ! Top Node
  Q = 2. * pi * Rc / aa * (h(nr-1,0) - h(nr,0)) / (r(nr) - r(nr-1)) * z(1) / (rez + 1.)

  ! Interior Nodes
  DO j = 1,nz-1
    Q = Q + 2. * pi * Rc / aa * (h(nr-1,j) - h(nr,j)) / (r(nr) - r(nr-1)) * &
      & (rez * (z(j) - z(j-1)) + z(j+1) - z(j)) / (rez + 1.)
  END DO

  ! Bottom Node
```

```
  Q = Q + 2. * pi * Rc / aa * (h(nr-1,nz) - h(nr,nz)) / (r(nr) - r(nr-1)) * &
    & rez * (z(nz) - z(nz-1)) / (rez + 1.)

END SUBROUTINE S_LinearQout

!=====================================================================================!
! \\\\\\\\\\\\\\\\\\\\\\\\\                                    ///////////////////////////// !
!                                 END SUBROUTINE: S_LINEARQOUT                              !
! /////////////////////////                                    \\\\\\\\\\\\\\\\\\\\\\\\\\\\\ !
!=====================================================================================!

!=====================================================================================!
! \\\\\\\\\\\\\\\\\\\\                                          ///////////////////////// !
!                              BEGIN SUBROUTINE: S_NONLINEARQOUT                            !
! ////////////////////                                          \\\\\\\\\\\\\\\\\\\\\\\\\ !
!=====================================================================================!

! This subroutine calculates the outflow rate using Forchheimer's Equation.
SUBROUTINE S_NonlinearQout(r, z, h, Q)

  USE constants
  IMPLICIT NONE

  ! Define dummy variables
  REAL, DIMENSION(0:nr), INTENT(IN) :: r
  REAL, DIMENSION(0:nz), INTENT(IN) :: z
  REAL, DIMENSION(0:nr,0:nz), INTENT(IN) :: h
  REAL, INTENT(OUT) :: Q

  ! Define temporary variables
  INTEGER j

  ! Top Node
  Q = pi * Rc * aa / bb * z(1) / (rez + 1.) * (                              &
    & SQRT(1. + 4. * bb * (h(nr-1,0) - h(nr,0)) / (aa ** 2 * (r(nr) - r(nr-1)))) - 1.)

  ! Interior Nodes
  DO j = 1,nz-1
     Q = Q + pi * Rc * aa / bb * (z(j+1) - z(j) + rez * (z(j) - z(j-1))) / (rez + 1.) *  &
       & (SQRT(1. + 4. * bb * (h(nr-1,j) - h(nr,j)) / (aa ** 2 * (r(nr) - r(nr-1)))) - 1.)
  END DO

  ! Bottom Node
  Q = Q + pi * Rc * aa / bb * rez * (z(nz) - z(nz-1)) *                          &
    & (SQRT(1. + 4. * bb * (h(nr-1,nz) - h(nr,nz)) / (aa ** 2 * (r(nr) - r(nr-1)))) - 1.)

END SUBROUTINE S_NonlinearQout

!=====================================================================================!
! \\\\\\\\\\\\\\\\\\\\\\\\\                                    ///////////////////////////// !
!                               END SUBROUTINE: S_NONLINEARQOUT                             !
! /////////////////////////                                    \\\\\\\\\\\\\\\\\\\\\\\\\\\\\ !
!=====================================================================================!
```

A.9 Matrix Operations

```
!========================================================================================!
! \\\\\\\\\\\\\\\\\\\\\\                                              /////////////////////////// !
!                                  BEGIN SUBROUTINE: S_LUDECOMP                                  !
! //////////////////////                                              \\\\\\\\\\\\\\\\\\\\\\\\\\\ !
!========================================================================================!

! This subroutine finds the LU decomposition for a banded matrix A.
SUBROUTINE S_LUDecomp(A, n)

  USE constants
  IMPLICIT NONE

  ! Define dummy variables
  REAL, DIMENSION(n,n), INTENT(INOUT) :: A
  INTEGER, INTENT(IN) :: n

  ! Define temporary variables
  INTEGER i, j, k
  INTEGER p, q

  p = nr + 1           ! Lower bandwidth
  q = nz + 1           ! Upper bandwidth

  ! LU decomposition of banded matrix A
  DO k = 1,n-1
    DO i = k+1,MIN(k+p,n)
      A(i,k) = A(i,k) / A(k,k)
    END DO
    DO i = k+1,MIN(k+p,n)
      DO j = k+1,MIN(k+q,n)
        A(i,j) = A(i,j) - A(i,k) * A(k,j)
      END DO
    END DO
  END DO

END SUBROUTINE S_LUDecomp

!========================================================================================!
! \\\\\\\\\\\\\\\\\\\\\\\                                             //////////////////////////// !
!                                   END SUBROUTINE: S_LUDECOMP                                   !
! ///////////////////////                                             \\\\\\\\\\\\\\\\\\\\\\\\\\\\ !
!========================================================================================!
```

```
!======================================================================================!
! \\\\\\\\\\\\\\\\\\\\\\                                              //////////////////////////// !
!                                   BEGIN SUBROUTINE: S_LUBKSUB                                   !
! //////////////////////                                              \\\\\\\\\\\\\\\\\\\\\\\\\\\\ !
!======================================================================================!

! This subroutine does the backsubstitution for an LU decomposed banded matrix A.
SUBROUTINE S_LUBkSub(A, x, n)

  USE constants
  IMPLICIT NONE

  ! Define dummy variables
  REAL, DIMENSION(n,n), INTENT(IN) :: A
  REAL, DIMENSION(n), INTENT(INOUT) :: x
  INTEGER, INTENT(IN) :: n

  ! Define temporary variables
  INTEGER i, j, k
  INTEGER p, q
  REAL sum1, sum2, arg

  p = nr + 1          ! Lower bandwidth
  q = nz + 1          ! Upper bandwidth

  ! Forward substitution for Ly=b
  DO i = 1,n
    sum1 = 0.
    DO j = MAX(1,i-p),i-1
      sum1 = sum1 + A(i,j) * x(j)
    END DO
    x(i) = x(i) - sum1
  END DO

  ! Back substitution for Ux=b
  DO i = n,1,-1
    sum2 = 0.
    DO j = i+1,MIN(i+q,n)
      sum2 = sum2 + A(i,j) * x(j)
    END DO
    x(i) = (x(i) - sum2) / A(i,i)
  END DO

END SUBROUTINE S_LUBkSub

!======================================================================================!
! \\\\\\\\\\\\\\\\\\\\\\\                                            ///////////////////////////// !
!                                     END SUBROUTINE: S_LUBKSUB                                   !
! ///////////////////////                                            \\\\\\\\\\\\\\\\\\\\\\\\\\\\\ !
!======================================================================================!
```

Appendix B
Collected Data

B.1 2008 Core Specimen Porosity Data

Core ID	W_s (g)	$W_{sub,total}$ (g)	$W_{sub,solid}$ (g)
1-1-T	3082.0	1385.0	1774.8
1-1-S	2673.3	1229.8	1542.6
1-2-T	3309.7	1473.5	1891.5
1-2-S	2450.1	1158.5	1420.3
1-3-T	2746.7	1313.9	1579.4
1-3-S	2283.1	1047.1	1313.0
2-1-T	2190.9	1100.0	1272.0
2-2-T	2206.1	1083.6	1270.1
2-3-T	1991.7	992.7	1154.3
3-1-T	2446.1	1254.0	1401.5
3-2-T	2060.8	1046.7	1176.6
3-3-T	2455.7	1233.5	1410.6

B.2 2009 Core Specimen Porosity Data

Core ID	W_s **(g)**	$W_{sub,total}$ **(g)**	$W_{sub,solid}$ **(g)**
1-i-T	2831.5	1360.0	1610.0
1-i-S	2164.4	1017.0	1252.0
1-ii-T	2856.4	1362.0	1633.0
1-ii-S	1928.6	928.0	1120.0
1-iii-T	2965.2	1405.0	1698.0
1-iii-S	2040.1	971.0	1182.0
2-i-T	2133.5	1073.0	1238.0
2-ii-T	2254.9	1121.0	1305.0
2-iii-T	2271.6	1133.0	1314.0
3-i-T	2546.2	1288.0	1451.0
3-ii-T	2694.1	1363.0	1542.0
3-iii-T	2638.5	1257.0	1505.0

B.3 2010 Core Specimen Porosity Data

Core ID	W_s (g)	$W_{sub,total}$ (g)	$W_{sub,solid}$ (g)
1-a-T	1519.1	738.4	880.8
1-a-S	1179.2	559.6	689.4
1-b-T	1484.3	670.8	855.2
1-b-S	1191.4	567.7	692.1
1-c-T	1573.8	769.3	902.8
1-c-S	1167.5	560.3	679.8
3-a-T	1376.2	699.1	789.4
3-b-T	1345.7	683.1	773.2
3-c-T	1371.3	697.3	791.3

B.4 2008 Core Specimen Constant Head Data

Core 1-1-T

Q (cm^3/s)	h_s (cm)
1.46	0.12
7.53	1.26
9.97	2.03
14.57	3.89
17.23	5.07
19.87	7.22
23.22	8.43
26.22	11.06
28.51	11.95
31.59	14.03
34.09	15.65
36.59	17.60

Core 1-1-S

Q (cm^3/s)	h_s (cm)
1.45	0.11
5.20	0.40
7.42	0.65
9.35	0.94
11.48	1.33
14.11	1.79
16.16	2.25
18.33	2.79
20.12	3.21
22.08	3.80
24.81	4.61
26.12	5.05
27.78	5.56
29.72	6.31
32.04	7.05
33.68	7.90
34.99	8.34
36.37	8.84

Core 1-2-T

Q (cm^3/s)	h_s (cm)
1.44	0.14
5.28	0.91
7.26	1.47
9.19	2.15
11.68	3.13
14.11	4.29
16.04	5.32
18.11	6.51
19.70	7.41
21.81	8.73
24.22	10.38
26.15	11.76
27.79	12.91
29.88	14.72
31.76	16.23
33.40	17.81
34.88	19.03

36.37	20.27

Core 1-2-S

Q (cm^3/s)	h_s (cm)
1.42	0.09
4.93	0.66
7.43	1.19
9.02	1.62
11.68	2.41
14.18	3.33
15.97	4.11
18.01	4.94
19.85	5.83
22.73	7.22
24.36	8.28
25.98	9.14
27.51	10.05
29.62	11.19
31.60	12.47
33.24	13.59
35.11	14.76
36.44	15.78

Core 1-3-T

Q (cm^3/s)	h_s (cm)
1.44	0.10
4.90	0.52
7.02	0.84
9.35	1.35
11.97	1.88
14.40	2.64
16.22	3.17
17.94	3.71
19.90	4.37
22.28	5.41
24.23	6.22
25.85	6.89
27.57	7.66
29.52	8.52
31.65	9.52

33.48	10.37
35.04	11.09
36.00	11.69

Core 1-3-S

Q (cm^3/s)	h_s (cm)
1.43	0.07
4.69	0.41
7.41	0.76
9.35	1.09
11.36	1.49
14.03	2.02
16.31	2.53
17.76	2.88
19.50	3.34
21.97	4.08
24.54	4.76
25.90	5.27
27.13	5.66
29.21	6.46
31.42	7.17
33.18	8.00
34.62	8.49
36.00	9.08

Core 2-1-T

Q (cm^3/s)	h_s (cm)
1.48	0.34
5.12	1.53
7.33	2.66
9.39	3.94
11.72	5.69
13.99	7.55
16.07	9.37
17.71	11.06
19.72	13.13
22.17	15.88
24.33	18.53
25.94	20.47
27.12	21.92

29.17	24.70
35.52	33.47
36.82	35.94
38.08	38.68
39.96	41.19

Core 2-2-T

Q (cm^3/s)	**h_s (cm)**
1.51	0.18
5.20	0.86
8.34	1.74
10.58	2.47
12.90	3.43
15.09	4.41
17.77	5.84
19.46	6.69
21.45	7.74
23.16	8.87
24.67	9.75
26.97	11.12
29.30	13.07
30.89	14.11
32.17	15.11
34.54	16.88
36.87	18.91
38.99	21.18

Core 2-3-T

Q (cm^3/s)	**h_s (cm)**
1.45	0.32
4.68	1.44
7.46	2.88
9.40	4.18
11.57	5.72
13.72	7.59
16.23	9.73
18.50	12.00
20.43	14.22
22.07	15.73
23.82	17.76

26.15	20.87
28.42	23.77
30.19	26.32
31.39	28.01
33.62	31.10
35.56	34.41
37.88	37.73

Core 3-1-T

Q (cm^3/s)	**h_s (cm)**
1.55	3.12
3.96	13.74
6.02	26.08
8.37	40.13
9.65	49.83

Core 3-2-T

Q (cm^3/s)	**h_s (cm)**
1.48	5.97
4.02	25.12
6.22	49.29

Core 3-3-T

Q (cm^3/s)	**h_s (cm)**
1.50	0.68
5.28	4.21
7.89	8.28
9.82	11.90
11.82	17.19
14.65	23.82
16.62	29.22
18.60	35.81
20.34	41.56
22.13	47.00
24.39	54.97

B.5 2009 Core Specimen Constant Head Data

Core 1-i-T

Q (cm^3/s)	h_s (cm)
1.29	0.11
1.53	0.08
2.22	0.15
3.15	0.27
3.93	0.40
4.66	0.51
5.07	0.52
5.32	0.63
6.25	0.76
7.79	1.15
7.91	1.19
8.13	1.06
10.25	1.58
12.50	2.13
14.53	2.79
16.68	3.48
19.19	4.44
21.39	5.23
23.45	6.08
25.31	6.86
27.18	7.82
28.99	8.80
31.50	10.25
32.98	11.07
34.17	12.09
36.15	13.38
38.92	15.11

Core 1-i-S

Q (cm^3/s)	h_s (cm)
1.21	0.06
1.48	0.09
2.22	0.12
2.97	0.17
3.63	0.22
4.36	0.30
5.06	0.38

5.31	0.43
5.89	0.47
7.56	0.66
7.57	0.65
7.86	0.68
9.78	0.79
11.87	1.14
14.51	1.49
16.22	1.84
18.20	2.16
20.04	2.47
22.30	2.91
24.25	3.40
25.74	3.71
27.97	4.31
29.49	4.74
31.60	5.37
33.29	5.89
34.50	6.33
35.63	6.76

Core 1-ii-T

Q (cm^3/s)	**h_s (cm)**
1.53	0.24
2.03	0.35
3.14	0.63
4.07	0.89
4.79	1.16
5.17	1.48
5.43	1.46
6.24	1.77
7.32	2.27
8.25	2.92
8.92	2.99
9.03	3.06
10.38	4.28
12.38	5.56
14.64	7.09
17.00	8.82
19.05	10.48
21.18	10.78

22.72	12.34
24.29	13.96
27.03	17.10
28.95	19.17
30.88	21.37
32.31	22.97
34.28	25.20
35.94	27.79
38.09	30.51

Core 1-ii-S

Q (cm^3/s)	h_s (cm)
1.46	0.12
1.51	0.12
2.71	0.23
3.86	0.36
4.65	0.46
4.83	0.46
5.33	0.59
6.18	0.72
7.05	0.88
8.11	1.03
8.93	1.31
8.97	1.32
10.32	1.50
12.34	1.96
14.42	2.55
16.28	3.10
18.36	3.75
21.45	4.87
23.16	5.50
24.66	6.20
26.65	6.71
28.41	7.55
30.49	8.63
32.20	9.57
34.21	10.59
35.89	12.19
37.70	13.32

Core 1-iii-T

Q (cm^3/s)	h_s (cm)
1.42	0.10
1.63	0.10
3.02	0.24
3.88	0.38
4.68	0.49
4.68	0.47
5.43	0.56
6.15	0.72
7.07	0.87
7.77	1.04
8.98	1.24
9.03	1.31
9.54	1.32
11.55	1.74
13.69	2.23
15.84	2.82
18.34	3.46
20.80	4.24
23.00	5.03
23.99	5.40
25.49	5.77
27.07	6.42
29.45	7.34
31.94	8.46
34.15	9.29
35.31	9.80
36.89	10.51

Core 1-iii-S

Q (cm^3/s)	h_s (cm)
1.46	0.22
1.53	0.22
3.02	0.48
3.89	0.72
4.63	0.91
5.05	1.14
5.45	1.19
6.17	1.43

7.23	1.79
8.03	1.89
8.48	2.33
9.08	2.57
10.11	2.71
12.12	3.75
14.43	5.11
16.78	6.53
19.32	8.18
20.75	9.10
22.17	10.18
23.93	11.53
26.05	13.14
28.51	15.22
30.79	17.12
32.24	19.47
33.88	21.20
35.61	23.10
38.85	26.77

Core 2-i-T

Q (cm^3/s)	**h_s (cm)**
1.30	0.47
1.43	0.55
2.83	1.18
3.78	1.68
4.48	2.19
4.62	2.52
5.19	2.70
5.89	3.28
6.78	3.97
7.53	4.71
8.14	5.11
8.69	5.60
9.52	6.51
11.75	12.64
13.88	14.88
16.38	18.40
18.40	21.13
20.44	24.68
21.78	26.60

23.45	29.33
25.68	32.62
28.32	37.26
30.21	41.04
31.82	42.24
33.27	45.24
35.07	49.01
38.16	55.49

Core 2-ii-T

Q (cm^3/s)	**h_s (cm)**
1.42	0.24
1.58	0.35
2.79	0.58
3.59	0.81
4.29	0.99
4.84	1.48
5.04	1.21
5.98	1.54
6.97	1.90
7.87	3.06
8.68	3.18
8.72	2.81
9.87	4.18
12.01	5.34
14.31	6.74
16.70	8.12
18.38	9.25
20.21	10.52
21.90	11.64
23.62	13.18
26.15	15.31
28.23	16.42
29.66	17.71
31.66	19.48
33.82	21.34
36.01	23.39
37.54	25.25

Core 2-iii-T

Q (cm^3/s)	h_s (cm)
1.54	0.18
1.54	0.18
2.79	0.43
3.63	0.55
4.31	0.70
4.85	0.80
5.11	0.88
5.88	1.04
6.78	1.24
7.88	1.55
8.22	1.62
8.60	1.74
10.43	2.28
12.13	2.86
14.80	3.83
16.66	4.61
18.78	5.86
21.62	7.29
23.94	8.50
25.92	9.70
27.69	10.86
29.79	12.08
31.76	13.45
33.35	14.63
35.57	16.23
37.56	17.76
40.41	19.84

Core 3-i-T

Q (cm^3/s)	h_s (cm)
1.41	2.08
1.73	2.225
2.67	3.61
3.40	5.185
4.01	6.61
4.77	8.72
4.80	9.43
5.74	11.91

6.30	14.13
7.66	18.76
7.99	20.37
8.19	18.68
9.78	23.98
10.87	29.49
12.58	34.60
14.36	44.90
15.68	52.85

Core 3-ii-T

Q (cm^3/s)	**h_s (cm)**
1.49	1.02
1.55	1.11
2.57	2.02
3.42	2.94
3.98	3.72
4.63	4.74
5.15	4.74
5.50	5.83
6.27	6.98
7.48	8.91
7.98	9.29
8.11	10.20
9.76	12.64
11.85	16.63
14.35	20.31
16.61	26.15
18.68	31.90
20.70	37.77
22.16	42.16
24.59	49.62
25.89	56.06

Core 3-iii-T

Q (cm^3/s)	**h_s (cm)**
1.54	0.85
1.55	0.86
2.53	1.65
3.37	2.34

3.94	3.04
4.64	3.91
4.83	4.52
5.29	4.77
6.20	5.94
7.49	8.17
7.70	9.50
8.16	9.62
9.68	13.58
11.85	16.11
13.49	20.98
15.76	27.59
17.35	32.34
19.32	39.11
21.07	45.64
22.61	50.66

B.6 Select 2008 and 2009 Core Specimen Falling Head Data

Core ID	**t_1 (sec)**	**t_2 (sec)**	**α (s/cm^2)**	**β (s^2/cm^5)**
1-1-S	3.55±0.05	10.18±0.02	0.1505	0.0050
1-2-T	5.42±0.21	14.84±0.16	0.1480	0.0135
1-2-S	4.81±0.10	13.09±0.26	0.1188	0.0110
2-1-T	11.14±0.10	31.43±0.20	0.4161	0.0516
2-i-T	9.72±0.05	25.90±0.04	0.4057	0.0405
2-iii-T	4.10±0.09	11.89±0.16	0.1873	0.0064
3-i-T	21.56±0.38	62.08±0.34	0.9443	0.1799
3-ii-T	13.21±0.07	37.43±0.12	0.5112	0.0715
3-iii-T	14.23±0.21	40.24±0.62	0.5413	0.0836

B.7 2010 Core Specimen Falling Head Data

Core ID	t_1 (sec)	t_2 (sec)	α (s/cm^2)	β (s^2/cm^5)
1-a-T	11.16±0.13	30.53±0.17	0.2997	0.0576
1-a-S	2.91±0.15	8.02±0.19	0.0868	0.0038
1-b-T	3.09±0.13	8.24±0.16	0.0524	0.0049
1-b-S	2.57±0.10	7.08±0.09	0.0750	0.0030
1-c-T	6.23±0.13	17.16±0.21	0.1804	0.0176
1-c-S	2.26±0.07	6.28±0.03	0.0737	0.0022
3-a-T	18.93±0.07	52.09±0.57	0.5464	0.1627
3-b-T	97.34±9.10	295.17±22.37	5.7616	3.0130
3-c-T	37.84±1.76	105.28±4.63	1.2329	0.6265

Symbology

α	linear modified Forchheimer coefficient
α'	significance level used for statistical decisions
β	nonlinear modified Forchheimer coefficient
ε	convergence criteria
η	transformed nonlinear modified Forchheimer coefficient
θ	θ-direction
μ	fluid dynamic viscosity
ξ	transformed linear Forchheimer coefficient
ρ	fluid density
Φ	hydraulic conductivity ratio
a	linear original Forchheimer coefficient
A	cross-sectional area
b	nonlinear original Forchheimer coefficient
b^*	transformed nonlinear original Forchheimer coefficient
b_c	core specimen thickness
c_1	slope relating linear Forchheimer coefficients
c_2	slope relating nonlinear Forchheimer coefficients
c_3	slope relating transformed linear Forchheimer coefficients
c_4	slope relating transformed nonlinear Forchheimer coefficients
c_w	empirical constant for nonlinear porous media flow
d	characteristic length scale
d_{10}	smallest 10% grain diameter
d_{50}	mean grain diameter
D_p	particle diameter
e	eastern half node

E	coefficient for east computational node
E	ratio of liquid-solid interaction pressure gradient to total pressure gradient
F	linear shape factor
f_k	friction factor
Fo	Forchheimer number
g	gravitational constant
h	hydraulic head
h^*	head distribution for infinite core
H_0	null hypothesis
H_a	alternate hypothesis
h_b	average head at outflow boundary
h_s	standpipe head
h_{sd}	measured standpipe head data
h_{sm}	modeled standpipe head
H_u	normalized unit head difference
i	index for radial direction
I	hydraulic gradient
I_r	radial direction hydraulic gradient
I_x	x-direction hydraulic gradient
I_y	y-direction hydraulic gradient
I_z	vertical hydraulic gradient
j	index for vertical direction
k	intrinsic permeability
k_0	intrinsic permeability for zero discharge
K	hydraulic conductivity
K_F	effective Forchheimer hydraulic conductivity
K_r	radial hydraulic conductivity
K_W	Kruskal-Wallis test statistic
K_z	vertical hydraulic conductivity

L	length dimension
L_∞	norm used for convergence criteria
m	power term for Izbash equation
n	northern half node
n	transformed nonlinear original Forchheimer coefficient or time level
N	coefficient for north computational node
N	number of data points
N_i	number of image pairs
n_e	effective porosity
n_r	number of elements in the radial direction
n_z	number of elements in the vertical direction
p	fluid pressure or convergence rate
P	coefficient for computational node
$P.D.$	percent difference
q	specific discharge
Q	volumetric flow rate
q_D	Darcy specific discharge
q_F	Forchheimer specific discharge
q_r	radial specific discharge
q_z	vertical specific discharge
r	radial direction
R	data value rank
Δr	radial difference
R_c	core specimen radius
Re	Reynolds number
Re_k	Reynolds number based on intrinsic permeability
r_{er}	radial expansion ratio
r_{er1}	radial expansion ratio under standpipe
r_{er2}	radial expansion ratio outside of standpipe

r_{ez}	vertical expansion ratio
r_i	radial node location
R_s	standpipe radius
R_w	well radius
s	southern half node
s	roadway slope
S	coefficient for south computational node
$S.E.$	standard error
t	time
T	Mann-Whitney test statistic
Δt	time step
t_0	initial time measurement
t_1	middle time measurement
t_2	final time measurement
t_a	confined aquifer thickness
v	average fluid velocity
V_s	volume of solids in core specimen
V_t	total core specimen volume
w	western half node
W	coefficient for west computational node
W_b	weight of plastic bag
W_s	oven dry weight of solids
$W_{sub,solid}$	submerged weight of core specimen
$W_{sub,total}$	submerged weight of core specimen and plastic bag
z	vertical direction or elevation head
z_j	vertical node location

Acronyms

ANOVA	Analysis of Variance
BMP	Best Management Practice
CDS	Central Difference Scheme
CRWR	Center for Research in Water Resources
HMAC	Hot Mix Asphalt Concrete
LID	Low Impact Development
OGFC	Open-Graded Friction Course
PFC	Permeable Friction Course
RHS	Right Hand Side
TCEQ	Texas Commission on Environmental Quality
TSS	Total Suspended Solids
TX	Texas
TxDOT	Texas Department of Transportation

Works Cited

ASCE (1992): *Design and Construction of Urban Stormwater Management Systems*, American Society of Civil Engineers, prepared by the Urban Water Resources Research Council and the Water Environment Federation, Reston, Virginia.

Barrett, M.E., P. Kearfott, and J.F. Malina (2006): "Stormwater Quality Benefits of a Porous Friction Course and Its Effects on Pollutant Removal by Roadside Shoulders," *Water Environmental Research*, Vol. 78, No. 11, pg. 2177-2185.

Barrett, M.E. and C.B. Shaw (2007): "Benefits of Porous Asphalt Overlay on Storm Water Quality," *Transportation Research Record*, No. 2025, pg. 127-134.

Bear, J. (1972): *Dynamics of Fluids in Porous Media*, American Elsevier Publishing Company, Inc., New York.

Bear, J. (1979): *Hydraulics of Groundwater*, McGraw-Hill, New York.

Bendtsen, H. and B. Andersen (2005): "Report 141: Noise Reducing Pavements – State of the Art in Denmark," Road Directorate, Danish Road Institute, Denmark Ministry of Transport.

Berbee, R., G. Rijs, R. de Brouwer, and L. van Velzen (1999): "Characterization and Treatment of Runoff from Highways in the Netherlands Paved with Impervious and Pervious Asphalt," *Water Environment Research*, Vol. 71, No. 2, pg. 183-190.

Bordier, C. and D. Zimmer (2000): "Drainage Equations and Non-Darcian Modelling in Coarse Porous Media or Geosynthetic Materials," *Journal of Hydrology*, Vol. 228, pg. 174-187.

Caltrans (2009): *Open and/or Gap Graded Asphalt Pavements Water Quality Project: Visual Inspection of Monitoring Location Pavements*, California Department of Transportation, Division of Environmental Analysis, Storm Water Program MS-27, Sacramento, CA.

Camacho-V., R.G. and M. Vasquez-C. (1992): “Comment on ‘Analytical Solution Incorporating Nonlinear Radial Flow in Confined Aquifers’ by Zekai Sen,” *Water Resources Research*, Vol. 28, No. 12, pg. 3337-3338.

CAMPO (2009): “TxDOT 5 County AADT Counts: 1990-2005,” 20 April 2009, Capital Area Metropolitan Planning Organization, Austin, Texas, <http://www.campotexas.org/programs_rd_traffic_counts.php>.

Candaele, R.M. (2008): *Porous Friction Course: A Laboratory Evaluation of Hydraulic Properties*, M.S. Thesis in Engineering, The University of Texas at Austin.

Carslaw, H.S. and J.C. Jaeger (1959): *Conduction of Heat in Solids*, Second Ed., Oxford University Press, Amen House, London.

Chai, K.C., S.A. Tan, and T.F. Fwa (2004): “Finite Element Analysis of Runoff Flow Within Porous Pavement System,” *Journal of the Institution of Engineers, Singapore*, Vol. 44, Issue 2, pg. 10-28.

Charbeneau, R.J. (2000): *Groundwater Hydraulics and Pollutant Transport*, Prentice-Hall, Upper Saddle River, NJ.

Charbeneau, R.J. and M.E. Barrett (2008): “Drainage Hydraulics of Permeable Friction Courses,” *Water Resources Research*, Vol. 44, W04417.

Charbeneau, R.J., J.B. Klenzendorf, and M.E. Barrett (in press): “Methodology for Determining Laboratory and In-Situ Hydraulic Conductivity of Asphalt Permeable Friction Course,” *Journal of Hydraulic Engineering*.

Chen, Z., S.L. Lyons, and G. Qin (2001): “Derivation of the Forchheimer Law via Homogenization,” *Transport in Porous Media*, Vol. 44, pg. 325-335.

Collins, R.E. (1961): *Flow of Fluids Through Porous Materials*, Reinhold, New York.

Conover, W.J. (1980): *Practical Nonparametric Statistics*, Second Ed., John Wiley & Sons, New York.

Darcy, H. (1856): *The Public Fountains of the City of Dijon*, English Translation by Patricia Bobeck (2004), Kendall/Hunt Publishing Company, Dubuque, Iowa.

Eck, B.J. (2010): *Drainage Hydraulics of Porous Pavements: Coupling Surface and Subsurface Flow*, PhD Dissertation in Engineering, The University of Texas at Austin.

Eck, B.J., M.E. Barrett, and R.J. Charbeneau (in press): "Note on Modeling Surface Discharge from Permeable Friction Courses," *Water Resources Research*.

Ergun, S. (1952): "Fluid Flow Through Packed Columns," *Chemical Engineering Progress*, Vol. 48, No. 2, pg. 89-94.

Ewing, R.E., R.D. Lazarov, S.L. Lyons, D.V. Papavassiliou, J. Pasciak, and G. Qin (1999): "Numerical Well Model for Non-Darcy Flow Through Isotropic Porous Media," *Computational Geosciences*, Vol. 3, pg. 185-204.

Ferziger, J.H. and M. Peric (2002): *Computational Methods for Fluid Dynamics*, Third Ed., Springer-Verlag, Berlin.

Fetter, C.W. (1994): *Applied Hydrogeology*, Third Ed., Macmillan College Publishing Company, New York.

Field, R., H. Masters, and M. Singer (1982): "Status of Porous Pavement Research," *Water Research*, Vol. 16, No. 6, pg. 849-858.

Forchheimer, P. (1901): "Wasserbewegung dur Bodem," *Zeitschrift des Verbundes der deutschen Ingenieurs*, Vol. 45, pg. 1782-1788.

Frasier, P.M. (2009): *Stormwater Quality Benefits of Permeable Friction Course*, M.S. Thesis in Engineering, The University of Texas at Austin.

Fwa, T.F., S.A. Tan, and C.T. Chuai (1998): "Permeability Measurement of Base Materials Using Falling-Head Test Apparatus," *Transportation Research Record*, No. 1615, pg. 94-99.

Fwa, T.F., S.A. Tan, and Y.K Guwe (1999): "Laboratory Evaluation of Clogging Potential of Porous Asphalt Mixtures," *Transportation Research Record*, No. 1681, pg. 43-49.

Fwa, T.F., S.A. Tan, C.T. Chuai, and Y.K. Guwe (2001a): "Expedient Permeability Measurement for Porous Pavement Surface," *International Journal of Pavement Engineering*, Vol. 2, pg. 259-270.

Fwa, T.F., S.A. Tan, and Y.K. Guwe (2001b): "Rational Basis for Evaluation and Design of Pavement Drainage Layers," *Transportation Research Record*, No. 1772, pg. 174-180.

Giorgi, T. (1997): "Derivation of the Forchheimer Law via Matched Asymptotic Expansions," *Transport in Porous Media*, Vol. 29, pg. 191-206.

Goggin, D.J., R.L. Thrasher, and L.W. Lake (1988): "A Theoretical and Experimental Analysis of Minipermeameter Response Including Gas Slippage and High Velocity Flow Effects," *In Situ*, Vol. 12, No. 1&2, pg. 79-116.

Hassan, H.F., A.A. Rawas, A.W. Hago, A. Jamrah, A. Al-Futaisi, and T. Al-Sabqi (2008): "Investigation of Permeability and Leaching of Hot Mix Asphalt Concrete Containing Oil-Contaminated Soils," *Construction and Building Materials*, Vol. 22, pg. 1239-1246.

Hassanizadeh, S.M. and W.G. Gray (1987): "High Velocity Flow in Porous Media," *Transport in Porous Media*, Vol. 2, pg. 521-531.

Helsel, D.R. and R.M. Hirsch (2002): "Statistical Methods in Water Resources," Techniques of Water-Resources Investigations of the United States Geological Survey, Book 4, Hydrologic Analysis and Interpretation, Chapter A3.

Hwang, H.C. and R.J. Houghtalen (1996): *Fundamentals of Hydraulic Engineering Systems*, Third Ed., Prentice Hall, Upper Saddle River, NJ.

Irmay, S. (1958): "On the Theoretical Derivation of Darcy and Forchheimer Formulas," *Journal of Geophysical Research*, Vol. 39, pg. 702-707.

Isenring, T., H. Koster and I. Scazziga (1990): "Experiences with Porous Asphalt in Switzerland," *Transportation Research Record*, No. 1265, pg. 41-53.

Izbash, S. (1931): *O Filtracii Kropnozernstom Materiale*, Leningrad, USSR.

Jackson, T.J. and R.M. Ragan (1974): "Hydrology of Porous Pavement Parking Lots," *Journal of the Hydraulic Division*, Vol. 100, HY 12, pg. 1739-1752.

Kadlec, H.R. and L.R. Knight (1996): *Treatment Wetlands*, CRC Press Lewis Publishers, Boca Raton, Florida.

Kanji, G.K. (2006): *100 Statistical Tests*, Third Ed., SAGE Publications Ltd, London.

Kelkar, M.G. (2000): "Estimation of Turbulence Coefficient Based on Field Observations," *SPE Reservoir Evaluation and Engineering*, Vol. 3, No. 2, pg. 160-164.

Kovacs, G. (1981): *Seepage Hydraulics*, Elsevier Scientific Publishing Company, Amsterdam.

Krishnan, J.M. and C.L. Rao (2001): "Permeability and Bleeding of Asphalt Concrete Using Mixture Theory," *International Journal of Engineering Science*, Vol. 39, pg. 611-627.

LCRA (2010): "Hydromet," 15 February 2010, Lower Colorado River Authority, Austin, Texas, <http://hydromet.lcra.org/>.

Li, D. and T.W. Engler (2001): "Literature Review on Correlations of the Non-Darcy Coefficient," *SPE 70015*, Proceedings of the SPE Permian Basin Oil and Gas Recovery Conference, Midland, Texas, USA, May 15-16.

Loaiciga, H.A. (2005): "Steady State Phreatic Surfaces in Sloping Aquifers," *Water Resources Research*, Vol. 41, W08402.

Ma, H. and D.W. Ruth (1993): "The Microscopic Analysis of High Forchheimer Number Flow in Porous Media," *Transport in Porous Media*, Vol. 13, pg. 139-160.

Masad, E., B. Muhunthan, N. Shashidhar, and T. Harman (1999): "Internal Structure Characterization of Asphalt Concrete Using Image Analysis," *Journal of Computing in Civil Engineering*, Vol. 13, No. 2, pg. 88-95.

Masad, E., B. Birgisson, A. Al-Omari, and A. Cooley (2004): "Analytical Derivation of Permeability and Numerical Simulation of Fluid Flow in Hot-Mix Asphalt," *Journal of Materials in Civil Engineering*, Vol. 16, No. 5, pg. 487-496.

Mathias, S.A., A.P. Butler, and H. Zhan (2008): "Approximate Solutions for Forchheimer Flow to a Well," *Journal of Hydraulic Engineering*, Vol. 134, No. 9, pg. 1318-1325.

Moutsopoulos, K.N. and V.A. Tsihrintzis (2005): "Approximate Analytical Solutions of the Forchheimer Equation," *Journal of Hydrology*, Vol. 309, pg. 93-103.

Muskat, M. (1982): *The Flow of Homogenous Fluids Through Porous Media*, International Human Resources Development Corporation, Boston, MA.

Pagotto, C., M. Legret, and P. le Cloirec (2000): "Comparison of the Hydraulic Behaviour and the Quality of Highway Runoff Water According to the Type of Pavement," *Water Research*, Vol. 34, No. 18, pg. 4446-4454.

Ranchet, J. (1995): "Impacts of Porous Pavements on the Hydraulic Behaviour and the Cleansing of Water" (in French), *Techniques Sciences et Methodes*, Vol. 11, pg. 869-871.

Ranieri, V. (2002): "Runoff Control in Porous Pavements," *Transportation Research Record*, No. 1789, pg. 46-55.

Ranieri, V. (2007): "The Functional Design of Porous Friction Courses," *2007 Annual Meeting of the Transportation Research Board*.

Reddy, N.B.P. and P. Rama Mohan Rao (2006): "Effect of Convergence on Nonlinear Flow in Porous Media," *Journal of Hydraulic Engineering*, Vol. 132, No. 4, pg. 420-427.

Regimand, A. and L. James (2004): "Systems and Methods for Determining the Porosity and/or Effective Air Void Content of Compacted Material," U.S. Patent 6,684,684 B2, Feb. 3, 2004.

Reynolds, O. (1900): "Papers on Mechanical and Physical Subjects," Cambridge University Press.

Ruth, D. and H. Ma (1992): "On the Derivation of the Forchheimer Equation by Means of the Averaging Theorem," *Transport in Porous Media*, Vol. 7, pg. 255-264.

Sen, Z. (1987): "Non-Darcian Flow in Fractured Rocks with a Linear Flow Pattern," *Journal of Hydrology*, Vol. 92, pg. 43-57.

Sen, Z. (1988): "Analytical Solution Incorporating Nonlinear Radial Flow in Confined Aquifers," *Water Resources Research*, Vol. 24, No. 4, pg. 601-606.

Sen, Z. (1990): "Nonlinear Radial Flow in Confined Aquifers Toward Large-Diameter Wells," *Water Resources Research*, Vol. 26, No. 5, pg. 1103-1109.

Sen, Z. (1992): "Reply," *Water Resources Research*, Vol. 28, No. 12, pg. 3339-3340.

Sidiropoulou, M.G., K.N. Moutsopoulos, and V.A. Tsihrintzis (2007): "Determination of Forchheimer Equation Coefficients *a* and *b*," *Hydrological Processes*, Vol. 21, pg. 534-554.

Smith, G.D. (1965): *Numerical Solution of Partial Differential Equations*, Oxford University Press, Amen House, London.

Srivastava, R. (2009): "Discussion of 'Effect of Convergence on Nonlinear Flow in Porous Media' by N. Bhanu Prakasham Reddy and P. Rama Mohan Rao," *Journal of Hydraulic Engineering*, Vol. 135, No. 6, pg. 533-535.

Stanard, C.E. (2008): *Stormwater Quality Benefits of a Permeable Friction Course*, M.S. Thesis in Engineering, The University of Texas at Austin.

Stanard, C.E., M.E. Barrett, and R.J. Charbeneau (2008): *Stormwater Quality Benefits of a Permeable Friction Course*, CRWR Online Report 08-03, Center for Research in Water Resources, The University of Texas at Austin.

Stotz, G. and K. Krauth (1994): "The Pollution of Effluents from Pervious Pavements of an Experimental Highway Section: First Results," *The Science of the Total Environment*, Vol. 146-147, pg. 465-470.

Tan, S.A., T.F. Fwa, and C.T. Chuai (1997): "A New Apparatus for Measuring the Drainage Properties of Porous Asphalt Mixes," *Journal of Testing and Evaluation*, Vol. 25, No. 4, pg. 370-377.

Tan, S.A., T.F. Fwa, and C.T. Chuai (1999): "Automatic Field Permeameter for Drainage Properties of Porous Asphalt Mixes," *Journal of Testing and Evaluation*, Vol. 27, No. 1, pg. 57-62.

Tan, S.A., T.F. Fwa, and Y.K. Guwe (2000): "Laboratory Measurements and Analysis of Clogging Mechanism of Porous Asphalt Mixes," *Journal of Testing and Evaluation*, Vol. 28, No. 3, pg. 207-216.

Tan, S.A., T.F. Fwa, and C.T. Chuai (2002): "Drainage Testing of Porous Asphalt Road Mixes," U.S. Patent 6,367,310 B1, Apr. 9, 2002.

Tan, S.A., T.F. Fwa, and C.T. Han (2003): "Clogging Evaluation of Permeable Bases," *Journal of Transportation Engineering*, Vol. 129, No. 3, pg. 309-315.

Tan, S.A., T.F. Fwa, and K.C. Chai (2004): "Drainage Considerations for Porous Asphalt Surface Course Design," *Transportation Research Record*, No. 1868, pg. 142-149.

Tarefder, R.A., L. White, and M. Zaman (2005): "Neural Network Model for Asphalt Concrete Permeability," *Journal of Materials in Civil Engineering*, Vol. 17, No. 1, pg. 19-27.

Thauvin, F. and K.K. Mohanty (1998): "Network Modeling of Non-Darcy Flow Through Porous Media," *Transport in Porous Media*, Vol. 31, pg. 19-37.

Theis, C.V. (1935): "The Lowering of the Piezometer Surface and the Rate and Discharge of a Well Using Groundwater Storage," *Transactions, American Geophysical Union*, Vol. 16, pg. 519-524.

Thiruvengadam, M. and G.N. Pradip Kumar (1997): "Validity of Forchheimer Equation in Radial Flow Through Coarse Granular Media," *Journal of Engineering Mechanics*, Vol. 123, No. 7, pg. 696-705.

TRB (2009): *Construction and Maintenance Practices for Permeable Friction Courses*, National Cooperative Highway Research Program Report 640, Transportation Research Board of the National Academies, Washington, D.C.

TxDOT (1993): *Special Specification 3231 – Porous Friction Course*, Texas Department of Transportation, Austin, TX.

TxDOT (2004a): *Test Procedure for Permeability or Water Flow of Hot Mix Asphalt*, Texas Department of Transportation, Construction Division, Designation Tex-246-F, Austin, TX.

TxDOT (2004b): *Item 342 – Permeable Friction Course (PFC)*, Texas Department of Transportation, Austin, TX.

Van Heystraeten, G. and C. Moraux (1990): "Ten Years' Experience of Porous Asphalt in Belgium," *Transportation Research Record*, No. 1265, pg. 34-40.

Venkataraman, P. and P. Rama Mohan Rao (1998): "Darcian, Transitional, and Turbulent Flow Through Porous Media," *Journal of Hydraulic Engineering*, Vol. 124, No. 8, pg. 840-846.

Venkataraman, P. and P. Rama Mohan Rao (2000): “Validation of Forchheimer’s Law for Flow Through Porous Media with Converging Boundaries,” *Journal of Hydraulic Engineering*, Vol. 126, No. 1, pg. 63-71.

Wang, X., F. Thauvin, K.K. Mohanty (1999): “Non-Darcy Flow Through Anisotropic Porous Media,” *Chemical Engineering Science*, Vol. 54, pg. 1859-1869.’

Ward, J.C. (1964): “Turbulent Flow in Porous Media,” *Journal of the Hydraulic Division*, Vol. 90, HY 5, pg. 1-12.

Wiles, T.J. and J.M. Sharp (2008): “The Secondary Permeability of Impervious Cover,” *Environmental and Engineering Geoscience*, Vol. 14, No. 4, pg. 251-265.

Wu, Y.S. (2002): “An Approximate Analytical Solution for Non-Darcy Flow Toward a Well in Fractured Media,” *Water Resources Research*, Vol. 38, No. 3, 1023.

Yates, S.R., A.W. Warrick, and D.O. Lomen (1985a): “Hillside Seepage: An Analytical Solution to a Nonlinear Dupuit-Forchheimer Problem,” *Water Resources Research*, Vol. 21, No. 3, pg. 331-336.

Yates, S.R., D.O. Lomen, and A.W. Warrick (1985b): “Solutions for a Dupuit Aquifer with Sloping Substratum and Areal Recharge,” *Computers and Geosciences*, Vol. 11, No. 4, pg. 477-469.

Zeng, Z. and R. Grigg (2006): “A Criterion for Non-Darcy Flow in Porous Media,” *Transport in Porous Media*, Vol. 63. pg. 57-69.